# Review of the critical current densities and magnetic irreversibilities in high Tc superconductors

S. Senoussi

Classification
*Physics Abstracts*
74.70 — 74.60 — 74.30C — 74.70V — 74.70Y

# Review of the critical current densities and magnetic irreversibilities in high $T_c$ superconductors

S. Senoussi

Laboratoire de Physique des Solides (*), Bât. 510, 91405 Orsay Cedex, France

(*Received 18 June 1991, revised 17 February 1992, accepted 30 March 1992*)

**Résumé.** — Ce papier de revue est consacré aux courants critiques ($J$) et aux irréversibilités magnétiques dans les nouveaux matériaux supraconducteurs (HTSC). Nous y comparons les densités des courants critiques effectives déduites à partir des techniques expérimentales les plus courantes (transport, cycle d'hystérésis, susceptibilité alternative, ...). L'influence de l'échelle du temps de la mesure et de la taille effective de l'échantillon sur les divers critères définissant $J$ est examinée en détail. La dépendance de ce courant en fonction des joints de grains (« liens faibles »), du degré de texture et des autres défauts physiques et chimiques est discutée. Le rôle du champ propre est clarifié. Le courant critique est très dépendant de l'anisotropie de l'échantillon dans pratiquement toutes les conditions expérimentales. L'ancrage intrinsèque est détérioré par les défauts. Le rôle des effets démagnétisants et de la surface de l'échantillon sur les résultats expérimentaux est passé en revue. Les modèles de l'état critique et de « flux creep » sont rappelés en insistant sur les aspects les plus spécifiques des HTSC. Un modèle théorique est proposé. Il tient compte de l'aimantation réversible, des aspects granulaires et reproduit à la fois les propriétés les plus typiques des cycles d'hystérésis et de la susceptibilité alternative. Plusieurs formules nouvelles généralisant le modèle de Bean en sont déduites. Elles montrent comment tenir compte des dimensions des grains (matériaux granulaires), du rayon macroscopique, de l'anisotropie et des effets démagnétisants, dans certaines conditions. Plusieurs limites au-delà desquelles les concepts classiques de l'état critique cessent d'être valides sont également examinés : (1) la limite élastique où le champ de mesure est trop faible pour dépiéger les vortex, (2) $H \approx H_{C1}$ de sorte que les interactions entre vortex sont exponentiellement faibles et (3) $H$ et $T$ voisins de la ligne d'irréversibilité où les forces de viscosité jouent un rôle prépondérant. (4) $H \gg H_{C1}$ de sorte que $J$ est imposé par l'ancrage collectif.

**Abstract.** — This review article is concerned with critical current density ($J$) and magnetic irreversibilities in high-$T_c$ superconductors (HTSC). The apparent $J$ derived from different experimental techniques (transport, hysteresis cycle, ac-susceptibility) are compared. The influence of time (relaxation effects) as well as the macroscopic size of the sample on the criteria defining $J$ are discussed. The dependences of the critical current on grain boundaries (« weaks-links »), texturing and other physical and chemical defects are examined in detail. The role of self fields is clarified. The critical current is strongly influenced by the anisotropy of the layered structure practically whatever the experimental conditions. Intrinsic pinning is lowered by

(*) Laboratoire associé au CNRS, URA n° 002.

defects. Demagnetizing effects and surface pinnings are reviewed. The usual critical state and flux creep models are recalled emphasizing the physical aspects most specific to HTSC. A theoretical model which takes into account the equilibrium magnetization and sample granularity is developed. It reproduces most of the characteristic features of both the hysteresis cycle and ac-susceptibility. A number of new formulae are introduced. They generalize the Bean model and show how to correct for the dimensions of the grains (granular materials), the macroscopic radius of the sample, anisotropy and demagnetization effects in certain situations. Several limits beyond which the usual critical state breaks down are discussed : (1) the quasi elastic limit where the variable field is too weak to depin the vortices, (2) $H \approx H_{c1}$ so that the interaction between vortex lines is exponentially weak and (3) $T$ and $H$ close to the « irreversibility line » where the influence of viscous forces are strong. (4) $H \gg H_{c1}$ so that $J$ is governed by collective pinning.

PLAN

## 1. Introduction.

Since the pioneering paper of Bednorz and Müller [1] on the high temperature superconductors (HTSC) $La_{1-x}Ba_xCuO_4$ and the ensuing discoveries of the now archetypal systems $La_{2-x}Sr_xCuO_4$ (Takagi *et al.* [2]), $YBa_2Cu_3O_7$ (Chu *et al.* [3]), (Michel *et al.* [4]) and other cuprate families [5-12], a huge number of articles have been devoted to investigate the critical current densities of these materials. From the very beginning of the high $T_c$ story, it was shown first by Oussena *et al.* [13] that the intragrain critical current density in $La_{2-x}Sr_xCuO_4$ was as high as $10^6$ A/cm$^2$. This result was obtained indirectly by means of magnetic measurements assuming the Bean model. Since then, magnetic as well as transport critical current densities up to $5 \times 10^7$ A/cm$^2$ are currently quoted in the literature, especially in highly textured epitaxial thin films of $YBa_2Cu_3O_7$ (Chaudhari *et al.* at 4.2 K, [14]). However, it turns out that for detailed analysis and interpretations of transport and magnetic experiments, the relation between the local current density $J$, entering the critical state force balance equation [15-17], and the apparent critical current density deduced from experimental data is generally extremely complex in HTSC. The same remark holds for the derivation of the pinning barriers associated with these currents. It is indeed known [18, 19] that type II hard superconductors are characterized by different kinds of supercurrents the manifestation of which depend both on the experimental conditions ($T$, $H$, dimensions of the sample, time scale of the experiment etc.) and the measurement technique employed. For single crystals and homogeneous materials, these currents can be classified into two different groups related to the equilibrium magnetization ($M_{eq}$) and to the irreversible magnetization ($M_{ir}$) respectively. $M_{ir}$ is in turn connected with pinning forces which act on the vortex lines and give rise to a local current density $J$. It is generally this local current density which is tacitly referred to in the literature as the critical current density. It is important to keep in mind that this critical current does not include the current associated with $M_{eq}$. In addition, because of their ceramic nature HTSC often exhibit both intragranular and intergranular currents. It is found that the critical current densities of high $T_c$ materials differ from those of conventional type II superconductors in many important aspects. I find it interesting to enumerate some of these aspects.

First, apart from their exceptionally high values at low $T$ and low $H$ (in crystallites and in thin films), the experimental critical current densities generally decrease extremely rapidly with temperature ($T$) [20-25], time ($t$) [26-34], and field ($H$) [20, 35-41] (especially near the irreversibility lines in the last case).

Secondly, the quasi-bidimensionality of HTSC makes their magnetic and transport properties strongly anisotropic [42-70]. A spectacular and very unusual consequence of the layered structure is the fact that, for arbitrary orientation of the applied field **H** with respect to the crystalline axes, the magnetic vectors **H**, **B** and **M** are no longer colinear. In particular, in the limit of infinite anisotropy the magnetization is at right angles to the $a$-$b$ basal planes, whatever the direction of **H** except when the angle of the applied field with these planes is strictly zero (but in such a case $M = 0$ as well, for infinite anisotropy). If the anisotropy is large but finite the angle of **M** with the $c$-axis is of the order of the mass anisotropy ratio $m_{ab}/m_c$ where $m_{ab}$ and $m_c$ are the effective masses of the conduction electrons moving parallel to the $a$-$b$ planes and perpendicular to these planes respectively. A serious problem then arises concerning the interpretation of magnetic data since most of commercial magnetometers used in laboratories measure not the total vector **M** but only one of its three components, generally the longitudinal component $M_L$ (i.e. that parallel to **H**). We shall see later that in some experimental conditions (ordinary magnetometers, Foner, SQUID) this measured component is negligible compared to the « hidden » transverse magnetization

$M_T$ which is habitually not detected (Note however that on the contrary torque measurements detect $M_T$ but not $M_L$).

A third unusual feature of HTSC concerns their ceramic-like tendency to form granular compounds leading in experiments to the coexistence of intergrain and intragrain currents which follow very different $H$ and $T$ behaviours.

In addition, both transport and magnetic data unavoidably include surface equilibrium currents ($\mathbf{J}_s$) circulating around the individual grains within the London penetration depth $\lambda$. These currents are related to the London-Abrikosov's equilibrium magnetization $M_{eq}$. Contrary to the local « semi-microscopic » critical current density defined by the critical state equations, these surface currents vary rather slowly with $T$ and $H$ and are independent of time. Also, as they are restricted to the surface of the specimen their mean value decreases with the effective radius of the specimen as $1/R$. For all these reasons, their contribution to the measured signal can become quite large, especially close to the irreversibility line where $J$ (the bulk critical current density) becomes vanishingly small. In addition, since their relative weight grows as $1/R$, the equilibrium currents can exceed the critical current density $J$ in granular materials and in thin films (if $H$ is parallel to the film surface in this case) at any temperature and field. For example, it can be shown from the data of the literature that for standard $YBa_2Cu_3O_7$ the two kinds of currents are generally comparable for a grain radius of $r_g \approx 1$ μm, at $T$ as low as 4.2 K. Then, as the irreversible magnetization drops sharply with $T$ the equilibrium currents rapidly become predominant at higher temperatures. Of course, real experiments involve both surface equilibrium currents $\mathbf{J}_s$ and bulk critical currents $J$ and the main question is how to extract out the contribution of interest. This is a very important task especially when we are interested in determining the pinning barriers which are related to the bulk current $J$ alone (i.e. not to $\mathbf{J}_s$) or $H_{c1}$ which depends on the London-Abrikosov's current exclusively. As a general rule it is easier to correct for equilibrium currents in magnetic measurements [71, 72] than in transport measurements. The difficulties are the same for the extraction of the local pinning energies.

Let us ignore for a while the equilibrium currents and consider the local critical current density $J$ alone. The measured current always represents some spatio-temporal average of the distribution of $J$ through the specimen. As a consequence the measured current depends on the experimental technique used, the time scale of the experiment, the shape of the sample, its magnetothermal history, energy losses or heatig and so on. For instance, the time constants involved in magnetic and transport measurements differ generally by several orders of magnitude [73] and this can lead to a difference in their apparent current densities because of the thermally activated flux creep and the associated time relaxation effects. A second distinguishing feature between magnetic and transport techniques, particularly important in the case of high $T_c$, concerns the role of anisotropy which manifests quite differently in the two cases. Also the influence of demagnetizing effects is generally more important in magnetic than in transport measurements. Finally, magnetic and transport critical current densities correspond to different averages over the volume of the sample and this also leads to different results for the two methods even for homogeneous materials. Of course, the situation is more complicated and the difference between the two measurements techniques more important in granular materials where, as we shall see, the useful Bean model [71, 72] breaks down completely.

This review paper is concerned with the critical current density in high $T_c$ materials. Owing to the above problems our objective is fourfold :

(i) Outline briefly the present status of investigations on the critical current density of HTSC.

(ii) Investigate in detail and, when possible, elucidate the relationship between the local

current density $J$ as defined by the critical state [72, 74-76] and the apparent critical current densities deduced from various physical measurement techniques (transport, hysteresis cycle, ac-susceptibility, torque etc.) commonly employed to determine such a quantity.

(iii) Review from'an experimental point of view' the results of the literature on $J$ and other related questions such as the pinning energy, the anisotropy..., having in mind the difficulties enumerated in the discussion above concerning the interpretation of the experimental data.

(iv) Point out that most of the typical features of magnetic (hysteresis cycle, ac-susceptibility) as well as transport properties of HTSC can be understood in a unique model [77] which takes into account simultaneously the intergrain currents connected with the weak-link network (for sintered granular samples), the intragrain currents and the equilibrium currents $J_s$ related to the London-Abrikosov's equilibrium magnetization [78-83]. In particular, this model will allow us to relate the critical current density $J$ to the peak of the imaginary part, $\chi''(T)$, of the a.c.-susceptibility [84-95] as well as to the low-$H$ hysteresis cycle exhibited by granular superconductors [96-102]. The model can also be applied to more classical superconductors such as Chevrel phases [103] which exhibit the same kind of low-$H$ hysteresis loop as HTSC. The same picture describes equally the hysteresis cycles of single crystals [77, 104] and reproduces some of the most unusual features (low-$H$ peak) of such cycles.

The subject of primary importance concerning the microscopic origin of the pinning potentials acting on the vortices and their anomalous temperature and field dependences [20-25, 30-41] is dealt with only very briefly here. However, we will pay a special attention to the intrinsic pinning due to the layered structure of HTSC. In particular, we shall show that : (1) this pinning generally provides a large contribution to the transport critical current, (2) contrary to ordinary pinning, it is probably deteriored by defects at any concentration and (3) it is very hard to derive from magnetic measurements.

Concerning intergranular currents, which is the object of sections 7 (experimental) and 9 (theoretical), we shall not discuss in detail the nature of the weak links (SNS, SIS, SSS) nor their spatial structure. Readers interested in a detailed investigation and in the classification of weak links are referred to the classical review paper by K. Likharev [105]. A detailed discussion of the intrinsic role of grain boundaries and other sensitive factors controlling the critical current density in HTSC can be found in reference [107] by P. Manuel (in French). Among recent review articles dealing with magnetic and transport properties of HTSC a paper by A. Malozemoff [108] and another by Tholence *et al.* [109] present complementary information on several aspects insufficiently or not at all developed here. A very general review by E. H. Brandt [110] is very enlightening from both the theoretical and experimental points of views especially concerning thermally activated depinning and the elastic properties of the vortex lattice (not studied here). Somewhat similar problems (thermal fluctuations, vortex-glass effects, phase transition etc.) are treated by D. S. Fisher *et al.* [106]. It is equally important to mention three interesting papers by Fisanick [111], by Ekin [112] and by Goodrich and Bray [113] which discuss in detail the various factors affecting $J$ and compare the criterions defining the experimental critical current $J$ (see also A. Gupta *et al.* [114] for the dependence of $M$ on the experimental technique). Comparison between magnetic (ac-technique) and dc-transport critical current densities in NbTi superconductor is carried out by Hampshire and Larbalestier [115]. Finally, many important aspects common to all type II superconductors (whether conventional or new) are treated in the very known review article of Campbell and Evetts [19] (from which some of the concepts recalled here have been borrowed).

1.1 ORGANIZATION OF THE PAPER. — The paper is divided into 18 sections and 2 appendices. It is conceived in such a way that each section is as independent as possible of the other

ones. Therefore, the reader interested in a given subject is not forced to read all the article. In addition, we tempted to proceed gradually beginning by a brief recall of some general results and concepts. When possible, we tried to adopt an « experimental point of view » always insisting on the experimental meaning of calculated formulae and on the limit of validity of common approximations tacitly accepted in the literature. We shall see that some of them are not valid for HTSC. To facilitate the understanding of the paper and give it a more concrete content we have made a very extensive use of numerical calculations together with many illustrative figures.

In section 2 we define and discuss briefly most of the physical parameters (currents, fields, magnetizations, characteristic lengths) used in this paper. When possible these definitions are illustrated in various figures : Section 3 deals with the usual critical state model and insists on some of the most common approximations explicitly or implicitly admitted in this picture : there are features of the hysteresis cycle for which these approximations are not justified, especially at low $H$. Section 4 concerns flux creep and relaxation effects. Here too, we insist on the approximations involved in the usual flux creep model and we try to define as clearly as possible the various energy barriers and the various magnetic terms intervening in relaxation experiments. It will be shown in the framework of the flux creep model that the exact spatial shape of the pinning potential $U(r)$ (experienced by the vortices) plays a fundamental role in HTSC and in the flux creep approach. Section 5 deals with the various criterions defining the experimental or apparent critical current densities. Magnetic current ($J_{mag}$, defined from the hysteresis cycle), transport current ($J_{tr}$, defined from *V versus I* characteristics) and resistivity criterions and their relation to the experimental conditions, in particular the time scale, are compared. We shall also show that the notion of critical current density loses its signification in the so called TAFF limit. In section 6 we consider the influence of the radius of the sample (assumed to be a very long cylinder to avoid usual demagnetizing effects) on the apparent critical current density as determined by transport and magnetic measurements. Three different *J versus H* models are considered. Here too we shall insist on the differences and the analogies between magnetic and transport critical currents. It will be seen that the apparent average critical current ($J_{measured} = \langle J(r) \rangle$) generally depends on the *J versus H* law and on the experimental technique used. Section 7 presents experimental results $J(H, T)$ on the intragranular current of most typical HTSC (single crystals, highly textured thin films and isolated oriented grains). The influence of physical and chemical pinnings, as well as thermal treatments on intragranular currents are reviewed. Section 8 deals with experiments on intergranular current density in polycristalline materials. Textured materials are the object of section 9 which compares various texturing techniques. It also discuss the physical and chemical parameters governing the properties of weak links. In section 10 we present a generalization of the static Bean model, calculate and reproduce the hysteresis cycle of single crystals and oriented grains dispersed in epoxy resin. The same model calculation is used in section 11 for the obtention of the hysteresis cycle of granular dense samples. The results are compared with experimental data. Complex ac-susceptibility (at high enough excitation field) is investigated in section 12 where $\chi'$ and $\chi''$ are calculated numerically using the same models as for the hysteresis cycle. Different laws for $J(H, T)$ are tried and compared in detail. The relationship between $\chi''$ and $J$ is clarified for both intra and intergranular current densities. Frequency effects together with the contribution of flux flow to $\chi''$ are examined. The information that can be extracted from $\chi'$ concerning the fractional volume of superconducting material are discussed at length. In section 13 we consider the case where the amplitude of the applied field is so small that the critical state cannot be applied (this experimental situation is encountered not only in some a-c susceptibility measurements conditions but more commonly in EPR, NMR and other low variable $h$ measurements). The implications for the hysteresis cycle, ac-susceptibility and ac-resistivity are outlined. We shall

show that when the amplitude $h_0$ of the alternating field is smaller than some threshold field $h_{2,\,th}(T, H, J)$ the magnetic response of the sample is controlled essentially by the elastic properties of the vortex line lattice (VLL) and the critical state model is no longer valid. In addition, it will be shown that the correct treatment of this important point requires a collective pinning formalism. The elastic penetration depth $\lambda_{el}$ (see definition in sect. 2) and the associated magnetizations are derived for various configurations of the applied fields and the crystalline axes. Anisotropy effects are delt with in section 14 where four different kinds of anisotropy sources are investigated. We also compare the influence of anisotropy on transport and magnetic measurements, especially in thin films, insisting on the influence of the various pinning potentials (both intrinsic and extrinsic). A two-component model for the interpretation of the cycle for $H$ oriented out of the symmetry directions is developed. Formulae are established allowing us to correct the experimental data from shape effects and then relate the anisotropy of magnetization to that of the apparent critical current. In section 15 we consider briefly demagnetizing effects particularly in the two particular limits of (1) a very thin film and (2) the case where the field penetration is very small compared to the dimensions of the specimens. Surface effects are the object of section 16 where two distinct (« intrinsic » and « extrinsic ») surface barriers are discussed. Section 17 deals briefly with thermal fluctuations, collective pinning and the irreversibility line. The general conclusion is the object of section 18.

## 2. Definition of the critical currents, the characteristic fields and other parameters used in this paper.

In most parts of this article we shall use usual notations employed for conventional superconductors. However, it is clear from the above discussion that for the sake of clarity, and for the detailed investigation of the critical current density, it is helpful to define the various currents, fields and other physical parameters intervening in transport and magnetic measurements taking into account the specific features (anisotropy, granularity) of HTSC. Many of these quantities will be re-examined in more detail later in the corresponding sections. Other less important parameters will be introduced at the appropriate moments. Concerning the units we shall often use the Gauss cgs system except for the formulae relating the apparent critical current density to the hysteresis cycle where $J$ will be expressed in A/cm$^2$. This introduces the so-called practical units obtained from Gauss ones simply by replacing c, the velocity of light, by 10 (we shall also use SI units in some special cases). This choice has been imposed to us by the diversity of the notations encountered in the literature on which this work is based. Correspondence between gaussian cgs and SI units will be summarized in appendix B.

2.1 THE VARIOUS CURRENTS ENCOUNTERED IN HIGH-$T_c$ MATERIALS. — Shown in figure 1 is a schematic representation of the most important current densities introduced in this paper.

$J_d$ : At the very microscopic level the supercurrent is defined by the Maxwell equation $\frac{c}{4\pi}$ Curl (**h**) where **h** is the local magnetic field defined on the atomic scale. Generally, these microscopic currents are not directly accessible experimentally except in some special and rather academic conditions as those discussed in appendix A. Here, we shall consider that $J_d$ is the depairing current. In HTSC, $J_d$ is estimated to be as high as $5 \times 10^8$ to $10^9$ A/cm$^2$ at $T = 0$ K.

$J_s$ : This is the surface current (invoked previously) corresponding to the London-Abrikosov's equilibrium magnetization. In HTSC, $J_s$ is of order 2 to $5 \times 10^7$ A/cm$^2$ at $T = 0$ K, $H \leqslant H_{c1}$ and in the $a$-$b$ planes. It is divided by the mass anisotropy ratio

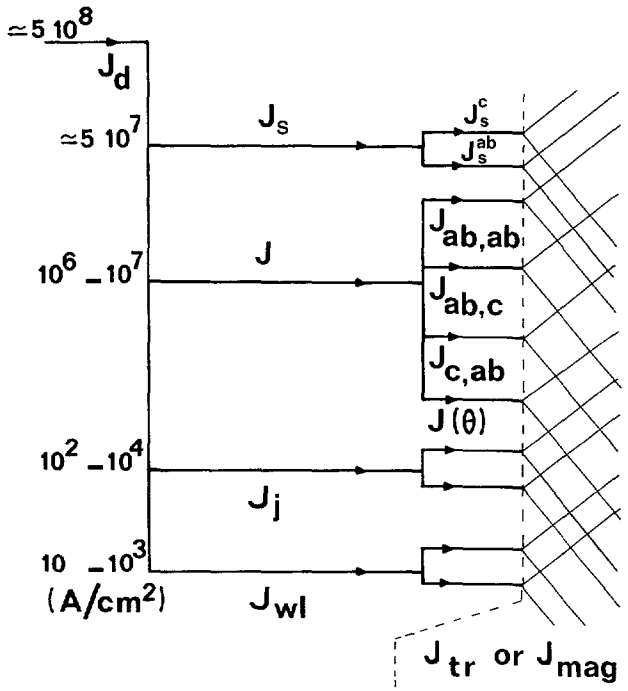


Fig. 1. — Schematic representation of the most important current densities exhibited by layered superconductors. These currents are defined in the text. Their relative contributions to the measured effective current depend on the measurement technique used (hysteresis cycle, transport, torque, magnetic susceptibility), the direction of the applied field with respect to the crystalline axes, the microstructure (granularity), the shape of the specimen and the time scale involved in experiments (the quoted values are for $T \ll T_c$).

$m_c/m_{ab}$ in the $c$-direction. Note that we shall keep the same notation, $J_s$, in the presence of a thermodynamic surface barrier which increases the surface current, see section 16.

$J$ : The critical state allows us to define a semi-microscopic local critical current density as $J = c \,.\, \mathrm{Curl}\, \mathbf{B}(\mathbf{r})/(4\pi)$ where $\mathbf{B}(r)$ is the average of the local field $\mathbf{h}(\mathbf{r})$ over a correlation volume $V_c$ containing a bundle of several vortices (see also [19] p. 231). This current will be called the local intragranular current (note that for the simplicity of notation we drop the usual subscript $c$ in the critical current using $J$ rather than $J_c$).

The relationship between these three current densities is discussed in appendix A. Here, we only note that there are physical arguments which show that for thick enough samples (thicker than about the London penetration depth) the critical current density $J$ can never exceed a small fraction of $J_d$, probably $J_d/K$ or $J_d \ln(K)/K$ where $K$ is the Ginzbur-Landau parameter. $K$ is of the order of 200 in the case of HTSC materials.

$J_{ab,\,c}$, $J_{c,\,ab}$, $J_{ab,\,ab}$ . In the case of single crystals of layered superconductors we are led to define at least three distinct critical current densities depending on the relative directions of the current under consideration, the magnetic induction (**B**) and the crystalline axes. The first index of $J_{i,j}$ defines the direction of the current (axis **c** or $a$-$b$ planes) whereas the second one refers to that of the induction **B** (also assumed along **c** or **a-b**). Of course, these three currents have the same value in isotropic materials but can differ by a factor as high as $10^4$ for $J_{ab,\,ab}/J_{c,\,ab}$ and 500 for $J_{ab,\,c}/J_{c,\,ab}$ in some HTSC such as Bi-Sr-Ca-Cu-O. This anisotropy is expected to be the highest at the lowest $T$ and $H$. Nevertheless, the situation might be quite

different at high enough temperature near the depinning line. This is because $J_{ab,\,c}$ is expected to fall off with $T$ and $H$ more rapidly than $J_{c,\,ab}$ [116]. This can be justified by two independent arguments. (1) Thermal fluctuations of the vortex line lattice are probably more important (hence more dramatic for $J$) when $H$ is parallel to the $c$-axis than for $H$ lying in the $a$-$b$ planes. (2) In conventional superconductors, at high enough field the critical current density drops with $H$ following a power law of the form $(1 - H/H_{c2})^n$. Then, the above claim follows from the anisotropy of $H_{c2}$ as $H_{c2,\,c} < H_{c2,\,ab}$ (see below). A more detailed definition of the currents $J_{i,\,j}$ will be given in section 14 dealing with anisotropy effects. It is important to keep in mind that the critical current $J$ or the associated $J_{ij}$ are defined according to the state of flux distribution in the sample during the time of the experiment. Because of flux creep these currents are lower than the most critical current $J_{\max}$ which would exist before vortices begin to creep over their barriers. In practice this $J_{\max}$ is inaccessible experimentally except when $T$ tends to zero. At this point, we note that throughout this paper we shall neglect any residual anisotropy in the $a$-$b$ planes (otherwise we should introduce six, rather than three, $J_{i,\,j}$ currents). This is not always strictly justified, particularly in the case of untwinned materials or in the presence of modulation structure existing only along the $b$-axis [117] (nevertheless, such a in plane anisotropies are readly negligible in general).

$J_{\rm tr}$ and $J_{\rm mag}$. Each of the current densities $J_{ab,\,c}$, $J_{c,\,ab}$, $J_{ab,\,ab}$ or $J_{\rm s}$ defined above can be obtained either magnetically ($J_{\rm mag}$) or by transport measurements ($J_{\rm tr}$). However, due to our unability to control completely the geometry of the flux lines, especially those associated with the self field, all of these four currents are in general simultaneously present in the experimental data. In addition, the four terms are often mixed in such a way that their relative weights depend both on the shape of the specimen and on the experimental technique employed.

In other words, we generally have :

$J_{\rm measured} = \alpha J_{ab,\,c} + \beta J_{c,\,ab} + \gamma J_{ab,\,ab} + \delta J_{\rm s}$ where $\alpha$, $\beta$, $\gamma$ and $\delta$ are weighting coefficients which depend on the experimental conditions.

$J_{\rm wl}$ and $J_{\rm wl,\,s}$. In the presence of weak links as in sintered granular materials, we can also define (following Josephson [18]) a « local » intergranular critical current density $J_{\rm wl}$ as well as an edge or surface like current $J_{\rm wl,\,s}$ typical of the junctions. The latter current has the same physical meaning as $J_{\rm s}$, the London-Abrikosov's current in bulk materials. As in this case, it is related to a « reversible magnetization » and restricted to the Josephson penetration depth $\lambda_{\rm J}$ at the periphery of the junction (for more details see [97]). $J_{\rm wl}$ will be called the local intergranular current. Naturally these currents depend not only on the nature of the junction (SNS, SIS, S'S'S) but also on the relative orientations of the crystallites bordering it (i.e ; the mismuch between the crystalline axes).

$J_{\rm wl,\,tr}$, and $J_{\rm wl,\,mag}$. Here too, it is useful to distinguish between the intergranular critical current densities derived either from transport or from magnetic measurements.

$J_{\rm J}$ is the reversible current of an ideal (defect free) Josephson junction. In analogy with $J_{\rm s}$ it is restricted to the Josephson penetration depth $\lambda_{\rm J}$.

We shall see that because of the self-fields (i.e. the fields created by the currents flowing in the sample) there are some situations, especially in the case of sintered materials, where the measured current ($J_{\rm wl,\,tr}(H)$, or $J_{\rm wl,\,mag}(H)$) at a given applied field $H$ is very different from the actual one ($J_{\rm wl}(H)$) at the same field. We shall also see that it is generally possible to define a characteristic radius $R_0$ above which both $J_{\rm wl,\,tr}$ and $J_{\rm wl,\,mag}$ are different from the local current $J_{\rm wl}$ and different between them.

$J_{\rm a}$ is the external applied current density (imposed by the power supply). It is used in resistivity measurements to recall that it is generally different from the critical current density $J$.

$I_P$. By analogy with the field $H_p$ of full flux penetration, it is the value of the applied current (in *V versus I* measurements) at which the current arrives at, or as close as possible, to the centre of the specimen. Note that this definition, which amounts to assume that the current penetrates the sample gradually as a function of the applied I, is only valid in the critical state model.

2.2 THE VARIOUS CHARACTERISTIC FIELDS AND TEMPERATURES ENCOUNTERED IN LAYERED MATERIALS. — Associated with some of the above critical current densities are the characteristic fields represented in figure 2.

$H_{c1,c}$ and $H_{c1,ab}$ are the first critical fields of individual grains and single crystals for $H$ parallel and perpendicular to the $c$-axis respectively. It is to be noted that the entry of vortices can eventually be delayed by the presence of a thermodynamic surface barrier (see section 16 for more explanations) introducing a second entrance field $H_s > H_{c1}$.

$H_s$ is the entrance field for a defect free material having a perfect surface (on the atomic scale in order to avoid local demagnetizing fields ; see § 16.3.1).

$H_{c2,c}$ and $H_{c2,ab}$ are the upper critical fields defined as above (some times called $H_n$ and $H_p$ respectively, in the literature).

$H_c$ is the usual thermodynamic field which is isotropic and approximately equal to $(H_{c1} H_{c2})^{1/2}$

$H_{c1}^*$ : It is the experimental first penetration field. Because of demagnetizing fields and imperfections in the vicinity of the surface, which hinder the movement of the vortices, the effective penetration field can be very different from both $H_s$ and $H_{c1}$ (see § 10.6 and Fig. 50). The experimental situation is extremely confusing at present.

$H_J$. It is the first critical field of a single Josephson Junction.

$H_{c1}^w$ : It is the apparent first critical field of the weak link structure as deduced from magnetic measurements. This filed is defined rather phenomenologically and is generally significantly higher than the true $H_J$. This point will be discussed later.

$H_{c2}^w$ is the apparent Josephson decoupling field between adjacent grains. Just as for $H_{c1}^w$ defined above, this field is generally badly defined from experiments.

$H_{J,k}^{ir}$. These fields represent the irreversibility lines (in the $T$-$H$ plane) defined mathematically by the equation $J_{J,k}(H, T) = 0$ (i.e. the vanishing of the critical current densities given in Fig. 1). This line is also called the depinning line.

It is to be emphasized that the real meaning of these lines is not clear at the moment, though it is almost certain that they do not correspond to a thermodynamic transition in the vortex lattice. In addition, if they are associated with the usual thermally activated flux creep then they should not be well defined and would represent a crossover region from flux creep to thermal assisted flux flow and to flux flow regimes. In this case, they should depend on the size and the preparation of the sample as well as on the experimental conditions including the technique of measurement employed. Systematic studies of such effects should help clarifying the present speculations, often unfounded, about the physical nature of these lines. In fact we believe that in most experimental conditions it is more correct to call it a $J$ (or $E$) constant line ($E$ is the electric field). This is because it is defined by some (more or less arbitrary) experimental condition such as $J = 0$ for the magnetic criterion. However we know that there is always some experimental uncertainty $\Delta J$ on the value of the measured current, even though this current is taken to be equal to zero within this uncertainty. As a consequence it is very obvious from the experimental point of view that the line will depend strongly on the experimental technique employed and on the sensitivity of the experiment. In particular it has not much meaning in transport measurements if one uses the usual electric field criterion $E$ = constant. Of course in this case it is a constant $E$ line. For the sake of simplicity we will

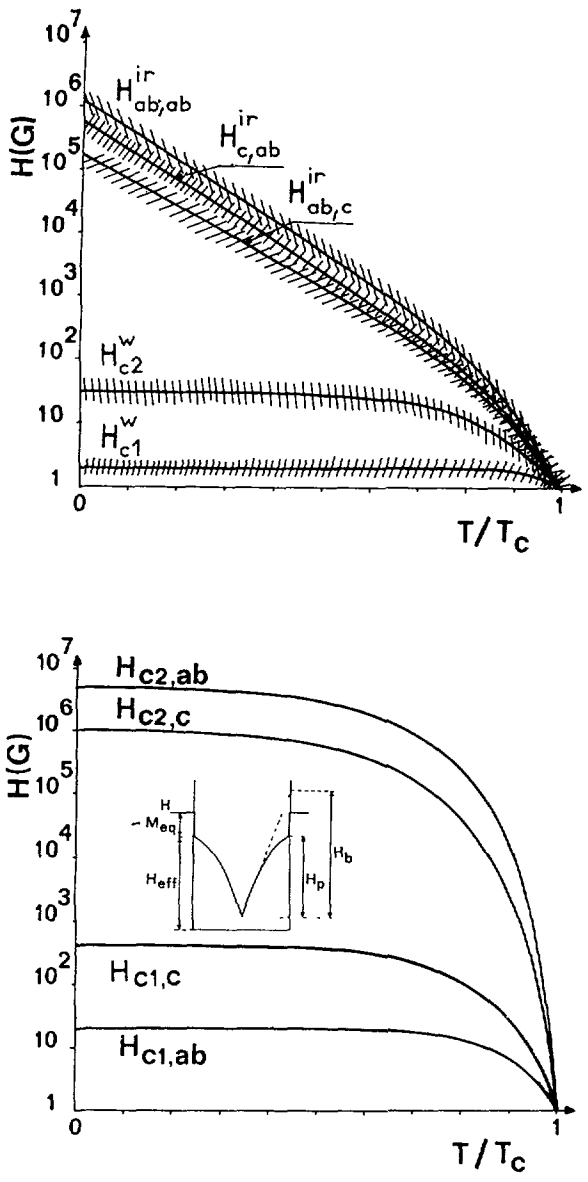


Fig. 2. — The lower graph is a schematic representation of the temperature variation (log $(H) - T$ scales) of the first critical fields $H_{c_1,\,c}$ and $H_{c_1,\,ab}$ (parallel and perpendicular to the $c$-axis respectively), the upper critical fields $H_{c_2,\,c}$ and $H_{c_2,\,ab}$. The upper graph corresponds to the field $H^{w}_{c_1}$ of the first penetration of vortices within the weak links. $H^{w}_{c_2}$ stands for the Josephson decoupling field of the same junctions. The irreversibility lines are defined by $H^{ir}_{ab,\,ab}$, $H^{ir}_{ab,\,c}$, $H^{ir}_{c,\,ab}$ which would correspond to the critical current density $J_{ij}$ sketched in figure 1. Inset : the solid curve represents the field profile within the sample (assumed to by cylindrical) and the field $4\,\pi M_{eq}$ induced by the London-Abrikosov's currents $J_s$ (this field is restricted to the London's penetration depth $\lambda \ll R$). Also defined are the field of complete penetration $H_p$ and the Bean field $H_b$ (dashed curve) obtained by the interpolation of the linear region of the field profile.

use the notation $H_{ir}$ to designate the irreversibility line when the anisotropy effects can be ignored.

$T_{ir}$ represents the temperature of the irreversibility line. It is defined by the implicit equation $J(T_{ir}, H_{ir}) = 0$ (to within the experimental uncertainties just discussed).

Apart from the applied external field $H$ we shall also introduce the following fields in the calculations :

$H_{eq}$ . The thermodynamic field relating the equilibrium magnetization and the magnetic induction. From the thermodynamic point of view $H_{eq}$ is defined by the gradient with respect to $B$ of $f$, the Helmoltz free energy per unit volume, by $H_{eq} = 4\pi \nabla_B f$ (see [19] p. 214 and 215, see also Fig. 4b for a schematic illustration). Note that we have used here the notation $H_{eq}$ to distinguish this field from the other thermodynamic field $H_c$ (already introduced) the square of which is proportional to the condensation energy :

$$\int_0 M_{eq}\, dH = H_c^2/8\pi .$$

$H_{eff,s}$ . It is the effective field existing at the surface of the specimen (including the demagnetizing contribution $H_d$ for samples of arbitrary shapes).

$H_{eff}$ . It is the effective field seen by the vortex lines at the surface of a very long cylindrical specimen (inset Fig. 2) : because of the field induced by the equilibrium currents circulating at the surface of the specimen this field is different from the applied field even for a cylindrical sample with no classical demagnetizing effect.

$B_0$ (or $H_0$) and $T_0$ . They define some characteristic scaling field and temperature governing the variation of $J = J(B/B_0, T/T_0)$ with $B$ and $T$. In other words, $J$ is assumed to depend on $T$ and $H$ through the reduced variables $B/B_0$ and $T/T_0$ (in the simplest situation).

$H_p$ . It is equal to the applied field at which the first flux lines just arrive and meet at the centre of the specimen during the experimental time scale (inset Fig. 2). $H_p$ is a shape dependent field.

$H_{p,max}$ is the field of full penetration which would exist in the absence of flux creep (such as at $T = 0$) or before flux creep takes place.

$H_b$ is the usual Bean field defined in the case where the critical current density $J$ is assumed to be independent of $H$ (as in the original Bean model). It coincides with $H_p$ when $B_0$ tends to infinity (inset of Fig. 2). Remember that the definition of the fields $H_p$, $H_b$ and $H_{p,max}$ assumes the validity of the critical state model.

$H_{cool}$ and $B_{fc}$ represent the cooling field and the associated magnetic induction respectively.

$H_\parallel$, $H_\perp$ . These fields intervene in the transport measurements of $J_{tr}$ and mean that the applied field is either parallel or perpendicular to the mean direction of the macroscopic current (more on these parameters in the appropriate sections).

$h_{1,th}$ . It is the field at which the Bean penetration depth $\Delta r$ is just equal to the range $r_p$ of the pinning well ($\Delta r$ and $r_p$ are defined below).

$h_{2,th}$ . This is a threshold field below which the critical state is no longer valid and the magnetic response imposed by the elastic displacement of the pinned VLL. It depends on the experimental conditions and is anisotropic (see section 13 for its exact definition). It is also the field at which $\Delta r = \lambda_{el}$ where $\lambda_{el}$ is the elastic (or Campbell's) penetration depth defind below. We shall see in section 13 that for the critical state model to be valid we must have $H \geq \max\ (h_{1,th}\ ;\ h_{2,th})$.

2.3 THE VARIOUS MAGNETIZATIONS ASSOCIATED WITH LAYERED SUPERCONDUCTORS. — Because of the anisotropy we must in principle indicate the direction of **H** in the definition of the measured magnetization. For the sake of simplicity we defer these definitions to section 14 concerning anisotropy effects.

$M_{eq}$ . It is the London-Abrikosov equilibrium magnetization already seen.

$M_{ir} = (M^+ - M^-)/2$ : This is the irreversible magnetization induced by vortex pinning. $M^+$ and $M^-$ correspond to the upper and the lower branches of the hysteresis cycle respectively (Fig. 3). The mathematical relationship between $M_{ir}$ and the applied field, $H$, depends on the considered branch of this cycle (see Fig. 3). As a consequence we are led to distinguish between the following magnetizations.

$M_{vg}$ . It is the virgin or initial magnetization measured after zero field cooling. It corresponds to a subcritical state in which the magnetic flux and the current loops have not yet reached the centre of the specimen (Fig. 3).

$M_{cyc}$ . The sample is in a critical cyclic state. It is this magnetization which is related to the critical current density in the famous Bean model (Fig. 3).

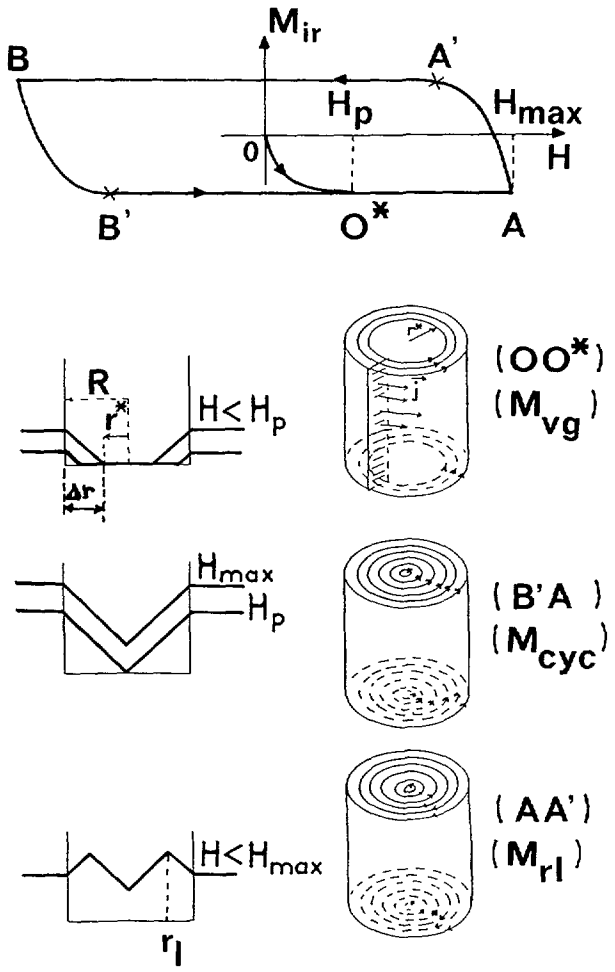


Fig. 3. — a) Schematic definition of the various branches of the hysteresis cycle of a hard type II superconductor. OO* is the virgin or initial magnetization. A'B and B'A define the cyclic critical state whereas BB' and AA' refer to reversal states. Also shown is the field $H_p$ at which magnetic flux just arrives at the centre of the specimen (assumed to be cylindrical). The lower figures represent the field and current profiles associated with $M_{vg}$, $M_{cyc}$ and $M_{rl}$ respectively. $M_{eq}$ is taken equal to zero (for simplicity) and $J$ is assumed to be independent of $H$ so that $H_p = H_b$ (see text).

$M_{rl}$ . This magnetization corresponds to a reversal state characterized by the existence of both clockwise and anticlockwise currents in the specimen (Fig. 3). Remember that in real conditions the hysteresis cycle has a more complicated shape than in figure 3.

$M_L$ and $M_T$ are the longitudinal and the transverse magnetizations defined with respect to the direction of the field **H** respectively.

2.4 THE VARIOUS CHARACTERISTIC TIMES AND LENGTHS TYPICAL OF LAYERED SUPERCONDUCTORS. — Because of their pronounced anisotropy and because of their large Guinzbur Landau parameter $K = \lambda/\xi$ ($\lambda$ and $\xi$ denote the London penetration depth and the coherence length, see below) high $T_c$ superconductors exhibit a large number of specific properties which are characterized by different time scales and lengths. Some of the parameters we are going to define are seldom used in this paper but are worth mentioning as they are currently employed in the literature. At first we define the effective masses of the charge carriers (electrons or holes) as they enter many fundamental quantities :

$m_{ab}$ and $m_c$ are the effective masses of the conduction electrons (or holes) moving parallel to the *a-b* basal planes and along the *c*-axis respectively. Many properties of HTSC are related to the factor $\Gamma = (m_c/m_{ab})^{1/2}$ (~ 6 for YBaCuO and ~ 60 for Bi and Tl based cuprates). This is illustrated in the equations of the characteristic lengths and fields given below

$$\lambda_{ab} = \left[ \frac{c^2 m_{ab}}{4 \pi n_s e^2} \right]^{1/2}$$

This is the London penetration depth associated with the screening currents flowing in the *ab* planes. We recall that $c$ is the velocity of light, $e$ the charge of the electron and $n_s$ the density of the superconducting charge carriers

$$\lambda_c = \left[ \frac{c^2 m_c}{4 \pi n_s e^2} \right]^{1/2}$$

This is the London penetration depth associated with the screening currents directed along the *c*-axis. The simplest way to visualize such a penetration depth is perhaps to imagine a slab semi-infinite in the *c*-direction with the applied field $H$ parallel to both the *a-b* planes and to the slab. Now, it is worth racalling that it is often assumed that $\lambda$ varies with $T$ and $B$ as

$$\lambda = \lambda_0 \left( 1 - \frac{B}{B_{c2}} \right)^{-1/2} [1 - (T/T_c)^4]^{-1/2}$$

This « two fluid » temperature law is empirical and has no firm theoretical basis. It is more appropriate for type I superconductors and gives the correct feature $[1 - T/T_c]^{-1/2}$ near $T_c$

$$\xi_c = \frac{\hbar v_{c,F}}{\pi \Delta(0)} = \hbar \frac{[2 E_F/m_c]^{1/2}}{\pi \Delta(0)}$$

is the coherence length along the *c*-direction for $T$ close to zero. Here $v_{c,F}$ and $E_F$ are the corresponding Fermi velocity (along the *c*-axis) and Fermi energy respectively, whereas $\Delta(T)$ is the energy gap

$$\xi_{ab} = \frac{\hbar v_{ab,F}}{\pi \Delta(0)} = \hbar \frac{[2 E_F/m_{ab}]^{1/2}}{\pi \Delta(0)}$$

is the coherence length in the *a-b* planes (see also Abrikosov's book [78b] p. 450, 451). It is worth recalling that near $T_c$, $\xi$ is often assumed to vary as

$$\xi(T) = 0.7\ \xi(0)\left[\frac{T_c}{T_c - T}\right]^{1/2} \quad \text{(generally valid near } T_c\text{)}.$$

The following remarks are of interest : (1) These expressions are calculated in the so called clean limit in which the electron mean free path (l) is much longer than the coherence length $\xi$. (2) It is clear that the anisotropies of $\lambda$ and $\xi$ are exactly inverse of each other. (3) It is worthrecalling that $\Delta(0)$ is related to $T_c$ by the formula $\Delta(0) = 1.864\ kT_c$ valid in the BCS theory. (4) However, it seems that this property is strictly true only if the energy gap $\Delta(T)$ is itself isotropic (a question not yet completely clarified in HTSC). (4) Finally it is important to remember that the critical fields $H_{c1}$ and $H_{c2}$ are related to $\lambda$ and $\xi$ by

$$H_{c1} = \frac{\Phi_0}{4\ \pi \lambda\,(T)^2} \ln\,(\lambda/\xi)$$

and

$$H_{c2} = \frac{\Phi_0}{2\ \pi \xi(T)^2}.$$

Here $\Phi_0 \approx 2 \times 10^{-7}$ G/cm$^2$ is the elementary flux quantum. Therefore, they will also exhibit opposite anisotropies.

$\lambda_J$ is the Josephson penetration depth.

$\lambda_{s,\,eff}$ is the effective penetration depth for non ideal samples : because of surface imperfections the experimental penetration depth (determined by magnetic techniques) is generally a combination of London and Josephson lengths. For this reason (among others), it is generally different from the one inferred from $\mu$SR experiments for instance. This is because in this case the penetration depth is averaged over the whole volume of the sample.

$\Delta r(H) = R - r^*$ (see Fig. 3) is Bean's penetration depth which depends on $J$ and $H$.

$\delta_{ff}$ is the flux flow skin depth.

$\delta_{staff}$ is the thermal assisted flux flow skin depth.

$\lambda_c$ is Campbell's penetration depth. When the applied field is not strong enough to depin the vortices the penetration of flux is controlled by the elastic properties of the VLL.

$\lambda_{el}$ and $\lambda_{ij,k\ell}$ are elastic penetration depths which generalize Campbell's penetration depth for various configurations of the applied fields with respect to both the surface of the sample and the crystalline axes (for anisotropic materials).

Depending on the experimental conditions (in particular on $T$, $H$, $\omega$ and the microstructure), the penetration of magnetic flux is governed by one or another of the above characteristic depths. As developed in § 13, these lengths depend also on the various kinds of anisotropy present in the material. In general, these lengths are most easily illustrated in ac-susceptibility measurements. However, in this paper we are mainly concerned with the critical state model (except Sect. 13) where the penetration of vortices is described by $\Delta r(H)$.

$X$ is the hopping or jump distance of the flux bundle.

$r_p$ is the range of the pinning potential (for the sake of simplicity these two parameters are assumed to be equal throughout this paper).

$V_b$ is the volume of the vortex bundle involved during flux creep events.

$V_c = L_c R_c^2$ is the correlation volume entering the collective pinning theory (To avoid any confusion, it is important to keep in mind that the same notation, $V_c$, is used to define the electric potential associated with the critical current $I_c$ when investigating the *V versus I*

characteristics). Here $L_c$ and $R_c$ are the longitudinal and transverse correlation ranges (i.e. along and perpendicular to the vortex direction respectively).

$V_p$ is the fractional volume (or packing factor) of the superconducting material.

$\nu = \nu_0 \exp[-U/kT]$ is the flux creep frequency while $\nu_{vl}$ and $\nu_p$ are characteristic frequencies of the VLL in the pure flux flow state and in the presence of strong pinning disorder ($U$ is an effective pinning potential). In the literature on superconductivity these frequencies are generally referred to indistinguishably as phenomenological attempt frequencies. In view of their central role in flux creep effects, particularly in resistivity data, we shall try to clarify their physical origins.

$\tau_0 (\approx \nu_0^{-1})$ is the time needed for the vortices to begin to creep out of their potential wells (formally speaking, $\tau_0$ measures the life time of the most critical state that could be built up immediately after an instantaneous application of a field equal or greater than $H_{p,max}$).

$\tau_{char} = \tau_{ff}$ or $\tau_{taff}$ is a diffusion characteristic time associated either with $\delta_{ff}$ or $\delta_{taff}$ respectively.

$\tau$ is a correlation time which enters the argument of the logarithmic relaxation $(\ln (t + \tau)/\tau_0)$ of the metastable magnetization $M_{ir}$ and which depends on the experimental conditions including $T$, $H$, $J$ and the size of the sample under study (*).

$\tau_{app}$ is the time constant of the measuring apparatus such as the integration time of a lock-in amplifier.

It is to be emphasized that all of the above factors (except $\tau_{app}$) are anisotropic as will be discussed in the appropriate sections.

2.5 THE VARIOUS PINNING POTENTIALS ENCOUNTERED IN HARD SUPERCONDUCTORS. — $U(r)$ : It defines the spatial profile of the pinning potential felt by a vortex line at site $r$ in the limit $J = 0$ (i.e. there is no flux gradient and no Lorentz force). Because of the interaction between vortices $U(r)$ can depend strongly on $H$ and $T$, especially in the limit of weak pinning where the collective pinning theory is more appropriated than the usual flux creep picture considered here : for the sake of simplicity we shall assume here that the pinning centres are independent from each other (except in few cases such as sections 13 and 17).

$U(T, H, J)$ : If $J$ is different from zero, a moving vortex (whatever the origin of this movement : creep, flow, thermal fluctuations, . ) has to work against the Lorentz force. This is why $U$ depends on $J$. Moreover, because the experimental time scales are generally much larger than the characteristic time scales of the VLL (for instance $\tau + t \gg \tau_0$ is generally true) the dependence of $U$ on $r$ is averaged out during flux creep and other vortex movements involving displacements larger than the range $r_p$ of the pinning potential.

$U_p$ . This is the amplitude of the pinning potential. $U_p \approx U(r \approx 0) \approx U(J = 0)$, though $U_p$ is generally a not well defined quantity.

$U_0^*$ : The effective potential barrier entering experimental data depends on the experimental technique employed. For the very usual magnetic measurements, it is noted $U_0^*$.

## 3. Critical state at zero temperature.

To help the understanding of the various subjects considered in this article it is useful to recall that first very briefly the magnetic and transport behaviours of ideal type II superconductors (i.e. without any extrinsic pinning forces) in which the critical current density $J$ (as defined by the critical state) is equal to zero if the material is isotropic (no intrinsic pinnings). Also, since

(*) It is often not realized that many experimental data depend on this factor which is generally not accounted for in comparing with theory. In many examples of the literature $\tau$ is taken equal to 1-10 seconds to avoid the divergence of ln $(t)$ at $t = 0$).

the notion of critical current density is closely related to the concept of the critical state it is important to discuss briefly the basic assumptions of this state. A short discussion of the more general model of collective pinning is presented in the last section of this paper.

3.1 FIELDS AND CURRENTS IN IDEAL TYPE II SUPERCONDUCTORS. — According to Abrikosov's theory [78] the vortex density $B(H)/\Phi_0$ in an ideal type II superconductor has the same value at any point of the specimen, except close to the surface in the London penetration depth $\lambda(T)$. In addition, $B(H)$ depends only on the applied field $H$ and not on the way the field has been increased from zero to its final value : in modern language this means that there is equivalence between the field cooled (fc) and the zero field cooled (zfc) states.

$M_{eq}(H)$ and the associated $B(H)$ curves are shown schematically in figure 4a and figure 4b respectively. The continuous curves correspond to conventional materials with relatively low

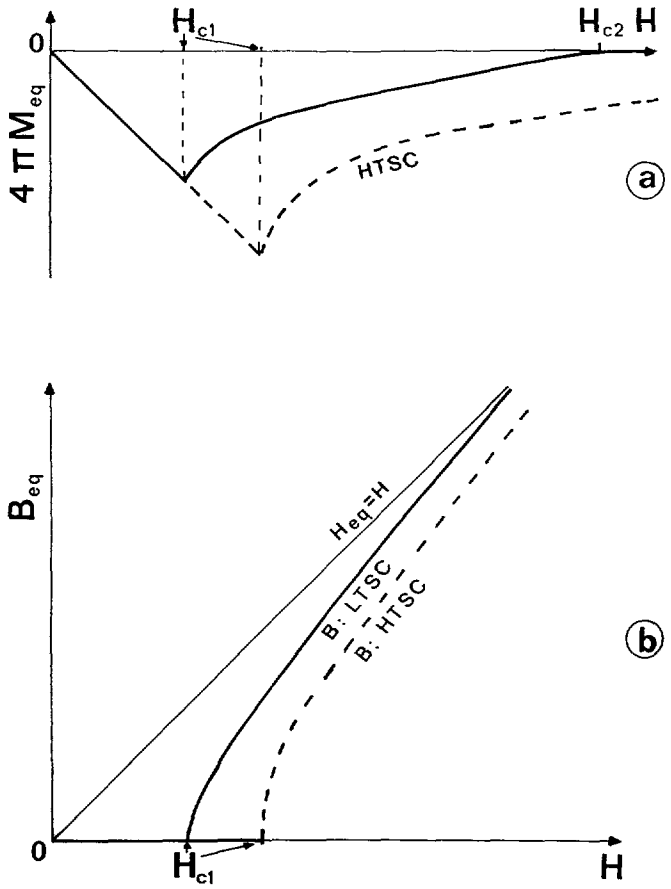


Fig. 4. — a) Schematic representation of the equilibrium reversible magnetization of conventional type II superconductors (solid line) with moderate and laboratory accessible $H_{c_2}$ and of HTSC with very high $H_{c_2}$ (dashed line, $T \ll T_c$). b) Schematic representation of the magnetic induction $B(H)$ of conventional type II superconductors with moderate $H_{c_2}$ (solid line) and of HTSC (dashed line, $T \ll T_c$). Recall that $B(H)$ is related to $M_{eq}(H)$ by equation (1) and that $H$ coincides with $H_{eq}$ here (no demagnetizing field).

$H_{c2}$. The dashed curves correspond to high $T_c$ for which $H_{c2}(T \ll T_c)$ is generally much higher than laboratory available fields.

Sketched in figure 5a and figure 5b are the distribution of the fields and the London surface currents associated with the equilibrium magnetization represented in figure 4a.

Shown in figure 6 is the distribution of currents within the same wire as in figure 5 but here the sample is fed with an external current whereas the applied field is equal to zero. It can be shown that in this case ($H = 0$) the average transport current density is about $H_{c1}/R$ (in the limit $R \gg \lambda(T)$ where $R$ is the radius of the specimen). At higher field such that $H_{\text{eff, s}} > H_{c1}$ we expect that the bulk critical current $J = 0$. However, the general case is probably more complicated. For example, it is likely that even in the mixed state (defined by $H_{\text{eff, s}} > H_{c1}$) a thin specimen of thickness comparable to $\lambda(T)$ and less is not necessarily in a dissipative flux flow state and could carry an apparent $J$ different from zero. This might happen either because the London-Abrikosov's surface currents or because the intrinsic pinning (for layered superconductor, but see anisotropy section (14) and appendix A for a more detailed discussion of this point).

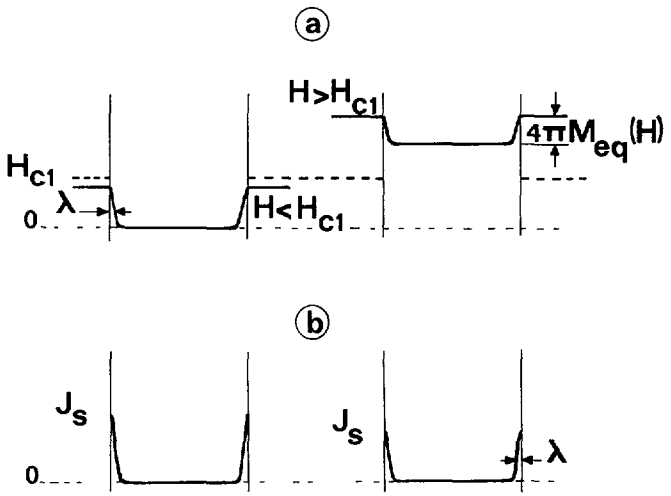


Fig. 5. — Profiles of the local induction $B(r)$ (a) and the associated reversible surface currents (b) in a cylindrical sample of a perfect type II material for $H \leq H_{c_1}$ (left side) and $H \geq H_{c_1}$ (right side). It is to be noted that in both cases the currents are restricted to the surface of the specimen within the London penetration depth $\lambda(T)$.

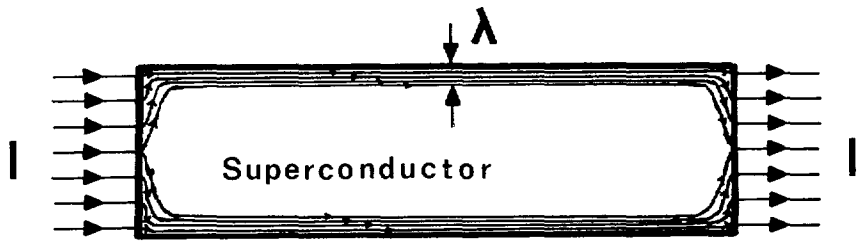


Fig. 6. — Distribution of currents within a perfect superconductor fed with an external current $I$ the self field of which satisfies the condition $H_{\text{self}} \leq H_{c_1}$. There is no external applied field.

In the above curves $H$, $B$ and $M_{eq}$ are related by Gauss equation :

$$B = H + 4\,\pi M_{eq}(H, T)\,. \tag{1}$$

The following remarks are of interest for the forthcoming discussions :

(i) For ideal type II superconductors $H$ coincides with the thermodynamic field $H_{eq}$ defined previously.

(ii) It is known ([78, 79], [118, p. 68-69], [120, p. 152]) that in the so called London approximation the theoretical $M_{eq}(H)$ curve has an infinite slope at $H = H_{c1}$ whilst it varies extremely slowly with $H$ for $H \gg H_{c1}$. Neglecting demagnetizing effects we have :

$$4\,\pi M_{eq}(H, T) = -H \qquad (H \ll H_{c1}) \tag{2a}$$

$$4\,\pi \left[\frac{\partial M_{eq}}{\partial H}\right]_{H \to H_{c1} \to \infty} \qquad (H - H_{c1} \to 0_+) \tag{2b}$$

$$4\,\pi \frac{\partial M_{eq}}{\partial H} = \frac{H_{c1}}{2\,H \ln\,(\lambda/\xi)} \qquad (H_{c2} \gg H \gg H_{c1})\,. \tag{2c}$$

(iii) Throughout this paper we shall use such classical London's approximation. It is to be noted however that more general theoretical treatments by Buzdin *et al.* [80, 81], by Zhidong Hao *et al.* [82] and by Zhidong Hao and Clem [83] reveal that these expressions are severely modified by vortex core effects, particularly near the critical fields $H_{c1}$ and $H_{c2}$. For instance, according to Zhidong Hao and Clem [83] the contribution of the currents circulating very close to the vortex cores lead to an equation of the form :

$$M_{eq} = -\,\beta\,(H, T)\,\frac{\Phi_0}{8\,\pi\lambda^2}\ln\,[\alpha\,(H, T)\,H/H_{c2}] \qquad (H \gg H_{c1})\,. \tag{3}$$

Here $\alpha\,(H, T)$ and $\beta\,(H, T)$ are fitting parameters which vary slowly with field and temperature (approximate values valid in restricted field domains are given in reference [83]).

(iv) The experimental occurrence of a singularity in $M_{eq}(H)$ at $H = H_{c1}$ requires that : (1) the material is perfect on a scale much larger than the London penetration depth $\lambda\,(T)$ and (2) the demagnetizing field is zero everywhere in the specimen. Both conditions are very difficult to realize in practice even for conventional superconductors. In fact, it can be shown that the higher the critical current density $J$ (see below) the smaller the change in the slope of the measured magnetization at $H = H_{c1}$, and thus the smaller the singularity at $H = H_{c1}$. The situation is expected to be more serious in HTSC because the vortices are softer here (especially near $H_{c1}$) and thus can be more easily deformed and attracted by the potential wells of any defect.

(v) Since, from Maxwell equations the local current is proportional to Curl ($\mathbf{B}(\mathbf{r})$), the spatial uniformity of $\mathbf{B}$ (far from the surface (Fig. 5)) implies that a perfect type II superconductor cannot carry any « volumic » or « bulk » current (Fig. 5b). It is to be recalled however that the specimen always carries surface shielding currents extending over the London penetration depth $\lambda\,(T)$. It is these currents which give rise to the equilibrium magnetization $M_{eq}(T, H)$. Therefore, ideal superconductors are of no use for technical applications (at least for materials thick compared to $\lambda$ (see also Appendix A for more details).

3.2 THE CRITICAL STATE AT T = 0, THE CRITICAL CURRENT AND THE PINNING FORCES. — In real materials there are imperfections which pin the vortex lines. Then, pinning leads to irreversibilities in the vortex distribution, i.e. in $\mathbf{B}$, and hence in the magnetization ($M = (-H + B)/4\,\pi$). The result is a non equilibrium magnetization ($M_{ir}$, Fig. 3) which adds

to the equilibrium magnetization discussed above. $M_{ir}$ is induced by local currents called critical currents densities $J$ (already involked) which exist within the interior of the specimen. Usually, the material is homogeneous and the critical current density does not depend explicitly on the point $r$ within the specimen. In this case, the dependence of $J$ on $r$ is indirect, *via* other parameters such as $B(r)$ and $T(r)$. This is not the case for sintered granular materials nor for insufficiently oxygenated single crystals for which $J$ depends directly on $r$. It is not the case for surface pinning either.

To relate the irreversible magnetization to the field and current profiles within the interior of the specimen, Bean [72] introduced the critical state concept and assumed that the critical current density at any point $r$ of the sample can only take one unique value among three different states $J$, $-J$ or zero, depending on the past electromagnetic history of the sample at point $r$. Moreover, in these conditions the resistivity of the specimen is assumed to be strictly zero and as a consequence there is no time relaxation effects in the magnetization (except those imposed by the Maxwell equations during variations of the external fields, see the end of Sect. 4.2). As will be discussed in the next section, this hypothesis is equivalent to the assumption that $T \approx 0$. Bean's model is particularly useful for $H > H_p$ where $H_p$ has been defined previously as the external field above which the sample is entirely penetrated by magnetic flux down to its core (these points will be developed in detail later). In such a critical state and under the assumption that $J$ depends only weakly on the applied field then the current density and the equilibrium magnetization are related to the hysteresis cycle by the two equations below [71, 72] in which $R$ is given in cm, $J$ in A/cm$^2$ and $M$ in emu/cm$^3$ (« practical units » obtained from c.g.s. units by replacing $c$, the velocity of light, by 10) :

$$J_{mag} = 15 \frac{M^+ - M^-}{R} = 30 \frac{M_{ir}}{R} \tag{4}$$

$$M_{rev} = \frac{M^+ + M^-}{2} \tag{5}$$

As introduced originally by Bean, the critical state concept was purely phenomenological. Its microscopic nature and foundation were clarified by Friedel *et al.* [75] and by Anderson [74] who showed that a vortex line is submitted to two kinds of force densities :

(i) A magnetic pressure exerted by the neighbouring vortices which, in some limit, is equivalent to a Lorentz force density $\mathbf{F}_L$ acting on the vortex under consideration and thus proportional to the critical current density $J$ at the vortex site.

(ii) A pinning force density acting on the same vortex line and arising from structural defects. The hypothesis of the critical state lies in the fact that this force can take any value up to a threshold limit $P_V$. As long as the amplitude of the Lorentz force $\mathbf{F}_L$ is lower than $P_V$ the vortex lattice is rigidly locked to the crystalline lattice through the defect structure. Naturally, this is only true if the defect itself is not mobile, a not impossible situation (near $T_c$) with light defects such as oxygen vacancies or perhaps traces of hydrogen atoms. Above $P_V$ the vortex lines are depinned and start to move under the resulting force $F_L - P_V$. Then, the material is said to be in a flux flow state in which the movement of the vortex lines is damped by viscous forces uniquely (we shall ignore these viscous forces for the moment, they will be considered briefly in the next section and in more detail in section 12 in relation with frequency effects. Keep in mind that $F_L$ and $P_V$ represent the forces acting on the vortices crossing the unit surface ([118], p. 83-84).

In the simplest case of homogeneous and isotropic materials the force balance equation of the critical state at $T = 0$ takes the form :

$$-\frac{B}{4\pi}\frac{\partial H_{eq}(B)}{\partial x} = -\frac{B}{4\pi}\frac{\partial H_{eq}}{\partial B}\frac{\partial B}{\partial x} = \frac{B}{c}\frac{\partial H_{eq}}{\partial B} J = P_V . \tag{6}$$

We recall here that $H_{eq}(r)$ is the thermodynamic field defined mathematically by equation (1) in which we must replace $H$ by $H_{eq}$ (thus $H_{eq}$ has no real existence within the material except that it coincides with the applied field at the surface of the specimen in the absence of demagnetizing effects (see Ref. [118] page 84]. It is related to the local $B(r)$ and to the equilibrium magnetization by equation (1) and, hence, can be deduced unambiguously from the curves of figure 4 for any value of $B(r)$ even for dirty superconductors. Remember however that the definition of $H_{eq}$ from equation (1) is only valid for ideal superconductors. In view of the considerable interest of the above equations it is important to keep in mind the conditions under which they can be applied for the analysis of experimental data.

(i) At first, the currents intervening in macroscopic measurements are related to curl $(\mathbf{B}(\mathbf{r}))$ and not to curl $(\mathbf{H}_{eq}(r))$.

(ii) Secondly, in the literature, it is commonly assumed that $B \approx H_{eq}$ and hence $\partial H_{eq}/\partial B \approx 1$ in equation (6) above. As can be seen from equations (2) and (3) this is justified only at very high field such that $H$ and $B(r) \gg H_{c1}$ everywhere in the specimen. Indeed, since we know (Eq. (2)) that $M_{eq}$ has a logarithmic singularity at $H = H_{c1}$, this assumption is only valid for $B(r) \gg H_{c1}$. To prove this claim we can put equation (1) in equation (6) and rewrite the latter as below (valid for isotropic materials) :

$$\frac{B}{c} J = \left[ 1 + 4 \pi \frac{\partial M_{eq}}{\partial H_{eq}} \right] P_V . \tag{7}$$

Customarily, it is assumed that at $H \ll H_{c2}$ the pinning force density, $P_V$, is proportional to the vortex density and thus to $B$. In other words $P_V/B$ is the pinning force per vortex. Then for individual pinnings and in the limit $\partial M_{eq}/\partial H_{eq} \approx 0$, $J$ should be independent of $H$. Then, in these conditions it is clear from equation (7) that for $H_{c2} \gg H \gg H_{c1}$ the critical current density should be independent of $B$ (and thus of $H$).

(iii) Nonetheless the above equation together with equations (2) and (3) predict that $J$ should be strongly enhanced (relatively to its high field value) in the region where the relation $B(r) \gg H_{c1}$ is not satisfied. We in fact believe that this effect explains to a large extent the characteristic peak exhibited by the hysteresis cycle of HTSC near the origin $H = 0$ (see Sect. 7-9). According to a suggestion by Aguillon, this peak can also be enhanced by anisotropy effects : at very low vortex density the vortices are bended by defects allowing for intrinsic current $J_{ab,\,ab}$. This current would be supressed by high $H$ (see Sect. 14 and 15 for details).

(iv) It is to be emphasized too that because of the anisotropy of HTSC, the vectors **B**, **H** and $\mathbf{M}_{eq}$ are not parallel for an arbitrary orientation of the applied field with respect to the crystalline axes. Obviously, in the presence of anisotropy equations (6) and (7) must be modified accordingly.

(v) In concrete problems the interaction between defects (which are not necessarily independent) and the rigidity of the vortex lattice render the computation of the resulting pinning force acting on this lattice extremely complicated.

To account for the long range structure and interactions of the vortex lattice, the notion of a Lorentz force (and the associated Eq. (6) must be replaced by a more general description based on the elastic constants of the vortex lattice [110, 126] (see also [19] page 233). For instance, the sharp peak sometimes exhibited by the $J(H)$ curve of conventional materials close to $H_{c2}$ [127] arises because the vortex lattice shear constant $C_{66}$ falls to zero quadratically as $H_{c2}$ is approached (see [19] p. 326) : the vanishing of $C_{66}$ allows each vortex to minimize its energy locally by locking with the local defects. When $C_{66}$ is very large the lattice is rigid and the pinning is very low as it is determined by the statistical pinning limit concerning the whole rigid lattice (see [110]). It turns out that using such a generalized formalism is even more

crucial in the case of HTSC because of their large anisotropic properties. The role of the tilt modulus $C_{44}$ is thought to be less important if the pinning defects are linear or very extended as in this case the vortex line does need to tilt in order to go onto the defect.

As will be reported elsewhere the central peak in the hysteresis cycle can be explained following the same arguments, namely the vanishing of the elastic constants as $H$ approaches $H_{c1}$.

There are also further physical phenomena such as dislocations and other defects in the vortex lattice which are thought to severely influence the effective pinning forces and time relaxation effects (see next section). Clearly, to account for these defects it is necessary to consider the long range vortex structure and the elasticity of the VLL which is beyond the ambition of the present paper (see however section 13 devoted to the very low field limit such that the Lorentz force is too small to overcome the pinning force).

3.3 CONCLUSION OF THIS SECTION. — In the above discussion we assumed that the superconducting material was homogeneous and isotropic. We have seen that even in this case the application of the usual critical state equations to the analysis of experimental results must be considered with caution especially for $H$ close to the critical fields $H_{c1}$ and $H_{c2}$. Naturally, the validity of the above equations is more restrictive in HTSC systems which are of interest here. For this reason, we wish to add the following remarks now.

(i) We shall see that in the limit where the demagnetizing field is negligible, the applied field parallel to a symmetry direction ($c$-axis or $a$-$b$ basal planes), $T$ and $H$ far below the irreversibility line (i.e. $T$ and $H$ sufficiently small) then both magnetic and transport critical currents (in single crystals and isolated grains) are correctly described by the critical state above at least in the case of $YBa_2Cu_3O_7$.

(ii) However, in so far as HTSC are concerned, it is important to keep in mind that for an arbitrary orientation of the applied field with respect to the symmetry directions the « scalar » critical state equations as written above (Eqs. (4, 6 and 7)) are not valid and must be extended to the case where the magnetic vectors **H**, **M** are not parallel. We believe that there is a need for more theoretical development in this case often encountered experimentally (see Sect. 14).

(iii) For the above reasons and because of demagnetizing effects Bean's formula (4) must be used with considerable caution except for a long cylinder with its axis parallel both to the $c$-axis and to **H**.

(iv) When the applied field is close to $H_{c1}$, it is not correct to replace **H** by **B** in the critical state equations and thus in the force balance equation (6).

(v) As we shall see later the critical state equations, including Bean's expression (4), do not apply for intergranular currents in polycrystalline materials.

(vi) We shall also introduce a characteristic length $R_0$ beyond which (i.e. for a sample of radius $R > R_0$) both the transport current ($J_{tr}$) and the magnetic current ($J_{mag}$, deduced from Bean's equation) are different from the local current density.

(vii) The above critical state picture is more or less severely modified by demagnetization effects, particularly for thin films (see Sect. 15).

(viii) The critical state picture breaks down totally at very low variable fields of amplitude $h_0 \ll h_{2,\,th}$, where $h_{2,\,th}$ is a threshold field calculated in section 13.

(ix) Concerning *ac*-measurements (susceptibility, resistivity, NMR, EPR etc.) the validity of the critical state depends also on the frequency of excitation (see Sect. 12.5 and 13).

(x) Because of relaxation effects the situation is even more complex at finite temperature, in particular close to the irreversibility or depinning line (thermal assisted flux flow (TAFF) and flux flow (FF) regimes). This is discussed in the next section.

**4. Flux creep theory.**

The critical state picture discussed just above predicts no relaxation effects in the magnetization (except time effects related to variations of the external applied field *via* Lentz law). To explain magnetic relaxation observed in conventional hard type II superconductors, Anderson proposed in 1962 [74] the so-called flux creep theory based on thermally activated flux motion. In this theory the rate at which « flux bundles » jump over the pinning barriers $U$ is given by an Arrhenius equation :

$$\nu = \nu_0 \, e^{-U(T, H, J)/kT} \tag{8a}$$

$$\nu_0 \approx \nu_p(T) + \nu_{vl}(T) \tag{8b}$$

$$\nu_{vl}(T) = c^2 \rho_n(T) \{B/B_{C2}\} \{1 - B/B_{C2}\} / \{16 \pi^2 \lambda^2(T = 0)\} \tag{8c}$$

or

$$\nu_{vl}(T) = 6 \times 10^{10}(s^{-1}) \{B/B_{C2}\} \{1 - B/B_{C2}\} \{\rho_n(\mu\Omega cm)^{-1}\} \{1\,000 \text{ Å}/\lambda(0)\}^2 \tag{8d}$$

Here $U(T, H, J)$ is an effective energy barrier which depends on $T$, $H$, the critical current density $J$ and the direction of the flux jump (forward or backward) with respect to that of the current density $J$ (we recall that the various pinning potentials that will be introduced in this section have already been defined and discussed briefly in § 2.5). Concerning equation (8b) we would like to emphasize that it is not rigorous and must be regarded with caution. Others combinations of $\nu_p$ and $\nu_{vl}$ such as $\nu_0 \approx [(\nu_p)^2 + (\nu_{vl})^2]^{-1/2}$ are possible. Our purpose here is to have some information on $\nu_0$ which is in general considered as a constant parameter in the literature. This is why we wish to discuss $\nu_p(T)$ and $\nu_{vl}(T)$ in more details below.

4.1 THE PHYSICAL ORIGIN OF THE ATTEMPT FREQUENCY $\nu_0$. — Apart from very few examples [110a, 121-124] $\nu_0$ is generally referred to in the literature on magnetic relaxation experiments as an attempt frequency the physical origin and the value of which are vaguely defined. Also the flux creep resistivity (see below) is proportional to this attempt frequency so that its vagueness often leads to confusion in the discussion of this important parameter. For this reason we believe that it deserves some comments. This frequency was first introduced by Anderson [128] as a phenomenological parameter, of order $10^6$ to $10^{13}$ Hz. It was noted by Anderson that the origin of $\nu_0$ was « readily not understood » (at this time). According to references [110, 126] it would be considered as a part of the more general problem of the Brownian motion of particles in a viscous medium treated first by Kramers [121] as early as 1940. Accordingly, $\nu_0$ would be given by equation (8c) in which $\rho_n$ is a normal state resistivity. It is not clear how to define this resistivity but we propose that $\rho_n$ can be obtained by extrapolating the normal state resistivity from $T > T_c$ (or $H > H_{c2}(T)$) to the temperature and the field of measurements. (This question is discussed in many details in Ref. [124]). It is interesting to note that this frequency is the same (within a numerical factor of about 4 $\pi$) as the one introduced by Fisher *et al.* [106] (in the limit $H_{c1} \ll H \ll H_{c2}$) when they investigated the problem of thermal fluctuations in disordered FLL. The calculation of the frequency term of (8b) as proposed by Brandt [110] for example assumes an ideal vortex lattice (or very weak pinning disorder), hence takes no account of strong pinning which probably prevails in such materials as YBaCuO. According to equation (8c), $\nu_0$ goes to zero as $B \to 0$. It seems that such a result is not physical for a disordered lattice. For this reason we added a phenomenological term $\nu_p$ in equation (8b) to account for the fact that isolated lines (limit $B \to 0$) would fluctuate within their own potential wells (see also Sect. 12 and 13 for other details). We believe that this pinning term should also somehow depend on $\rho_n$. Indeed the

localized eigenmodes of the pinning potential should be damped by the flux flow resistivity just as in the case of $\nu_{vl}$. The existence of $\nu_p$ can be justified qualitatively as follows : as noted by de Gennes and Matricon a long time ago [119] the presence of pinning disorder should lead to a gap in the energy spectrum of the VLL such that $\omega = \omega_0 + Dk^2$ for long wavelengths. Finally it is obvious that equations (8b, c, d) will be valid only in the limit of flux creep theory.

A possible second approach is that of Coffey and Clem [123] who calculated the frequency — dependent complex resistivity $\rho_v(\omega)$ associated with the local vortex motion in the elastic limit (see Sect. 13). They found that $\rho_v$ depends on the angular frequency $\omega$ *via* a dimensionless factor $\omega\tau$ in which $\tau$ is a characteristic time given by $(\eta/K_p)[I_0^2(\nu)/I_0(\upsilon)\, I_1(\upsilon)]$. Here $\upsilon = U_0/2\, kT$, $I_p(\nu)$ is a modified Bessel function of the first kind of order $p$, $\eta$ is the viscous drag coefficient and $K_p$ is the so called Labush parameter (defined as the average value of the second derivative $\langle d^2U/dr^2\rangle$ of the pinning potential through the specimen). $U_0$ is defined in [123] as the barrier height of the potential. We find that this formula can be rewritten (in SI units) approximately as $\tau \approx (B_{c2}\, r_p/\rho_n\, J)[I_0^2(\nu)/I_0(\upsilon)\, I_1(\upsilon)]$ where $r_p$ is the spatial range of the pinning potential ($\sim \xi$) while $\rho_n$ is a normal state resistivity defined in [124]. Another approach involving similar characteristic time scales has been carried out by Martinoli *et al.* [125].

4.2 THE VARIOUS POTENTIAL BARRIERS DEDUCED FROM MAGNETIC AND TRANSPORT MEASUREMENTS. — Flux creep theory was further extended by Anderson and Kim in 1963 [128] to include thermo-transport properties. They also showed that the pinning barrier $U(J)$ should be a decreasing function of $J$ and took a linear law (represented by the upper curve of Fig. 7) to account for this decay. Later, the relationship between $U$ and $J$ was discussed in more detail and greatly clarified by Beasley *et al.* [129]. This question was reexamined more recently by Xu *et al.* [130] in relation to HTSC oxides (in the flux creep limit).

It results from these investigations that the exact expression for $U(J)$ depends upon the spatial shape of the true energy barrier (i.e. upon $U$ *versus* $r$ function, see $U(J)$ curves of Fig. 7 and the associated insets). It is found that for sinusoidal $U(r)$ law [129] and for potential wells of various depths $U_p$ (with a large variety of assumed shapes and spacings [130]) the effective activation potential should approximately obey a relation of the form :

$$U(T, H, J) = U_p\left[1 - \frac{J(T, H)}{J_{max}(T, H)}\right]^n \qquad \frac{3}{2} \leqslant n \leqslant 2\,. \tag{9a}$$

We recall that $J_{max}$ is the maximum critical current density which could exist before flux creep takes place and which is not accessible except at $T \to 0$. Note that : (1) a more exact relationship between $U$ and $J$ is obtained by replacing in equation (9a) the ratio $J/J_{max}$ by the ratio $\nabla B/\nabla B_{max}$ of the gradients of $B$ and (2) it is assumed that the jump (or hopping) distance, $X$, of the flux bundle and the range, $r_p$, of the pinning potential are approximately equal (otherwise the ratio $J/J_{max}$ in Eq. (9a) must be replaced by the factor $(J/J_{max})(X/r_p)$). It turns out that this condition $X \approx r_p$ is realized either for a very dense system of pins or for a very dense VLL such that $B > 0.2 \times B_{c2}$ (for the sake of simplicity we neglect these effects here). It is to be recalled too that in the original paper of Anderson and Kim [128] as well as in the recent work of Hagen *et al.* [135, 136] on HSTC the exponent $n$ was taken tacitly equal to one (linear approximation). Then, using the above power law for the function $U$, Xu *et al.* [130] calculated the apparent pinning energy $U_0^*$ which enters the time dependent equation controlling $M_{ir}$. Their result is :

$$U_0^*(T, H, J) = nU_p \frac{J}{J_{max}}\left[1 - \frac{J}{J_{max}}\right]^{(n-1)} \tag{9b}$$

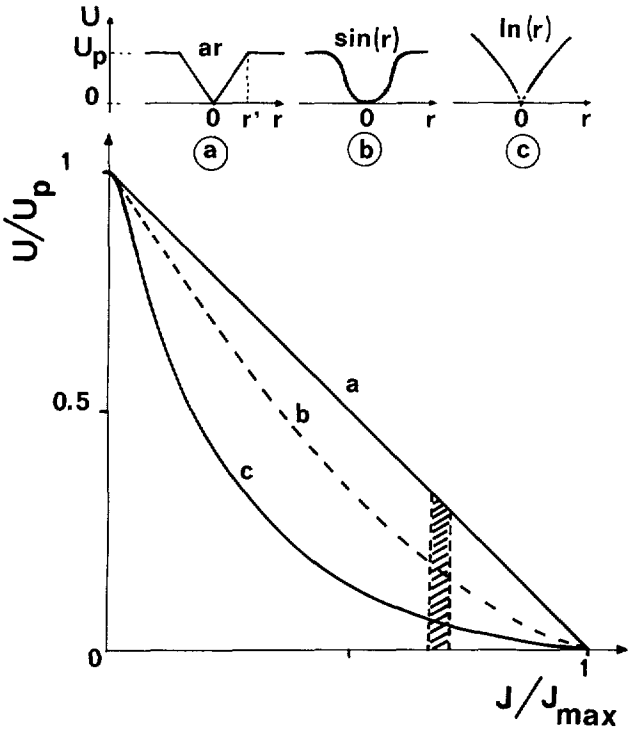


Fig. 7. — Variation with the critical current density $J$ of the effective energy barrier seen by the vortices and entering Arrhenius formula (8a) of the text. The relationship $U(J)$ depends on the spatial shape of the actual potential barrier $U(r)$. The upper curve (a) corresponds to the initial model of Anderson and Kim [128] in which $U(r)$ varies linearly with $r$ up to a certain threshold limit $r'$ and then becomes constant (inset a). The middle curve (b) corresponds qualitatively to the sinusoidal example first discussed by Beasley *et al.* [129] (inset b). The lower curve (c) is intended to represent HTSC oxides for which $U(r)$ seems to behave logarithmically at large $r$ [139-141] (inset c). The dashed portions are intended to represent the regions spanned during the duration of the experiment at given $T$.

It is to be emphasized that it is this apparent barrier (and neither $U(J)$ nor $U_p$) which is deduced from magnetic relaxation. In fact we can show that the apparent magnetic barrier is related to the derivative of $U(J)$ at $J$ by $U_0^* = (J/J_{max})(\partial U/\partial J]$ while that deduced from transport data is closer to $U(J)$ or $U_p$ depending on the analysis of these data (see Refs. [131-133] and subsection 5.5.3).

To calculate $U_p$ and relate it to the experimentally accessible quantity $U_0^*$ we can use the following procedure which is expected to be valid in the limit $T \ll T_c$ and in the approximation where the above power law for $U(J)$ is justified. Then, from measurements of $M_{ir}$ as a function of both time and $T$ we can determine both $U_0^*$ and $J$ as well as $J_{max}$ by the interpolation of the $J(T)$ curve to $T = 0$ (this is valid if $T \ll T_c$). In other terms we have :

$$U_p = \frac{J(0)}{J(T)} \frac{U_0^*(J)}{n[1 - J(T)/J(0)]^{n-1}}, \qquad (T \ll T_c, J_{max} \approx J(T = 0)) . \tag{10}$$

It turns out that equations (9-10) above are badely (i.e. not rigorously) obeyed even by conventional superconductors if one takes $n = 1$. The result is that in the linear ($n = 1$) approximation used originally by Anderson and Kim [128], the time decay of

$M_{ir}$ is given by :

$$M_{ir}(T, H, t) = M_{ir}(T, H, 0)\left[1 - \frac{kT}{U_p(T, H, J)} \ln (t/\tau_0)\right] \tag{11}$$

with ($U_p \gg kT$, $t \gg \tau_0$, $n = 1$).

Here $\tau_0$ is a relaxation time related to equations (8b), (8c) of order $10^{-6}$ to $10^{-12}$ s [128, 135, 136], but as we have just seen depends on many experimental conditions. This linear equation was also used more recently by Hagen and Griessen [137] to interpret the time decay of the magnetization of HTSC. Using Monte Carlo simulation and the same $U(J)$ linear law, Hagen and Griessen also showed that at extremely long elapsed times such that $M_{ir}(t)/M_{ir}(0) < 0.05$ the $t$-dependence of $M_{ir}(t)$ goes over from the above logarithmic behaviour to an exponential law (diffusion process). It is to be emphasized that equation (11) is only valid for $n = 1$. This important point will be discussed briefly at the end of § 4.3.

If the linear equation (11) is valid, then $M_{ir}(T)$ and the associated $J(T)$ should decrease linearly with $T$, in contradiction with the exponential decay observed experimentally for single crystals. To explain the temperature dependence of $M$, Hagen and Griessen [135, 136] assumed that there is a wide distribution of energy barriers ($U_p$) extending from $U_p = 0$ to $U_p \gg kT$. Under these conditions, at a given temperature the strength of the experimentally accessible magnetization and its decay with time are governed by the barriers such that $U_p \gg kT$ (i.e. lower barriers are irrelevant). As we will now show the exponential decay of $J(T)$ can also be explained in the framework of other plausible models for $U(r)$ without the need for a wide distribution in $U_p$ (even though some distribution in $U_p$ is physically unavoidable). Also, the collective pinning theory predicts an exponential $J(T)$ relationship. Finally, there is no doubt that the pinning potential intervening in Anderson's equation is already a mean quantity averaged over the whole volume of the vortex bundle. Clearly this will contain a large number of individual pinning sites except perhaps in the case of extended defects as those considered in reference [139]. Finally, it is to be added that model calculations of the magnetic relaxation $(dM_{ir}/d \ln t)\, M_{ir}^{-1}$ in the presence of both narrow and broad distributions of the pinning potentials, assumed to have a general shape of the form given by equation (9a), can be found in references [137, 142, 143].

Turning back to the $U(T, H, J)$ relationship, it is now worthy to note that in the flux creep regime the critical current density is derived from the implicit equation :

$$U(T, H, J) = kT \ln \left(\frac{\nu_0 BX}{E}\right) \tag{11b}$$

where $E$ is the electric field within the material just at the moment of measurement. We feel that $E$ is generally constant ($\sim 10^{-5}$ to $10^{-6}$ V/cm) in transport measurements. However, in static magnetic experiments, $E$ can be determined from Maxwell equation (curl (**E**) $= -\partial B/\partial t$) and Bean's equation (4) and flux creep equation (11). At intermediate time scale $t$, it is probably of the form :

$$E \approx R \frac{\partial B}{\partial t} \approx \alpha R \frac{\partial M_{ir}}{\partial t} \approx \alpha R^2 \frac{kT}{U_0^*} \frac{J(T, H)}{t} \tag{11c}$$

Taking the following realistic values : $\nu_0 \approx 10^{10}$ Hz, $B = 1$ Tesla, $X = 1$ nm and $E = 10^{-9}$ to $10^{-12}$ V/m we find $\ln (\nu_0 BX/E) \approx 20$ to 30. Note that in the case where $U$ is given by equation (9a) one has :

$$J = J_{max}\left[1 - \frac{1}{n}\left(\frac{kT}{U_p}\right)^{1/n} \ln \left(\frac{\nu_0 BX}{E}\right)\right]. \tag{11d}$$

Finally, it is to be added that if $H$ varies with time (as during hysteresis cycle registrations or in ac-susceptibility experiments), $E$ will also include an externally induced large term proportional to $-R\,dH/dt$. Note that at short times $t$ must be replaced by $t + \tau$ in equation (11c), where $\tau$ is defined below.

4.3 THE LINK BETWEEN THE APPARENT PINNING BARRIER, THE REAL BARRIER AND $M_{ir}(T)$. — Turning back to the case where $M_{ir}(T)$ is controlled by a very narrow distribution of potential barriers, we note that in the above equation $U_p$ is the real energy barrier (seen by isolated vortices), $J$ the critical current density at the time $t$ of the measurement whereas $M_{ir}(T, H, 0)$ is the irreversible magnetization corresponding to $J_{max}$ or equivalently to the most critical state which would be realized before flux creep has had time to occur (i.e. for $t < \tau_0$). Of course, such an $M_{ir}(T, H, 0)$ is not accessible in real experiments (except eventually by interpolating the experimental results to the limit $T = 0$). Moreover, as far as HTSC are concerned equation (11) is generally not valid (in its above form) and has led to many erronous conclusions concerning the amplitude of the potential barriers. This is due to the fact that both the experimental magnetization $M_{ir}(T, H, t)$ and the apparent energy barrier ($U_0^*$) are as a rule very different (several orders of magnitude are usual) from those assumed in the right hand side of equation (11). Therefore, it is essential to emphasize once again that the above equation is only valid in the very restrictive approximation where $U$ varies linearly with $J$ (i.e. $n = 1$ in Eq. (9a)). Since $U_0^*$ is related to the slope of $U(J)$ it is clear from figure 7 (dashed region) taht this slope can differ considerably owing to the real $U(r)$ law.

We propose that the variation with time of the irreversible magnetization can be written in the more general form (but restricted to the flux creep regime) :

$$M_{ir}(T, H, t) = M_{ir}(T, H, t_0)\,\frac{1 - \dfrac{kT}{U_0^*}\ln\dfrac{\tau + t - t_0}{\tau_0}}{1 - \dfrac{kT}{U_0^*}\ln\left(\dfrac{\tau}{\tau_0}\right)} \tag{12a}$$

with :

$$U_0^*(T, H, J) = U_0^* \gg kT \ln\left(\frac{\tau + t - t_0}{\tau_0}\right), \qquad (t > t_0) \tag{12b}$$

$$\tau \approx \frac{H_{p,\,max}(T) - H_p(T)}{dH/dt} \qquad \text{(to be justifed in § 4.7)}. \tag{12c}$$

The reference time $t_0$ refers to the starting of the first measurement. This initial time depends on the experimental conditions but can be taken equal to zero provided that we remember that $M_{ir}(H, T, 0)$ is in this case the value of the measured irreversible magnetization at the beginning of the experiment (assuming condition (12b) true), whereas in equation (11) it corresponds to the value of $M_{ir}$ at $J = J_{max}$ (a situation never realized in practice). In addition, we have introduced a correlation time $\tau$ which is found experimentally to depend on the field $H_p(T, R)$ of full penetration and which is inversly proportional to the sweep rate $dH/dt$ of the applied field. Qualitative arguments that will be developed later in subsection (4.6) show that $\tau$ should also depend on the penetration field $H_{p,\,max}(T, R)$ corresponding to the most critical state which would exist at $J = J_{max}(T)$ before flux creep has had time to begin. Note that $\tau$ is expected to vary both with $T$ and $R$ through the penetration fields. We find that in usual experimental conditions with vibrating sample magnetometers $\tau$ is generally of the order of 10 to 100 s and one to two orders of magnitudes longer for SQUID magnetometers. This leads to a departure from the logarithmic law at short time scales (often erronously

ascribed in the literature to « some fundamental effects »). However we emphasize that the exact dependence of $\tau$ on $H_p$, $H_{p,max}$ and $dH/dt$ certainly needs more investigations. For instance, in the simple model of Bean, the penetration field is proportionnal to the product of the critical current density times the radius $R$ of the specimen. Then using equation (11) gives :

$$\tau = \left[ RJ_{max}(kT/U_p)^{1/n} \ln\left( \frac{\nu_0 BX}{E} \right) \right] / (12\, n\pi\, dH/dt) .$$

Naturally, when in relaxation experiments one has $t/\tau \gg 1$ together with inequality (12b) we can rewrite equation (12a) in the following form commonly encountered in the literature :

$$\frac{1}{M_{ir}(T, H, t_0)} \frac{dM_{ir}(T, H, t)}{d \ln t} = - \frac{kT}{U_0^*(T, H, J)} , \qquad t_0 \gg \tau_0 \tag{13a}$$

$$U_0^*(T, H, J) = J(dU/dJ) . \tag{13b}$$

We wish now to emphasize some important points.

(1) At first, it is to be recalled that the potential barrier $U_0^*$ in equation (13) depends on $T$, $H$ as well as on the critical current density $J = J(T, H, t_0)$. In addition, $J$ is assumed to be given by the Bean equation (4) which is only valid in the limit where $J$ is spatially homogeneous (i.e. does not depend explicitly on $r$ as in granular or in multiphased materials). $J$ is also assumed to be approximately independent of $H$. It is clear from equation (13) above and from figure 8 (comparing $U_p$ and $U_0^*$) that $U_0^*$ is related to the real $U(J)$ as well as to the potential well height $U_p$. However, it is also clear from this figure that under no physically realizable conditions is $U_0^*$ equal to $U$ or to $U_p$.

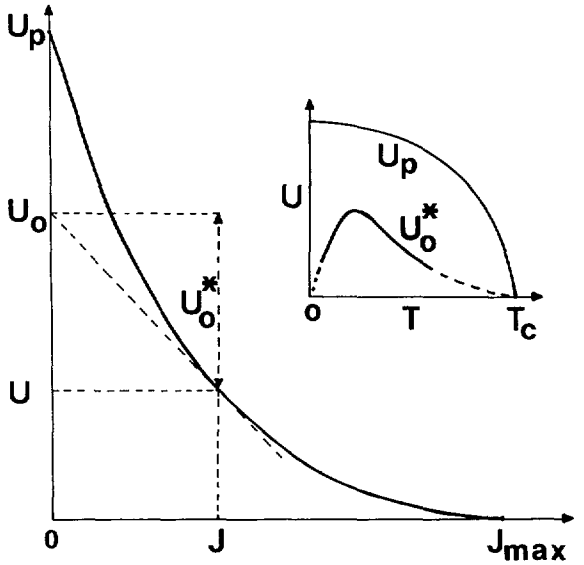


Fig. 8. — Definition of the various pinning energies intervening in the flux creep theory (see text). The inset is a schematic representation of the temperature dependence of the apparent pinning potential $U_0^*$ as deduced from magnetic relaxation experiments and the height $U_p$ of the expected real potential in the absence of any current $J$.

(2) It is important to remember that this equation is not an exact solution (except for $n = 1$) and corresponds to the linearization of the flux creep equation around the point $(U, J)$. This implies that it might happen that equation (13) is not obeyed over a wide range of $t$.

(3) Often in the literature on HTSC equation (13a) is written in the form $(1/M)$ $(dM/d \ln t) = -kT/U = S$ with the factor $1/M$ referring sometimes to the total magnetization (including $M_{eq}$) and sometimes to the measured irreversible magnetizations $M_{ir}(t)$, $M_{ir}(t_0)$ or $M_{ir}(0)$. To avoid such confusions we intentionally expressed the parameters $M$, $J$ and $U$ entering equation (13) in a more explicit way, insisting on the fact that $M$ is the value of $M_{ir}$ at the beginning of the measurement (in the limit of Eq. (12b). Therefore, it is the experimentalist who chooses the time origin according to his experimental conditions.

(4) However, from the experimental point of view it is not always clear how to define the time origin because of transient effects particularly when these transient times are comparable or higher than the correlation time $\tau$ given by equation (12c). Such transient effects can have many different origins among which the eddy currents (flux flow) induced by the variation of the external field, the time constant of the measuring set up including that of the magnet producing the external field and the difficulty to avoid small instabilities (small oscillations during a short time) of the applied field just after stopping the variation of this field. The last difficulty is due to the fact that these oscillations lead to an inhomogenous distribution of the currents (i.e. positive and negative currents, a small reversal branch) near the surface of the sample thus influencing the apparent time decay. In terms of the hysteresis cycle of figure 3 these oscillations imply that the sample is in the reversal branch (for example just below point A of such a branch, Fig. 3), through generally not far from the desired unperturbed value. A last undesirable and more general effect is the fact that the electric field, $E_{ind}$, induced by the variable field, $H(t)$ leads to local dissipation and thus heating. Therefore, if the effective thermal conductivity of the superconducting material plus the surrounding exchange fluid is high this can lead to some extra heating of the sample during the field sweeping time. Such an effect should also depend on the specific heat as well as the effective size of the specimen. This point is discussed further below. All these effects are neglected in this paper except eddy currents which will be reconsidered briefly below in subsection 5.5 (devoted to thermal assisted flux flow (TAFF) effects) and later in relation with frequency effects in a.c.-susceptibility measurements, section 12.

(5) Close to the irreversibility line (or depinning line), in particular close to $T_c$, the effective pinning forces and the associated $U_0^*$ are vanishingly small. This implies that the condition $U_0^* \gg kT$ on validity of equations (12) and (13) is no longer satisfied. In fact we have seen that in this limit the logarithmic relaxation is replaced by an exponential decay law. In addition, within this limit flux flow effects become important as will be discussed in relation with a.c.-susceptibility data in section 12.

(6) We have already mentioned that the variation of the pinning potential $U$ with $J$ (Beasley curve), $T$ and $r$ are not independent. In particular, it was shown very recently independently by Manuel *et al.* [139] (from magnetic data at $T \ll T_c$) and by Zeldov *et al.* [140, 141] (from resistivity measurements near $T_c$), that the spatial variation of the pinning potential $U(r)$ would follow a logarithmic behaviour at large distance $r$. As a consequence, we expect that in HTSC oxides the apparent potential $U_0^*$ associated with this logarithmic behaviour would be much smaller than the height $U_p$ of the same potential. This is illustrated schematically in figure 7 which shows $U(J)$ curve in the linear approximation of Anderson and Kim [128] together with the more realistic approximation of Beasley *et al.* [129] for conventional materials and the expected behaviour for HTSC materials [139].

(7) Recent experiments on HTSC [144, 145] showed that magnetic relaxation persists down to $T$ very close to 0 K (from the extrapolation of the data to $T = 0$) suggesting the existence of vortex depinning *via* quantum tunneling. This quantum tunneling has been investigated recently in two theoretical papers by Blatter *et al.* [146] and by Fisher *et al.* [147] and seems to exist in conventional superconductors as well (see Ref. [3-5] in [146]). This fascinating effect

is at present the object of intense experimental investigations, in the temperature domain down to $10^{-2}$ K.

(8) Turning back to equation (10), it is interesting to see that at very low temperature the experimental critical current of HTSC is expected to be linear in $T$ ($J \approx J(0) \exp(-T/T_0) \approx J(0)\{1 - T/T_0\}$). Then, as $U_p$ reaches its highest value at $T = 0$ it is easily seen from equation (10) that as $T$ approaches zero the apparent pinning energy $U_0^*$ should vary as $T^{n-1}$ and hence should go to zero if $n > 1$. Putting this value into equation (13), it is easily seen that $[dM/d \ln (t)]/M$ goes to zero as $T^{2-n}$ Since from equation (8) we have $n > 1$, we see that the temperature derivative of this expression diverges as $T$ tends to zero. In other terms, if $n$ is close to 2 this factor will not extrapolate to zero with $T$ suggesting that flux creep might persist down to the lowest temperature of measurement ($T \approx 0$).

On the other hand, from the experimental point of view it is possible that due to the very low thermal conductivity $K$ of HTSC, especially at $T \ll T_c$, it is likely that flux creep will result in a continuous drift of the effective temperature felt by the vortices. In other words, at very low $T$ the establishment of thermal equilibrium can be very slow due to heat dissipation accompanying each flux creep event. The clarification of this point requires the simultaneous resolution of the equations of thermal and flux diffusions.

It is usually assumed that there are no thermal instabilities during the experiment so that the function $U(J)$ (Eq. (9)) does not depend directly on time. This hypopthesis is not always easy to satisfy at very low temperatures, particularly for large single crystals with large $J$. When this condition is fulfilled the pinning barrier depends on $t$ only *via* $J$ and we can write $U(J) = U(J(t))$. Then at a given fixed temperature $T \neq 0$, the point $U(J_{max})$ of Beasley curve (i.e. the intersection of this curve with the $J$ axis, Fig. 7) would correspond to the initial instant of establishement of the hyper-critical state ($J(t \ll \tau_0) \approx J_{max}$) whereas $U(J = 0) = U_p$ would correspond to $t$ equal infinity ($J(t \to \infty) = 0$). Of course, the time scale involved in real experiments is finite so that the measured $J$ is comprised between these two extreme limits as illustrated by the dashed sections of the curves in figure 7 : this dashed region represents in fact the portions of the curves described during the duration of the experiment. It is clear from this figure that except for the linear model of Kim-Anderson the apparent effective pinning potential $U_0^*$, which is proportional to $dU(J)/dJ$, should increase with time since $J$ decreases with time. It can be shown that in this case the linear logarithmic relaxation of $M$ and $J$ is not strictly obeyed. It can also be shown that in a first approximation the term $(kT/U_p) \ln (t)$ entering equation (11) must be replaced by $[(kT/U_p) \ln (t)]^{1/n}$ where $n$ is the exponent of (Eq. (9a)). Such a possible deviation from the linear logarithmic relaxation is easier to detect at very long experimental time and close to the irreversibility line where the relaxation is expected to be more rapid. Relaxation effects are an important topic which needs more discussion and more clarification but this is beyond the scope of this paper.

Defined schematically in figure 8 are the various pinning energies intervening in the flux creep theory. Sketched in the insert of this figure is the temperature variation of both the apparent energy potential $U_0^*$ intervening in magnetic relaxation measurements and the height $U_p$ of the real pinning barrier. It is clear that $U_0^*$ is generally much lower than the actual energy $U_p$. In the classical model of Anderson, the variation of the real $U_p$ with $T$ is principally *via* the physical parameters $\lambda(T)$ and $\xi(T)$ and thus would be significant only close to $T_c$ as these quantities diverge at $T_c$. Therefore, neglecting other possible causes of variation of $U$ with $T$ (other less direct causes are the volume of the flux bundle and its jump distance), we expect that $U(J)$ would be practically independent of $T$ for $T \ll T_c$.

It is equally clear from the above discussion that only a very narrow portion of the $U(J)$ curve is spanned in real experiments at fixed $T$ and $H$. The question is then how to

determine this curve experimentally and extract the real pinning potential $U_p$ . it turns out [148-150] that this is partially possible if one accepts that the $U(J)$ is to a first approximation independent of temperature. In this case, increasing $T$ from zero to $T_c$ amounts to moving the interval of measurement in figure 8 from point $U(J_{max})$ towards the point $U(J = 0)$. Of course, the reality is probably more complicated especially at high temperature since $U_p$ goes to zero at $T = T_c$. This scaling procedure would be valid for $T \leqslant T_c/2$. In fact, it is known that resistivity measurements as a function of $T$ can give $U_p$ by interpolation of $\rho$ to low temperatures $T \ll T_c$ (see Sect. 5.5.2).

4.4 TYPICAL EXPERIMENTAL RESULTS IN HTSC. — Figure 9a shows a typical example of hysteresis cycle (*M versus H*, upper figure) together with two relaxation curves (*M versus t*) registred at points A of the cycle. This corresponds to the longitudinal magnetization of granular $YBa_2Cu_3O_7$ measured by means of a vibrating sample magnetometer. Illustrated in figure 9b is the relaxation of the transverse magnetization (in a semilog scale) of a single crystal of $YBa_2Cu_3O_7$ as deduced from torque measurements [153]. The comparison with conventional materials [152] shows that the relaxation is considerably faster here though the logarithmic law is exhibited in both cases. It is found that the logarithmic relaxation is followed in most experimental conditions except very close to the irreversibility-line, a situation encountered in Bi oxides but rarely in $YBa_2Cu_3O_7$ compounds (see § 5.5 and [165, 166] for more details). It is found that the logarithmic relaxation rate $M_{ir}^{-1}$ ($dM_{ir}/d \ln (t)$) varies notably with temperature in a way which depends considerably on $H$ and on the

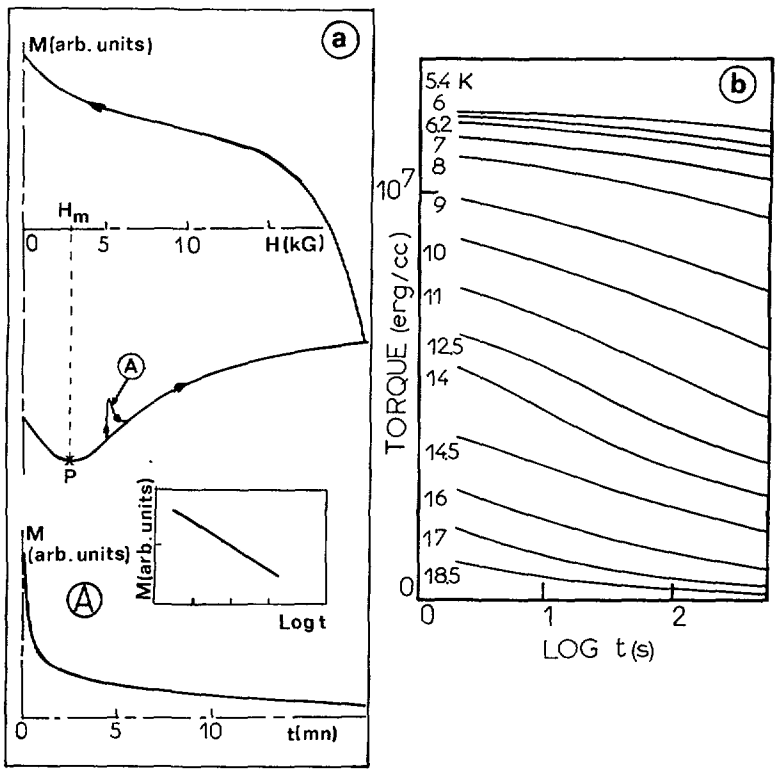


Fig. 9. — a) Hysteresis cycle (upper) together with magnetization *versus* time (lower) at point A of the cycle [155]. b) Torque relaxation in a single crystal of BiSnCaCuO (after Fruchter [153]).

dimensions of the sample under consideration. This is illustrated in figure 10 taken from reference [154].

As already mentioned, in some conventional superconductors [152] the relaxation rate of $M_{ir}$ is generally quite slow and more conveniently (but not rigorously) described by the linearized Anderson's theory (for $U(J)$) in usual experimental time scales ($t$ ranges from a few seconds to several hours). From figure 10 it is seen that the situation is very dramatic in high $T_c$ oxides (more especially in Bi families not shown here) where :

(1) Large and fast relaxations are observed [26-34].

(2) The apparent pinning barrier $U_0^*$ (related to the relaxation rate of figure 10 by

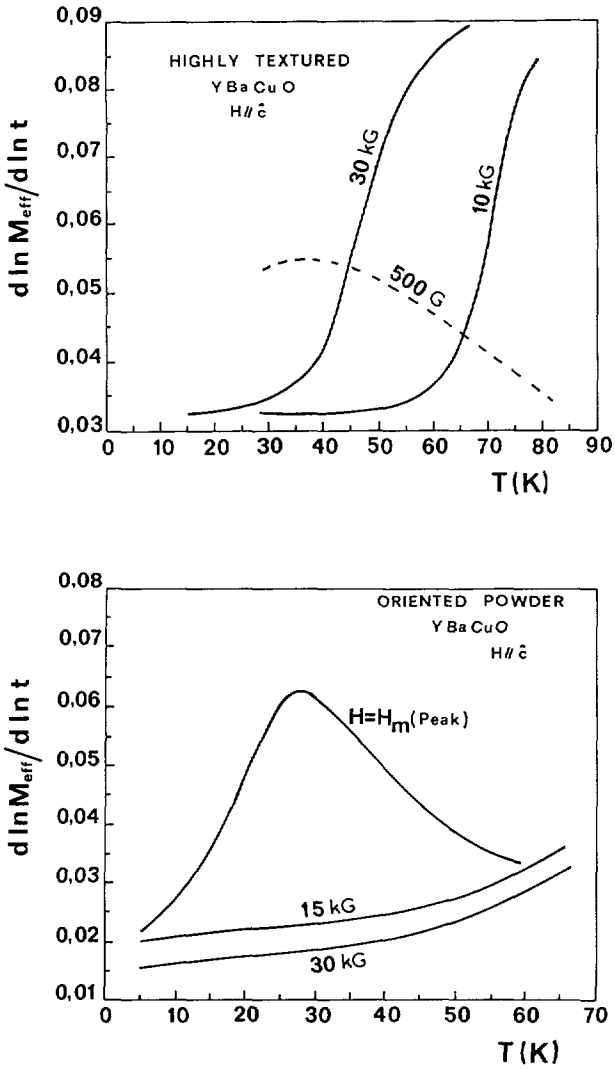


Fig. 10. — Temperature dependence of the logarithmic relaxation rate $S = \partial \ln M/\partial \ln t$ for various $YBa_2Cu_3O_7$ samples. Note the anomalous behaviour both at $H = 500$ oe and at the low-$H$ peak of the hysteresis cycle (the peak is indicated by point P in Fig. 9). Recall that the field $H_m$ of the peak varies with $T$ (after Ref. [154]) and that $S$ is related to the effective pinning potential by $U_0^* = kT/S$.

$U_0^* = kT\,(\mathrm{d}\ln M_{\mathrm{eff}}/\mathrm{d}\ln t)^{-1}$) is very low (compared to what is seen in some conventional materials such that NbTi) at low temperature and passes by a maximum with increasing $T$ [130, 116] and then tends to zero at $T_c$. In addition, this $T$-behaviour is very different from one HTSC family to another [153-161]. It is to be recalled that according to the preceding discussion the large difference in the apparent energy barriers does not necessarily imply that the amplitudes $U_p$ of the real barriers are so different.

(3) The critical current density $J$ which is proportional to $M_{ir}$ falls off sharply (approximately exponential in $T$) in many cases [20-25].

(4) The low $U_0^*$ value is not a unique specific feature of HTSC since Chevrel phases exhibit even smaller $U_0^*$ (~ 15 mV [152]).

(5) At high temperature, in particular near the irreversibility line, $J$ also drops dramatically with $H$ [20, 35-41]. Here too the behaviour is very different from one HTSC family to another. For instance, in Bi based oxides $J$ is often virtually zero in $B = 1$ Tesla at $T \geqslant T_c/2$. This is to be compared with the case of conventional superconductors [162-164] for which $J$ stays notably large at high fields and temperatures and vanishes only near $H_{c2}$. This means that in classical systems the irreversibility line coincides virtually with $H_{c2}$. This is illustrated schematically in figure 11 which compares the field dependence of $U_0^*$ of classical (upper curve) and HTSC (lower curve) at $T$ far from the irreversibility line. Because of the uncertainties on $U_0^*$ due to both the constraints of measurements and to temperature (when $U_0^*$ becomes comparable to $kT$), it is difficult to decide (from the experimental data) whether $U_0^*$ extrapolates to zero at some irreversibility field $H_{irr} (< H_{c2})$ or goes to zero only at $H_{c2}$.

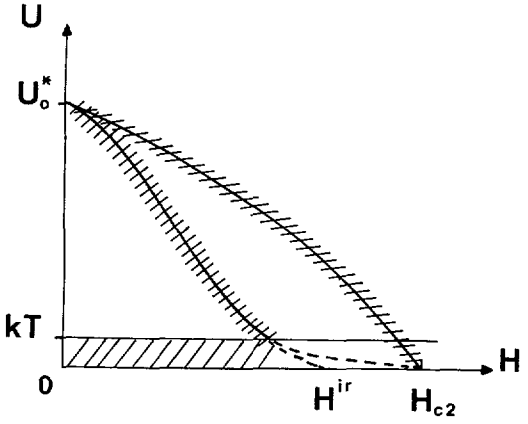


Fig. 11. — Schematic illustration of the variation of $U_0^*$ with the applied field for $T$ close to the irreversibility line. Upper and lower curves would correspond to classical and high $T_c$ superconductors respectively.

4.5 THEORETICAL PREDICTIONS OF THE FLUX CREEP MODEL. — Shown in figure 12 are the results of Monte Carlo calculations of Hagen and Griessen [135, 136] in the conditions explained previously. Apart from the choice $n = 1$ in equation (8) (linear approximation) this calculation is valid with no restriction on the ratio $kT/U_p$ and whatever the time scale. However, when comparing with experimental data it is important to remember that other time effects such as eddy currents can become preponderant near the irreversibility line and must be accounted for more properly (see TAFF paragraph 5.5 in the next section and

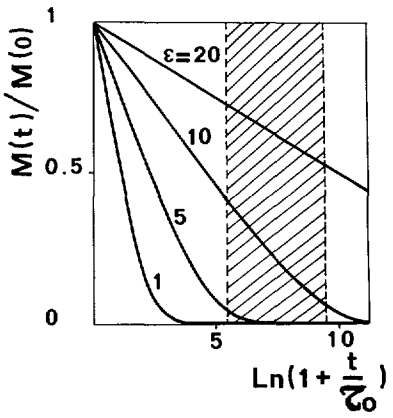


Fig. 12. — Calculated magnetization *versus* $\ln(1 + t/\tau_0)$ with $\tau_0$ is a reference time [135]. The right hand side of the dashed region would correspond to time scales where time effects are accessible in magnetic relaxation experiments. The left hand portion of the same dashed region would be closer to the time scales of transport measurements $\varepsilon = U(T)/kT$.

section 12 on a.c.-susceptibility). Also, the analysis of the short time scale data is extremely difficule as it depends critically on the experimental conditions (see paragraph 4.7 for instance). At this point it is interesting to emphasize that long-term non logarithmic relaxation is observed experimentally in Y-Ba-Cu-O single crystals [165, 166]. Note that the time scale used in the calculated curves of figure 12 is somewhat arbitrary because of the fact that the characteristic relaxation times $\tau_0$ is unknown ($10^{-6}$ to $10^{-12}$ s), $\tau_0$ is related to $\nu_0$ of equation (8b).

4.6 FIELD AND PINNING ENERGY PROFILES WITHIN THE SAMPLE. — It is now interesting to discuss briefly the evolution of the field gradient and the energy barriers inside the material as a function of time and the magnetothermal history of that material. In the insert of figure 2 (Sect. 2) we showed the field profile within the sample as predicted by the critical state model. In this example the field gradient and the corresponding irreversible magnetization were assumed to be independent of time (or equivalently the temperature was assumed to be zero). However, we have just seen that because of flux creep this is never realized in practice even for $T/T_c$ as low as $5 \times 10^{-4}$ [144] in HTSC. The same problem happens with some other families of superconductors [167, 168].

According to the flux creep model, the evolution of the distribution of flux and currents within the specimen with time can be represented schematically in the various but equivalent ways sketched below.

Figure 13 corresponds to a sample in the field cooled state (i.e. the sample was cooled in a certain field $H_{cool}$ down to the measuring temperature, fc-state) : figure 13a presents the energy barriers experienced by the vortices in this fc-state, far from the surface of the specimen. The field profile associated with this same state is depicted in figure 13b. In this case $J$ is close to zero and the effective $U$ is large. In term of $U(J)$ curves (Figs. 7 and 8) this means that we are describing the top regions of these curves. The time variation of the fc-magnetization ($M_{ir,\,fc}$) [169] probably arises from currents at and near the surface of the sample and should be negligible in large single crystals. The physical origin of this effect can be understood as follows : Because the field cooled magnetic induction $B_{fc}$ is related to the magnetization by $B_{fc}(T) = H_c + 4\,\pi M_{fc}(H_c, T)$, it is expected to decrease with $T$ as $H_c + 4\,\pi M_{eq}(H_c, T)$ in the reversible region of the $T$-$H$ plane (i.e. down to the irreversibility

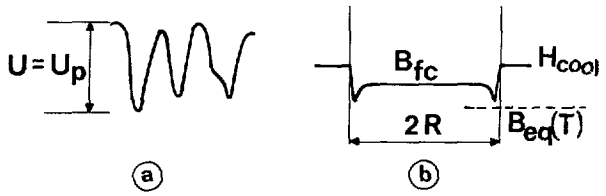


Fig. 13. — a) Energy barriers in the field cooled (fc) state far from the surface of the specimen. b) Field profile in the same fc-state. The local vortex density is constant far from the edges. This situation would correspond to the top ($J \approx 0$) of Beasley curves of figure 7. The discontinuity of field at the surface is due to London-Abrikosov's shielding currents.

line temperature $T_{ir}(H_c)$. It then becomes constant, at least if this line is traversed very fastly (quenched vortex state). This means that for any temperature $T < T_{ir}(H_c)$ one has $B_{fc}(T) \approx B_{eq}(H_c, T_{ir}(H_c))$. The relaxation of $B_{fc}(T)$ is then due to the fact that one has $B_{fc}(T) \approx B_{eq}(H_c, T_{ir}(H_c)) > B_{eq}(H_c, T)$. This also means that there are more vortex lines in the sample than needed for thermodynamic equilibrium at the measurement temperature $T$. Since the vortices (in excess) lying near the surface will be the first to leave the sample, this results in a field profile of the form sketched in figure 13b. The exact interpretation of time effects is certainly more complex in the fc-state.

Figure 14a, b provides schematic representations of the energy barriers (a) and the field profile (b) in the extreme case where the sample is assumed to be in the most critical state (hypercritical). Formally speaking, this means that the sample has been cooled in zero field (zfc-state) and then submitted instantaneously (i.e. in a time $t < 1/\nu_0$) to an external field high enough to build up the full critical state everywhere in the specimen. This implies that the critical current density has its largest possible value $J_{max}$ at the specified $H$ and $T$, whereas the effective pinning barrier is zero. Of course, in real experiments this critical state is never reached, even at temperature as low as 50 mK in the case of $YBa_2Cu_3O_7$ [145]. In many ordinary experimental conditions the shortest reasonable time is of the order of 1 s. This time is generally notably larger in SQUID measurements (5 to 10 mn).

The curves in figure 14c, d have the same meanings as those in figure 14a, b but correspond to a more realistic experimental time scale. In this example the critical current and the

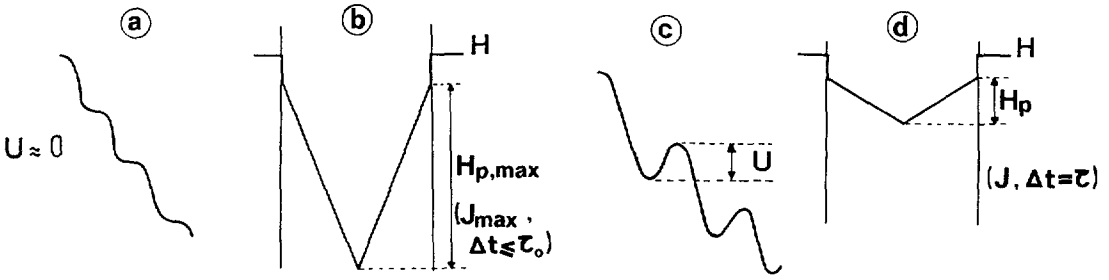


Fig. 14. — a) Schematic plot of the energy barriers in the most critical state. b) Field profile in the same critical state. The gradient of the vortex density has the highest possible value obtained before flux lines begin to jump across the energy barriers ($\Delta t < 1/\nu_0 \approx \tau_0$, a purely theoretical assumption used in the flux creep model, see text). This defines the current density $J_{max}$ used in the previous figures. (c, d) The curves have the same meaning as in (a and b) but correspond here to a more realistic time scale of the order of the experimental or observation time $\tau$ (see text).

associated magnetization have decreased by about two orders of magnitudes relatively to their full critical values represented formally in figure 14b. This is approximately the real case for $YBa_2Cu_3O_7$ in a few Tesla at about 70 K. The difference between the two quantities is even more dramatic at present in the case of Bi-based oxides where $J$ is virtually zero for the same $T$ and $H$. Clearly, in this limit it seems unphysical to represent these very different values of $J$ by the same equation as it is done in equation (11).

4.7 THE CORRELATION TIME $\tau$ INTERVENING IN THE FLUX CREEP EQUATION. — We can now use the results of figure 14 above to estimate qualitatively the correlation time $\tau$ intervening in equations (12a, c), as illustrated in figure 15 (recall that $H_p$ and $H_{p,\,max}$ in this figure have been defined previously as the complete penetration fields corresponding to the experimental and the maximum critical current densities $J$ and $J_{max}$ respectively). Let us imagine the following experimental process : (1) First we assume that at some time $t$ the « experimental » field profile is represented by the heavy line labelled $t$ and corresponding to an applied field $H(t)$ and to the « experimental » critical current density $J$. (2) The field is then suddenly increased (in a time less than $\tau_0$) from the value $H(t)$ to $H(t) + (H_{p,\,max} - H_p)$. Since the increase $(H_{p,\,max} - H_p)$ in $H(t)$ was faster than the time needed for the flux to start creeping, the corresponding field profile $dH/dr$ would correspond to the current $J_{max}$ and would be like the dashed curves labelled $t + \tau_0$. (3) To get the new « experimental » flux profile (corresponding again to $J$) we must wait a time equal to the correlation time $\tau$ we are searching for. Consequently, the latter is defined by the equality $H_{p,\,max} - H_p = H(t + \tau_0 + \tau) - H(t) \approx (dH/dt)\,\tau$, assuming that in a first approximation $H$ varies linearly with $t$. We stress again that the above considerations are only qualitative and must be considered as a first step approach to this complicated problem. Recall also (point 4 of paragraph 4.3) that the interpretation of magnetic relaxation experiments can present other experimental difficulties at short time scale.

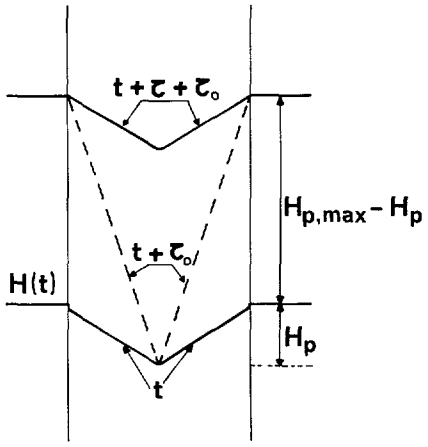


Fig. 15. — At the time $t$ and field $H(t)$ the field profile is represented by the curve « $t$ ». If the field is then increased instantaneously (in a time shorter than or equal to $\tau_0$) from this $H(t)$ value to $(H(t) + H_{p,\,max} - H_p)$ the resulting field gradient is the highest possible as schematized by the dashed curves labelled $t + \tau_0$ and by figure 14b. However because this is a highly metastable state and because the ensuing flux creep, the field gradient will tend to the experimental profile after a correlation time of the order of $\tau_0 + \tau$.

4.8 CONCLUDING REMARKS OF THIS SECTION. — In summary, the first problem faced by many experimentalists when analyzing relaxation experiments is the fact that flux creep theory includes many unknown parameters.

First of all, we do not measure the actual energy height $U_p$ but an apparent term $U_0^*$ which depends on $T$ and the value of $J$ at the instant of measurement (with $J$ in turn depending on $T$, $H$ and $t$).

Secondly, the theoretical model includes at least two other experimentally inaccessible quantities $J_{max} = J(T, H, t = 0)$ and $\tau_0$.

Thirdly, the measured magnetization, $M_{tot}$, depends on the shape of the sample (especially its diameter) and includes the equilibrium magnetization ($M_{eq}$) which is not always easy to obtain. In addition, the simplest Anderson's equation (11) is in principle only valid in the limit of a single energy barrier $U(r)$ with a very special spatial shape (short range interaction).

Fourthly, we have seen that other $U(r)$ laws give very different $J(T, H, t)$ functions [139, 140]. In clear, the spatial shape of the pinning potential has a fundamental bearing on the apparent potential.

Finally, in the above discussion we ignored the structure of the vortex bundle involved in flux jumps and the associated physical parameters (correlation volume $V_c$, jump distance $X$, . .) which probably vary with temperature, field and perhaps time (thermal instabilities). We also firmly believe that at very low temperature internal heating effects connected with the very low thermal conductivity $K$ (and diffusivity) of HTSC should play a significant role in relaxation experiments, especially for large samples. We also believe that such heating effects are generally quite important in pulsed field hysteresis cycle measurements. These effects are generally not accounted for in the literature and could explain some anomalous $T$ and $H$ behaviours of $J$, in pulsed field experiments. Also, we believe that heating is generally at the origin of the very asymmetrical hysteresis cycles deduced from these experiments.

It turns out that the combination of all these effects make the apparent $U_0^*$ of HTSC much lower than the real $U_p$ (at low $H$) so that the latter is probably in the range of 1 to 2 eV as deduced from some resistivity data [170, 171]. It is to be added that for better understanding of the data it is recommended to analyze temperature and time effects simultaneously when possible.

A more general question concerns the correct treatment of collective thermal fluctuations in the vortex lattice and the validity of the classical flux creep model outlined above, in particular near the irreversibility line. Concerning this point, it is possible that other more sophisticated models [172-174] incorporating characteristic effects of HTSC (such as the anisotropy, the high temperatures involved, ...) would be more appropriate for some of these materials. For instance, according to a recent paper by Markiewicz [176], thermal fluctuations and thermal depinnings could also be incorporated in the melting theory to generalize the flux creep model and investigate the important question concerning the meaning of the irreversibility line (see also Brandt [110]).

Finally it is clear that as long as we are not able to control the nature, the distribution and other features of the defects responsable for vortex pinning it is difficult to propose any clear cut interpretation of the experiment data. Also, as already mentioned many experimental data such as a.c.-susceptibility or « vibrating reed » experiments [177] are probably related to flux creep and flux flow phenomena but are often analysed as manifestations of a thermodynamic transition in the vortex lattice (see [178]).

## 5. Criteria defining the experimental critical currents $J_{mag}$ and $J_{tr}$.

As pointed out first by Anderson and Kim [128], the fact that the magnetic flux profiles (depicted in Figs. 13-15) evolve with time implies the existence of a finite electrical field $E$

(Lentz law $e = -\,\mathrm{d}\Phi/\mathrm{d}t \approx 2\,\pi RE$) across the specimen, and thus a non zero resistivity. This means that for practical purposes the critical current density must be defined from the *V versus I* characteristics by setting a minimum acceptable electric field. In other terms, this means that the critical current density must be defined in relation to a measurement criterion and depends on the application considered [73, 112, 113]. We have seen that the most common methods used to determine $J$ are, by increasing order of importance : (1) the transport or resistive technique ($J_{tr}$) (*via V-I* curve), (2) the magnetic hysteresis cycle ($J_{mag}$) and (3) inductive methods including a.c.-susceptibility through its imaginary part $\chi''$ (this point will be clarified later). In this and in the next section we wish to compare and discuss the apparent critical current densities corresponding to transport and magnetic methods and the influence of time and spatial averages on each of these currents.

5.1 *V VERSUS I* CHARACTERISTICS. — One generally encounters in the literature two different procedures for the analysis of the $V(I)$ relationship. First, it is known [73] that in the flux creep regime, conventional hard superconductors exhibit a *V versus I* characteristic often written in the form of a power law as below :

$$V = kI^{m} \tag{14a}$$

Here $k$ and $m$ can be considered as constant, but only for a given specimen of a well defined shape. For conventional superconductors, such as NbTi and $Nb_3Sn$, the exponent $m$ is extremely large and varies approximately from 15 to 150 [73], but far below $T_c$. It is to be noted that the above *V versus I* power law is rather empirical and has no firm physical justifications. It turns out that it is especially useful for the characterization of the material when the shape and other structural parameters of the specimen undr study are not well defined. For instance, this seems to be often the case for granular HTSC. For well defined specimens, this equation is less appropriate especially for the study of more microscopic and more fundamental properties. The flux creep model predicts a rather different relationship which is more suited in this case. It depends on the relative value of $U_0^*$ and $kT$. Let $L$ be the length of the sample under study, $X$ the distance moved by the flux bundle during the jump and let $n = 1$ in equation (9a) (linear approximation). Then the flux creep model gives :

$$V = LX\,\Delta B\,\nu_0\,\mathrm{e}^{-U_p(1 - J_a/J_{max})/kT} = V_0\,\mathrm{e}^{-U(J_a)/kT}, \quad \frac{U_p J_a}{kTJ_{max}} \gg 1 \tag{14b}$$

$$V = 2\,LX\,\Delta B\,\nu_0\,\frac{U_p J_a}{kTJ_{max}}\,\mathrm{e}^{-U_p/kT} = 2\,V_0\,\frac{U_p J_a}{kTJ_{max}}\,\mathrm{e}^{-U_p/kT}, \quad \frac{U_p J_a}{kTJ_{max}} \ll 1\,. \tag{14c}$$

Here $J_a$ is the applied current density : the subscript a is intended to recall that in transport measurements the current density can take any value according to the experimentalist choice. This is in contrast to the case of magnetic measurements where the current density is generally (not always) close to its critical value at the working $T$ and $H$. The limit $U_p J/J_{max} \ll kT$ (Eq. (14c)) corresponds to the TAFF regime discussed later (we shall also call this creep domain the diffusive regime). The other limit is the usual flux creep regime. Having in mind that the electric field is simply related to the electric potential $V$ by $E = V/L$ and to the resistivity by $\rho = E/J$, it is interesting to rewrite these equations in terms of flux creep and TAFF resistivities $\rho_{cr}$ and $\rho_{taff}$ respectively

$$\rho_{cr} = (X\,\Delta B\,\nu_0/J_a)\,\mathrm{e}^{-U_p(1 - J_a/J_{max})/kT} = \rho_0\,\mathrm{e}^{-U(J_a)/kT}, \quad \frac{U_p J_a}{kTJ_{max}} \gg 1 \tag{14d}$$

$$\rho_{taff} = 2\,X\,\Delta B\,\nu_0\,\frac{U_p}{kTJ_{max}}\,\mathrm{e}^{-U_p/kT} = \rho_{0,\,taff}\,\mathrm{e}^{-U_p/kT}, \quad \frac{U_p J_a}{kTJ_{max}} \ll 1\,. \tag{14e}$$

Other $V(I)$ laws have been predicted theoretically [174, 179] and seem to be observed experimentally [180]. The induction $\Delta B$ is probably dominated by that induced by $J_a$.

For completeness we also give the flux flow resistivity, $\rho_{ff}$, [181] associated with the so called flux flow regime which sets in when the pinning force becomes small in comparison with the viscous force $\eta v$ experienced by the normal electrons of the cores of Abrikosov vortices moving at a velocity $v$

$$\rho_{ff} = \rho_n B/B_{c2} \qquad (J_a \gg J_{max}(T)) . \tag{14f}$$

Here $\rho_n$ is the normal state resistivity that would exist if all the superconducting electrons were normal at the field and temperature of measurements [125].

For completeness we note that, (1) the viscous drag in a conventional Josephson junction was first treated by Lebwohl and Stephen [182] and (2) Clem and Coffey [183] determined the flux flow resistivity induced by the motion of vortices (treated as Josephson lines) between a-b sheets in HTSC. It is to be added that all these calculations are based on the idea that the cores of the vortices are made of normal electrons. However, as shown first by Caroli *et al.* [184] and then in more detail by Barden *et al.* [185] this property does not hold at sufficiently low temperature (probably below about 20 to 30 K in the case of YBaCuO, see Ref. [125] for the evaluation of these temperatures). Note that the viscosity coefficient $\eta$ is related to $\rho_{ff}$ (Eq. (14f)) by the equation $\eta = B^2/\rho_{ff}$. This is easily shown by eliminating the velocity $v$ from the equations $\eta v = JB$ (viscous force = Lorentz force) and $E = (d\Phi/dt)/L \approx B(dr/dt) = Bv = J\rho_{ff}$.

Figure 16a and figure 16b illustrate schematically the various regimes associated with $V$ *versus* $I$ characteristics. All of these regimes are encounterted in resistivity data while the sample is cooled down from the normal state. It is clear from (16b) that the transport criterion defining $J$ loses any meaning at low $J$, since it gives a finite value even in the normal state.

At this point we recall again that the above results are expected to be more or less modified by thermal fluctuations, anisotropy and collective pinnining all of which have been neglected up to now. In particular, according to the collective pinning theory disorder induced pinning of a 3D VLL would lead to the formation of a « vortex glass » phase [174] characterized by the absence of long range crystalline order in the VLL. What is then important to note is that the vortex glass phase would lead to very high energy barriers between different metastable states of the VLL and as a consequence to a zero resistivity in the weak current limit. Nevertheless, we have already mentioned that there are both theoretical and experimental arguments against the vortex glass concept. We shall come back briefly to the complicated subject of collective pinning at the end of this paper. We also believe that the above « flux creep » picture of Anderson provides an excellent starting approach to the physics of the VLL.

5.2 TRANSPORT CRITERION AND TRANSPORT CRITICAL CURRENT. — The transport critical current is generally defined from the $V(I)$ curve assuming an electric field $E$ of $10^{-5}$ to $10^{-8}$ $Vcm^{-1}$, depending on the experimental conditions. Because of the large value of the exponent $m$ in the flux creep regime (Eq. (14a)), the exact choice for $E$ is in fact of little influence on $I_c$ (see Fig. 16a). Using realistic values of $m$ and $k$ in equation (14a), we can show that one order of magnitude variation in $V$ leads to only few percent changes in the transport current density $J_{tr}$. It is to be emphasized again that this is only true in the flux creep regime, which in practice means that we are far from the irreversibility line. At this point it is interesting to note that the time scale intervening in transport measurements is the « creep time » : $\tau_{creep} \approx \nu^{-1} = \nu_0^{-1} \exp[U/kT]$ (see Eq. (8a)).

In terms of the electric field criterion, the critical current density deduced from magnetic data would generally correspond to $10^{-8}$ to $10^{-12}$ $Vcm^{-1}$ depending on the time scale of the

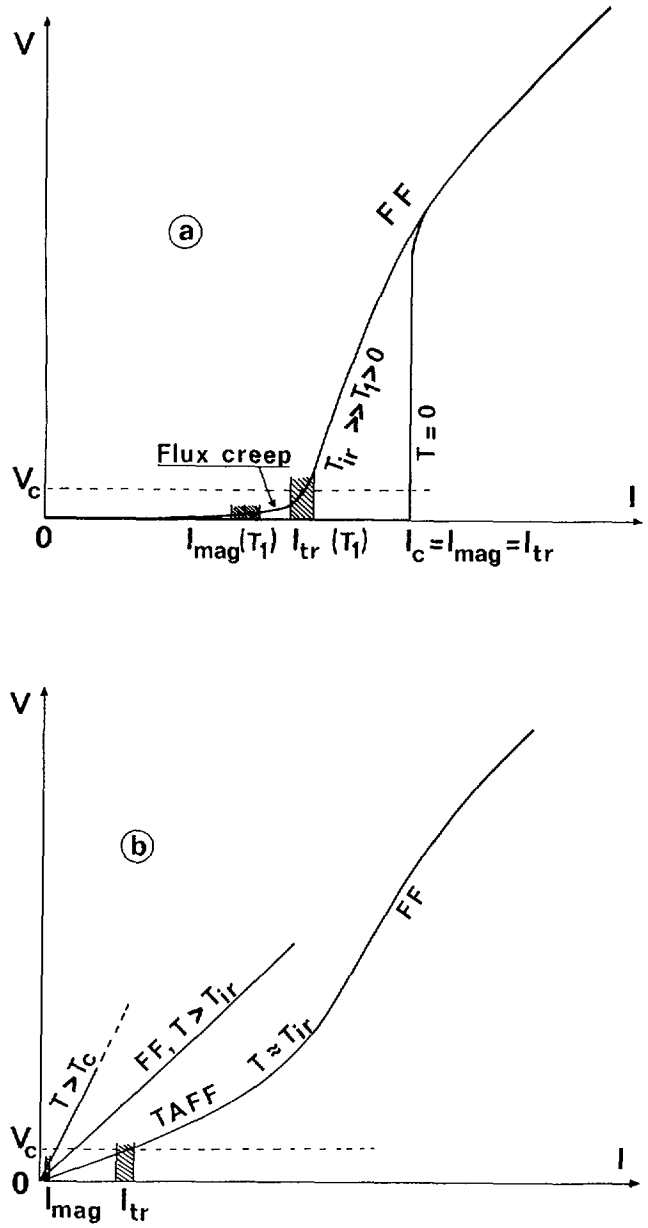


Fig. 16. — Schematic representations of *V versus I* characteristics. a) Flux creep regime with $T \ll T_{ir}$. The dashed region on the right hand side would correspond to the transport critical current for electrical fields in the range $10^{-5}$ to $10^{-8}$ V/cm. The left hand dashed side would correspond to electric fields ($10^{-8}$ to $10^{-12}$ V/cm) accessible with magnetic measurements. The difference between $J_{tr}$ and $J_{mag}$ is about zero at $T \approx 0$ but increases with $T$. b) In the TAFF, FF or normal phases, the *V versus I* curves are roughly linear in $J$. This makes it difficult and unphysical to define a transport critical current and to distinguish between these regimes including the fluctuation regime very close to $T_c$.

experiment, the dimension of the sample and other conditions ($E$ is in fact roughly proportional to $JR^2/t$ if $R$ is the dimension of the specimen ; see Eq. (11c) and Sect. 4.2). For instance, taking $m = 13$ in the above formula yields a magnetic current $J_{mag}$ 1 to 2 times smaller than the transport one (see below). In principle, this difference depends on $T$ and $H$. It would be zero at $T = 0$ (Fig. 16a) and remains small in the flux creep domain, but would increase with $T$ and $H$ becoming very large near the irreversibility line (determined from magnetic data) where we believe that the transport criterion looses any physical meaning. This is because $J_{tr} = E_c/\rho(T)$ has always a $J_{tr}$ different from zero solution, even in the normal state (see Fig. 16b). This and other effects discussed previously (such as the reversible currents) can explain the difference in the irreversibility lines determined from the two experimental methods. As suggested by figure 1 and as will be discussed in section 14, anisotropy is another source of large discrepancy between $J_{tr}$ and $J_{mag}$.

5.3 MAGNETIC CRITERION AND MAGNETIC CRITICAL CURRENT. — As we know the magnetic critical current density is determined from the hysteresis cycle *via* the critical state and Bean's model (Eq. (4)). However, because of the flux creep phenomena we have just discussed, the measured current depends on the time scale of the experiment in particular on the time spent to plot the whole cycle. This is illustrated qualitatively in figure 17 which displays the evolution of the $M(H)$ loop as a function of the sweeping rate of the applied field at a given fixed temperature. Note that curve (4) of figure 17 is obtained by interpolation of $M(H, t)$ from the predictions of the flux creep theory (see also subsect. 4.7). It would approximately correspond to the shortest transport time scale and thus to the transport critical current. Indeed, from the flux creep approximation, the transport time scale discussed in the preceding paragraph would be in the range $10^{-8}$ to $10^{-12}$ s. We recall that at very short time scales the relaxation effects are controlled by the so called attempt frequency $\nu_0 = \tau_0^{-1}$ the value of which is unknown at present (see Eq. (8b) however) and by eddy currents neglected here. However, it turns out that $\tau_0$ is generally in the range $10^{-6}$ to $10^{-12}$ s and can probably be in some conditions comparable to the effective time scale in transport experiments. As an extreme example we take $\tau_0 = 10^{-13}$ s, then we can check that for most experimental conditions the ratio $J_{tr}/J_{mag}$ is generally of the order of 1 to 3. More generally, this ratio would tend to 1 close to $T = 0$ and would increase considerably as one approaches the irreversibility (or depinning) line.

5.4 EXPERIMENTAL $V$-$I$ CHARACTERISTICS OF HTSC THIN FILMS AND SINGLE CRYSTALS. — To our knowledge the $V$ *versus* $I$ relationship is still practically unknown in the case of high $T_c$ single crystals. However, this relation is presently extensively investigated in highly textured thin films of YBaCuO [186-189] oxides where $V$ is found to increase extremely rapidly with $J$. Very often the experimental results are interpreted in terms of the classical flux creep predictions outlined above (Eqs. (14b)) but there are several points which are difficult to understand in this model. For instance, it is often found [60, 188] that the resistance is rather insensitive to the orthogonality requirement of the Lorentz force. Another probably related problem is that epitaxial thin films generally exhibit gross microstructural features [186, 188, 189] which could perturbate severly the local directions of the currents and hence the orthogonality with the local field. In addition, there are fine details in the curvature of $V(I)$ characteristics [190, 191] which are not consistent with the flux creep model. It seems to us that such changes in the curvature of $V(I)$ could also be considered as the signature of weak link effects [192, 193]. Finally, as will be discussed in sections 14 and 15, it is probable that the $V(I)$ of thin films is to a large extent imposed by intrinsic pinning.

Other laws of variations of $V$ with $I$ were also reported in the recent literature on HTSC : $V$ proportional to $\exp(-a/J)$ [180] for example (a being a constant). Such laws are often

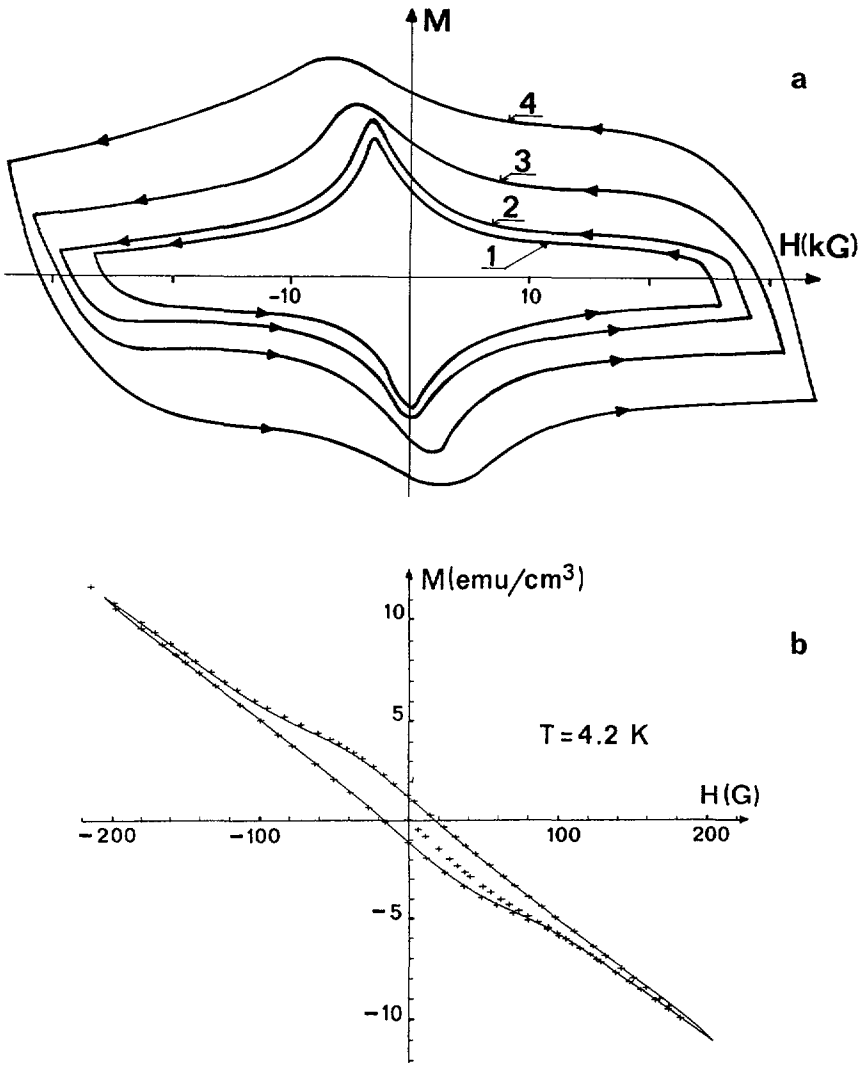


Fig. 17. — a) Evolution of the hysteresis cycle of YBaCuO at 4.2 K as a function of the sweeping rate $dH/dt$ of the applied field. Cycles 1 and 2 represent measurements performed with an ordinary VSM magnetometer ($dH/dt$ = 10 to 100 G/s). Cycle 3 corresponds to experiments in pulsed fields where $dH/dt$ is of the order $10^5$ G/s. Cycle 4 is only schematic and would correspond to the time scales of transport measurements. b) Low-$H$ cycle in granular materials recorded at two different frequencies (discrete points correspond to about $10^{-3}$ Hz while continuous line refers to $10^3$ Hz [198]. We see no detectable difference between the two.

described in terms of a thermodynamic transition at the irreversibility line (but further comments will be made at the conclusion of this section).

5.5 THERMALLY ASSISTED FLUX-FLOW (TAFF). — The notion of thermal assisted flux flow (TAFF) is a new terminology which appeared with high $T_c$ materials [194]. Its exact definition is not yet quite clear for us and differs slightly from one author to another. It seems to correspond to the region of the $T$-$H$ plane where creep is controlled by equation (14c), in

which the electric field $E$ is proportional to $J$, the critical current density. In other words the resistivity ($\rho = E/J$) is independent of $J$ as illustrated by the low $I$ portion of figure 16b. This is to be compared with the other and more usual creep limit of equation (14b) where $\rho$ varies exponentially with $J$. TAFF has the same physical origin and obeys the same basic equation (8a) as flux creep. It also satisfies the same continuity equation for the magnetic induction $B$, which expresses flux conservation. The main difference with respect to the flux creep case is that reverse vortex hopping is no longer negligible. It turns out that TAFF exists in conventional superconductors as well [196]. Since equation (14c) defining the TAFF domain of $H$-$T$ plane is valid only in the limit $UJ/J_{max} \ll kT$, it is in practice only observable close to the irreversibility line. In the case of YBaCuO's system, this region is practically limited to a few degrees (~ 10 K in ordinary experimental conditions) below $T_c$. It is more extended in BiSrCaCuO compounds and other related families. It is thought that in this $H$-$T$ domain the time behaviour of the irreversible magnetization obeys a diffusion of the form $M_{ir}(T) = M(t_0) \exp[-t/\tau_{ff}]$ where $\tau_{ff}$ is given by equation (14g). Concerning YBaCuO such an exponential decay law has been observed [165] close to $T_c$ ($T = 0$ to 80 K and $H = 2$ to 4 kG) after a very long observation time (~ five days). This diffusion regime is expected to occur at much shorter times in the case of Bi and Tl based cuprates. For a deeper insight on this topic see Dew-Hughes [197].

5.5.1 *Some experimental and theoretical difficulties of the TAFF concept.* — We would like to make the following comments now.

(i) Firstly, since in the TAFF region the electric field $E$ is approximately linear in $J$ (Eq. (14c)), the criterion defining $J$ becomes very unclear conceptually and needs to be reconsidered in this region. In addition, in term of $\rho$, it is possible that for very low $J$ the criterion will be satisfied by the flux flow resistivity or even by the normal state resistivity (see discussion below, § 5.8, concerning the implication of these criteria for the resistivities of some very pure metals).

The comparison between criteria defining $J$ via a given fixed electric field $E$ or a given fixed resistivity $\rho$ is done in references [112, 113].

(ii) Secondly, we may wonder if the very popular Bean picture is still valid. We believe that this picture, in particular the notion of critical current density, looses any physical meaning in the TAFF limit. Indeed, the famous field diagram of Bean, such as that displayed in figure 3 (which is very helpful for the interpretation of magnetic data) is no longer justified in this case. The reason of this is outlined in the next paragraph.

(iii) One important deficiency of the TAFF model is the neglect of flux flow effects which are expected to become preponderant above the irreversibility line. In particular, it is obvious that $\rho_{taff}$ (Eq. (14e)) does not tend towards $\rho_{ff}$ (Eq. (14e)) when the pinning force approaches zero.

(iv) To our knowledge, there is at present no satisfactory theory which treats flux creep, TAFF and flux flow simultaneously, on the basis of the same model. This is particularly true when the pinning is strong because most of the collective pinning theories assume that the pinning is weak. This makes the interpretation of the experimental data difficult in many conditions.

(v) Fortunately, there are some limiting examples where TAFF and FF are treated simultaneously : (1) An interesting approach is that of Feigel'man *et al.* [122] who calculate the critical current density $J$ starting from the unperturbed (i.e. defect free material) flux flow state in which the sample is assumed to carry an applied current density $J_a$. Then, they introduce pinning disorder gradually and look to the reduction $\delta v$ in the initial flux flow velocity $v_{ff}$ as a function of the increasing disorder strength. The critical current is defined at the point where the velocity of the vortices is reduced by 100 % (that is to say when

$v \approx v_{ff} - \delta_v \approx 0$, which means that the VLL is totally pinned within this first order perturbation calculation). In other terms, as the disorder is increased the applied current density $J_a$ becomes equal to the critical current $J$ at $v_{ff} - \delta v \approx 0$. (2) A second interesting approach initiated by Coffey and Clem [123] takes into account simultaneously both TAFF, FF as well as flux creep, but this theory is only valid in the limit of nearly elastic displacement of the VLL (this model will be reexamined more extensively in Sect. 13).

5.5.2 *The penetration depths associated with the various flux regimes : flux creep, TAFF, FF and normal.* — We recall that in Bean's model the penetration depth $\Delta r = R - r^*$ depends on the field. For small fields and for the virgin branch of the hysteresis cycle it is given by

$$\Delta r = RH/H_b \,. \tag{14g}$$

This formula is no longer valid in the diffusive or TAFF region where it must be replaced by an exponential decay length [110, 194] given (in SI units) by

$$\delta_{taff} \approx [\rho_{taff}/2\,\mu_0\,\omega\,]^{1/2} \tag{14h}$$

This length can be called the TAFF skin depth in analogy to the usual normal state skin depth (remember that $\omega$ is the angular frequency of the applied variable field). The same kind of equation has been derived some time ago by Clem *et al.* [195] in the flux flow domain :

$$\delta_{ff} \approx [\rho_{ff}/2\,\mu_0\,\omega\,]^{1/2} \tag{14i}$$

We note that these « screening » lengths tend to diverge in the dc-limit. Then, it is interesting to see that strictly speaking this implies that the sample cannot sustain any « persistent » current, or equivalently the magnetic critical current density is equal to zero. In practice however, the above equations suggest that in the FF and TAFF regions of the *H-T* plane any induced magnetic current (or equivalently any irreversible magnetization) will vanish over a period of time

$$\tau_{char} \approx 2\,\mu_0\,\delta^2/\rho = 2\,\mu_0 R^2/\rho \qquad (\text{if } \delta \approx R)\,. \tag{14j}$$

As usual, $R$ is the radius of the sample (note that we have dropped the subscripts « taff » and « ff » for simplicity).

At this point it is interesting to see that the characteristic time $\tau_{char}$ can be deduced quite simply from the usual time constant $\mathfrak{L}/\mathfrak{R}$ of a superconducting coil magnet having a self inductance $\mathfrak{L}$ and shunted by a resistance $\mathfrak{R}$ : On the one hand, assuming that the sample is a cylinder of length unity we have by definition $\mathfrak{L} I = \Phi \approx \Delta B\, S \approx \Delta B\, (2\,\pi R \delta)$ and $\Delta B \approx \mu_0 I$ (Ampere's theorem). On the other hand we can write $I = J\delta$ and $\mathfrak{R} = \rho\,(1/S) = \rho\,(2\,\pi R/\delta)$. Combining these equations we easily obtain $\mathfrak{L}/\mathfrak{R} \approx \mu_0\,\delta^2/\rho$ which is equal to the above characteristic time within a numerical factor of about 2.

More general treatments of field and current penetrations within the sample will be considered in section 13. Later (§ 12.63, Eqs. (68)), we will use the above equations to derive the crossover lines between the flux creep regime and the other regimes as a function of $\omega$. Now, we wish to discuss some experimental problems that can be encountered in transport measurements.

5.5.3 *Comparison between ZFC and FC transport measurements.* — As a general rule the interpretation of transport experiments are based on equations (14a-f) which assume tacitly that the distribution of currents within the sample is homogeneous. There are however several experimental examples where this condition is not satisfied, in particular in *V versus I* measurements. More precisely, as discussed previously in connection with equation (14f) the distribution of the current within the sample is expected to be uniform at very low frequencies of measurements, in both the FF and the TAFF limits. However, it is likely that this

distribution becomes inhomogeneous in the flux creep regime. This is illustrated schematically in figures 18a, b, c which assume that the current penetration across the sample as the applied current is increased evolves following three successive steps defined in these figures, in analogy with the field penetration in magnetic measurements (see Fig. 3). This analogy can be justified qualitatively if we note that the penetration of current is accompanied by that of the self field and the associated vortices. In standard $V(I)$ measurements, the current $I$ is increased (at constant $T$) from zero to some maximum value $I_{max}$ greater than the critical current $I_c$. At first we expect that at low excitation levels the average current density within the sample is determined by the London-Abrikosov current $J_s$. For instance, when the self-field is equal to $H_{c_1}$ the corresponding average current density would be given approximately by $J_s(R)\, 2\,\lambda/R \approx (1 \text{ to } 5) \times 10^7\, \lambda/R \approx 2\, H_{c_1}/R$ (for $T < 77$ K and $\lambda \ll R$ typically ; see appendix A). Since the contribution of this term (which produces no dissipation ($\rho = 0$) to the total current is proportional to the ratio $\lambda/R$, it is expected to become preponderant at high enough $T$ as $\lambda/R$ diverges as $T = T_c$.

Let us now neglect such a London current (an assumption generally valid at $T \ll T_c$ or $R \gg \lambda$) and assume that, like in magnetic measurements, the applied current penetrates and develops into the sample from the surface as assumed in figure 18b (but see Sect. 13 for other possible modes of penetration). Then, it follows that the local current density is highly inhomogeneous while the average current density $\langle J \rangle$ entering the measured $V(I)$ is given by $J_p(1 - r^{*2}/R^2)$, for $\langle J \rangle$ lower than the current $J_p$ of full penetration of the sample. It is only when the biasing current exceeds $\pi R^2 J_p$ that the critical current density becomes eventually uniform (see next Sect. 6 for other possible causes of unhomogeneties in the current distributions) and the application of equation (14b) becomes justified. From the above considerations it seems probable that upon cycling the current $I$ up and down this effect will, in some conditions, lead to a regime of low hysteresis between the virgin (or initial) and the cyclic branches of the $V(I)$ curve (Fig. 18d). It is also possible that the zero current state realized after such a $V$-$I$ cycling exhibits macroscopic remanent currents (in the form of closed loops) and is thus different from the virgin one. The above predictions need experimental confirmations, e.g. they can be tested either by decoration experiments or by means of microscopic Hall sensors (of dimension comparable to the remanent current loops) placed very close to the specimen. Finally, the $V$-$I$ characteristics considered above must be regarded as ZFC experiments. Equivalent FC and ZFC magnetic susceptibility measurements are considered in § 12.5.

The situation is expected to be much simpler in ordinary resistivity ($\rho$) measurements than in $V(I)$ characteristics just discussed. This is because $\rho$ is usually measured under field cooled and current cooled conditions. In this case indeed, the repartition of the current within the specimen and the associated field gradient are created at $T > T_c$ (or eventually above the irreversibility line) and $J$ is then relatively uniform (Figs. 18e, f, g) whatever its value (assuming that the influence of the self field is negligible, see however next Sect. 6 for the consequences of self fields). Therefore, $\rho$ measurements (in static conditions) are equivalent to FC- experiments whereas $V(I)$ (Fig. 18h) characteristics are equivalent to ZFC-conditions.

Of course, we can also carry out ZFC resistivity experiments by applying the current at low $T$ and then heating the specimen up to the normal phase. ac-resistivity presents great interest but is more difficult to interpret and depends on the amplitude, $i_0$, of the alternating current as well as on the measurement frequency, $\nu$. It is probable that for large enough $h_0$ and low $\nu$ the ac-resistivity is equivalent to the ZFC one just discussed while for very low $h_0$ and high frequencies it is governed primarily by the elastic response of the VLL and includes a large quadratic term (see Sect. 13 for more details).

Finally, it is extremely important to note that the above considerations apply also to

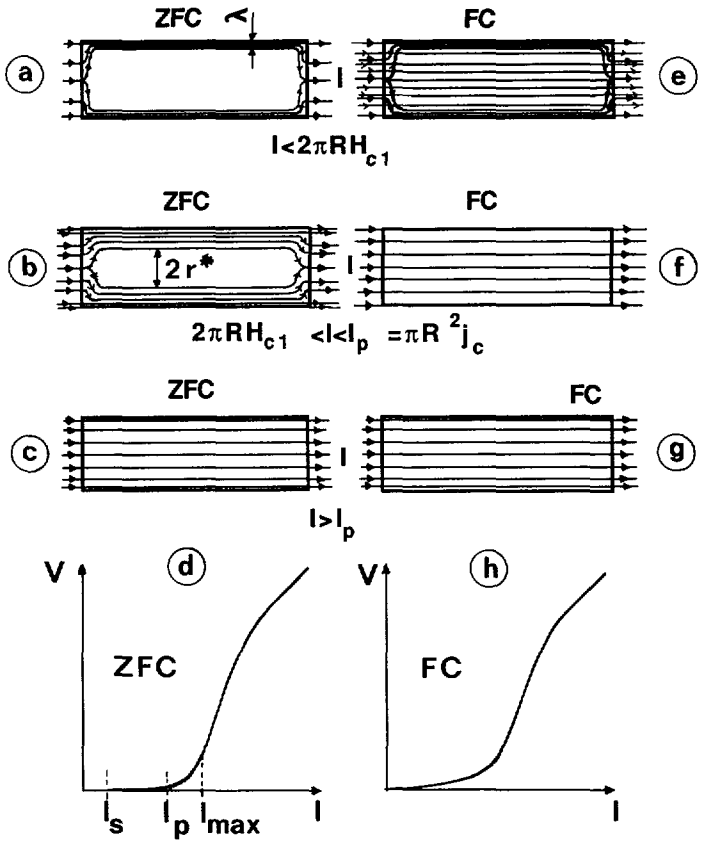


Fig. 18. — Suggested current distributions within a sample prepared in two different cooling states. a, b, c) The sample is cooled in zero field and zero current. The current is then increased continuously from zero to some value $I_{max} > I_c$. d) A schematic $V(I)$ curve which would correspond to the field profiles of figures a, b, c.

Fig. 18e, f, g. — The sample is cooled in an external constant current $I$. In this case the current is expected to be approximately (not rigorously) uniform across the sample. h) Intended to represent the $V(I)$ curve corresponding to this « field cooled » state. Curve (h) is expected to be more consistent with the theoretical models (see text) than curve (d). Such an fc-curve would correspond to usual resistivity measurements.

$V(I)$ characteristics of granular samples where the situation is even more complicated because of the extreme sensitivity of these systems to the self fields (generated by the applied current) which make $J_{wl}$ very inhomogeneous through the sample whatever the experimental conditions (ZFC, FC or AC, see below for more details). It is clear that more theoretical and experimental investigations are needed to clarify these important points.

In the following paragraph we limit our attention to the FC-resistivity which is, as we have just seen, more appropriate for comparison with the theoretical predictions of equations (14).

5.5.4 *The link between the FC-resistivity and the apparent pinning potential.* — Now, we are in position to discuss resistivity measurements in some detail and ask the two important questions : (1) how to derive the apparent pinning potential from such measurements ? and (2) what is the exact meaning of the resulting potential barrier ? Firstly, to avoid

complications from the London currents we shall assume that the effective field (including the self-field) is larger than $H_{c_1}(0)$. If there is no external field this implies $I_a > 2\,\pi R H_{c_1}(T = 0)$ (see lower region of Fig. 18i) where $I_a$ is the applied current and $R$ the radius of the sample. Secondly, also for the sake of simplicity, we shall restrict the quantitative discussion mainly to the TAFF region of the $T$-$H$ plane (Eq. (14e)). In the previous analysis of magnetic relaxation we did not pay much attention to the fact that the pinning barrier depends in fact on temperature. This was justified because most magnetic measurements are performed well below $T_c$ in the pure flux creep regime. This is not generally the case in resistivity data as in most experimental conditions $\rho$ is significantly different from zero only close to $T_c$. Moreover, as illustrated by the dashed lines labelled « $I_1$ », « $I_2$ » and « $I_3$ » (Fig. 18i), we expect that the TAFF domain spanned during resistivity measurements increases as $I_a$ increases (recall that the self-field associated with $I_a$ is given by $H_{sf}(I_a) \approx I_a/2\,\pi R$). The figure suggests that $H_{sf}(I_a)$ is expected to have the same broadening effect (on the resistive transition) as an external field $H$. This implies that the analysis of $\rho$ in the framework of the TAFF model is less justified at very low $I_a$. However, in practice $H_{sf}(I_a)$ is often very small (generally much less than 1 œ) implying that $\rho(T)$ goes to zero in a very narrow temperature domain known as the width of the resistive transition.

Many workers assume that the pinning potential varies with $T$ as

$$U(B, T) = U(B)[1 - (T/T_c)^n]^{3/2} \tag{14k}$$

with the exponent $n = 1$ to 2. Quite often, experimentalists [87, 131-133, 140] analyse their data in plotting $\mathrm{d} \ln \rho / \mathrm{d}(1/T)$ as a function of $T$. Then putting equation (14k) in (14e) gives

$$\frac{\mathrm{d} \ln \rho_{\mathrm{taff}}}{\mathrm{d}(1/T)} = \frac{\mathrm{d} \ln \rho_{0,\,\mathrm{taff}}}{\mathrm{d}(1/T)} - \frac{U(B, T)}{k} \frac{1 + (1.5\,n - 1)(T/T_c)^n}{1 - (T/T_c)^n} \tag{14l}$$

Generally the first term of the right hand side of (141) is thought to be negligible. Accepting this approximation we can get directly both $U_p(B)$ and $n$ from the experimental data. Therefore, in contrast to magnetic measurements resistivity experiments can give direct

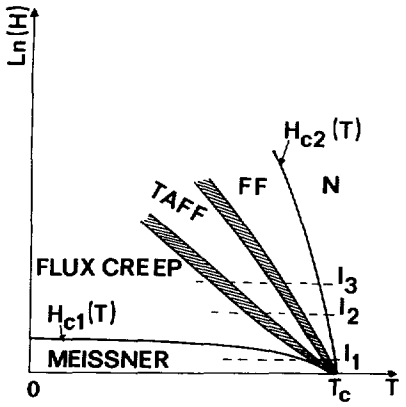


Fig. 18i. — During field cooling, the sample undergoes several flux regimes and always crosses the FF and the TAFF regions where $\rho$ is linear in $I$. If there is no external field the applied field is equal to the self-field. Moreover, if $I = I_1 \leqslant 2\,\pi R H_{c_1}$, it is in the Meissner state where $\rho = 0$. The dashed areas mean that the border lines between the various flux regimes are ill defined.

access to the strength of the real pinning potential. This could explain many apparently conflicting data of the literature. Figure 18j presents schematically the *U versus J* relationship at various fixed temperatures and compares the *U versus* the experimental *J* curves obtained at different temperatures by means of either magnetic relaxation (dashed curve of Eq. $J = J_{mag}(T)$) or resistivity measurements (thin vertical line of Eq. $J = J_a$ = Cte). Note that the dashed curve represents also the equation of $U(J_{mag}(T), T)$ in which $J_{mag}(T)$ is the magnetic critical current at the temperature $T$. At $T \ll T_c$, the pinning barrier does not depend directly on $T$ (in the flux creep model) but only through $J(T)$. However, close to $T_c$ it depends on $T$ both directly and *via* $J_{mag}$ and tends to zero rapidly. For investigations on magnetic relaxation and $U(J)$ at $T$ very close either to $T_c$ or to the irreversibility line see reference [134].

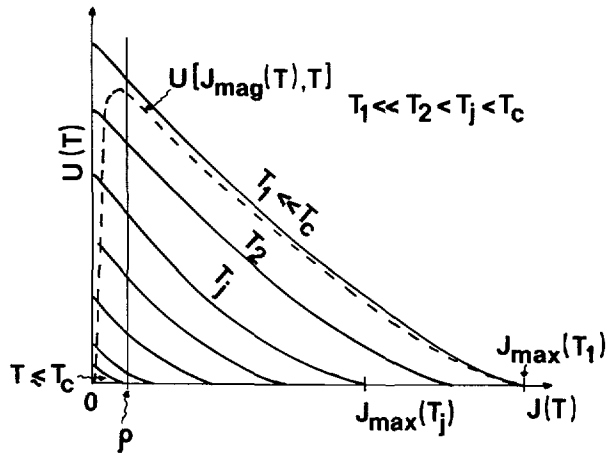


Fig. 18j. — Compares the points of the *U-J* diagram spanned in resistivity measurements at constant *J* (vertical line labelled $\rho$) and in magnetic relaxation experiments (dashed curve) defined by the equation $U(J) = U(J_{mag}(T), T)$. Usually, at low temperatures $U$ does not depend directly on $T$ and thus $U(J_{mag}(T), T)$ merges with $U(J)$ at $T \approx 0$.

5.6 GRANULAR SUPERCONDUCTORS. — It turns out that for sintered high $T_c$ materials the exponent $m$ equation (14a) is only of the order of 10 to 20 instead of 20 to 150 typical of conventional materials [73]. However, $m$ is related here to the weak link network and the associated intergrain current. As a consequence, it would obey different flux pinning mechanisms and thus leads to a different $V(I)$ relationship. Moreover, it is likely that for granular materials the exponent $m$ is strongly dependent on the shape of the sample [39, 73, 196]. This is because of the self-field which will be discussed in the next section. For the same reason, the $V(I)$ relationship is sometimes hysteretic as the applied field is swept upwards and backwards. This is due to up and down fields trapped by the grains whenever $H$ exceeds (or had exceeded) $H_{c_1}$ for such grains. It is important to realize that the physical origin of the hysteresis exhibited by the *V versus I* curves is different from that responsible of the hysteresis in the $M(H)$ curves. The existence of hysteresis here implies that the parameters $m$ and $k$ formula (14a) depend on the magnetic history of the specimen. Hereafter, we shall neglect irreversibilities in $V - I$ characteristics.

5.7 TIME DEPENDENT EFFECTS IN GRANULAR MATERIALS. — In the previous section on flux creep, we only considered homogenous materials. Here we wish to examine quickly the case of intergranular currents in granular materials. At present there seems to be no strong evidences of time dependent effects in the low-$H$ hysteresis cycle ascribed to intergranular currents of granular materials. This is illustrated by figure 17b from Maury [198] which shows a low-$H$ magnetic cycle recorded at two very different sweeping frequencies (about $10^{-3}$ and $10^{+3}$ Hz). It is clear that $M$ is approximately independent of the sweeping rate of the measuring field (within the experimental accuracy) over this wide frequency range and at $T \ll T_c$. In the same way, a.c.-susceptibility measurements close to $T_c$ reveal almost no frequency effects up to about 1 MHz (this will be reexamined later). This quasi absence of relaxation phenomena has led many authors to the conclusion that the pinning barriers associated with intergranular currents is excessively large, up to 35 eV. We believe that the absence of any significant time effect together with other unusual properties such as size effects (see section 6 below) suggest that the flux creep model is probably inadequate for the description of time and temperature dependences of the intergrain currents considered here (we recall that in the flux creep formalism, the variations of $J$ with $t$ has only one physical origin : the creep of the vortices over the barriers). In any case, it is clear from this discussion that the question of time dependent effects in granular systems requires more systematic investigations. (We shall come back later to this question and see that time effects can be detected in some special experimental conditions such as the field induced by persistent currents in the centres of toroidal samples, in apparent contradiction with magnetic measurements). However, in these experiments (persistent $I$ in toroids) the time effect is perhaps connected with trapped flux in the grains, due to the fact that $H$ has exceeded $H_{c_1}$ somewhere.

5.8 COMPARISON WITH THE RESISTIVITIES OF SOME ORDINARY NORMAL METALS. — Let us consider again the transport critical current $J_{tr}$ and assume that the corresponding electric field $E$ is limited by the experimental precision to $10^{-5}$ Vcm$^{-1}$ (this is a rather low field value but corresponds to the usual criterion used in magnet construction and is meaningful for the following comparison). It is then interesting to compare the associated creep resistivity defined here as $E/J_{tr}$ with the resistivities of some ultra-pure ordinary metals at liquid helium temperature. On the one hand, we can easily see that for granular ceramics where $J_{tr}$ is generally less than $10^3$ Acm$^{-2}$ the creep resistivity is about $10^{-8}$ $\Omega$cm$^{-1}$, which is comparable to the value of most commercial Cu wires at liquid helium temperature. On the other hand, intragranular current density $J$ (in single crystals) is of the order of $10^6$ Acm$^{-2}$ (at 4.2 K) corresponding to a creep resistivity of $\approx 10^{-11}$ $\Omega$cm$^{-1}$. Again, this value is comparable to that of very pure gallium, potassium or aluminium at 4.2 K and $H = 0$ (for these metals, especially for gallium, residual resistivity ratios RRR as high as $2 \times 10^5$ have been reported in the literature).

5.9 DISCUSSION AND CONCLUSION. — Current-voltage characteristics (and more generally resistivity broadenings) are generally used to determine the energy barriers entering equation (14b, 14c). These energy barriers were also discussed in this section in terms of magnetic relaxation. The values ($U_0^*$) deduced from magnetic relaxation are often one to two orders of magnitudes lower than those inferred from resistivity data. As we have seen, this is probaly because of the fact that the apparent barrier ($U_0^*$) in magnetic data does not correspond to the actual energy potential but to an apparent term which depends on the associated region of the $U(J)$ curve. On the contrary, according to section 5.5.3 the apparent potential barrier deduced from resistivity data is closer to the real one. A second possible

cause of this difference could be due to the fact that the time scales involved in the two experimental techniques are generally very different.

Careful analysis of the *V-I* characteristics of thin films [190, 191] reveals some fine details (in particular some changes in the curvature of the $V(I)$ curve) not consistent with the usual flux creep model, in particular with equation 14b, c. Such effects have often been ascribed to a melting transition [180] or to a vortex glass like transition [106, 174]. Also, there is some evidence that relaxation effects persist in the limit $T = 0$ which is not consistent with classical thermal flux creep. As we know other interpretation problems arise in zero field cooled *V versus I* experiments because the distribution of the current through any transverse section of the sample is not uniform.

However, despite the many important work which has been achieved in thin films and in granular materials, we believe that the detailed interpretation of *V-I* characteristics is still too complicated to draw any convincing conclusion concerning possible transitions in the vortex lattice. This is because of the influence of the microstructure. It is also likely that the interpretation of the data is made very unclear because of the fact that the measured current generally includes various contributions of different origins (see the discussion in the introduction and Fig. 1) the respective weights of which depend on many different factors ($T$, $H$, the microstructure, the geometrical shape of the specimen, the experimental technique etc.).

The qualitative consideration above show that the usual transport criterion ($E \sim 10^{-6}$ Vcm$^{-1}$) can be quite appropriate for some applications such as transport of electric energy at long distances but is generally not sufficient for the production of high permanent fields (such as permanent magnets). This is for instance the case in NMR applications in the persistent mode where a relative stability (for $J$) of the order of $10^{-6}$ (and better) is required over a long period of time (several weeks or months). Clearly, the magnetic criterion is more suitable for this last example. Finally, we must emphasize that the above comparison is not very rigorous from the applications point of view since the creep resistivity is not very significant by itself from the economic aspect : Economic factors such as the cost of liquid $N_2$ compared to that of liquid helium (among many other economic considerations) have to be taken into account. Here we are only interested in a qualitative discussion to illustrate the notion of critical current.

In this section we showed that the apparent $J$ depends on the experimental method because of the different time scales involved (Fig. 17). Presented in the following section are some striking examples demonstrating that the apparent $J$ can also depend differently on the shape of the sample through the self-fields.

## 6. Interplay between the apparent critical current density, the size of the sample and the self field.

In the precedent two sections, it was assumed that $J$ was approximately independent of $H$ and uniform within the specimen. However, we have seen that in real situations the measured critical current depends on the time scale of the experiment and represents some spatial average of the actual one. As a consequence, for the same applied field the measured critical current will depend on the exact shape of the sample, on the experimental technique employed and on the exact $J(H)$ relationship. In other words, one has in general $J(H) \neq J_{tr}(H) \neq J_{mag}(H)$, even in the limit $T = 0$ where normal relaxation effects are zero. Among other causes of this discrepancy is the fact that even for perfectly homogeneous and isotropic materials, $J$ will vary through the sample because of the self-field (i.e. the field induced by the currents circulating within the sample). As we shall see later this phenomenon is particularly important for intergranular currents in ceramic samples. It also depends

strongly on the demagnetizing field, though it exists even for very long cylinders with no usual such field. For this reason we wish to pay some attention to this point now.

To illustrate the various influences of the size of the sample and the associated self-field on the apparent critical current we first calculate numerically and compare the transport and magnetic currents in the simplest example of a long wire (thus without ordinary demagnetizing field) of radius $R$ submitted to its own induced field (i.e. applied field $H = 0$) and with homogeneous pinning forces. We also assume that $H(r)$ (equal to the the self-field since the applied field is zero) and $J(r)$ have axial symmetry and neglect the equilibrium magnetization and the associated shielding current. To illustrate further the shape effects in magnetic data we also calculate the field $H_p$ of complete flux penetration for various $J(H)$ models. Finally, in the last paragraph we shall discuss briefly the effects of usual demagnetizing effects in the extreme limit of thin films where it is shown that $H_p$ is approximately proportional to the thickness of the film but depends only logarithmically on its radius (demagnetizing field will be reexamined in more detail in section 15). The main idea of this section is the introduction of a characteristic length $R_0$ below which self-fields are negligible.

**6.1** LINEAR DECREASE OF THE CRITICAL CURRENT DENSITY WITH $H$. — To point out the physical origin of the size effect we first consider the *ansatz* first used by Koppé [199] where $J$ (in A/cm$^2$) varies with $B$ as :

$$J(|B|) = J_0(1 - |B|/B_0), \qquad (0 < B < B_0) \tag{15}$$
$$J(B) = 0, \qquad (|B| \geqslant B_0)$$

$$R_0 = \frac{5 B_0}{2 \pi J_0}. \tag{16}$$

Here $B_0$, expressed in gauss ($B_0 < B_{c_2}$), is some characteristic field controlling the field dependence of $J(B)$. Note also the introduction of a characteristic length $R_0$ (in cm) the role of which will become clear later. Let us now calculate the apparent magnetic and transport currents corresponding to this linear law.

**6.1.1** *Transport current in zero applied field (Koppé model).* — The relation between the transport critical current $J_{tr}$ and the real one $J$ can be defined quite generally by the equation below, valid for axial symmetry (the simplest configuration) :

$$J_{tr}(B) = \frac{2}{R^2} \int_0^R J(r)\, r\, dr \tag{17}$$

with $R$ being the radius of the cylindre. The spatial variations of $J$ and $B$ are related by Maxwell's equation which, for cylindrical symmetry with $J$ parallel to the cylinder axis, takes the form :

$$\frac{\partial B_\varphi}{\partial r} + \frac{B_\varphi}{r} = \frac{4 \pi}{10} J(B_\varphi). \tag{18}$$

Here $B_\varphi$ is the azimuthal self-field generated by the transport current flowing along the wire axis. After resolving this equation for zero applied field and putting in equation (17) we obtain the transport current density (in A/cm$^2$) :

$$J_{tr}(H = 0) = \frac{5 B_0}{\pi R} \left[ 1 - \frac{R_0}{R} (1 - e^{-R/R_0}) \right] \tag{19}$$

with the characteristic length $R_0$ defined by equation (16). A Taylor expansion of this

equation as a function of $R$ (recall that $R$ is the sample radius) shows that at small $R$ ($R \ll R_0$) we have $J_{tr} \approx J(H = 0) \approx J_0$ while at large $R$ ($R \gg R_0$) $J_{tr}$ becomes independent of the initial $J_0$ and inversely proportional to $R$ :

$$J_{tr} = J_0 \qquad (R \ll R_0) \tag{20a}$$

$$J_{tr}(H = 0) = \frac{5 B_0}{\pi R} \qquad (R \gg R_0) . \tag{20b}$$

Let us turn back to the Maxwell relation in equation (18) and discuss its consequences for the transport currents. Because of the term $B_\varphi/r$ which goes to infinity as $r$ approaches zero (i.e. the centre of the wire), no stable critical state can occur if $B_\varphi(r)$ does not reach zero at any point of the specimen. According to Campbell and Evetts [19] and to Koppé [199] this condition introduces a characteristic radius $R'$ below which the vortex rings around the current are unstable and collapse. This threshold radius is reached when the radial tension (which varies as $1/r$) tending to collapse the ring is just equal to the pinning force. What is important for the present discussion is the fact that this seems to imply also that for very large specimens the apparent transport current density $J_{tr}$ should drop as $1/R$ whatever the initial $J(B)$ law [199]. As we shall see below, this makes a big difference with the magnetic current which sometimes decreases more slowly with $R$.

It is interesting to note that measurements of transport critical current in zero field can provide a much more accurate determination of $H_{c_1}$ if the radius of the sample is smaller than $R'$ [19, 199]. This is because the pinning forces and the associated irreversibilities (which make an accurate determination of $H_{c_1}$ very difficult) are balanced by the radial tension in this limit. In practice, the limit $R'$ is very low to allow the determination of $H_{c_1}$ by means of presently realizable HTSC wires.

We now consider the persistent magnetic critical current in zero applied field, associated with the remanent magnetization $M_r(B = 0)$ in the hysteresis cycle (this is the right quantity to be compared with $J_{tr}$ in zero applied field).

6.1.2 *Remanent magnetic current $J_{mag}$ (Koppé model).* — It can be shown that the magnetic critical current as defined by the critical state formula $J_{mag} = 30\, M_{ir}/R$ can be rewritten in the following way (for cylindrical symmetry with $B = B_z$ now parallel to the axis of the wire) :

$$J_{mag}(H) = \frac{3}{R^3} \int_0^R J(r)\, r^2\, dr \tag{21}$$

with

$$\frac{\partial B_z}{\partial r} = \frac{4\pi}{10} J(B_z) . \tag{22}$$

After resolving Maxwell's equation (22) for the function $J(B)$ given by equation (15) and putting in equation (21) we obtain for the remanent magnetic current (at applied field = 0 and for the cyclic critical state) :

$$J_{mag}(H = 0) = \frac{15 B_0}{2 \pi R} \left[ 1 - 2 \frac{R_0}{R} - 2 \left( \frac{R_0}{R} \right)^2 (1 - e^{-R/R_0}) \right] \tag{23a}$$

$$H_p = H_0 [1 - e^{-R/R_0}] . \tag{23b}$$

We recall that $H_p$ is the field of complete flux penetration within the sample. Again we can easily see that at small $R$ ($R \ll R_0$ given by Eq. (16)), $J_{mag}$ reduces to the real $J_0$ (at $H = 0$) but

varies as $B_0/R$ at large $R$, that is :

$$J_{mag} \approx J_0 \qquad (R \ll R_0) \tag{24a}$$

$$J_{mag}(H = 0) = \frac{15\, B_0}{2\, \pi R} \qquad (R \gg R_0)\,. \tag{24b}$$

We can also see from equation (23b) that for $R \ll R_0$ the field $H_p$ of full flux penetration reduces to the Bean field $H_b = 2\, \pi J(0)\, R/5$, proportional to $R$, whereas at large $R$ it is equal to $H_0$, and hence independent of $R$. Comparing equations (15), (20) and (24) we can make the following remarks :

1) The variation of the apparent current with $R$ can be very complex and different for transport and magnetic measurements.

2) In the limit where $R$ is much smaller than the characteristic field $R_0$ ($R \ll R_0$ defined by Eq. (16)) the two methods give the same critical current $\sim J(H = 0) = J_0$.

3) In the opposite limit $R \gg R_0$, the apparent critical current depends strongly on the size of the sample and decreases with $R$ as $1/R$ in both cases. More strikingly, in this limit it is independent of the real $J_0$ for both cases (transport and magnetic) as well.

4) In the limit $R \gg R_0$, $J_{mag}$ is larger than $J_{tr}$ by a factor 3/2 for the present example.

However, it is not clear whether or not for large $R$ the apparent current always behave as $B_0/R$ and become independent of $J_0$ (regardless of the particular $J(B)$ law). It seems that this is probably the case for the transport current. However, it turns out that the $1/R$ asymptotic law is not always followed in the case of magnetic data. To answer this question we further calculated the hysteresis cycle and the associated magnetic remanent currents for two other models at zero applied field : (1) in the approximation where the actual $J$ varies as $J_0 \exp(-B/B_0)$ and (2) for the Kim model in which the actual $J(B)$ drops with $B$ as $J_0/(1 + B/B_0)$. The results are summarized below.

**6.2** EXPONENTIAL DECREASE OF THE CRITICAL CURRENT WITH $H$. — Now we assume that the critical current drops exponentially with $H$ :

$$J(|B|) \approx J_0\, e^{-|B|/B_0} \tag{25}$$

**6.2.1** *Magnetic current (exponential law).* — The whole hysteresis cycle is calculated analytically in reference [77] in the approximation where $J$ drops exponentially with $H$. In particular, the remanent magnetic current (i.e. for zero applied field) is given by formula (26a), valid for all $R$. The field of complete penetration is given by equation (26b)

$$J_{mag}(H = 0) = \frac{15\, B_0}{2\, \pi R}\left[-\frac{3}{2} - \frac{R_0}{R} + \left(1 + \frac{R_0}{R}\right)^2 \ln\left(1 + \frac{R}{R_0}\right)\right] \tag{26a}$$

$$H_p = H_0 \ln(1 + R/R_0)\,. \tag{26b}$$

We can again expand equation (26a) in a Taylor series as a function of $R$ and show that at small $R$ it reduces to $J_{mag} = J_0$ whereas at very large $R$ it becomes independent of $J_0$ and decreases as $1/R$. The result is :

$$J_{mag} \approx J_0 \qquad (R \ll R_0) \tag{27a}$$

$$J_{mag}(H = 0) \approx \frac{15\, B_0}{2\, \pi R}\left[\ln\left(\frac{R}{R_0}\right) - \frac{3}{2}\right] \qquad (R \gg R_0)\,. \tag{27b}$$

Here too, it is clear that for $R \gg R_0$ (where $R_0$ is still defined by Eq. (16)) the apparent

current drops as $B_0/R$ (if one neglects the additional logarithmic variation). We can make the same remarks as above concerning $H_p$ which varies from $H_B$ ($R \ll R_0$) to $H_0$ for $R \gg R_0$.

It is possible to make a rapid estimation of the apparent current at large $R$ if one remembers that because of the very rapid drop of $J(H)$, the current density, across any section of the sample, can be considered as constant within a shell of thickness $R_0$ and vanishingly small for $r < R_0$. Then, putting this spatial variation of $J(r)$ in the general formula (21) with the limits of integration $R - R_0$ and $R$, one obtains $J_{mag} \approx \left(3 \int Jr^2\, dr\right)/R^3 \approx 3\, J_0\, R/R_0 = 15\, B_0/(2\,\pi R)$ (after making use of the relation $B_0 = 2\,\pi\,.\,J_0\, R_0/5$ of Eq. (16)). This is to be compared with the factor in the right hand side of equation (27). The above simple physical argument shows why when $R \gg R_0$, the apparent current density is almost independent of the initial $J_0$ and drops rapidly with $R$.

6.3 KIM MODEL. — A frequently used $J(B)$ relationship was introduced a long time ago by Kim [200] :

$$J(|B|) \approx \frac{J_0}{1 + \dfrac{|B|}{B_0}}\,. \tag{28}$$

6.3.1 *Magnetic current (Kim model).* — Using equations (21) and (22) together with Kim's model (Eq. (28)) yields a persistent magnetic current (in the remanent cyclic state) of the form :

$$J_{mag}(H = 0) = J_0\left[\frac{2}{5}\left(\frac{R_0}{R}\right)^3\left\{\left(1 + 2\frac{R}{R_0}\right)^{5/2} - 1\right\} - 2\left(\frac{R_0}{R}\right)^2 - 3\frac{R_0}{R}\right] \tag{29a}$$

$$H_p = H_0\left[\sqrt{1 + 2\frac{R_0}{R}} - 1\right]. \tag{29b}$$

Here too we can easily develop $J_{mag}$ in powers of $1/R$ and test that for $R \ll R_0$, we have $J_{mag} = J_0$ whereas at large $R$ we have :

$$J_{mag}(H = 0) \approx 8\left(\frac{J_0 B_0}{5\,\pi R}\right)^{1/2} \qquad (R \gg R_0) \tag{30a}$$

$$J_{mag} \approx J_0 \qquad (R \ll R_0)\,. \tag{30b}$$

What is new with respect to the two precedent examples is that now $J_{mag}$ is proportional to the square root of $J_0 B_0$ and drops as $1/\sqrt{R}$ at large $R$. Also $H_p$ increases with $R$ as $\sqrt{R/R_0}$ in the Kim model. Shown in figure 19a are the calculated variations with $R$ of the reduced transport current $J_{tr}/J_0$ corresponding to equation (19) and the three different magnetic currents $J_{mag}/J_0$ corresponding to equations (22, 26, 29) in semi-logarithmic scales. Also shown for comparison is $J_{tr}$ of equation (19) ; the corresponding $J_{mag}$ is noted $J_{mag\,3}$.

We shall learn later that intragranular current can not be described by a single characteristic lengh $R_0$ but at least two different $R_0$ are needed. One is associated with the rapid variation of $J$ at low $H$ (low-$H$ peak in the hysteresis cycle) and the other one with high-$H$ variation of $J$. The corresponding size effect is sketched in figure 19b (a more rigorous calculation will be reported elsewhere, see also section 10). Comparing the curves of figure 19a we see that at

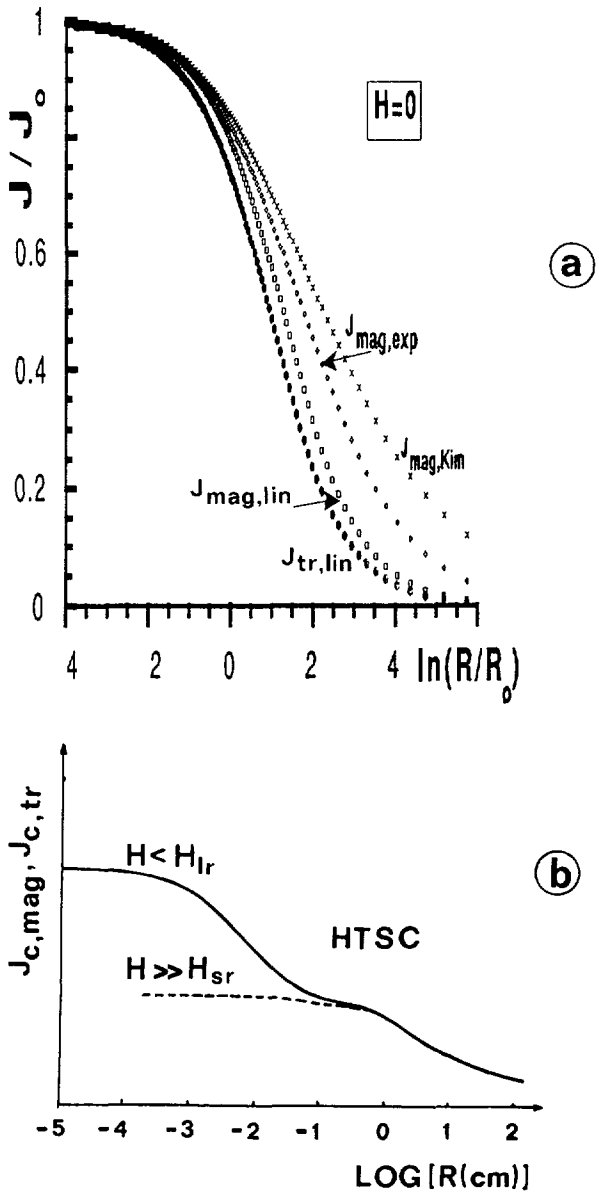


Fig. 19. — a) The reduced transport ($J_{tr}/J_0$) and magnetic ($J_{mag}/J_0$) currents as a function of the reduced radius $r = R/R_0$ (note the semi-logarithmic scale). $J_{tr,\,lin}$ corresponds to equation (19), $J_{mag\,3}$ to equation (23a), $J_{mag,\,lin}$ to equation (26a) and $J_{mag,\,Kim}$ to equation (29a). These curves are qualitatively valid for the intergrain currents. b) Expected behaviour for intergrain currents.

large $R$ the transport current ($J_{tr}$, Koppé [199]) deviates more rapidly from $J_0$ (the real current in zero field) than the associated magnetic term $J_{mag\,3}$ (Eq. (15)). However, it is possible that the difference between the two methods of measurement (transport and magnetic) would become less dramatic in the presence of an applied field much larger than the self-field. This is because in this limit the vortex structure would be imposed principally by the applied field and would therefore be approximately the same in the two situations (eventhough a definitive

conclusion requires more investigations, we find that the self-field effects disappear for $H \gg H_0$ in magnetic data). Note that the curves of figure 19a would be valid (especially the exponential law) for intergranular currents in HTSC.

6.4 FIELD PENETRATION IN THIN FILMS. — In all of the above examples we have assumed that the sample was a long cylinder with negligible demagnetizing field. In this case the field $H_p$ of complete flux penetration was easily calculated in all the three models considered above and found to tend towards the Bean's ($H_b = 2\ \pi JR/5$) for $R \ll R_0$. However, this result is completely wrong when the usual demagnetizing field becomes nonnegligible, particularly in thin films. A useful formula approximately valid in the case of thin films in the limit where $J$ is independent of $H$ is as follows :

$$H_p = \frac{\pi}{5} eJ \ln (R/r^*) . \tag{30c}$$

Here $2\ e$ is the thickness of the film of radius $R$ whereas $r^*$ defines the border circle inside which the sample is still in the virgin state ($B(r) = 0$, $r < r^*$). It is related approximately to the virgin magnetization by $M_{vg} \approx M_{cyc}[1 - (r^*/R)^3]$ with $r^*$ necessarly greater than $e$. Assuming $r^* \approx R/10$ in the above equation shows that for thin films (with $J$ = Const.) $H_p$ is given roughly by the same expression as for $H_b$ (of long cylindrical samples) but with $R$ (and this is very important) replaced by $e$. Demagnetizing effects are the object of section 15 where the above expression (30c) will be demonstrated rigorously.

Another point which is important to emphasize as well is that transport and magnetic currents can appear very different because of the anisotropy. This point is considered in section 14.

6.5 DISCUSSION AND CONCLUSION. — To conclude this section, it seems that if $J$ depends only on the reduced variable $B/B_0$, then regardless of the exact relationship $J(B/B_0)$ (among those considered in this section), it is always possible to define a characteristic dimension $R_0$ (Eq. (16)) below which the measured critical current (in applied field much smaller than $H_0$) reflects the real critical current whereas for larger $R$ it depends on the experimental technique used and decreases according to some power law of $1/R$. It turns out that intragranular current of high $T_c$ materials cannot be described by a single scaling law $J(B/B_0)$ of the sort studied before and we need two different terms $B_0$ corresponding to very different field domains. We found that $YBa_2Cu_3O_7$ at 4.2 K, the characteristic length $R_0$ associated with the high field regime $H \gg H_{c_1}$ is of the order of 2 to 5 mm for intragranular current density single crystals at $T \ll T_c$ (and probably larger at high $T$), but only 20 to 50 μm for intergrain currents [77]. This shows clearly that in the last case we are practically always in the $1/R$ regime. Thus, intragranular currents are characterised in fact by two different $R_0$. It is of interest to add that because the relative influences of $J_0(T)$ and $H_0(T)$ on the measured current depend on $R$, it is expected that the $J$ *versus* $T$ law of the experimental current should depend on $R$, particularly in granular materials. At large $R$ it would reflect the $T$-dependence of $H_0(T)$ whereas for very thin specimens it would correspond to $J_0(T)$ (see also § 8.3). Finally it is important to emphasize that when the applied field is very large compared to $H_0$ we recover the Bean model in which $M$ scales with $R$ and the apparent critical current density (obtained by the Bean model) represents really the local one. In other terms, if one tries to generalize this idea of a characteristic $R_0$ to the high field domain it seems that $R_0$ varies more or less inversly to $J(H)$. Then, since $J(H)$ decreases with $H$ this implies that $R_0(H)$ increases with $H$ and should exceed the radius $R$ of the sample at some field value. Because of the size effect emphasized in this section, it seems that the experimental critical current density in zero applied field is not a sufficient means to judge of the quality of the

material. For this purpose, it would be better to measure the critical current in some fixed field much higher than any self-field. As far as granular, no textured, HTSC superconductors are concerned an applied field of about 50 œ would be quite sufficient. Clearly more investigations are needed to clarify this point.

**7. Critical current in single crystals, oriented grains and highly textured thin films.**

This section concerns the investigation of intragrain critical current densities in single crystals, decoupled grains and highly textured epitaxial thin films of HTSC. We wish to emphasize the most characteristic features common to these systems. In particular, we shall consider the influence of field, temperature, the microstructure (chemical and physical defects) as well as the macroscopic shape of the sample on the « experimental » critical current densities.

We know that direct transport measurements of critical currents in single crystals (intragranular current) are very difficult to realize and are rather scarce in the literature at present. Therefore, this section will principally focus on the determination of $J$ from magnetic measurements (we recall that for notational simplicity we call the critical current density $J$ instead of $J_c$). We have seen in section 4 concerning the experimental criteria defining $J$ that because of the difference in the time scales involved, the transport critical current is expected to be somewhat larger than the magnetic one. We have also seen that, on the opposite, spatial averaging favours $J_{mag}$ if $R \gg R_0$ (with $R$ being the radius of the sample whereas $R_0$, given by Eq. (16), is a characteristic dimension of order 1 to 4 mm for YBaCuO single crystals and for $H \gg H_{c_1}$). Indeed, we shall see that except in a narrow field domain of about $10 \times H_{c_1}$ around the origin (defined by the low-$H$ peak region of the hysteresis cycle ; see below) the magnetization scales with $R$ and hence represents (to a good approximation) the local critical current density $J$. This claim is valid for single crystals as well as highly textured epitaxial films, when the radius of the specimen is less than a few millimetres (a condition generally satisfied in most experiments ; see Fig. 19). Therefore, we believe that as far as these systems are concerned most of the quantitative data deduced from magnetic measurements are either very close to the transport critical current or represent a lower limit of this current, particularly at low temperatures when flux creep is negligible. Nevertheless, this conclusion is certainly less justified very close to the irreversibility (or depinning) lines where relaxation effects are often very strong and favours $J_{tr}$ rather than $J_{mag}$. Again, for the sake of notational simplicity we shall assume in this section that $J$, $J_{mag}$, and $J_{tr}$ are identical (unless otherwise specified). Also, to avoid complications from anisotropy effects (which will be discussed separately later in Sect. 14) we shall equally assume that the applied field is directed along a symmetry direction ($c$-axis or $a$-$b$ plane) and that the vectors **H**, **B** and **M** are aligned along the same direction. Finally, we shall see in section 14 about anisotropy effects that $J_{ab,\,ab}$ (i.e. the current in the $a$-$b$ planes with the Lorentz force perpendicular to these planes) is hardly accessible by means of usual magnetic measurements so that for the experimental results considered here the measured critical current is $J_{ab,\,c}$ (for $H /\!/ \mathbf{c}$) or $J_{c,\,ab}$ (for $H \perp \mathbf{c}$).

Some of the most characteristic features of intragrain currents have been already mentioned but it is of interest for the present discussion to recall the following results :

1) $J$ is generally as high as $10^6$ to $10^7$ $Acm^{-2}$, at low temperatures and fields. Such very large current values have been first observed in $La_{1.85}Sr_{0.15}CuO_4$ by Oussena *et al.* [13] before the discovery of $YBa_2Cu_3O_7$ by Chu *et al.* [3] and then confirmed for other high $T_c$ families in particular by direct transport measurements in Y(123) thin films by Chaudhary *et al.* [14].

2) In general the magnetic critical current drops very sharply with temperature (exponentially for $T \leqslant 2\,T_c/3$ in the case of Y(123)), as well as with field at high $T$. For instance, in the

case of Y(123) $J$ is reduced by two orders of magnitude when $T$ varies from 4.2 to 77 K [20-25, 201, 202]. Close to $T_c$ it follows a power law. The situation is generally much more dramatic in the case of the Bi [60, 203-205] and Tl cuprates [206, 207].

7.1 THE HYSTERESIS CYCLE AND THE FIELD DEPENDENCE OF THE ASSOCIATED CURRENT DENSITY $J_{mag}$. — **$YBa_2Cu_3O_7$**. Some representative examples of the hysteresis cycles of melt textured samples and single crystals of $YBa_2Cu_3O_7$ are displayed in figures 20 and 21 (respectively) for $H$ parallel to the $c$-axis and in figure 22 for $H$ perpendicular to that axis. The same kind of plots are presented in figures 23 and 24 for oriented grains of $YBa_2Cu_2O_7$ [25, 154]. It is seen that whatever the experimental conditions the cycle exhibits a well defined peak close to $H = 0$ (« central peak »). It is also seen that for **H** parallel to the $c$-axis the $M(T)$ curve (butterfly like shape) of the single crystal exhibits a minimum, in some temperature region (~ 50-80 K here) but it is to be emphasized that no minimum is seen for **H** parallel to the $a$-$b$ basal planes whatever the temperature. More puzzling, to the best of our

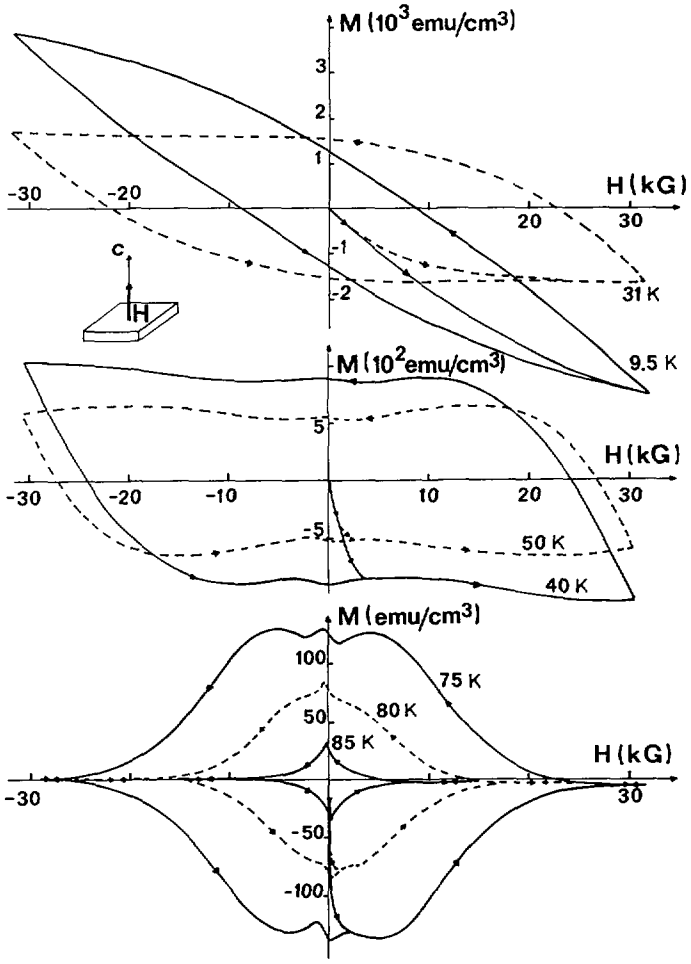


Fig. 20. — Evolution with temperature of the hysteresis cycle of a highly melt textured specimen of $YBa_2Cu_3O_7$ for $H$ parallel to the $c$-axis (from Aguillon [25, 154]).

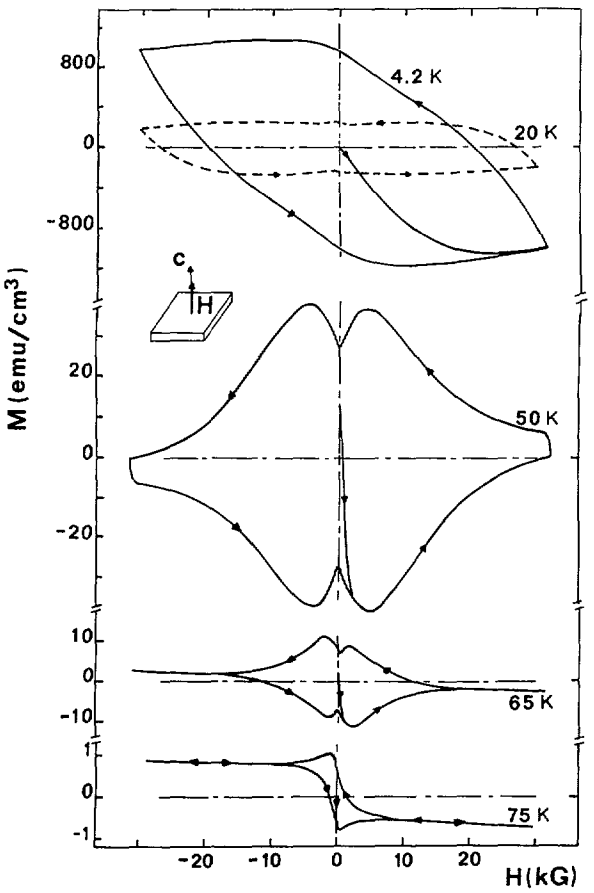


Fig. 21. — Same experiment as in figure 20, but for a single crystal of $YBa_2Cu_3O_7$ of almost spherical shape ($R \approx 0.3$ mm, $T_c \approx 85$ K) (after Ousséna [380]).

knowledge no pronounced minimum of this kind is seen in the hysteresis cycle of oriented (well oxygenated) grains prepared in the usual conditions ($r_g \leqslant 20$ mμ typically) for any orientation of the applied field. Concerning $M_{ab}(H)$ (i.e. the magnetization for **H** in the *a-b* planes) it is to be stressed that because the shape and the amplitude of the cycle are both extremely sensitive to any deviation of the *H*-direction from the *a-b* plane, the measured cycle with *H* assumed in the « basal planes » seldom represents the true magnetization for *H* strictly within these planes. It is indeed often dominated by the magnetization induced by the projection of *H* on the *c*-axis. More or less similar field behaviours are exhibited by other HTSC families, as illustrated below.

**Bi and Tl based high $T_c$ materials :** From figure 25a, [314] it is seen that at very low temperature Bi (2212)-oxide exhibits very much the same $M(H)$ curves as $YBa_2Cu_3O_7$ (for *H* parallel to the *c*-axis) but as the temperature is increased the magnetization drops much more rapidly with both *T* and *H* than that of Y (123) compound. Because of the large anisotropy of Bi cuprates the magnetization $M_{ab}$ for *H* strictly parallel to the basal planes is found to be practically zero in high quality single crystals. In fact, we recall that we find it extremely difficult to obtain **H** strictly parallel to the *a-b* planes. Most of the « *a-b* » magnetizations

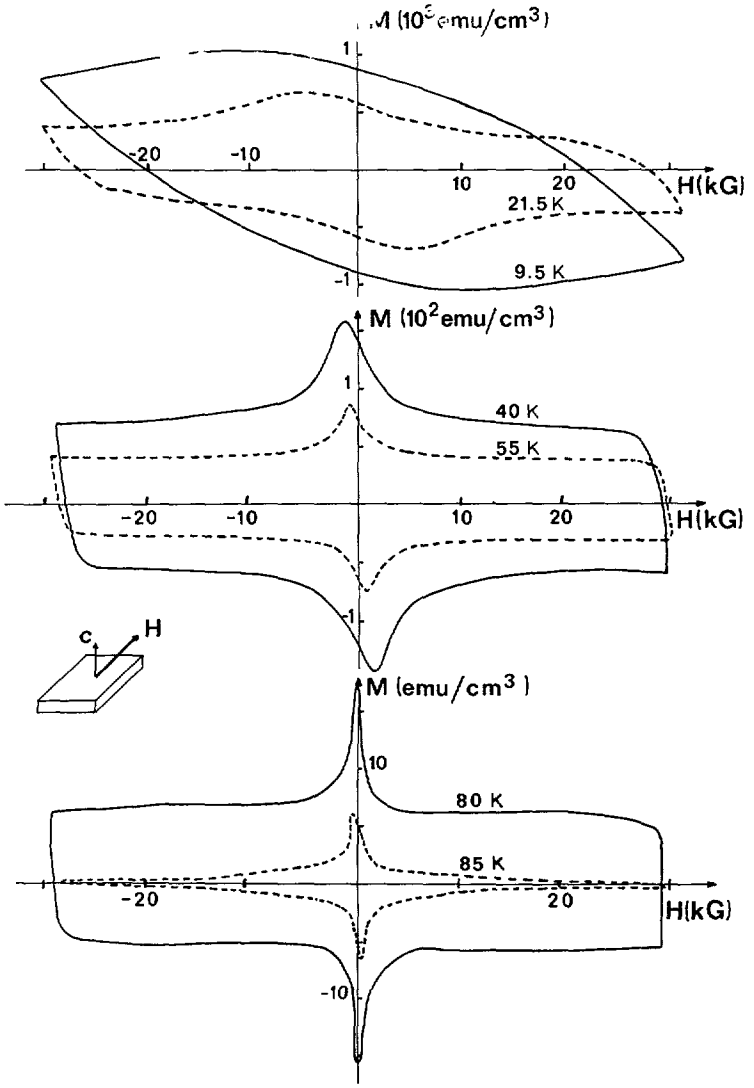


Fig. 22. — Evolution with $T$ of the hysteresis cycle of a single crystal of $YBa_2Cu_3O_7$ for $H$ « parallel » to the $a$-$b$ basal plane [154].

reported in the literature may probably be explained by this qualitative projection model (see Sect. 14) which means that the measured magnetization is due principally to that induced by the projection $H_z$ of **H** on the $c$-axis. In fact this component can be increased considerably by the demagnetizing field : $H_{z,\,\mathrm{eff}} \approx H_z/(1 - N_z)$ at low field and low flux penetration and where $N_z$ is the demagnetizing factor for $H$ parallel to the $c$ direction (see [50, 358] and § 15.2 for more details). A necessary but not sufficient condition for **H** to be in the $a$-$b$ planes is to make the transverse magnetization (i.e. the component $M_T \approx M_z$ along the $c$-axis in this case) equal to zero. Unfortunately, for this purpose we need a two-axis-magnemeter to measure $M_T$ and $M_L$ simultaneously. After correcting approximately for such misorientation errors we estimate that at very low $T$ and $H$ (i.e. not very close to the depinning line) $J_{c,\,ab}/J_{ab,\,c}$ is probably less than $10^{-2}$ to $10^{-3}$ in Bi-systems (see anisotropy Sect. 14 for more details). It is

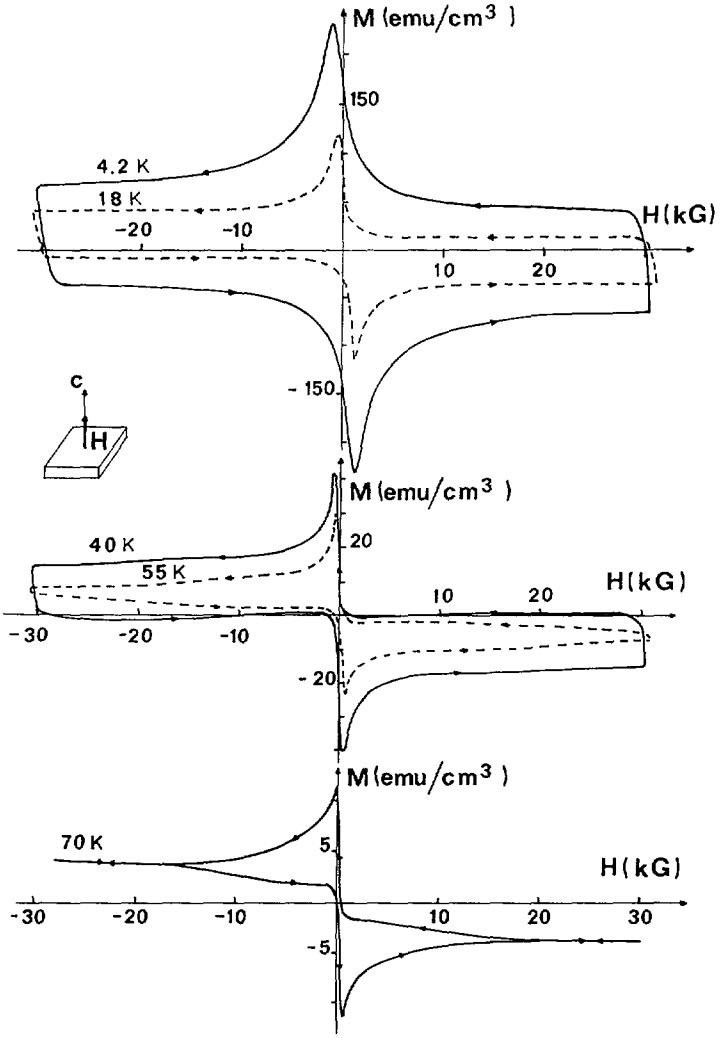


Fig. 23. — Evolution with $T$ of the hysteresis cycle for an $YBa_2Cu_3O_7$ sample with oriented grains. $H$ is approximately parallel to the $a$-$b$ basal plane [154].

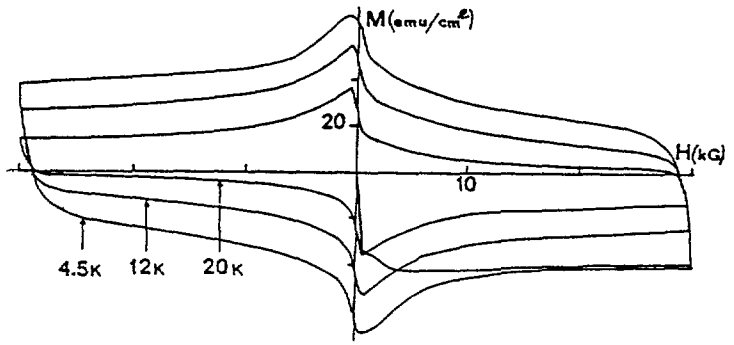


Fig. 24. — Examples of temperature dependence of the hysteresis cycle of oriented grains sample of $YBa_2Cu_3O_7$ for $H$ parallel to the $c$-axis [154].

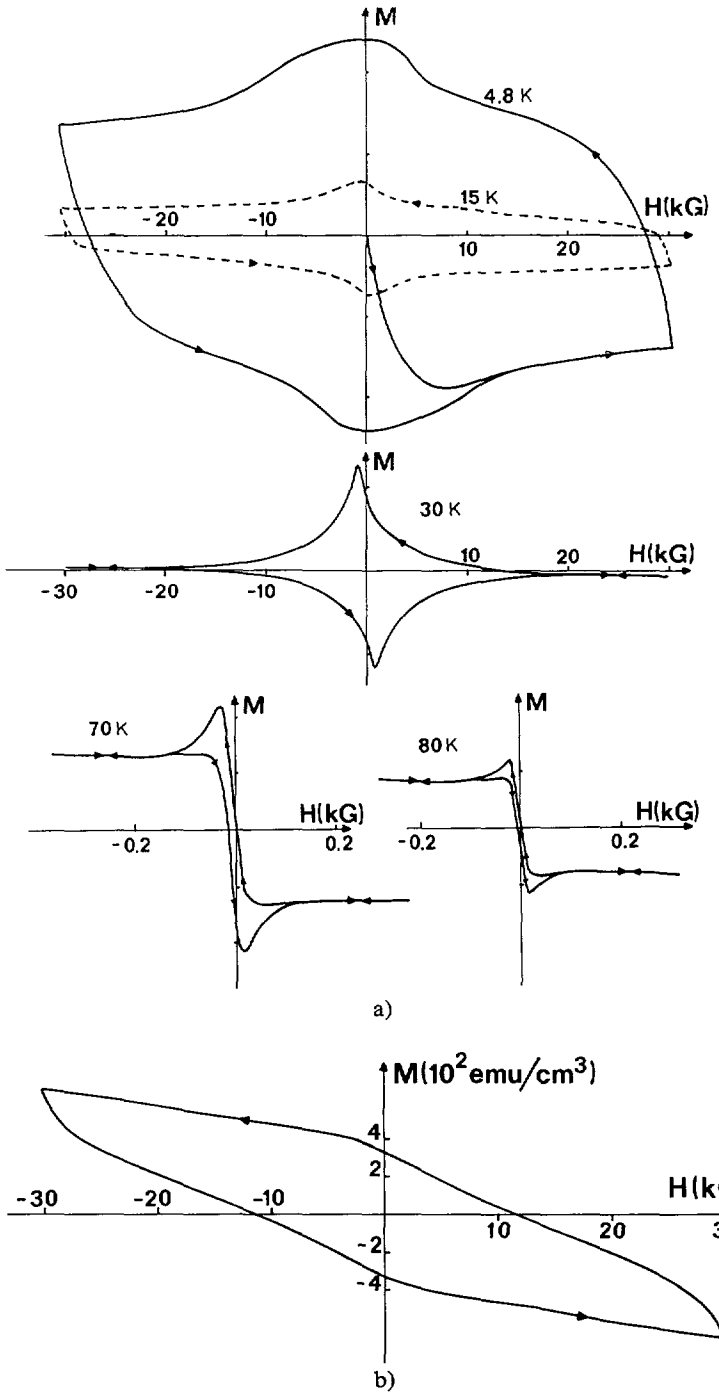


Fig. 25. — a) Temperature dependence of the hysteresis cycle of a single crystal of BiCaSrCuO (2212) for $H$ parallel to the $c$-axis. b) $H$ is « perpendicular » to the $c$-axis : it is likely that in most experimental results the magnetization for $H$ parallel to the $a$-$b$ planes is principally due to the extreme difficulties to make $H$ strictly parallel to the $a$-$b$ plane everywhere in the specimen and is in fact due to small in planes currents, $J_{ab,c}$ produced by the residual projection $\Delta H_z$ of $H$ on the $c$-axis. At low-$H$ $\Delta H_z \approx H_z \cdot \Delta\theta/(1 - N_c)$ where $N_c$ is the demagnetizing factor for $H /\!/ \mathbf{c}$.

now of interest to note the following two points :

(1) No minima of the sort exhibited by $YBa_2Cu_3O_7$ cycles (Fig. 21) are seen here in our Bi single crystals from different sources and of different dimensions. However, there are many examples in the recent literature where Bi oxides show butterfly shaped cycles of roughly the same form as in in the case of $YBa_2Cu_3O_7$ single crystals but this is not as general as in the latter system. In fact we still do not know for the moment the reasons why Bi oxides sometimes exhibit such a butterfly effect and sometimes not. It seems that the presence of the butterfly shape is accompanied by a very low apparent critical current density $J_{mag}$. However it is not clear whether this low $J$ value is due to very bad quality single crystals (containing a lot of weak links) or on the contrary to high quality single crystals with very little defects to pin the vortices. We believe that a very systematic study of the hysteresis cycle of Bi oxydes as a function of $T$ and $H$ will help answering this question, in particular in the region $H \leqslant H_{c_1}$ for the search of possible weak links.

(2) We emphasize again that if for any reason the field is not strictly parallel to the $a$-$b$ planes everywhere in the material the apparent magnetization $M_{ab}$ could be quite large even though the real $M_{ab}$ is zero. This is because of the combination of demagnetization and anisotropy effects mentioned above which can give rise to a large component $M_z$ along the $c$-axis. To prove this claim we consider two limits : (i) At sufficiently low field such that $H_z \ll H_p$ one has $H_{z,\,\mathrm{eff}} \approx H \cos \theta/(1 - N_z)$ and $4\,\pi M_z = -H \cos \theta/(1 - N_z)$. Therefore, in this limit the measured longitudinal magnetization reads

$$\mathbf{M}_L = \mathbf{M} \cdot \mathbf{H}/H = M_z \cos \theta \approx -H \cos^2 \theta/4\,\pi(1 - N_z)$$

(we recall that $\theta$ is the angle of $\mathbf{H}$ with the $c$-axis, Sects. 12 and 15). (ii) In the opposite limit $H_z \gg H_p$ we have $M_z \approx -J_{ab,\,c} R/30$ (Bean's model) and $M_L = \mathbf{M} \cdot \mathbf{H}/H \approx -J_{ab,\,c} R \cos \theta/30$. Very often, Bi single crystals have the shape of a very thin slab, hence with $N_z$ close to one. For example the sample reported in figure 25 is about 30 $\mu$ thick and 1 mm diameter. We believe that the « $M_{ab}$ » magnetization reported in figure 25b is consistent with the above projection picture if one accepts a misorientation of a few degrees. Such an error in $\theta$ is always present due to various unavoidable imperfections. In summary, this yields a finite projection $\Delta H_z$ of $H$ on the $c$ axis and hence to some in-plane current and thus to some magnetization $\Delta M_z$ along the $c$-axis. These considerations apply also to Tl based compounds. Due to technical difficulties the latter have recieved less attention than Bi systems up to now, but recent results on the critical current density of Tl based HTSC [208-210] are encouraging.

Note that in the above qualitative analysis we assumed that the in-plane current was equel to $J_{ab,\,c}$. The true current probably includes some contribution from the « intrinsic » term $J_{ab,\,ab}$ and is therefore expected to be slightly larger than $J_{ab,\,c}$ (since the inequality $J_{ab,\,ab} > J_{ab,\,c}$ is always true ; see section 14 for more explanations).

**$La_{2-x}Sr_xCuO_4$ .** The development with temperature of the hysteresis loop of some $La_{2-x}Sr_xCuO_4$ single crystals is presented in figure 26 and figure 27 for applied fields $\mathbf{H}$ either perpendicular or parallel to the $a$-$b$ planes [50, 154, 213]. Other examples of $M(H)$ curves can be found in references [214, 215]. Obviously, the cycles shown in the above figures have globally very similar shapes as those of the two preceding examples, especially $YBa_2Cu_3O_7$. In particular one observes roughly the same low-$H$ peak and the same butterfly-shaped cycle in a limited temperature domain for $H$ parallel to the $c$-axis. However, the variation with $T$ is somewhat slower here, in particular for $H$ oriented along the basal planes. Note also that for $La_{2-x}Sr_xCuO_4$ the anisotropy ratio $J_{ab,\,c}/J_{c,\,ab}$ is at present estimated to be about 200. This is an intermediate value between that of $YBa_2Cu_3O_7$ which is about 20 to 40 and that of Bi-based systems which is probably larger than 1 000. We shall equally see that the other anisotropy ratio $J_{ab,\,ab}/J_{c,\,ab}$ is even higher than these values). The same remarks as for Y and Bi cuprates

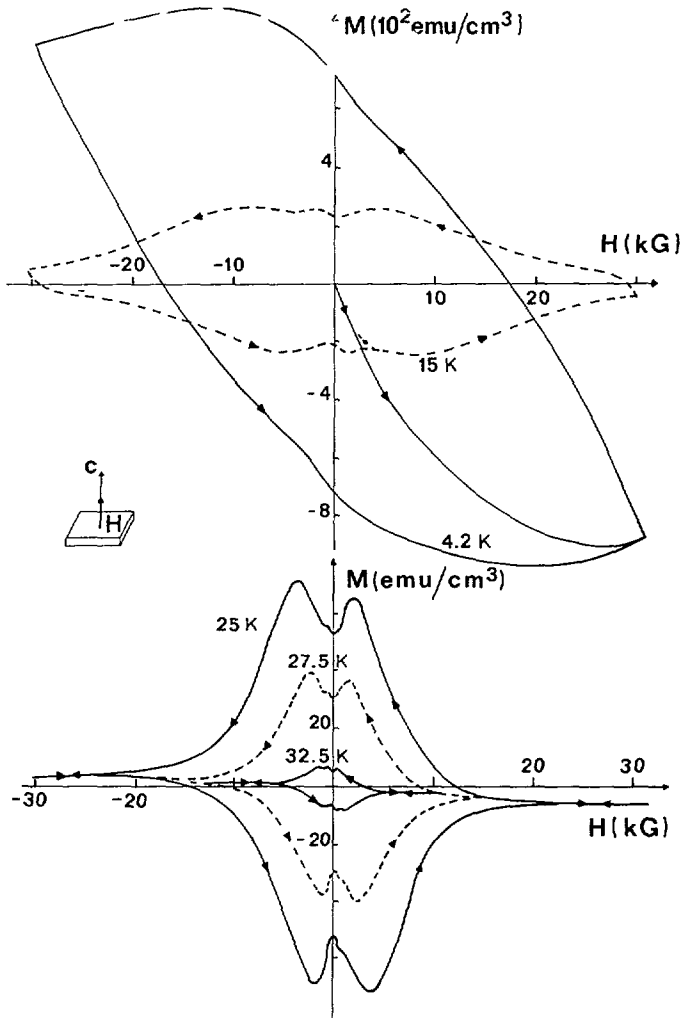


Fig. 26. — Evolution of the hysteresis cycle with temperature of $La_{2-x}Sr_xCuO_4$ single crystal for $H$ parallel to the $c$-axis (Aguillon [154], Khishiol *et al.* [216]).

is valid concerning the sensitivity of the measured $M_{ab}$ to small disorientations of **H** with respect to the basal planes.

7.2 TEMPERATURE VARIATION OF INTRAGRANULAR CURRENT DENSITIES. — **$YBa_2Cu_3O_{7-\delta}$**. Shown in figure 28 is the temperature dependence of the magnetic critical current density for various $YBa_2CU_3O_7$ samples with $H$ parallel to the $c$-axis. Also shown as a dashed line is the temperature dependence of the critical current density of a thin film. It is clear that the critical current of thin films is larger than that of single crystals and, more interestingly, varies more slowly with $T$ (for zero applied field). However, we know from previous discussions that for a number of reasons (for example demagnetizing fields, anisotropy, time dependent effects, contribution of surface London-Abrikosov's currents, etc.) it is much more difficult to interpret critical current data in thin films than in single crystals. In addition, we shall see later in section 14 on anisotropy and section 15.2 about

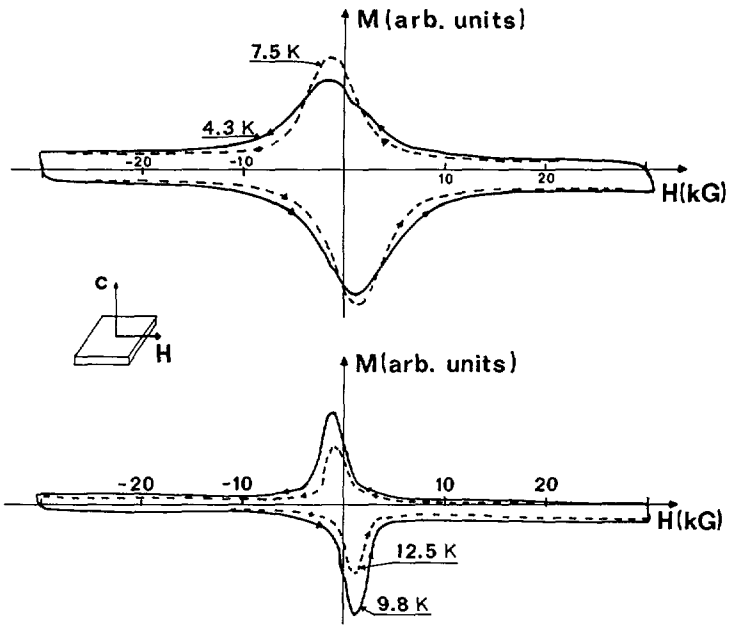


Fig. 27. — Evolution of the hysteresis cycle of $La_{2-x}Sr_xCuO_4$ single crystal with temperature for $H$ perpendicular to the $c$-axis (the same as in Fig. 26).

demagnetization effects that the experimental transport and magnetic critical currents ($J_{tr}$ and $J_{mag}$ respectively) in thin films can include a large intrinsic contribution $J_{ab,\,ab}$ generally not significant in $J_{mag}$ for thick single crystals.

It is found that $J_{ab,\,c}$ drops exponentially with $T$ for $T \ll T_c$ from the hysteresis cycles of single crystals or decoupled grains. The critical current density in the $c$-direction ($J_{c,\,ab}$) is also found to decrease very rapidly with $T$. However, in this case a marked change in the slope in the log ($J$) – $T$ curve is observed at about 15 K. This « accident » is observed in millimeter size single crystals as well as in oriented decoupled grains of radii as low as 1 μm [208-210]. This anomaly is also present in other HTSC families ($La_{2-x}Sr_xCuO_4$) [208, 216]. Its physical origin is still unclear at present. Similar temperature variations as described just above are exhibted by intragranular currents of sintered and textured $YBa_2CU_3O_7$ materials.

It is interesting to note in figure 28 that the depairing current $J_d$ is about two orders of magnitudes higher than the highest critical current density shown on the same figure (i.e. that of thin films). This difference between the two currents is discussed in appendix A. Here we only recall that the depairing current is defined formally as the limit wheere the kinetic energy ($\varepsilon_c$) of such a current is approximately equal to that of the condensation energy (see appendix A). Again formally speacking, this implies that a material which would carry a current density of about $J_d$ will have an effective energy gap of about zero ($\Delta_{eff} = \Delta - \varepsilon_c \approx 0$) and thus a transition temperature approaching zero too. This is to be compared with the usual assumption that the critical current density $J$ and the associated pinning centres do not perturbe the superconducting state to a first approximation, in particular $T_c$.

**Bi and Tl — based families :** We have seen that the influence of $H$ and $T$ on the critical current are much more dramatic in **Bi** and Tl cuprates than in Y(123). The temperature variation of the critical current density of Bi(2212) single crystals [203, 204] and of Tl oxides [206, 207] is illustrated in figure 29. Here too, it is found that the critical current density of

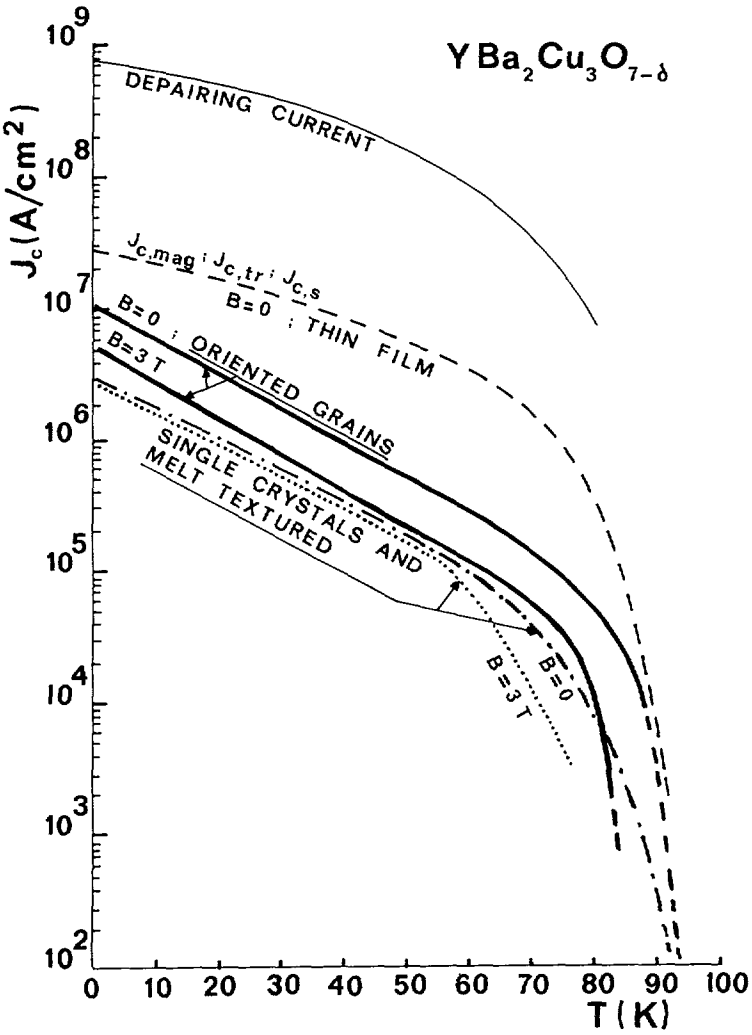


Fig. 28. — The evolution of the critical current density of a single crystal, an oriented granular sample and a melt textured sample of $YBa_2Cu_3O_7$ (deduced from the hysteresis cycle) are compared as a function of temperature. The dashed curve corresponds to a thin film [25]. In this latter case the field and its direction with respect to the crystalline axes is not rigorously defined because of both demagnetizing effects and vortex bendings. Also depicted schematically is the depairing current.

thin films drops less sharply with $T$ than in single crystals at least for zero applied fields. The situation is less clear at « relatively » high fields (on the order of 1 $T$) where $J$ drops dramatically with $T$ in both cases. We believe that this is consistent with the idea that the experimental critical current density of thin films reflects several contributions including reversible London-Abrikosov's currents as well as intrinsic critical currents $J_{ab,\,ab}$. The critical current density in highly anisotropic oxides such as Bi-systems will be reconsidered in connection with anisotropy effects in section 14. It is not possible to decide whether the low $J$ value at high $T$ given in the literature and discussed above has some fundamental origin (thermal fluctuations and anisotropy in particular) or is simply due to our inability at present

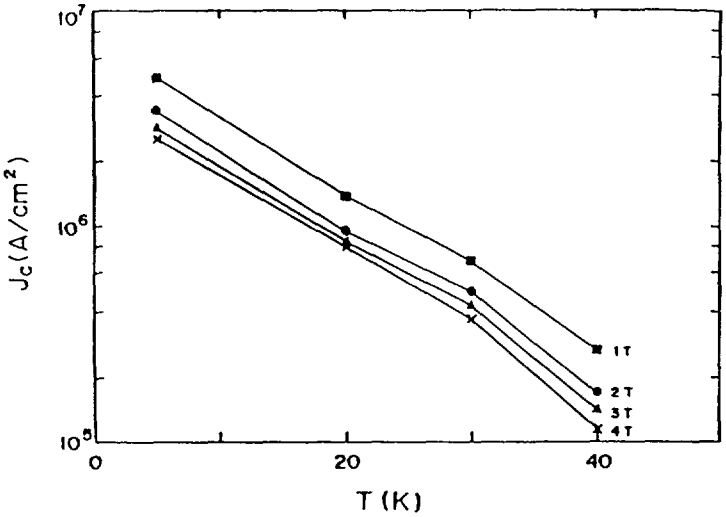


Fig. 29. — Evolution of the critical current density for a single crystal of Bi (2212) compound (deduced from the hysteresis cycle) as a function of temperature. The field is perpendicular to the *a-b* planes [206].

to optimize the microstructure of Bi single crystals and films (very recent data on textured Bi(2212) are in favour of the last hypothesis [211, 212], see section 9).

**$La_{2-x}Sr_xCuO_4$.** Due to the difficulty to prepare single crystals of $La_{2-x}Sr_xCuO_4$ of sufficient quality, there is at present much less data on the critical current densities of these compounds than in the two preceeding HTSC (Y and Bi) compounds. The temperature dependence of the magnetic critical current density of some single crystals of $La_{2-x}Sr_xCuO_4$ is displayed in figure 30 for $J_{ab,c}$ (i.e. $H$ parallel to the $c$-axis) [208-210, 216]. Here as well,

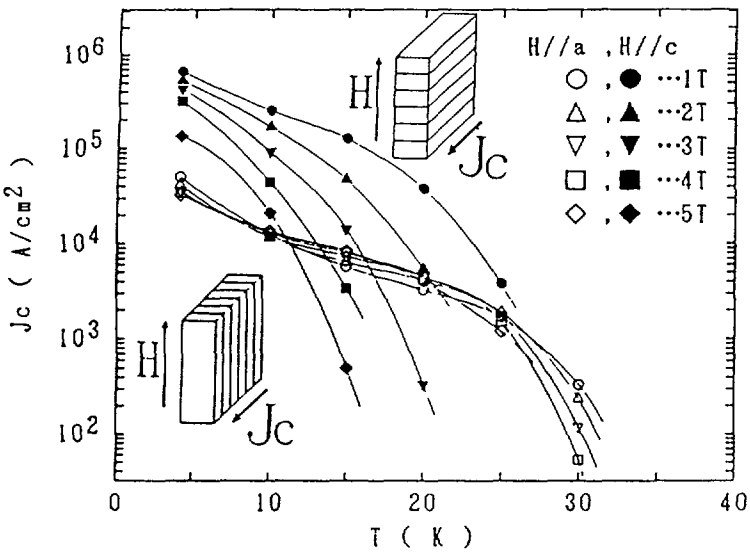


Fig. 30. — Evolution of the magnetic critical current density for a single crystal of $La_{2-x}Sr_xCuO_4$ (dimensions of about 4 × 2 × 1 mm$^3$) as a function of temperature. The field is perpendicular to the *a-b* planes [216].

$J_{ab,\,c}$ falls rather sharply with temperature even though less rapidly than for the case of Y or Bi compounds. It is to be emphasized however that the variation of $J_{c,\,ab}$ (i.e. $J$ along the $c$-direction) is found to differ markedly from one single crystal to another [208, 216]. In some cases, especially at high enough field (far from the peak region of $M(H)$), $J_{c,\,ab}$ is almost independent of $T$ from 1.2 K to 10 K and then decreases rapidly with $T$. It is not clear whether this distinctive behaviour has an intrinsic origin or is due to a difference between the microstructural defects responsible of flux pinnings.

**The *J versus T* relationship :** For Y and Bi single crystals with $H$ parallel to the $c$-axis, the critical current $J_{ab,\,c}$ varies (in a first approximation) as :

$$j(B, T) = J_0(B)(1 - (T/T_c))^n \, e^{-\frac{T}{T_0}} \tag{31}$$

with in many cases $T_0 \approx 20$ K for Y(123) [20, 139] and $T_0 \approx 5$ to 6 K for Bi(2212). As we shall see later we find that n is of the order of 1 to 1.5 (for $T$ not very close to $T_c$ and for laboratory available fields). We emphasize that the above expression is not intended to be rigorous espetially very close to the irreversibility lines for which we have almost no experimental data.

We have already mentioned (Sect. 4) that the above expression for $J(T)$ can be interpreted in different ways : Firstly, it can always be described by a distribution of the strengths of the pinning barriers [135, 136]. Secondly it is also consistent with a pinning potential $U(r)$ which varies logarithmically with $r$ at large distances [139-141]. Thirdly we have also seen in section 4 that other mechanisms (more typical of HTSC) based on collective pinning and collective thermal fluctuations [172-175] have been suggested to account for temperature, field and time dependences of the magnetization. However, it turns out that none of these models can explain the anomalous drop of $J$ with $T$ for all of the three HTSC families considered above, in particular for H oriented along other directions than the $c$-axis. In fact, at the microscopic level the interpretation of the temperature dependence of $J$ is closely related to the question concerning the origin of flux creep in HTSC as well as to the physical meaning of the irreversibility lines. This important point will be further discussed when examining this line in section 17.

In any case, it is clear that the identification and the control of the pinning mechanisms which are at the origin of $J$ should help resolve this question. Therefore, the next two sections deal with the dependence of $J$ on physical and chemical defects particularly in Y(123).

7.3 EXTRINSIC PINNINGS : INFLUENCE OF CHEMICAL AND PHYSICAL DEFECTS ON $J_{ab,\,c}$ AND $J_{c,\,ab}$. — The most classical route to improve the critical current is to add to the superconducting matrix an appropriate amount of pinning centres, with dimensions comparable to the coherence length $\xi$. The concentration of pinning centres must be high enough to anchor a maximum number of flux lines but not too high to avoid perturbing significantly $T_c$ and other fundamental parameters such as $\xi$ and $\lambda$. In conventional materials this is often achieved by the addition of some ordinary metals and then applying some appropriate heat treatments and mechanical work. Unfortunately, the situation is more complicated in HTSC, the superconducting properties of which are strongly sensitive to small deviations from the stoichiometric composition of oxygen and copper and cannot be plastically deformed. Concerning deviation from stoichiometry, it is important to keep in mind that very small deviations can increase the critical current density. However, to our knowledge there is not yet systematic investigations to determine the threshold limit below which this deviation will cease to improve $J$ and becomes to deteriore it. This threshold value is not an intrinsic quantity but would depend on the local distribution of the defects and thus on heat treatments

and other factors affecting this distribution. This is because $J$ depends strongly both on the chemical nature of the defect and on the shape and the dimension of the clusters formed by such defects. It turns out that clusters of dimension 2 to 6 $\xi$ (the coherence length) provide the most favourable critical current density. Defects of this size would indeed allow the vortices to lower significantly both their core and their electromagnetic energies [139] without perturbing very much the superconducting state (at least for isolated clusters). Clearly, this is a very important topic which needs more experimental as well as theoretical investigations.

7.3.1 *Substitution of Cu, Bi, Tl, Nd by other metallic elements.* — It turns out that at the present state of the art, direct substitution of Cu by other ordinary elements (such as silver, gold, aluminium [217-224], zinc [225-228]) or by transition metals (Fe, Co, Ni [229-231]) is either practically impossible (immiscibility of Ag, Au, Al in HTSC) or yields no encouraging improvement of the critical current and often has even negative effects on $J$ (iron, zinc, . . at least for the usual range of nominal concentration above 1 %). Of course this is when the substitution is possible. However from a number of works it is found that in appropriate conditions silver improves mechanical properties (ductibility, casting) as well as intergrain currents for granular or textured materials especially for Bi compounds [232-234], but also for YBaCuO systems [235-237]. It is however of interest to note that partial substitution of Bi[238] or Tl[206] by Pb and Y by Ca in $Y_2Ba_2Cu_4O_8$ (denoted 124) [101] improves $J$ significantly in the corresponding oxides. A very promising technique for the improvement of $J$ is *via* the use of dispersive fine precipitates of secondary phases [239-234]. As emphasized just above, the dependence of $J$ on these defects would be very sensitive to the concentration, the shape and the dimension of the clusters formed by such defects.

7.3.2 NEUTRON, ION AND ELECTRON IRRADIATIONS. — Another encouraging technique for the improvement of $J$ is neutron bombardments [244-251] at small and moderate fluences. The results are very positive not only for Y-compounds but also for Bi and other oxides and concerns single crystals, textured epitaxial thin films as well as intragrain currents in sintered and textured materials. It is indeed found that $J$ can be increased significantly (more than one order of magnitude) by means of neutron irradiation. What is very interesting from the point of view of technical applications is that the enhancement of $J$ is much more efficient at high temperature ($T \geq 60$ K) than at 4.2 K, as illustrated in figure 31 of references [244, 250]. The influence of electron [252-255] and ion [256-258] irradiations is less clear (in many examples) and seem to be rather damaging for $J$ in the case of electrons and somewhat more positive in the case of ions. However, recent bombardment of YBaCuO single crystals by 500-MeV Sn-ions [258] revealed strong increase of $J$ at all temperatures together with a large displacement of the irreversibility line towards high $T$ and high $H$ values. The results depend also on the fluence and the kinetic energy of the incident particles and their nature. The effects of both neutrons and ions as well as ectrons are discussed extensively in two complementary papers by Kirk [259a]. In fact, the idea which emerges from theses papers is that the variation of the critical current as a function of both the nature of the incident particles, their fluences and their energies can be described by a unique function (related to the critical current density) and a unique variable called « recoil parameter $\varepsilon$ ». In the case of electrons, this function is very narrow, sharp and centered at relatively low $\varepsilon$. It is broader and centred at higher $\varepsilon$ for ions. Finally, it is much more smoother and rather weak for neutrons. The recoil notion is very useful as it tells us how to optimize the « extrinsic » critical current in irradiation experiments. The physical factors relevant for the improvement of $J$ in irradiation experiments have been also extensively investigated and clarified very recently by Hardy *et al.* [259b].

7.3.3 *Influence of twin boundaries and stacking faults.* — Twin boundaries are also found to

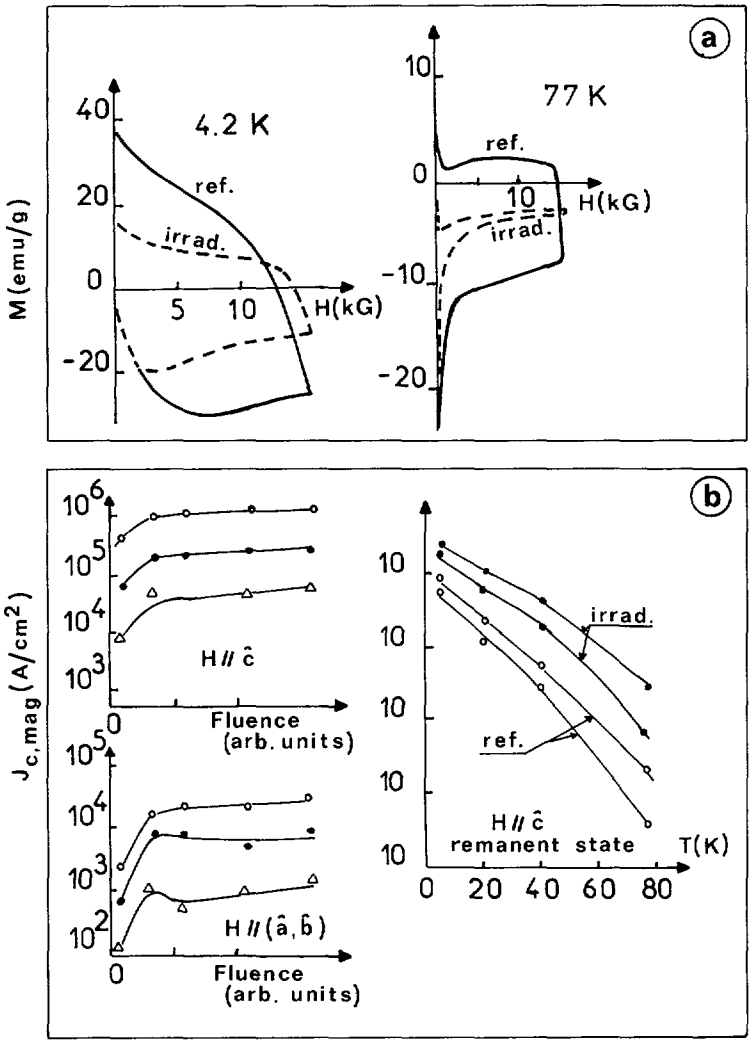


Fig. 31. — Change of the hysteresis cycle at the indicated temperatures as a result of neutron irradiation according to Wisniewski *et al.* [244] (a), and to Sauerzopf *et al.* [250] (b).

improve the intragranular critical current density more efficiently at high $T$, especially at $T$ of the order of 70 K and above [63, 261-263]. Direct counting of the vortex density around twin boundaries in decoration experiments [264] shows no detectable influence of the twin boundaries at low temperatures (decoration performed at helium temperature). The vortex gradient is not imposed by twin boundaries but rather by smaller defects, invisible to SEM, in normal resolution mode. Theoretical models [261, 265] also predict enhancement of the critical current density by twins. There are however some contradicting claims in the literature that $J$ is either enhanced [266] or very strongly decreased [267] in untwinned materials. We believe that twin boundaries do not behave like weak links and have quite a positive influence on $J$ at least at high temperature. This will be justified in section 9.4 concerned with weak links. This is also in agreement with the effect of other extended defects such as stacking faults [268, 269]. For a review paper on twins see Hoff *et al.* [265]. It is likely that other defects

abundantly present in the sample (small inclusions, small voids of dimension $\approx \xi$, stacking faults [270] etc.) will also contribute to the pinning forces and hence to $J$. It was shown recently by Aguillon *et al.* [154] that dislocations lying in the *a-b* basal planes enhance $J_{c,\,ab}$, that is the pinning forces parallel to these planes acting on the vortices parallel to the same planes.

More quantitative conclusions on the influence of these kinds of defects require systematic investigations of the microstructure by transmission electron microscopy and subsequent correlations of the microstructure with macroscopic measurements of $J$. There are several groups attempting to carry out such kinds of investigations at present, but the results are rather slow due to the extreme difficulties to carry out correct analysis of the experimental data.

7.4 INFLUENCE OF INTRINSIC PINNINGS ON $J$. — It is to be recalled that due to their layered structures, high $T_c$ materials also exhibit strong intrinsic pinning barriers (these forces have been introduced briefly in § 2.1 and will be defined more precisely in § 14.2). However, these barriers and the associated critical current density $J_{ab,\,ab}$ are hardly detected by means of conventional magnetic measurements. $J_{ab,\,ab}$ is also difficult to probe by transport current measurements as the latter can be severely reduced by the presence of any kind of weak links in the material (see Sect. 10 concerning textured samples for a more detailed discussion of this point). As a consequence, the temperature dependence of $J_{ab,\,ab}$ is still completely unknown at present. In fact, it is not impossible that the intrinsic pinning force remains very large up to higher temperatures (that is to say 77 K), even for Bi and other HTSC families. This is inferred from equations (9a) and (11b). One argument in favour of this claim is that, since the spatial variation of the intrinsic pinning barriers is periodic in the $c$-direction ($U_i(r + \mathbf{c}) = U_i(r)$ where $\mathbf{c}$ is the lattice spacing vector in the $c$-direction), its spatial dependence would be closer to a sinusoidal pinning potential of the kind considered by Beasley *et al.* [129] and by Xu *et al.* [130] than to the logarithmic potential of Zeldov *et al.* [140, 141] and Manuel *et al.* [139]. We have seen in section 4 that the latter leads to an exponential drop of $J$ with $T$ whereas the former yields a simple power law for $J(T)$. It is certainly of great interest to calculate the expected temperature behaviour of the intrinsic current and the associated $U(J)$ of Beasley-like curve in the flux creep model. Chakravarty *et al.* [271] have investigated thermally activated flux creep (across the intrinsic barriers) in strongly layered HTSC, using collective pinning and thermal fluctuations theory. At this point we would like to add the following remark : thermal fluctuations of the vortices through the intrinsic barriers are expected to be much lower (probably by a factor of the order of the mass anisotropy ratio $m_{ab}/m_c$) than when the vortices are parallel to the $c$-direction. Therefore, this is a second argument supporting our idea that $J_{ab,\,ab}$ remains very large up to 77 K. A third proof in favour of this claim will be given in sub-sections 15.5 and 15.6 concerning the critical current of thin films.

The above discussion about intrinsic pinning assumes tacitly that the material has no defects (or equivalently $J_{ab,\,c} = 0$). We believe that the presence of imperfections, especially weak links, reduces the intrinsic current $J_{ab,\,ab}$. This can be proved in several limiting examples.

The first problem is how to get rid of weak links the effect of which is probably more dramatic (on the basis of the topological arguments below) in the case of intrinsic pinning than in that of extrinsic pinnings. To see the physical origin of this effect, let us consider a linear defect of transverse dimension greater than or of the order of $\xi$ (such as a dislocation) lying in an *a-b* plane. If the uniaxial anisotropy is low the currents circulating in this *a-b* plane can pass round the defect and are thus not seriously affected by such a defect. On the contrary, for highly anisotropic materials the currents are forced to pass through the linear defect. Since the latter has a diameter larger than $\xi$ it behaves like a weak link and hence imposes a severe

reduction of the contribution of the considered *a-b* plane to the critical current density (this point is discussed further in Sect. 9.4). To end with this matter, we would like to add the following remarks valid whatever the shape of the defect : (i) At first, assuming that axis *c* is parallel to the *z*-direction we note that intrinsic pinning is expected to be proportional to $[\max |\Psi(z)|^2 - \min |\Psi(z)|^2]$ where $\Psi(z)$ is the *z*-dependent order parameter. (ii) For highly anisotropic layered materials, we have $\min |\Psi(z)| \approx 0$. (iii) We also expect that $\max |\Psi(z)|^2$ is in general decreased by defects. (iv) As a consequence, we can conclude that, contrary to $J_{ab,\,c}$, $J_{ab,\,ab}$ should be lowered by defects at any concentration. (See Sect. 14 for other details concerning intrinsic pinnings.)

We know that there are essentially three conventional techniques to probe the intrinsic forces in single crystals and in thin films with no weak links. These are :

(1) Transport measurements with **J** and **H** perpendicular and both lying in the *ab*-planes. We have seen that the main problem in this case is how to correct for surface London-Abrikosov currents, especially in thin films.

(2) Torque measurements performed during tilting the direction of the applied field (of constant amplitude) up and down around the *a-b* planes. This experimental technique is generally very powerful. The major problem in this case concerns the interpretation of the data as it is likely that the vortices do not follow rigidly the rotating field (kink effects). Other serious problems appear at low tilting angles (or fields) as the critical state can break down in some conditions. See section 13 for more development on this point.

(3) A third method for the determination of the intrinsic energy barriers is by means of conventional magnetic measurements. As will be discussed later in section 14 about anisotropy effects, this method works only for extremely thin samples in the *c*-direction, with an aspect ratio (width to thickness of the sample) of the order of or larger than the current anisotropy ratio $J_{ab,\,ab}/J_{c,\,ab}$. This is $\approx 200$ for Y(123), probably about 1 000 for $La_{2-x}Sr_xCuO_4$ and 10 000 for Bi families. Nevertheless, if by some means the above conditions were fulfilled (not impossible for Y(123)), then magnetic measurements would become extremely interesting. In this case we know how to correct for the London-Abrikosov current (see Sect. 10). In addition, in such direct magnetic measurements the vortices do not need to be inclined with respect to the *a-b* planes and therefore the analysis is not complicated by kink effects.

## 8. Intergranular critical current in sintered materials.

This section is devoted to experimental intergrain critical current densities ($J_{wl}$) in granular materials in the limit where the degree of alignment between grains is negligible (random distribution of the crystalline axes) and the Josephson coupling weak, but not zero. We shall, in particular, consider the experimental variation of $J_{wl}$ with *T*, *H*, *R* and $r_g$. We shall also examine the influence of metallic alloying as well as ion, electron, and neutron bombardments on this current. Contrary to the case of intragranular currents (in single crystals and isolated grains) considered just above most of our knowledge on intergranular currents is obtained by means of transport measurements. There are essentially two reasons for this. Firstly, we know that in general intergranular current densities are rather low and hence relatively easy to measure directly because of the moderate Joule heating. Secondly, until very recently, due to the complexity of the weak links problem, there have been no quantitative models relating the hysteresis cycle of granular materials to the macroscopic critical currents. The same is equally true concerning the a.c.-susceptibility. However, we shall present in the following sections a quantitative model developed by Senoussi *et al.* [77, 104] which allows us to relate the magnetic critical current density ($J_{mag}$) to the low field structure of the magnetization of polycrystalline materials (see Figs. 32a-c) as well as to the imaginary part of the ac-

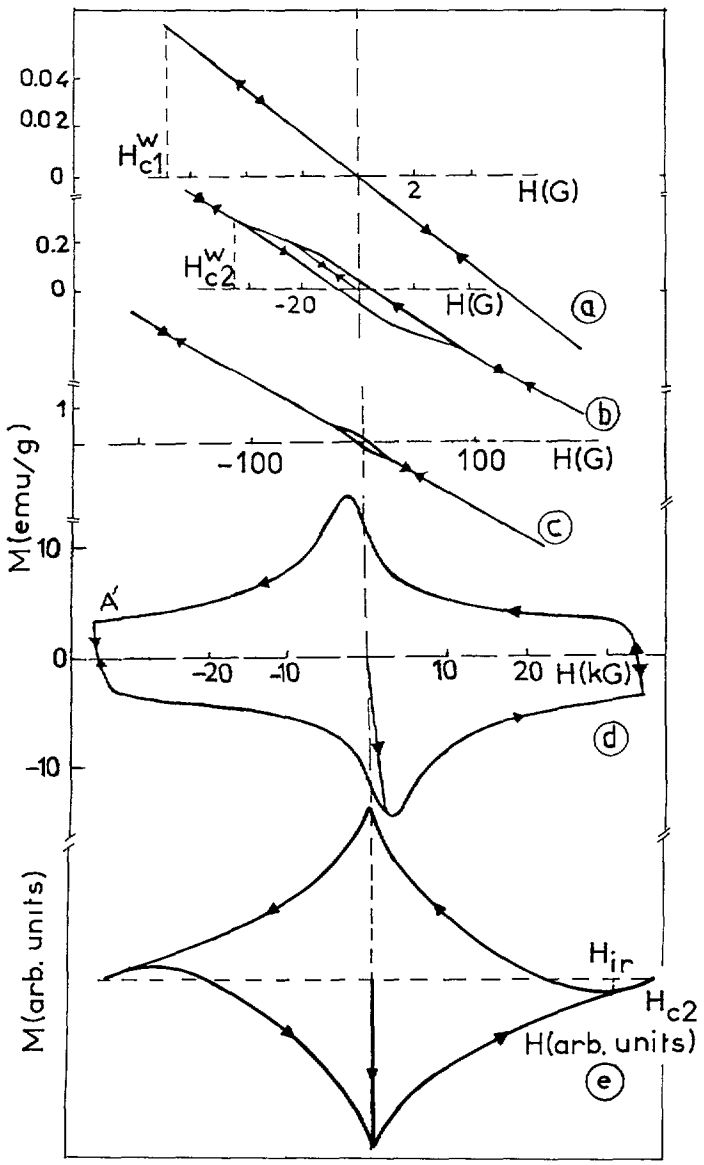


Fig. 32. — Experimental magnetization loops of granular $YB_2Cu_3O_7$ at increasing field scales (a, b, c, d) extending from $H < H_{c_2}^{w}$ to $H^{ir}$. (e) Schematic variation of $M$ in the depinning line region. This example is typical of sintered granular superconductors. At very low-$H$ $M$ is linear, reversible and exhibits perfect screening.

susceptibility (the latter will be deferred to Sect. 12). Very often indeed, the *M versus H* relationship exhibits two well separated loops as a function of $H$ the low field of which is connected with the weak link network [96-98, 104] whereas the high field one corresponds to intragrain currents flowing in independent grains. The physical interpretation of these hysteresis cycles is presented schematically in figure 33 which are based on the model developed in section 11.

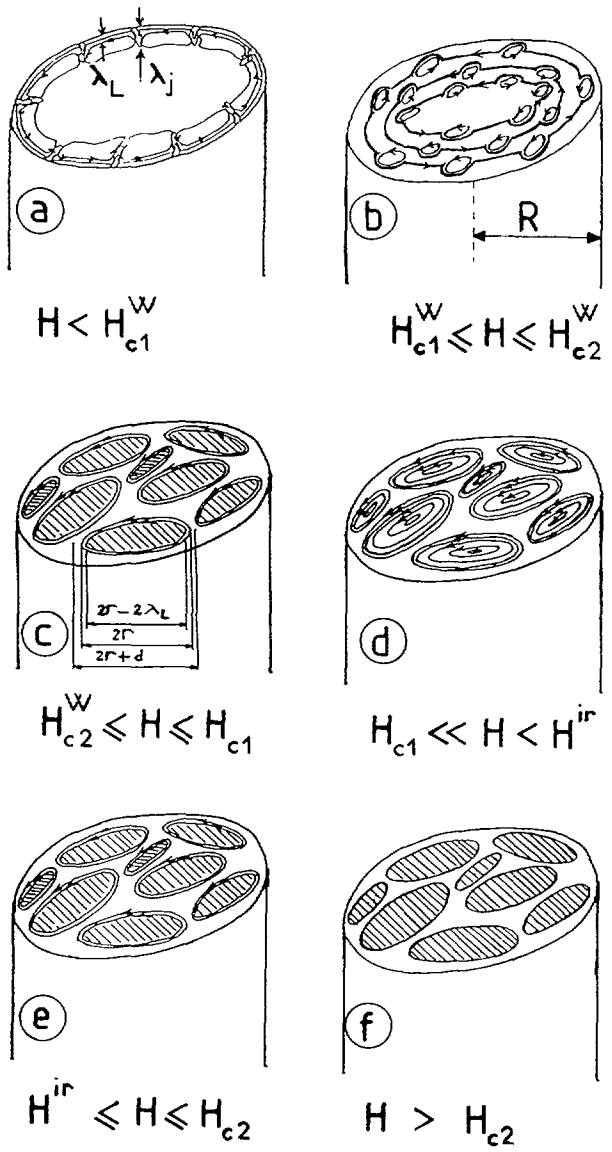


Fig. 33. — Qualitative illustration of the way magnetic flux and currents penetrate and develop through the sample as a function of the applied field (see Fig. 32 for the correspondence with the hysteresis loops a, b, c, d, e). In (a) the current is restricted to the depth $\lambda$ in the grains and to $\lambda_J$ in the junctions between grains. (e) : Above the depinning line the current is restricted to a surface region of depth $\lambda$ as for $H < H_{c_1}$.

Figure 33a shows that for $H$ smaller than $H_{c_1}^{w}$, the first critical field of the weak links, the currents and fields are restricted to the Josephson penetration depth $\lambda_J$ in the junction and to the London penetration depth $\lambda$ around the grains ($\lambda$ is determined by different techniques in [275-280]). As $H$ is further increased above the characteristic field $H_{c_1}^{w}$ (Fig. 33b), flux lines together with the associated currents penetrate the sample *via* the weakest links. This gives rise to macroscopic current loops (extending over the whole sample) as well as to microscopic

loops of London currents circulating around individual grains (note that these London currents are not present in the measured intergranular transport critical current). At fields larger than the weak link decoupling field ($H > H_{c_2}^{w}$, Fig. 33c) the macroscopic current (or intergranular current) vanishes and the magnetic behaviour is governed solely by the London currents surrounding decoupled grains ($H \leqslant H_{c_1}$). Finally, at still higher fields, exceeding the first critical field $\mathbf{H}_{c_1}$ of the grains, vortex lines and the associated intragrain currents propagate into the interior of the grains (Fig. 33d). Above the depinning line the current is restricted to the London-Abrikosov's surface current $J_s$ (Fig. 33e) and becomes zero only above $H_{c_2}$. The hysteresis cycles corresponding to the five situations of figure 33 are illustrated in figure 32 for granular $YBa_2Cu_3O_7$ at 4.2 K. A more systematic investigation of the hysteresis cycle of $YBa_2Cu_3O_7$ as a function of field and temperature is reported in references [13, 96, 97].

8.1 FIELD DEPENDENCE OF INTERGRANULAR CURRENT DENSITY $J_{wl,\,tr}$. — A vast amount of data reported in the literature indicate that $\mathbf{J}_{tr,\,wl}$ decreases severely with the applied field. This is illustrated in figure 34 from Evetts and Gloacki [73] where it is seen that the current drops practically to zero in less than 60 G. This abrupt drop of $J$ with $H$ seems to be very general (whatever the material and the method of preparation employed) when the degree of texturing is negligible and whatever the temperature.

From numerous examples reported in the literature on HTSC it is found that at slightly higher fields such that $H > H_{c_1}^{w}$ (see Figs. 32, 33 for the definition of $H_{c_1}^{w}$) the macroscopic current varies as $1/H^n$ with $n$ generally ranging from 1 to 2 [41]. Sometimes, the field variation of $J_{tr}$ is even more rapid and approaches an exponential law for junctions of highly metallic character (SNS). Of course, the field dependence is faster at high temperatures near $T_c$. Also, the $J_{wl,\,tr}$ *versus* $H$ relationship is often very different from sample to sample even for specimens prepared exactly in the same conditions. As discussed in section 5 and section 6 this is probably because of irreversibility effects in the current [39, 40, 73] and because of the self-field (see also discussion below) which depends on the shape (but in particular the diameter $D$) of the sample.

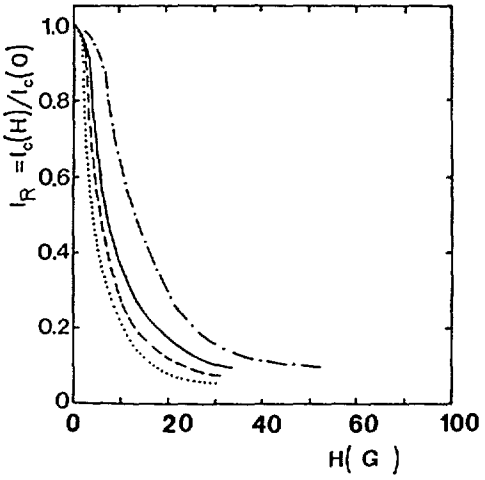


Fig. 34. — Field dependence of the transport critical current of granular $YBa_2Cu_3O_7$ prepared in different conditions (———) sintered at 940 °C ; (------) sintered at 910 °C ; (—) $YBa_2CU_3O_7$ + 0.1 wt% $SiO_2$ sintered at 910 °C ; (... ) $YBa_2Cu_3O_7$ + 1 wt% $SiO_2$ sintered at 910 °C ; after Evetts and Gloacki [73].

8.2 ON THE ABSENCE OF VARIATION OF $J_{tr}$ WITH THE DIRECTION OF $H$. — Another very unusual feature typical of granular materials as well is the fact that $J_{wl,\,tr}(H)$ is found to be generally independent of the angle between the applied field and the direction of the macroscopic current. In other terms, for granular materials (with no texturing) one has $J_{wl,\,tr}(H_{\parallel}) \approx J_{wl,\,tr}(H_{\perp})$ where $H_{\parallel}$ and $H_{\perp}$ indicate parallel and perpendicular to the average direction on the transport current. This apparent isotropy of the granular transport current has often been interpreted as a proof for the absence of a Lorentz force in these materials. This affirmation is probably wrong and a more realistic interpretation ascribes the « macroscopic isotropy » of $J_{wl,\,tr}(H)$ to the fact that the directions of the local currents (contributing to the macroscopic current) are to a first approximation randomly distributed within some solid angle probably of about 180°. The angular distribution of the directions of the local current density is produced by the combination of the granular structure and the strong anisotropy of the Josephson current [282, 283] which make the current paths very complicated. Consequently, the Lorentz force in granular materials is not zero locally but its average strength would be, to a first approximation, independent of the direction of $H$ with respect to the direction of the global transport current.

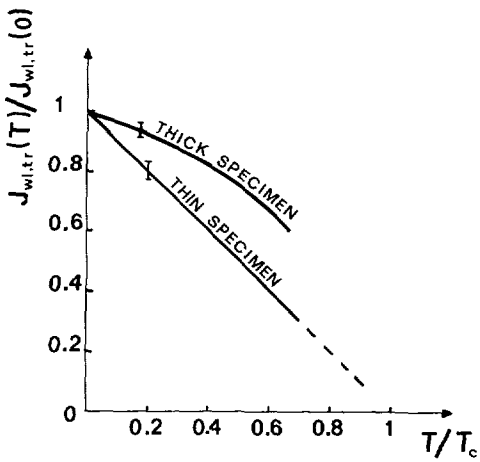


Fig. 35. — Temperature dependence of the transport critical current at zero applied field of a granular $YBa_2Cu_3O_7$ prepared in different conditions (Kormann *et al.*, private communication).

8.3 INFLUENCE OF THE RADIUS $R$ OF THE WIRE ON THE CURRENT, MACROSCOPIC SIZE EFFECT. — There are at present many experimental studies [285, 286] proving that the macroscopic current of sintered materials decreases with the radius $R$ of the wire as $1/R$. This is illustrated in figure 36 from references [281, 285, 286]. The physical origin of this behaviour has already been extensively discussed in section 6. It is likely that this size effect is due to the self-field of the current circulating along the wire. At first sight, these experimental results suggest that the transport current can be increased illimitedly (or at least very largely) for arbitrary thin wires. Unfortunately, we know from the results of section 6 that the $1/R$ behaviour is a characteristic feature of thick samples and that both $J_{wl,\,tr}$ and $J_{wl,\,mag}$ must reach a saturation value $J_0 = J(B = 0)$ as soon as the radius $R$ becomes smaller than some characteristic length $R_0$ given by equation (16). To get an order of magnitude estimate of $R_0$ in sintered HTSC we take $B_0 \approx 10^{-3}$ T and $J_0 = 2$ to $5 \times 10^3$ A/cm$^2$. This yields $R_0 \approx 20$ to 50 μm. We have seen that the experimental $J_{wl,\,tr}(B)$ law depends on the radius of

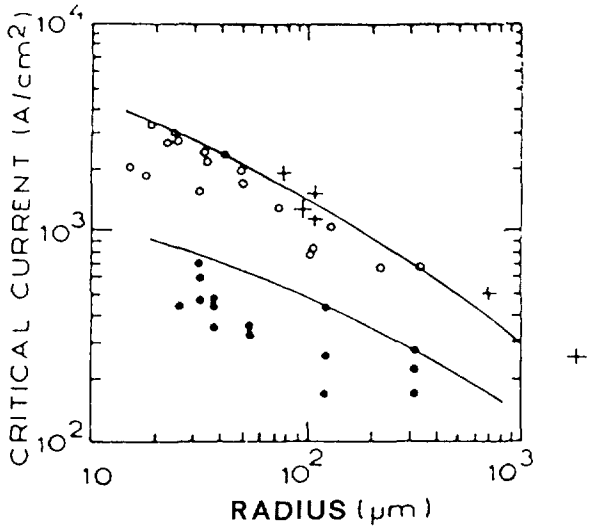


Fig. 36. — Variation of the transport critical current density of sintered $YBa_2Cu_3O_7$ as a function of the radius $R$ of the wire from various sources of the literature (particularly from [285] and [286]). We observe an $1/R$ behaviour of the critical current, presumably connected with the self-field discussed in section 6.

the wire. We shall show later using numerical calculations for $J$ as a function of both $H$ and $R$ that the increase of $J$ due to the reduction of $R$ has some drawback as well : it leads to more sensitivity (i.e. a more rapid decrease) of the experimental current to the applied field $H$.

Figure 35 (from R. Kormann, private communication) shows that the temperature dependences of the critical current densities of two ceramic samples of very different thicknesses extracted from the same batch, are quite different. This is probably connected with the results of section 6 which showed that for very thin specimens ($R \leqslant R_0$) the measured intergrain current should reflect the real current $J_0(T)$ of the junction network whereas for thick specimen it would be more related to the characteristic field $H_0(T)$ and thus would reflect the temperature dependence of this parameter. This is an interesting effect which needs more experimental studies.

8.4 INFLUENCE OF THE DIMENSION OF THE GRAINS ON THE CURRENT, MICROSCOPIC SIZE EFFECT. — There are a number of indications from magnetic measurements [287, 288] that the critical current of granular YBaCuO is approximately proportional to the inverse $1/r_g$ of the radius of the grains composing the sample. This is illustrated in figures 37 and 38 from [287]. However, to our knowledge there is not yet any direct confirmation of such size effect by transport measurements. This interesting point will be reexamined in more detail later in relation to the interpretation of magnetic data at low fields. At this point it is of interest to add that the critical current density of some conventional materials is also found to vary as $1/r_g$ [289].

8.5 TEMPERATURE VARIATION OF $J_{wl,\,tr}$. — Figure 39 shows the variation of $J_{tr}$ as a function of temperature for different $YBa_2Cu_3O_7$ specimens reploted from different sources [189, 290, 292]. It is to be emphasized that this kind of curves does not seem to follow any general or universal law even for samples prepared in the same conditions (i.e. extracted from the same batch). This is presumably connected with the nature of the weak links (metallic, insulating, semiconducting, . ) as well as with the shape of the sample *via* the self-field

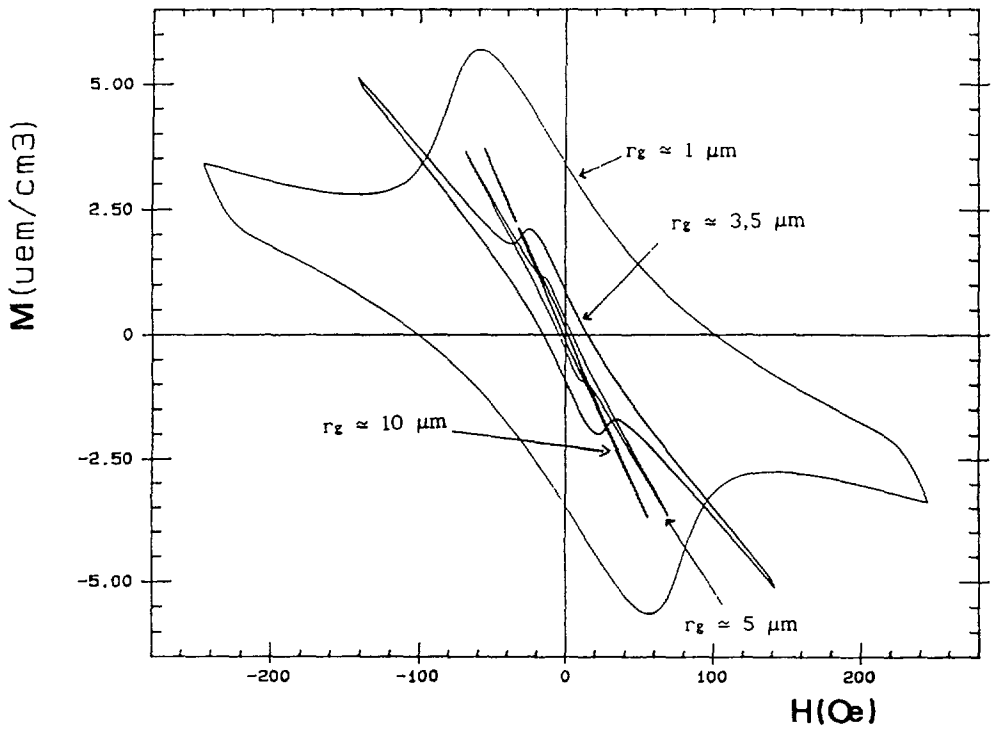


Fig. 37. — Evolution of the low-$H$ hysteresis cycle as a function of the average radius $r_g$ of the grains [287]. Note that the smaller the grains the larger the hysteresis. The quantitative relation with $J_{mag}$ is given in section 10.

(depending on the ratio $R/R_0$ where $R_0$ is defined by Eq. (16)). Of course $R_0$ is expected to vary with $T$ making the interpretations more complicated. This shows that it is in fact nonsense to compare the experimental results with classical theories on weak links unless the condition $R < R_0$ is well satisfied (we have seen that for present HTSC polycrystals $R_0$ is generally smaller than 50 μm at low $T$).

Indeed, according to equations (20b, 24b, 27b, 30a) which correspond to different model calculations in zero applied field we are in general measuring not the local $J_{wl}(T)$ but the field $B_0(T)$ (which controls the variation of $J_{wl}$ with $H$) since for sintered materials the condition $R/R_0 \gg 1$ is generally realized.

8.6 EFFECTS ON $J_{wl}$ OF IRRADIATIONS AND ALLOYING WITH ORDINARY METALS. — By analogy with ordinary superconductors, there are at first sight three classical routes to enhance intergranular currents. (1) The most natural method is texturing in order to reduce the number of incoherent Josephson junctions between grains with different crystalline orientations [107, 282, 283] ((see next Sect. 9) on textured samples for details). (2) The other classical possibility to increase intergranular current is to introduce an appropriate amount of defects at the interface between grains and therefore increase the pinning forces acting on the vortices within these junctions (as we shall see later there are probably more defects naturally in the junction than necessary to pin the vortices). (3) The third method is to improve the quality of the junction as measured, for instance, by its normal state conductivity. These three ways of improving $J_{wl}$ are in fact not independent and seem even contradictory in the case of the last two (it is in principle not possible to increase the density of pinning defects and reduce

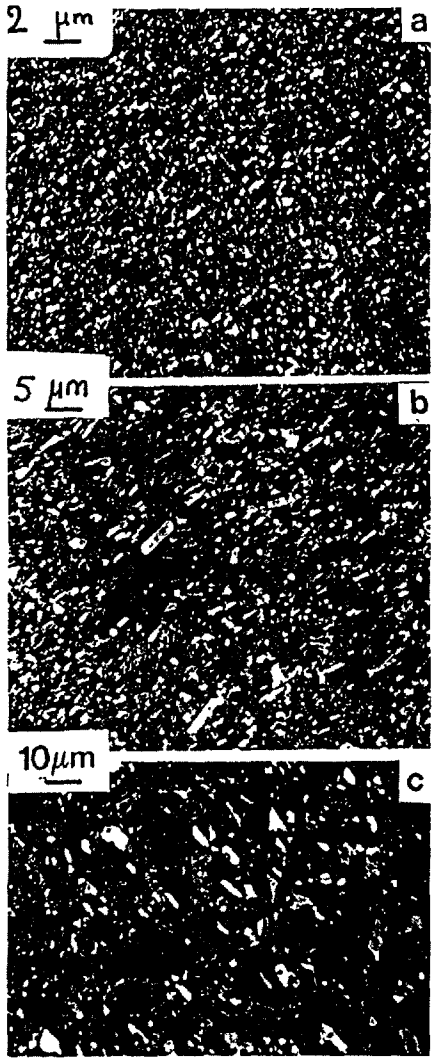


Fig. 38. — Micrographs corresponding to the material the hysteresis cycles of which are shown in figure 37.

the resistivity at the same time). It is indeed known that the most familiar procedure to increase the critical current in conventional superconductors is by the creation of a optimum density of defects with the right dimensions and distributions within the material. This fact led several groups to the conclusion that the transport current of bulk materials can be enhanced by increasing the density of defects within the junctions by means of ion, electron or neutron bombardments. However, the results of these bombardments were generally revealed unsuccessful and rather resulted in a deterioration of the intergrain current $J_{wl,\,tr}$. This is to be compared with the case of intragrain current which is found to be strongly improved by the same bombardment (at small fluence, [244-251]). Since the defects induced by irradiation are expected to increase the local resisitivity $\rho$ everywhere, in particular in the junctions themselves, it seems that the diminution of inter-grain current is directly correlated with the growth of the electrical resistivity due to irradiations.

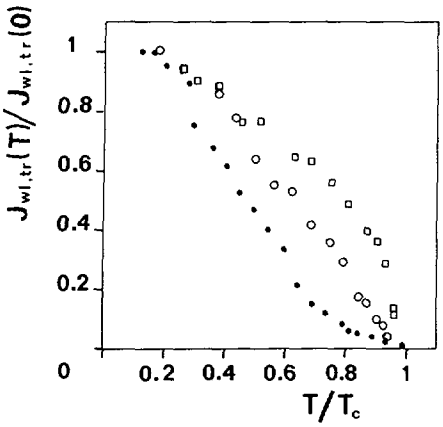


Fig. 39. — Temperature variation of $J_{tr}$ for granular $YBa_2Cu_3O_7$ materials. We see that the *J versus T* relationship is not universal but depends on the sample preparation and dimension [189, 290].

Some studies [293, 294] indicate that intergranular current can be slightly improved, typically by a factor of 2 to 3, by the introduction of a small amount of silver in the grain boundaries. In addition, this is generally accompanied by a sharp drop of the electrical resistivity $\rho$ of the material suggesting that the improvement in $J_{wl,\,tr}$ is not due to the increase of the pinning forces but is rather connected with the drop of the resistivity, in agreement with theoretical predictions (see below the Ambegaokar-Baratoff formula). However, to our knowledge there are not yet many systematic observations (by transmission electron microscopy or by other microscopy techniques) investigating the distribution of Ag within the junctions and thus to clarify the correlation between $J_{wl,\,tr}$ of granular ceramics, $\rho$ and such a distribution of Ag. It is indeed likely that the current pathways are drastically disrupted by segregation of silver the resistivity of which is generally much lower than the normal resistivity of the granular material under consideration. Then, the silver rich regions should act as short circuits for the current and lower the apparent resistivity of the sample making quantitative comparisons with theory not very meaningful.

8.7 DISCUSSION AND CONCLUSION CONCERNING EXPERIMENTAL DATA IN GRANULAR MATERIALS. — The most important conclusions of this paragraph are that $J_{wl,\,tr}$ of sintered materials is generally very low and decreases rapidly with field. The field dependence of the transport current has often been interpreted phenomenologically [295-298] in terms of an average over a statistical distribution of the dimensions ($\sim r_g$) of the Josephson barriers assuming that the current threading each individual junction is given by a Fraunhofer-like formula (see below Sect. 9).

As a matter of fact, these procedures for the calculation of $J_{wl,\,tr}$ were discussed by several authors, in particular by Evetts and Gloacki [73] who pointed out that a number of additional factors make a quantitative fit with the experimental data of doubtful value. From the analysis of the most common experimental conditions, it seems that none of these hypotheses is satisfied in real materials. This point was also discussed in several papers by Senoussi *et al.* [97, 98, 104] some time ago from the point of view of magnetic measurements and from the systematic comparisons between magnetic and transport currents $J_{wl,\,mag}$ and $J_{wl,\,tr}$ respectively. The main conclusions drawn from these investigations were :

1) First of all, magnetic measurements show without any doubt that the intergrain current is related to irreversibility effects and thus to flux traping within the junction network.

2) The junctions are highly ramified, not independent and extend over the whole sample. As a result magnetic flux enter the sample not uniformly but gradually starting from the surface and moving [299, 300, 301] continuously through the weakest barriers to the centre of the specimen.

3) Since $J_{wl,\,tr}$ is found to depend strongly on $H$, the self-field (neglected in the above models) should play a crucial role and must be taken into account in the calculation of $J_{wl,\,tr} \approx \langle J_{wl}(H + H_{sf}) \rangle$ averaged over the sample.

4) If the weak links are of SNS rather than SIS type, as it is probably the case for most sintered YBaCuO materials [73, 192, 193], their critical current will vary more or less exponentially with $H$ instead of the $1/H$ law predicted by the Fraunhofer-like models.

5) Finally, since the Josephson penetration depth diverges when $J_{wl}$ approaches zero, in particular when $T$ approaches $T_c$, the condition $\lambda_J \gg r_g$ is always satisfied near $J_{wl} \approx 0$ and the Fraunhofer picture could be justified in this particular limit. However, it seems that in this temperature region the physical properties controlling the $V(I)$ relationship are very different from that of the flux creep domain and involve percolation problems [302], dimensionality effects as well as spin-glass like effects and so on [304, 305]. We have seen that for the same granular materials prepared in the same conditions the variation of $J_{wl,\,tr}$ with $T$, $H$ and time $t$ can differ considerably depending on the diameter of the sample because of the self-fields.

From the above data and discussion it turns out that with the methods of preparation available at present the most efficiency way to increase $J$ is to improve the quality of the Josephson junctions as measured for example by resistivity. It turns out that this can be achieved through texturing, which is the object of the next section.

## 9. Textured HTSC materials.

In the previous sections (7, 8) we investigated the critical currents in single crystals and in sintered granular materials prepared by standard techniques. We have seen that intragrain current density was in general extremely large in crystalline materials at low $T$. Unfortunately, the dimensions of these materials were very small, of the order of few millimeters in the best cases. Obviously, in view of large scale applications of HTSC, we need long lengths of wires and tapes with sufficiently high $J$ at high enough temperature and field; $J(T = 77\ \text{K}, B = 3\ \text{T}) \geqslant 10^4\ \text{A/cm}^2$ is a reasonable goal. At present, it seems that among the known HTSC oxides only $YBa_2Cu_3O_7$ exhibits the desired $J(T, B)$ value. Unfortunately, the mechanical properties of this material and the conditions of preparation of long wires and tapes are raising great difficulties in this case. On the other hand, it turns out that Bi oxides (BSCCO, BPSCCO, especially the (2223) and 2212 phases) present appreciable deformation when cooled and a nonnegligible critical current in zero field at liquid nitrogen temperature. However, we know that the latter decreases dramatically with the applied field at 77 K and becomes practically of no use at $B > 0.2$ T. Consequently, it appears that for the near future, it would be interesting and realistic to envisage the development of Bi oxides for applications at 4.2 K hoping for more favourable conditions for solving the present difficulties at 77 K or discovering new HTSC which would satisfy all the required conditions (but see subsection 9.3 for very recent and encouraging data). However, even at 4.2 K much development work is still needed, though very encouraging results on Bi systems have been accumulated by a number of groups throughout the world.

Considerable efforts are made presently to overcome the weak link problem and produce highly textured bulk materials. We wish here to emphasize three popular techniques among others.

9.1 MELT TEXTURED GROWTH AND DIRECTIONAL SOLIDIFICATION TECHNIQUES. — The melt textured growth procedure was first introduced by Jin *et al.* [306-308] and further developed by other workers [309-314]. In this technique the grain growth is controlled by the temperature gradient and by the growth rate of the crystallites. Zone melting has also been used with some success to develop texture in Y and Bi based oxides [315-319]. In this procedure a molten zone is moved along the sample at a controlled rate. These two methods can be considered as a variant of the directional solidification technique. Both have the advantage of minimizing the amount of unreacted materials at the grain boundaries, therefore improving the qualities of the Josephson junctions. Critical current density as high as $7.5 \times 10^4$ A/cm$^2$ at 77 K was first obtained by Jin *et al.* [306-308] along the easy current direction (i.e. in the *a-b* planes) of textured samples of YBaCuO. On the other hand, more recently Chaffron *et al.* [313] and Aguillon *et al.* [25, 314] were able to obtain critical current densities of about $7 \times 10^3$ A/cm$^2$ along the hard current direction (*c*-direction) of YBaCuO prepared by the directional solidification method. This value was derived from both transport and magnetic measurements as illustrated in figure 40 below. It can also be deduced from figure 40 that $J$ might be as high as $2 \times 10^6$ A/cm$^2$ at 4.2 K which is the same value as in standard single crystals. Note that the transport point is slightly above the magnetic one. This can be explained by relaxation effects which, as we know (Sect. 4), are more important in magnetic measurements.

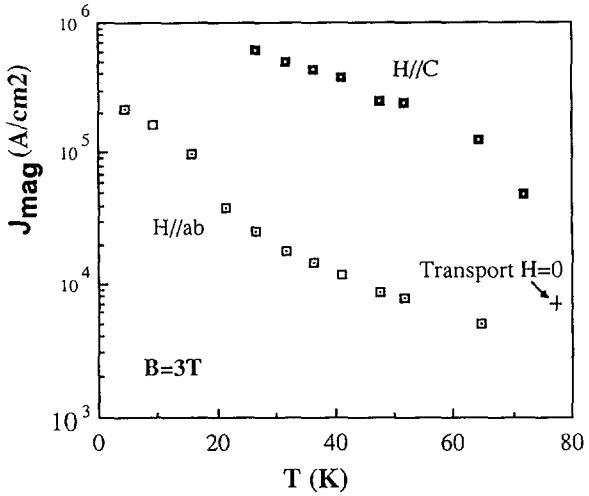


Fig. 40. — Critical current density of a YBaCuO prepared by the directional solidification technique (after Aguillon *et al.* [25]) for $H$ parallel to the *c* direction and $H$ lying in the *a-b* planes. The cross point corresponds to transport measurements at 77 K whereas the other data are deduced from hysteresis cycle recordings using the macroscopic radius ($\approx$ 1 mm) of the sample in Bean formula.

Even though the above techniques mark a considerable progress with respect to the standard sintering samples, so far the dimensions produced in this way have been of the order of few centemetres, thus still very small for suitable applications. From the practical point of view one of the problems of these methods is the excessively long time (several weeks) required for the obtention of these highly textured but relatively short samples.

9.2 MAGNETIC FIELD INDUCED TEXTURING. — A second texturing method which is begining to be explored is through the application of a magnetic field in the melted phase [320-325]. In

this case the alignment of grains in the solid state is very poor (virtually zero). Therefore, high degree of texturing by magnetic methods requires : (1) the existence of a sufficiently large anisotropy ($\Delta\chi$) in the paramagnetic susceptibility near the melting temperature and (2) the coexistence of a liquid phase with crystallites of large enough dimensions so that the anisotropy ordering energy $vH^2\Delta\chi/2$ is larger than the thermal disordering energy $kT$. Here $v$ is the average volume of the crystallites.

Detailed analysis of the mechanisms governing the dynamics of the alignment of paramagnetic grains in a viscous medium can be found in references [322-325]. The case where yttrium is substituted with other rare earth ions (ReBaCuO) has been investigated by Ferreira *et al.* [324]. The major interest of magnetic alignment lies in the fact that it can be relatively rapid. For instance, according to the calculation of Regnier *et al.* [321], in realistic experimental conditions (grains embedded in epoxy resin at room temperature, but the same calculation can be applied in other experimental conditions) only a few minutes should be sufficient to obtain 90 % alignment at 1 Tesla. By combining the calculations of Regnier *et al.* [321] and those of Ferreira *et al.* [324] we can show that the time $t$ required to get a given fixed degree of alignment (90 % for instance) varies as the factor :

$$\exp(-\eta\beta VH^2/T^3)\,. \tag{32}$$

Here $\eta$ is the viscosity coefficient in the liquid state and $\beta$ is a numerical factor proportional to the paramagnetic anisotropy at $T = 300$ K ($\Delta\chi$ (300 K)). We see from this formula that the time of alignment can be made relatively short (a few minutes to a few hours probably) even at very high temperatures, using the highest available magnetic fields (10 to 15 T typically). This is to be compared with the annealing time of several weaks involved in the melt textured growth procedure. Since the degree of alignment increases exponentially with the volume of the crystallites it is clear that the magnetic method is not efficient before the crystallites have reached some critical size. The drawback is then in the possible formation of agglomerates of polycristalline particles before attaining this critical size.

To date the degree of texturing as well as the length of the specimens obtained by the magnetic method are notably smaller than in the directional solidification procedures recalled above. It is probably possible and recommended to combine the two methods to obtain the associated advantages.

9.3 THE SILVER SHEATHED OR THE POWDER TUBE TECHNIQUES. — We have seen that in the two techniques described just above the dimensions of the textured material were, up to now, limited to few centimetres. It is likely that much longer specimens will be achieved soon using these techniques. However, the main problem in these cases is the difficulty to control the shape of the specimen, thus reducing the possibilities of industrial applications based on these techniques. Perhaps a more promising route, at least for Bi based oxides, is the so called powder tube or silver sheated method. This technique seems to be very promising for Bi based oxides especially at 4.2 K where values of $J$ up to $2 \times 10^4$ A/cm$^2$ in $B = 30$ Tesla were achieved first by Mimura *et al.* [324]. This method is extensively investigated at present [325-338]. Magnetic critical current densities of order $10^4$ A/cm$^2$ to $4 \times 10^4$ A/cm$^2$ are obtained in Bi oxides at 77 K in zero field [332, 337]. Unfortunately, in this case $J$ drops severely with $B$ becoming negligible at less than one Tesla at 77 K. However, very encouraging results have been reported recently by Sumitomo Electric group in Osaka [211] who found critical currents $J_{tr}$ (Bi compounds) as high as $J(T = 4.2\text{ K}, B = 23\text{ T}) = 1.3 \times 10^5$ A/cm$^2$, $J(77\text{ K}, 0\text{ T}) = 4.7 \times 10^4$ A/cm$^2$, $J(77\text{ K}, 0{,}1\text{ T}) = 3.1 \times 10^4$ A/cm$^2$, $J(77\text{ K}, 1\text{ T}) = 1.1 \times 10^4$ A/cm$^2$. We would like to note that these transport values probably represent what we have termed intrinsic current density $J_{ab,\,ab}$ which is, as discussed previously, expected to be much less

sensitive to thermal fluctuations than $J_{ab,\,c}$. We recall that $J_{ab,\,ab}$ is extremely difficult to probe by magnetic measurements especially for Bi and Tl based cuprates.

Figure 41 (inspired from Jin *et al.* [306]) compares qualitatively the values and the field dependences at 4.2 K of the various $J$ obtained by the different techniques just discussed and by the more usual procedures investigated in the preceding sections (7, 8) (note that the recent data of Sato *et al.* [211] are not included in this figure).

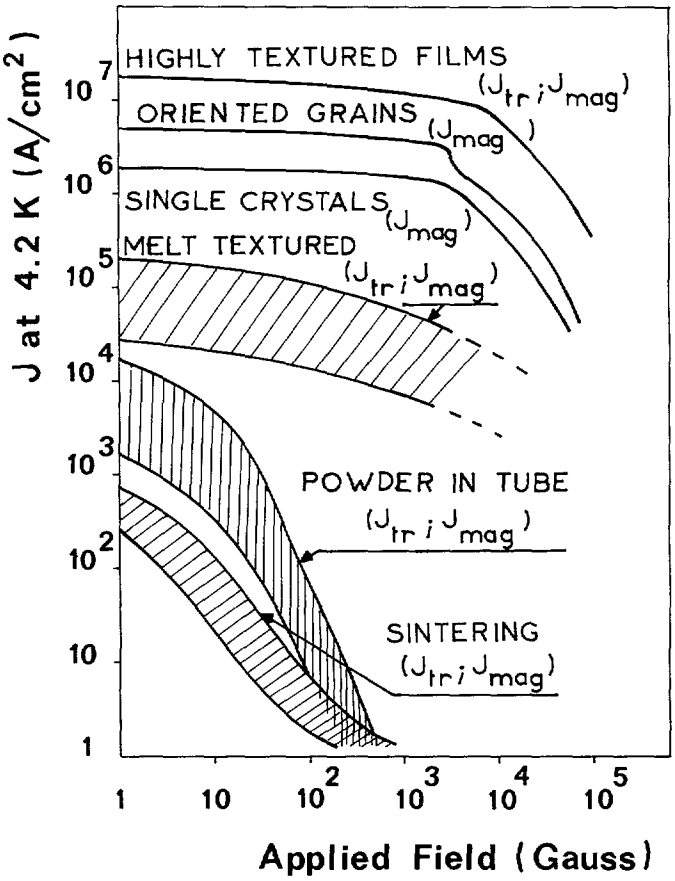


Fig. 41. — Qualitative diagram (note the logarithmic scales) of the critical current densities in the basal *a-b* planes of YBaCuO achieved by the various preparation techniques discussed so far. From the top to the bottom of the figure we have successively : thin films, fine oriented grains, single crystals, directional solidifications and melt textured samples, powder in tube and standard sintering methods.

At present we do not readily know the physical origin of the fast drop of $J_{ab,\,c}$ with $H$ and $T$ in Bi cuprates. In particular, it is not yet clear whether this dramatic fall off is due to weak links or to the lack of appropriate pinning defects or to a more fundamental mechanism such as the melting of the vortex lattice (assisted by anisotropy). However, the results of [211] mean that the density of weak links is very low in their systems (see next section for more quantitative estimates of this density). This implies that it is now possible to decide whether the dramatic exponential drop of the magnetic current, ($\approx J_{ab,\,c}$) with $T$ and $H$ is due to weak links or to one of the two other mechanisms just mentioned. We believe that in any case,

weak links should play a major role in textured materials. This is why we wish to discuss this point briefly now from a semi-microscopic point of view.

We know from the previous section that one of the easist way to detect the presence of weak links is by means of low field measurements (low-$H$ cycle). This point will be further clarified in the next section.

9.4 THE CRITICAL CURRENT IN THE PRESENCE OF WEAK LINKS. — To help clarifying the physical situation we first recall the magnetic and transport behaviours of a single Josephson junction as a function of its width ($w$) relative to its penetration depth $\lambda_J$ (Fig. 42). We know from early theoretical works by Ambegaokar-Baratoff [339] that at finite temperature the current density of a given ideal Josephson junction (in zero effective field) is inversely proportional to its normal state resistivity $\rho_J$ and is given by :

$$J_J \approx \frac{\pi}{2e} \frac{\Delta(T)}{\rho_J} \tanh\left(\frac{\Delta(T)}{kT}\right) \tag{33}$$

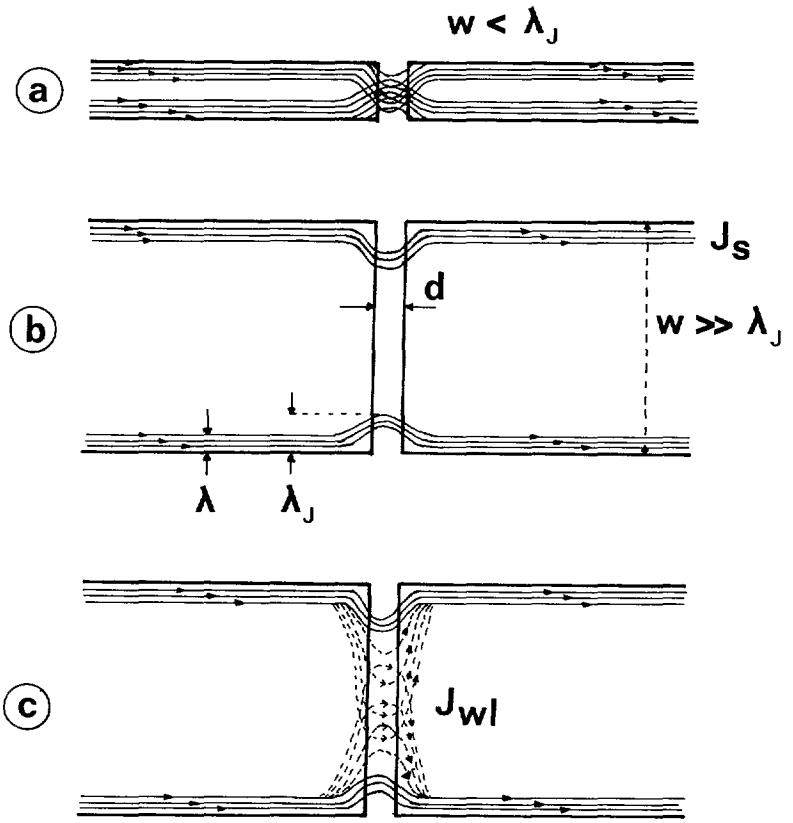


Fig. 42. — Schematic repartition of intergrain currents within various kinds of Josephson junctions. a) The junction is ideal (no defects) having a width $w$ much smaller than the associated Josephson penetration depth ($\lambda_J \gg w$). b) The junction is still ideal but now $\lambda_J \ll w$. Here, like in type II superconductors there is no bulk current except in the edge region within a depth $\lambda_J$. c) The junction is very large ($\lambda_J \ll w$) but inhomogeneous with holes and voids allowing for vortex pinnings and thus giving rise to a non zero bulk current.

where $\Delta(T)$ is the energy gap in the grain and $e$ the electric charge of the electron. We emphasize again that this expression is only valid when the effective field, including the self-field, is negligible compared to the Josephson first critical field $H_J$ defined below (in Gauss units) :

$$H_J \approx 8\ \pi J_J\ \lambda_J/c = \Phi_0/[\pi(2\ \lambda + d)\ \lambda_J] \tag{34}$$

with the Josephson penetration depth given by

$$\lambda_J = \left[\frac{c\Phi_0}{8\ \pi^2 J_J(2\ \lambda + d)}\right]^{1/2} \tag{35}$$

Here, $c$ and $\Phi_0$ have their usual meanings (i.e. velocity of light and the flux quantum respectively) and we have used Gauss units for $J_J$.

It is of interest to note that we can use equation (33) to decide when a tunneling Josephson junction can be considered as a weak link. Obviously, a necessary condition is $J_J \ll J_d$ where we recall that $J_d$ is the depairing current of the perfect material. As a typical example we can consider the case of twin boundaries in $YBa_2Cu_3O_7$ single crystals the resistivity of which can be estimated approximately from the extrapolation of the normal state resistivity of the sample to $T = 0$ and by assuming that this resistivity is imposed principally by the twin boundaries within the single crystal (see [97, 98] for more details). We find that the critical current of the twin boundaries calculated this way is of the order of $5 \times 10^8$ A/cm$^2$. This is quite comparable to the estimated depairing current $J_d \approx H_c/\lambda \approx 10^9$ A/cm$^2$ at $T = 0$ ($H_c$ is the usual thermodynamic field ; see also § 2.1 and Appendix A).

According to Ferrell and Prange [340], to Josephson [341] and to Clem *et al.* [342, 343] (see also [105] by Likharev) a weak link of thickness $d$ (Fig. 42) would behave like a type II superconductor with its own Josephson (i.e. London-like) penetration depth, $\lambda_J$, its own first critical field $H_J$, ($\approx H_{c_1}^w$), a decoupling field $H_{c_2}^w$ and finally its own edge or surface current (equivalent to the London current) given by Ambegaokar Baratoff equation (33) above. Knowing the characteristic dimensions ($w$, $d$ and $\lambda_J$) of the junction we can consider three physical limits and determine qualitatively the transport and magnetic behaviours in these special cases.

1) The junction is ideal and small compared to $\lambda_J$ ($\lambda_J \gg w$, Fig. 42a). This is the best known case for which the transport current density (in $H = 0$) should be of the order of $J_J$ (Eq. (33)) whereas the field dependence of the maximum of the total current that can thread the junction should be given by the Fraunhofer diffraction pattern of equation (36) below

$$I_c(H, w) = I_c(0)\left|\frac{\sin[\pi\Phi(H, w)/\Phi_0]}{\pi\Phi(H, w)/\Phi_0}\right|. \tag{36}$$

Here, $H$ is the applied field and $\Phi$ the magnetic flux threading the whole barrier of thickness $w$ ($w \sim \mathbf{r}_g$ in the remaining of this paragraph). At this point it is important to recall that as developed originally by Josephson [341] the Fraunhofer description assumes tacitly that the junction is ideal, isolated (no percolation with other junctions), insulating (tunnel barriers) and, more importantly, of dimension $w$ much smaller than the Josephson penetration depth $\lambda_J$ given by equation (35). It is important to keep in mind that it is only under these circumstances that the response of a given fixed junction to an applied field parallel to its barrier would be given by the Fraunhofer like function.

Many of the present models on weakly coupled granular materials consider the junctions as

ideal, neglect percolation problems and assume that the junctions behave independently and have lateral dimensions of the order of the average diameter $2\,r_g$ of the adjacent grains. Taking $J_0 \approx 2 \times 10^3$ A/cm$^2$ and $2\,\lambda + d \approx 1$ μm in equation (35), we find that $\lambda_J$ is typically of the order of 2 to 4 μm, whereas we know from the literature that $r_g$ varies widely from sample to sample (1 to 10 μm typically).

However, this kind of ideal junction considered in many examples of the literature is not consistent with experimental data and is easily ruled out by magnetic measurements which show unambiguously that the transport current has the same origin as the magnetic one and that the latter is related to irreversibility effects [97, 98] and therefore to some kind of pinnings of the vortices by defects. It is also inconsistent with the fact that in granular materials the junctions form a percolating network of dimension comparable to the macroscopic diameter of the sample, hence much greater than $\lambda_J$.

2) Secondly, the junction is very large compared to $\lambda_J$ but still ideal with no inhomogeneities (Fig. 42b). This situation is very similar [97, 98] to that of a perfect type II superconductor except that the current within the junction is restricted to the penetration depth $\lambda_J$ while it is restricted to the London depth $\lambda$ in the crystallites (see Refs. [18, 202]). For such large but ideal junctions the average critical current would drop towards zero very rapidly with increasing thickness $w$.

3) Thirdly, the Josephson barriers are very large and inhomogeneous with vortex trapping regions. It is possible now for the current to be carried by the interior of the junction just as in dirty superconductors of the second kind. This case is schematized in figure 42c showing both the edge or « reversible Josephson current » and the bulk non equilibrium current associated with the pinning forces within and near the junction. Moreover, it appears now quite natural to assume that this kind of junction is closer to the real situation and to identify the critical fields $\mathbf{H}_{c_1}^{w}$, $\mathbf{H}_{c_2}^{w}$ deduced from low field magnetic measurements as the averaged first and second critical fields of the weak link network. In the following section we shall use this description to calculate the hysteresis cycle of granular superconductors.

In the above examples it was assumed that all the junctions are roughly identical (i.e. the distributions in $J_0$ and in $\lambda_J$ are not very large). Because of the strong anisotropy of high $T_c$ oxides the situation is probably more complicated in these systems and we must represent HTSC granular materials by at least two kinds of very different junctions, parallel and perpendicular to the $a$-$b$ planes respectively, as illustrated in figure 43a. From the inspection of figure 43 it is seen that in this example the transport current is not well defined because of the presence of weak links. The transport critical current is determined by the current conservation condition which imposes that the maximum possible current is smaller than or equal to the lowest of the two currents w.u. $J_{ab,\,ab}$ and w.v. $J_{c,\,ab}$. (Note that $u$, $v$ and $w$ are the average thickness, width and length of the grains composing the material ; see Fig. 43a.) This means that the apparent current density is given roughly by :

$$J \approx \inf \{J_{ab,\,ab}\,;\ (v/u)\,J_{c,\,ab}\}\ . \tag{37}$$

To derive this expression we assumed that the small (vertical) junctions of the figure carry negligible current while the large horizontal ones are quasi perfect and have little influence on $J_{c,\,ab}$. We know that for Bi oxides the ratio $J_{ab,\,ab}/J_{c,\,ab}$ is very large, probably of the order of $10^4$. This suggests that the critical current density would be generally limited by the current density in the $c$-direction unless the aspect ratio $v/u$ is of the same order of magnitude as the anisotropy ratio $J_{ab,\,ab}/J_{c,\,ab}$. This implies that, even in highly textured materials the local directions of the current within the sample should be to some extent distributed with respect to the macroscopic direction. This is because weak links of the sort sketched just above are difficult to eliminate completely over a very large areas even in highly textured materials.

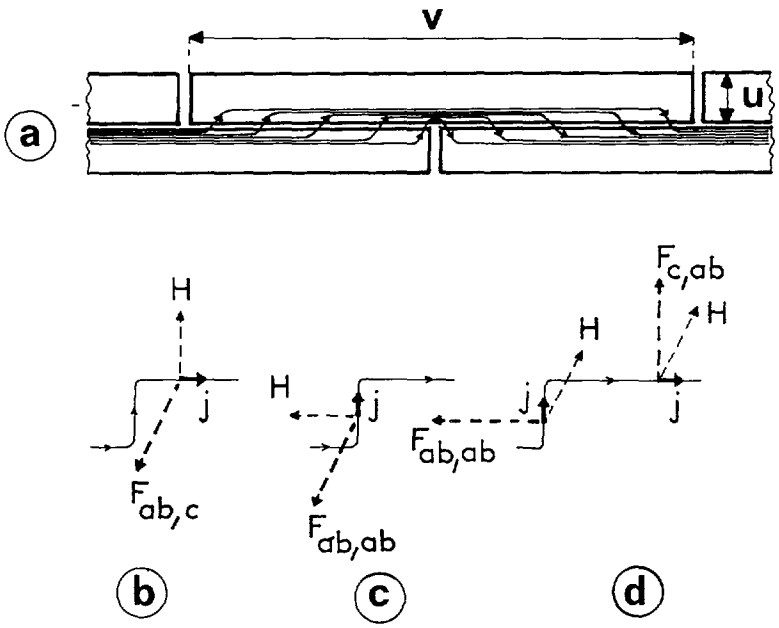


Fig. 43. — a) Schematic representation of the current pathways in a highly textured anisotropic sample. u and v are respectively the average thickness and the average length of the elongated crystallites. b) and d) Lorentz forces in the « orthogonal » configurations. ($H = H_\perp$, i.e. perpendicular to the average direction of the current). c) « longitudinal » configuration in which the applied field is parallel to the direction of the macroscopic current ($H = H_\parallel$), but this not true locally in the presence of weak links. Note that this kind of weak links will lower considerably the apparent anisotropy of the current.

This weak link effect would be easy to detect by looking at the variation of $J_{tr}$ with $H_\parallel$ (i.e. in a « longitudinal field » $H$, parallel to the mean direction of the excitation current). It is indeed known for conventional materials that if the vector $\mathbf{J}_{wl}$ is strictly parallel to the field $H_\parallel$ everywhere in the sample then the total critical current $I_c = \pi \cdot R^2 J_{tr}$ should be rather independent of or slightly increasing with $H_\parallel$. Therefore, if $J_{tr}$ decreases with the strength of $H_\parallel$ we can safely say that the direction of the local current is not constant. We believe that such an anisotropy effect should exist in epitaxial thin films and perhaps even in single crystals as the vortices can be distorted by the combination of defects and anisotropy. It is also of interest to note that the same kind of effect is observed in the resistive transition of most HTSC which is broadened by « longitudinal » fields. This is contrary to expectations for straight current lines. The physical origin of this broadening (in a longitudinal field) is probably the same as at low $T$ though in the last case some of the broadening can be due to vortex distortions by thermal fluctuations. In summary, the vortices and the associated currents can be distorted locally either by weak links or by defects assisted by anisotropy or (due to the high temperatures involved in HTSC) by thermal excitations assisted by anisotropy.

9.5 DISCUSSION AND CONCLUSION OF THIS SECTION. — In the preceding section we have seen that the conductivity in the normal state of sintered materials is decreased by irradiation-induced defects. Therefore, it seems that the claim according to which $\mathbf{J}_{wl}$ would be improved by introducing a desired amount of defects in the junction seems at first sight in contradiction with the predictions of equation (33) of Ambegaokar-Baratoff which shows that $J_J$ decreases

with the resistivity $\rho_J$ (or $\rho_{wl}$) of the junction and hence with the density of imperfections in this junction. However, according to the usual flux creep theory the improvement of the critical current density by defects is valid only in the limit where the vortex structure and dimensions ($\lambda$ and $\xi$) are not changed by such defects. Of course, this is not the case inside the junctions where the perturbation is generally very strong. There are general arguments which show that the pinning forces acting on the vortices should decrease in the same way as the transverse dimensions of the vortex. As far as the Josephson junctions are concerned, these dimensions are very large compared to the unperturbed ones and are measured either by $\lambda_J$ or by $\xi_J$ (the Josephson penetration depth and the Josephson coherence length respectively). These latter lengths are increasing functions of the normal state resistivity $\rho_{wl}$ of the weak link structure. To compare with experimental data we use the notation $\rho_{wl}$ rather than $\rho_J$ introduced for an ideal junction. Consequently, the two contradicting effects above are in fact not independent and must be considered simultaneously in order to find out the best trade-off between the two requirements (which state that to have large $I_c$ we need large pinnings and low $\rho_J$ at the same time). It is interesting to recall that the same situation can exist in bulk materials where $\lambda$ and $\xi$ depend in fact on $\rho$. This is particularly the case in the so called dirty limit in which the electron mean free path of the conduction electrons in the normal state is smaller than $\xi_0$.

From the microscopic point of view it is not clear how to realize the best compromise between the need for strong pinning centres and the need for clean junctions with the lowest possible $\rho_{wl}$ as required by equation (33). Nonetheless, we can argue that $\rho_{wl}$ is sensitive to all kinds of defects whereas the pinning forces should only depend on inclusions of dimension comparable to $\xi_J$. At this point, it is important to remark that voids at the intersection between several grains probably provide the most natural pinning centres which satisfy reasonably well the above requirements. Therefore, it seems that the first necessary condition for the enhancement of $J_{wl}$ is to improve the quality of the junction and as a rule to reduce the normal state resistivity of the weak link network at the working temperature. The problem is then how to relate the measured resistivity (which also includes intragrain electron scattering) to $\rho_{wl}$. We assume that in most practical cases it is reasonable to accept that : (i) this resistivity is approximately proportional to the residual resistivity of the granular sample, extrapolated from above $T_c$ to $T \approx 0$ as illustrated in figure 44a ; (ii) the residual resistivity is largely

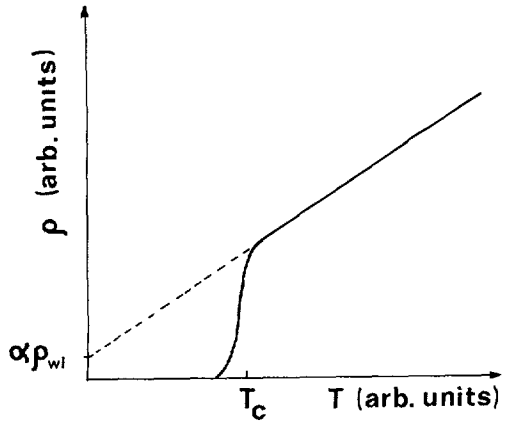


Fig. 44. — Resistivity as a function of $T$. The dashed curve is an extrapolation of the high temperature resistivity to obtain the normal state resistivity entering equation (33).

dominated by that of the grain boundaries. It is clear that when trying to make quantitative correlations between the total resistivity $\rho$ and $J_{wl}$ it is not $\rho$ which is the most relevant parameter but some resistivity $\rho_{wl}$ of the weak link. The latter would be (to a first approximation) obtained by dividing $\rho$ (of the whole sample) by the number of junctions per unit length. This number is of order $1/r_g$. Thus, to a first approximation we expect that $\rho_{wl}$ would be proportional to $\rho/n = \rho r_g$ (for a sample of length unity).

After the above discussion, the next fundamental question is then to what extent it is possible to reduce the normal state resistivity of the junction and therefore to enhance $J_J$ *via* equation (33). It is obvious that as far as the adjacent grains have their crystallographic axes strictly parallel, it is theoretically possible (but practically difficult) to reduce the resistivity of the junction infinitely (i.e. theoretically to zero) leading ultimately to a single crystal. One way to achieve or at least to approach this ideal limit is through texturing as discussed before. This conclusion is also in agreement with the experimental results discussed in the previous section which showed that $\mathbf{J}_{wl}$ can be improved by making the junction more metallic (thus reducing their $\rho_{wl}$), while the same intergrain current is drastically deteriored by ion, electron and neutron irradiations even at vary low doses.

The question concerning the possibility of reducing the resistivity of the junctions between disoriented grains (for instance *a-b* and *c-a* (or *c-b*) boundaries) is more difficult to answer. It is indeed possible that in this case the junction could behave like an insulating region with a rather large resistivity (though depending on the superconducting material) even in the best possible conditions. This is not only because of the unavoidable discontinuity of the periodic potential seen by the conduction electrons (which results in some resistivity), but more seriously, it is believed that the mismach between the crystalline directions of adjacent grains can be accompanied by a diminution of oxygen concentration either side of the junction leading probably to a much larger perturbation than in the coherent case.

## 10. Interpretation of the hysteresis cycle and determination of the real $J(T, H)$ relationships in single crystals.

We have already mentioned that most of our knowledge on the intragranular critical currents of high $T_c$ single crystals are inferred from magnetic measurements the interpretation of which is often not straightforward. This is especially true for the low-$H$ peak region (seen in all of the preceding figures of sections 7, 8 from Fig. 20 to Fig. 32) where the Bean model (as given by Eq. (4)) breaks down. We shall also see that at very low temperature the « reversible » magnetization given by formula 5 of Fietz and Webb is generally very different from the actual $\mathbf{M}_{eq}(T, H)$ of the ideal material. Naturally, the relationship between the intergranular current $J_{wl}$ and the low-$H$ cycle (Fig. 32b) is even more complicated. Getting quantitative information on the critical current, the microscopic and macroscopic structures from susceptibility data is another hard problem. In an attemp to clarify these points, we now concentrate on the interpretation of the hysteresis cycle as a function of both $H$ and $T$ and then try to go back to the actual variation of the local $J$ with $T$ and $H$. We have already seen that such a relation is made very complicated by size effects (Sect. 6), especially those arising from the spatial variation of $J$ induced by self-fields. As a consequence, the very useful Bean model gives an apparent current ($J_{mag}(H)$) which is sometimes quite different from the actual one ($J(H)$) at the measuring field. For instance, it was shown recently by Senoussi *et al.* [77] that the low-$H$ peak exhibited by the hysteresis cycles of HTCS (Figs. 21-32) cannot be understood in the framework of current $J(H)$ models (as those considered in Sect. 6) but is probably due to a competition between long range and short range vortex interactions obeying very different laws as a function of $H$ (this point was discussed briefly in Sect. 3 and will be discussed further later in this section). A further complication (also discussed before)

comes from the equilibrium magnetization which, in addition to its own direct contribution to the cycle, changes the effective field seen by the local current $J$ even in the absence of any conventional demagnetizing field as in a very long cylinder (such a field can be viewed as the contribution of $M_{eq}$ to the screening of the applied field). This effect was already illustrated in the inset to figure 2 and in figure 5 where it was seen that for a long cylinder with no usual demagnetizing factor ($N = 0$) the effective field seen by the vortices at the surface of the specimen is $4\pi\mathbf{M}_{eq}(H) + H$. The influence of this additional induced field on the shape of the hysteresis loop can be very important for samples of small size, in particular at high temperature [77] where the irreversible magnetization is generally dominated by the peak contribution. The anomalous behaviour of this low-$H$ peak of the hysteresis cycle as a function of $H$, $T$ and $R$ are considered below.

**10.1** THE RELATION BETWEEN THE LOW-$H$ PEAK OF THE HYSTERESIS CYCLE AND THE INTRAGRAIN CRITICAL CURRENT DENSITY. — Let us again consider the hysteresis cycles of figures 21-29. We have seen that all of them exhibit a marked hump near the origin. As far as we know, such a peak exists for all high $T_c$ materials and had recieved no explanation up to very recently [77, 344] (in fact, this kind of peak seems to exist in conventional superconductors as well [344, 345]). It exhibits the following characteristic features.

1) For a given material such as (Y (123) or Bi (2212)), the peak is generally more pronounced for small grains, in particular for decoupled oriented grains, than for large single crystals. More explicitly, it does not scale with $R$ (the radius of the sample) and its amplitude increases rather slowly with $R$. As a rule, it differs by a factor of only 3 to 10 between oriented grains (where $r_g \approx$ few μm) and single crystals (where $R \approx$ few mm). This is to be compared with the high field signals (i.e. far away from the peak region, $H \gg H_{c_1}$) of the same materials which scale with $R$ and can differ by as much as three orders of magnitudes between fine grain samples and large single crystals.

2) For a given crystal the low-$H$ peak is sharper for **H** parallel to the $a$-$b$ plane than for perpendicular. This is observed whatever may be the shape of the sample. This property together with the fact that the peak depends only weakly on $R$ implies that it cannot be due to demagnetizing effects.

3) Its relative contribution to the total magnetization and its sharpness both increase with $T$.

4) It is never centred at $H = 0$. This simple fact rules out the possibility that the peak could be induced by some kind of surface pinning.

5) Its position on the $H$-axis depends on the magnetic history of the sample and it is always sharper for the cyclic curve of the hysteresis loop than for the virgin (or initial) cycle. This is also not consistent with surface pinning since this would depend mainly on the value of $H$ at the surface but not on the magnetic history.

To bring out the physical origin of this peak we return back to figure 19 of section 6 where it is seen that the variation of $J$ with $R$ (recall that here $J$ is connected with $M_{ir}$ by Eq. (4)) tends towards saturation (or becomes almost independent of $R$) when the radius $R$ of the specimen exceeds some characteristic length $R_0$ defined by equation (16). Since $R_0$ is proportional to the characteristic field $B_0$ (Eq. (16)) which controls the field dependence of $J$, this suggests that the low-$H$ peak could be associated with a small characteristic field $B_{0,\,lr}$ (we recall that the subscripts « lr » and « sr » stand for long range and short range interactions between vortex lines respectively). In other terms, such a peak would correspond to some long range interactions which drop very rapidly with $B$. Therefore, it is likely that the hump is connected with some interaction mechanism that varies much more rapidly with $H$ than that controlling the high field magnetization ($H \gg H_{0,\,lr}$). The latter is more probably connected with the core and the kinetic energy of the currents in the surrounding region of the vortex lines [139]. The

former is probably connected with long range interactions between the vortex lines. In fact, we shall see that the low-$H$ peak has essentially the same physical origin as the peak which arises in some conditions near $H_{c_2}$. Namely : the possibility for the vortex lines to minimize locally their energy independently of their neighbours ; in the region $B \leq B_{c_1}$ where the interaction between lines vanishes exponentially. This is indeed accompanied by the vanishing of the elastic constants $C_{ij}$ of the VLL except for the line tension. As a consequence, an isolated vortex lines will tend to go through its neighbouring defects to minimize its energy. This effect is limited only by the induced elastic energy associated with the line tension. On the contrary, for a very rigid vortex lattice (strong vortex-vortex interaction) the vortices have no internal degree of freedom to modify their shape and minimize their energy locally so that the resulting pinning is generally very low. It is interesting to emphasize that the pinning mechanism is the same as in weakly anisotropic ferromagnets where a given domain wall tends to rearrange its spatial shape to pass through a maximum number of defects.

**10**.2 A THREE CURRENT MODEL FOR THE CALCULATION OF THE HYSTERESIS CYCLE. — In order to calculate the hysteresis cycle and give some support to the above hypothesis concerning the physical origin of the low-$H$ peak we assume that the total current density varies as :

$$J_{tot} = J_{sr}(B/B_{sr}) + J_{lr}(B/B_{lr}) + J_s(T, H, r) \tag{38a}$$

where the first term on the right hand side would describe the high field behaviour ($B_{sr}(T = 0) = B_{0, sr} \approx 200$ to 400 kG) whereas the second one would correspond the low-$H$ domain ($B_{lr}(T = 0) = B_{0, lr} \approx 2$ to 5 kG, peak region). The third current is the equilibrium London-Abrikosov's term which depends explicitly on both $H$ and $T$ as well as $r$. For concrete calculations we are using exponential laws (but the same calculation can be performed with other models such as those considered in Sect. 6, but see section 13 for the limit of validity of the critical state concept assumed implicitly here) :

$$J_{tot}(B(r)) = J_{sr}(T)\, e^{-\frac{|B(r)|}{B_{sr}(T)}} + J_{lr}(T)\, e^{-\frac{|B(r)|}{B_{lr}(T)}} + J_s(T, B, r)\,. \tag{38}$$

The field seen by the vortices at the surface is given by :

$$H_{eff}(R - \lambda) \approx H + 4\,\pi M_{eq}(H)\,. \tag{39}$$

To reproduce the experimental cycle the only important required condition is the coexistence of long and short range forces with $B_{sr} \gg B_{lr}$.

We note that $B(r)$ in equation (38) includes a contribution to the effective field from the surface current $J_s(T, H, r)$. The model reported in reference [77] takes into account this effect and assumes that the coupling between the irreversible magnetization and the London-Abrikosov equilibrium magnetization can be accounted for as follows : the vortices closest to the surface are not in equilibrium with the external applied field $H$, but rather with an effective field including the applied field and the field induced by the equilibrium currents flowing near the surface in the London depth $\lambda$. Then, for a cylindrical sample of length $L \gg R \gg \lambda$ the effective field seen by the vortices at the surface is given by equation (39). For the numerical calculations, we have taken

$$M_{eq}(T, H) \approx -\frac{H}{4\,\Pi}, \qquad (H < H_{c_1}) \tag{40}$$

$$M_{eq}(T, H) \approx -\frac{H_{c_1}}{4\,\Pi}\frac{\ln (H_{c_2}/H)}{\ln (\lambda/\xi)}, \qquad (H \gg H_{c_1})\,. \tag{41}$$

This was already illustrated schematically in figures 2 (inset), 13 and 14 in which we assumed that $M_{eq}(H)$ was induced by London-Abrikosov's currents flowing in the London penetration depth $\lambda$.

**10.2.1** *A possible origin of the critical current $J_{lr}$ responsible for the low-H peak in $M(H)$.* — We expect that a peak like that discussed above can be connected either with a pinning potential $U(r)$ of very long range ($\sim \lambda$) or with the vanishing of long range interactions between the vortex lines (see discussion in Sect. 10.1). It turns out that it is very difficult to picture physically plausible potentiel barriers with the required very long range interaction on a scale of the order of $\lambda$, especially for $H$ parallel to the $a$-$b$ planes where $\lambda(T = 0) = \lambda_0$ is as large as 8 000 Å (see Refs. [275-280] for $\lambda$ measurements). Therefore, as already discussed in section 3 we suggest an explanation based on the second mechanism, i.e. related to the weakness of the repulsion between vortex lines in this field region.

Indeed, we have seen in section 3 that in the field region where the condition $\partial H_{th}/\partial r \approx \partial B/\partial r$ is not satisfied the critical current density (and the associated apparent pinning force) is multiplied by a factor $1 + 4\pi\,\partial M_{eq}/\partial H_{eq}$ (see Eq. (7) of Sect. 3) which is notably greater than unity close to and slightly above $H_{eq} = H_{c_1}$ and tends to 1 for $B \approx H_{eq} \gg H_{c_1}$. Then, the comparison with the critical current component $J(T, B) = J_{sr}(B/B_{sr}) + J_{lr}(B/B_{lr})$ (formula 38) suggests the following identification :

$$J(T, B) = J_{sr}(T)\, e^{-\frac{|B|}{B_{sr}(T)}} + 4\pi \frac{\partial M_{eq}}{\partial H_{eq}} J_{sr}(T)\, e^{-\frac{|B|}{B_{sr}(T)}} \tag{42}$$

In other words, we propose that $J_{lr}$ is related to $J_{sr}$ by : $J_{lr}(B/B_{lr}) = 4\pi\,[\partial M_{eq}/\partial H_{eq}]\, J_{sr}(B/B_{sr})$. We also recall that $M_{eq}$, $H_{eq}$ and $B$ are related by equations (1-3) as explained in section 3. Experimentally, it is found that as far as YBaCuO (123) is concerned the two currents $J_{sr}(B/B_{sr})$ and $J_{lr}(B/B_{lr})$ in equation 38 follow approximately the same exponential variation with $T$, in agreement with formula 42. This is not true in the case of Bi and Tl based systems. The reason of this is connected with the fact that in the case of YBaCuO (123) the pinning disorder can be considered as very strong (in ordinary conditions of preparation of the material) both at high and low fields. This is not the case for Bi and Tl compounds where it is thought that at high $H$ the pinning is generally very low (at least in ordinary conditions of preparation of the material) and due to oxygen vacancies, but always strong in the peak region of the cycle. Other arguments are developed briefly below and more extensively in [344].

In this model the physical origin of the second current term on the right hand side of equation (42) lies in the fact that for $H$ slightly above $H_{c_1}$ the repulsion between lines are very weak (they vary like $e^{-d_v/\lambda}$ where $d_v$ is the vortex spacing) and as a consequence the lines can sustain more current than in the region $H_{c_1} \ll H \ll H_{c_2}$ (or equivalently in the limit $\lambda \gg d_v$) where the interaction between lines is much stronger and varies approximately like $\lambda/r$. A rigorous treatment of this point requires quantitative computation of $M_{eq}$ of HTSC in the presence of pinning forces and anisotropy, but this is beyond the scope of the present paper. It is probable that the rather qualitative Abrikosov formula [78] magnetization $M_{eq}$ (used here) needs to be improved in the case of HTCS [80-83] for quantitative comparison with experiments.

Finally, it is to be added that it can be shown that other suggested explanations (for the low $H$-peak) based on demagnetizing field effects [346], time relaxation effects [347] or surface pinnings [348] are not consistent with experimental data as already mentioned before. Of course, all of these effects, particularly the demagnetizing field, certainly influence the

experimental data whichever the physical mechanism readily responsible for the observed peak in $M(H)$, but these effects are difficult to account for rigorously in concrete calculations.

**10.3** CALCULATION OF THE HYSTERESIS CYCLE. — For the numerical calculations of $M_{eq}(T, H)$ we have taken $H_{c_1}(T = 0) = H_{c_{10}} = 150$ œ, $H_{c_2}(T = 0) = H_{c_{20}} = 10^6$ œ, $\lambda/\xi = 200$ and BCS laws for the temperature variation of $H_{c_1}$ and $H_{c_2}$. Note also that the interpolation between the two above limiting behaviours (Eqs. (40, 41)) was chosen so as to give a sharp positive slope in $M_{eq}$ at $H$ just above $H_{c_1}$.

To compare the calculated magnetizations with the temperature dependence of the measured cycles we need the exact temperature dependences of both $J_{ij}$ and $B_{0,ij}$ entering equation (38) (recall that $ij$ = « sl » = short range or « lr » = long range). At present, it is extremely difficult to get these relationships exactly. In addition, it is not certain that the same laws will work for all samples because of the possibility that different samples with different defects will exhibit different $T$ and $H$ dependences even for the same HTSC oxide. Nonetheless, we know that $J(T)$ for YBaCuO and other high $T_c$ families vary exponentially with temperature over a large $T$ domain [20-25] and follow a power law as $T$ approaches $T_c$. The $T$ dependences of the fields $B_{0,ij}(T)$ are more difficult to determine correctly, both because of the complexity of the $M(H)$ curves and because of their very high values compared to available fields. However, to compare the theoretical loops semi-quantitatively with experimental data we do not need the exact $J(T, H)$ relationships. Here, as suggested by formula 39 for the currents (and also for the sake of simplicity) we take the same temperature variation for $J_{sr}$ and $J_{lr}$ on the one hand and for $B_{lr}$ and $B_{sr}$ on the other hand. We also neglect for the moment other possible current terms such as that responsible for the butterfly shaped cycles (Sect. 7) which only exists in very special conditions and in a limited region of the ($T$-$H$) plane

$$J_{il}(B_{eff}, T) = J_{0,il}(1 - T/T_c)^n \, e^{-\frac{T}{T_{il}}} \, e^{-\frac{B_{eff}}{B_{il}(T)}} \tag{43}$$

$$B_{il}(T) = B_{oil}(1 - (T/T_c)^m) \, . \tag{44}$$

Here $T_{ij}$ is some characteristic temperature of the order of 15 to 25 K for $YBa_2Cu_3O_7$ and about 5 to 6 K for Bi (2212) (we recall that the exponential decay with $T$ is not valid for thin films). What is important to recall too is that at the surface of the specimen $B_{eff}$ is equal to the external applied field plus the field induced by the London-Abrikosov currents circulating in a shell of depth $\lambda$. A reasonable fit with experimental data in $YBa_2Cu_3O_7$ is obtained for $n \approx 1$ to $n = 1.5$, $m \approx 2$ and $J_{olr} \approx 2\, J_{osr} \approx 2 \times 10^6$ to $7 \times 10^6$ A/cm$^2$, whichever the sample radius and the method of preparation. In the present calculation we take $n = 1$. For the sake of simplicity we shall not consider other choices for the fitting parameters here.

**10.4** COMPARISON WITH EXPERIMENTAL DATA. — Shown in figure 45 are the calculated cycles (for the parameters given in the caption of this figure ; see [77] for the details of the calculation) using the various equations above. We observe a strong similarity with the cycles of oriented grains samples of figure 23 except that the calculated cycles present a small discontinuity at $H = H_{c_1}$. It is to be noted, however, that in the experimental data this discontinuity is smoothed out because of both demagnetizing effects and unavoidable inhomogeneities in the sample. The shape of the calculated cycle depends on the maximum applied field and on the ratio $J_{sr}/J_{lr}$. This is illustrated in figure 46 for $r_g \approx 6$ μm, $J_{lr} = J_{sr} = 7 \times 10^6$ A/cm$^2$ and for $J_{sr} = 4 \times 10^6$ A/cm$^2$, $J_{lr} = 7 \times 10^7$ A/cm$^2$. As can be seen the loop of figure 46 (for which $J_{lr} \approx 2\, J_{sr}$) is more consistent with the experimental cycles.

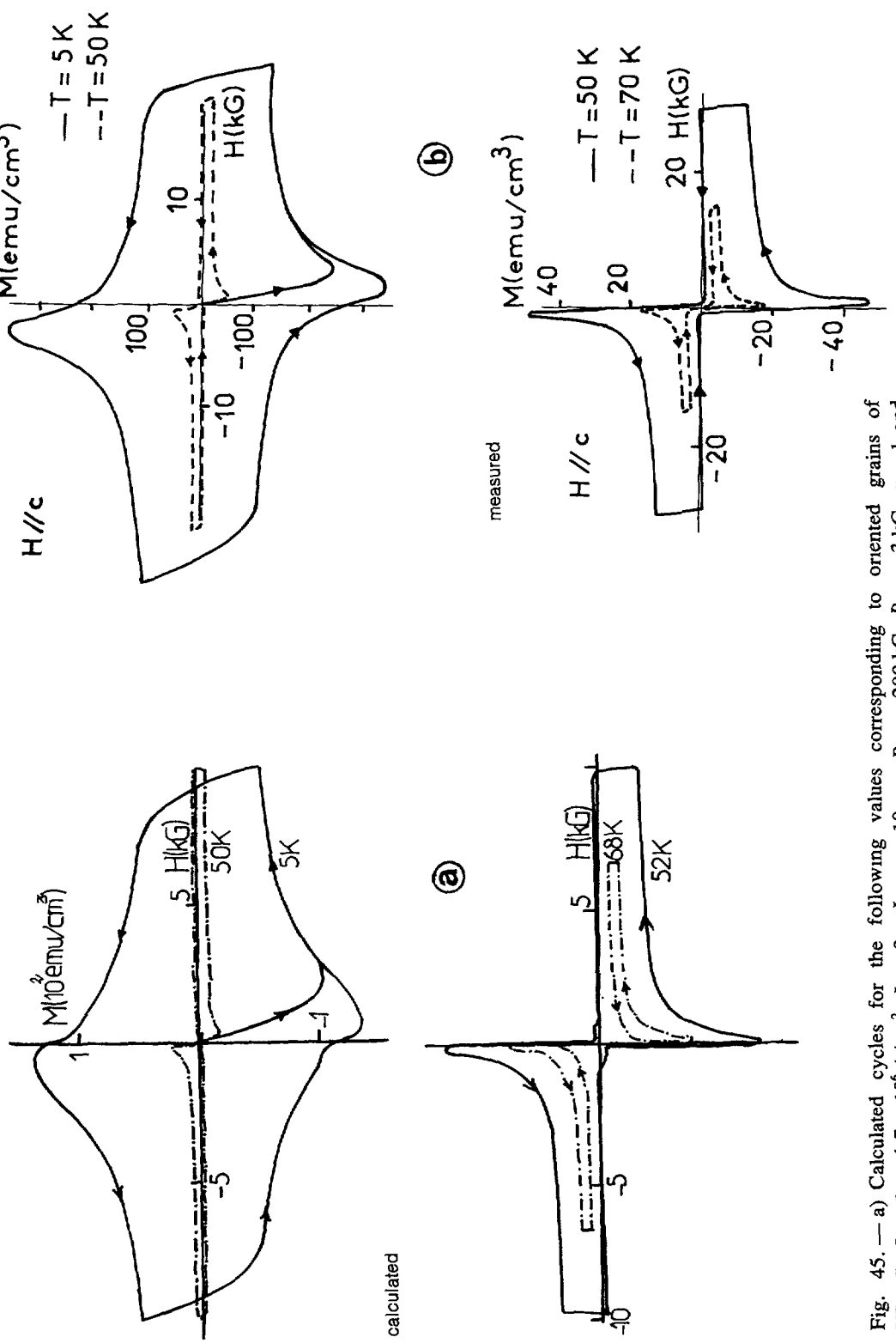


Fig. 45. — a) Calculated cycles for the following values corresponding to oriented grains of $YBa_2Cu_3O_7$ : $J_{01} \approx 1.7 \times 10^6$ A/cm$^2$, $J_{02} \approx 2 \times J_{01}$, $r_g \approx 10$ μm, $B_{0\,st} \approx 200$ kG, $B_{0\,l\,r} \approx 3$ kG, $n = 1$ and $m = 2$. b) Measured hysteresis cycles of the same oriented grains.

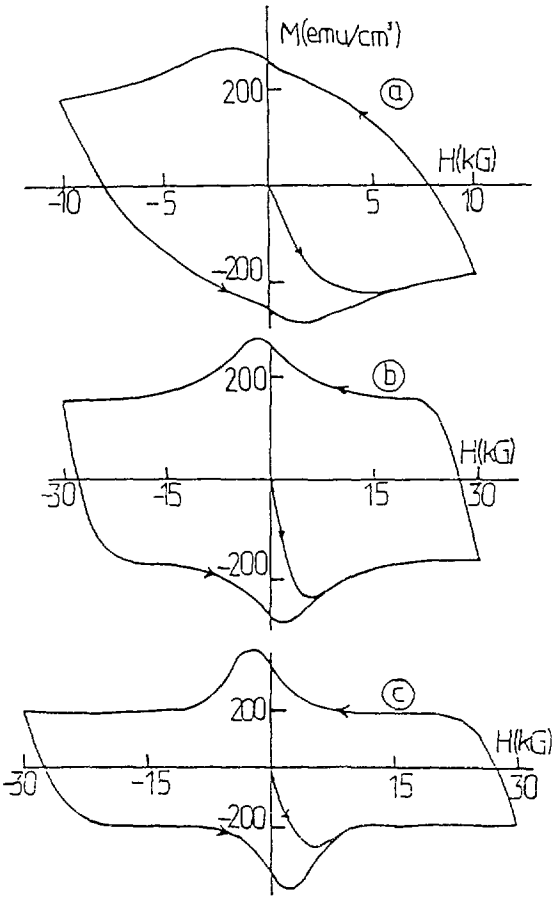


Fig. 46. — Calculated cycles at two different field scales and for the following parameters ; a, b) $J_{lr} = J_{sr} = 7 \times 10^6$ A/cm$^2$ ; c) $J_{sr} = 4 \times 10^6$ A/cm$^2$ and $J_{lr} = 7 \times 10^6$ A/cm$^2$ ; $r_g \approx 6$ μm, $B_{0\,sr} \approx 400$ kG, $B_{01\,r} \approx 2$ kG, $n = 1$ and $m = 2$, $T = 4$ K.

The evolution with the maximun applied field of the calculated cycle is presented in figure 47 for $J_{sr} = J_{lr} = 10^6$ A/cm$^2$ and $r_g = 500$ μm (single crystal, see figure caption for the values of the other parameters).

Very close to the irreversibility line, in particular near $T_c$, the shape of the hysteresis cycle is expected to be very sensitive to the exact variation with $T$ and $H$ of all the currents ($J_{lr}$, $J_{lr}$ and $J_s$ in formula 38) contributing to the hysteresis loop. A typical example is shown in figure 48 which compares calculated (a) and measured (b) cycles for $T$ approaching $T_c$. Other shapes observed experimentally can be easily reproduced using different parameters in the calculations. In fact we find that at high enough temperatures the shape of the cycle depends significantly on the relative rapidity of the variations with $T$ of $J(T)$ on the one hand and of $B_{sr}(T)$ and $B_{lr}(T)$ on the other hand.

The above results confirm that to describe the most characteristic features of the hysteresis cycle we need at least the three different currents given in equation (38). This description is probably valid very close to the irreversibility lines but since the variation with $T$ and $H$ are much more rapid in this region, it is necessary to know the various $J(T, H)$ relationships with

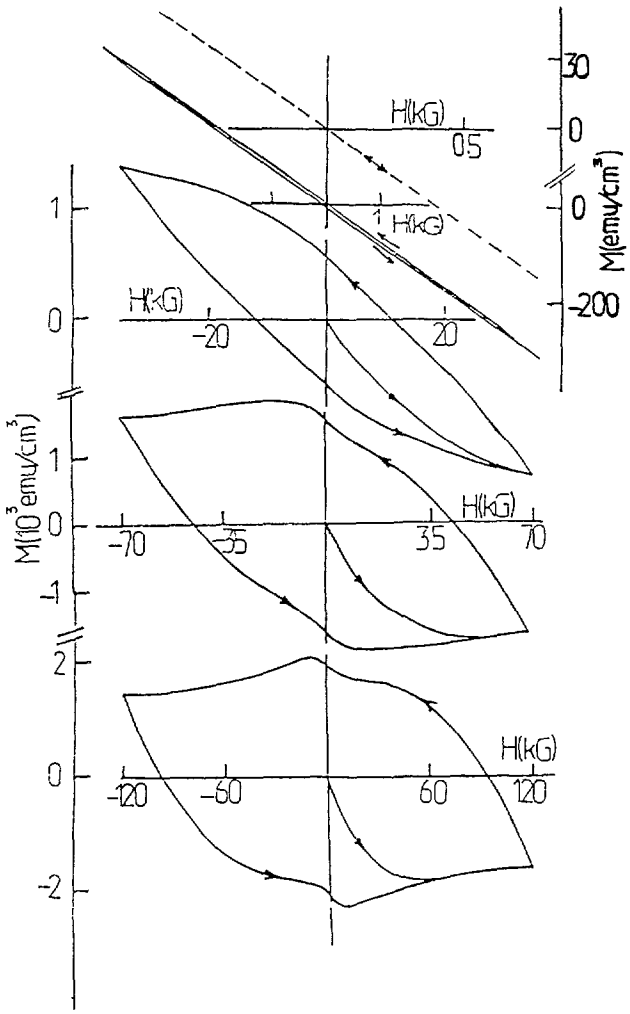


Fig. 47. — Development of the calculated cycle ($T$ = 4 K) as a function of the maximum cycling field for $J_{ir} = J_{sr} = 10^6$ A/cm$^2$, $r_g \approx 0.5$ mm, $B_{0\,sr} \approx 400$ kG, $B_{01\,r} \approx 3$ kG (a). Measured hysteresis cycle of a granular YBaCuO for $T$ very close to $T_c$ ; $T/T_c \approx 0.95$ (b).

more precision there than in equation (38) to reproduce the fine details of the curves. Other hysteresis cycle calculations can be found in references [351, 352].

**10.5** BUTTERFLY SHAPED CYCLE AND OTHER UNUSAL HYSTERESIS LOOPS FOR HTSC SINGLE CRYSTALS.

**10.5.1** *Anomalous hysteresis cycles.* — In some conditions high $T_c$ oxides exhibit the very unusual magnetic cycles displayed in figure 49 (lower loop, $\theta \approx 0°$) for $H$ oriented very close to the $c$-axis and in figure 49 (upper loop, $\theta \approx 83°$) for $H$ almost (but not exactly) parallel to the $a$-$b$ planes. The two effects have very different physical origins. The latter (Fig. 49b) has been invoked in section 7 and is an anisotropy effect which exists only when $H$ is not rigorously parallel to the $a$-$b$ planes. If the anisotropy is very high it can be explained quite satisfactorily by means of the projection model discussed briefly in section 7. This model will

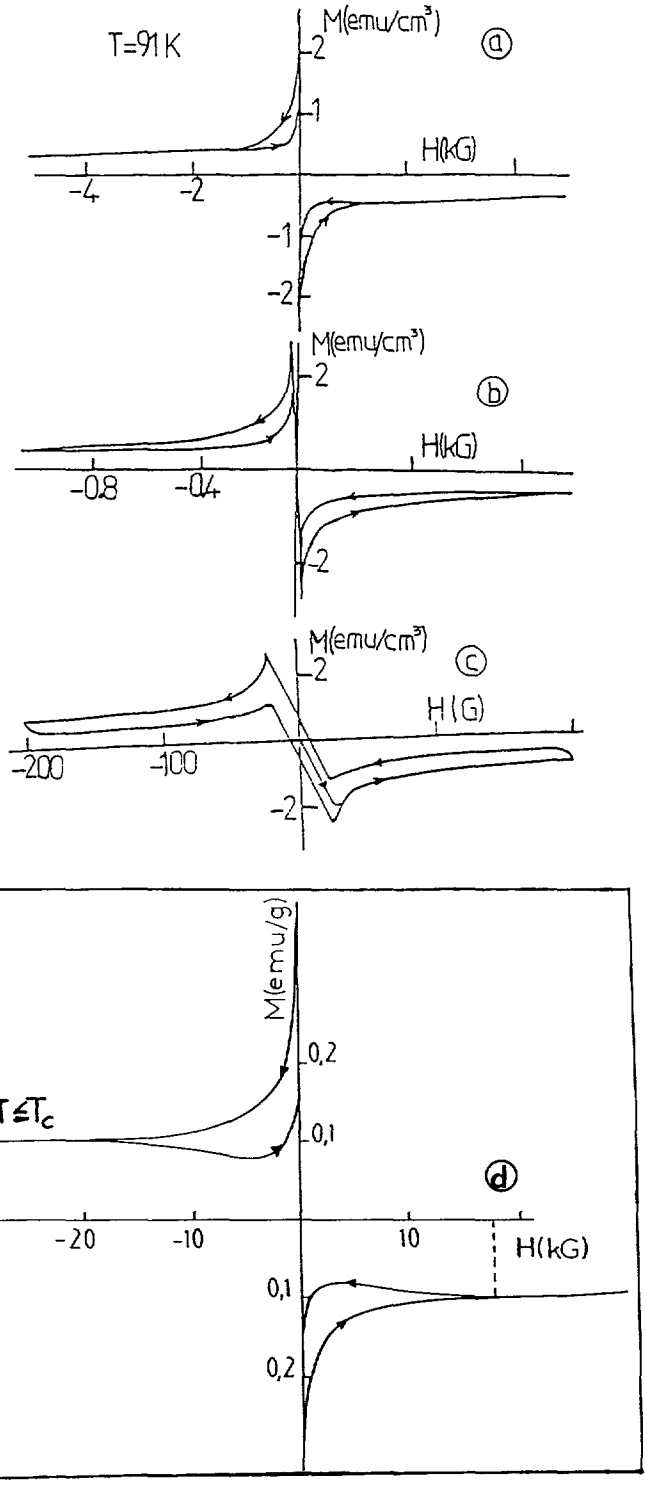


Fig. 48. — a, b, c) Calculated cycle at $T/T_c = 0.96$ (very close to $T_c$) at different field scales with $J_{lr} = J_{sr} = 10^6$ A/cm$^2$, $B_{0\,sr} \approx 200$ kG, $B_{01\,r} \approx 5$ kG, $r_g \approx 1$ mm. d) a measured cycle [13].

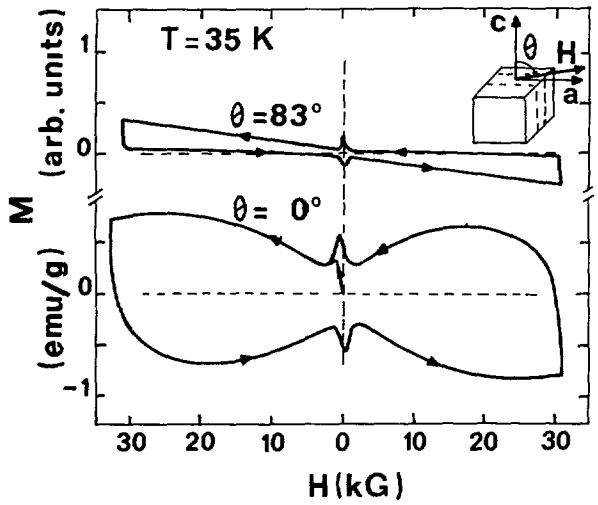


Fig. 49. — In some experimental conditions HTSC exhibit these kinds of hysteresis loops. Lower loop : the field is parallel or close to the *c*-axis ; upper cycle : the field is very close to but not parallel to the *a-b* planes.

be developed later (Sect. 15) in more detail. The butterfly like cycle of the lower figure 49 is generally observed only for large single crystals of some HTCS, for **H** oriented far from the *a-b* planes and in a limited *T*, *H* domain (*). This unusual cycle can also be reproduced by the model discussed above if one adds to the right hand side of equation (38) (i.e. to $\mathbf{J}_{sr} + \mathbf{J}_{lr} + \mathbf{J}_s$) a fourth current term of the form $J_{bf}[H - H_{bf}/H_{bf}]$ where $J_{bf}$ is some field dependent function presenting two symmetrical maxima at $H = \pm H_{bf}$. Its physical origin is still unknown. According to Aguillon (private communication), it could be due to the resonance of the vortex lattice with some periodic structure of the defects. We can also invoke some anomalous softening of the elastic coefficients $c_{66}$, $c_{44}$ of the vortex lattice for some unknown reason. It is indeed well known that this kind of softening effect occurs in conventional superconductors close to $H_{c_2}$ and is termed as the « peak effect » [127]. Other explanations were discussed by different authors [109, 350] : the idea here is based on the experimental fact that single crystals are generally badly oxygenated and would for this reason present statistically poorly oxygenated regions where supraconductivity is weak. Then, increasing the field would gradually destroy supraconductivity in these regions, thus providing extra pinning centres to the vortex lattice, but this is without affecting significantly the other parameters governing *J*. A third possibility proposed by Senoussi *et al.* in reference [20] is the possibility of thermally activated Frank-Read sources of dislocations in the vortex lattice at sufficiently high temperature. However, whichever the final explanation it should also account for the disapearance of the butterfly shaped cycle for *H* parallel to the *a-b* planes as well as for its non observance in granular samples prepared following standard methods. A further tempting mechanism could be a local rearrangement of oxygen vacancies (or other possible light defects such as traces of hydrogen) to stabilize the spatial structure of the vortex lines in some *T-H* region. The absence of this effect in granular systems may be due to the fact

(*) However, recent results from Mosbah, private communication, show that highly oxygenated oriented grains exhibit a small butterfly cycle, but at much higher field (about 60 kG) than in the case of single crystals.

that the latter are generally well oxygenated compared to large single crystals. We suggest this possibility by analogy with ferromagnetic materials where it is known that domain walls are stabilized by migration of nonmagnetic defects towards the domain wall location to lower the domain wall energy. Here, these phenomena may be favourable for two distinct reasons : the oxygen vacancies are rather light and the diffusion distances involved are very short (varying between two extreme limits : the vortex spacing $d_v$ at most and $\xi$ at least). With this idea in mind, it would be interesting to test the evolution of the cycle as a function of oxygen content in oriented grains specimens. The mechanism we are suggesting here is developed in the next subsection.

**10.5.2** *A possible explanation of the butterfly shaped cycle.* — This model allows the interpretation of other anomalous effects which are generally observed at the same time as the butterfly-shaped cycle : in particular, the returning branch of the magnetic loop sometimes presents a very extended linear field region ($M_{rl}$ proportional to $(H_{max} - H)$) which is usually typical of surface pinnings. This can be understood as follows : if the single crystal is insufficiently oxygenated (this is generally the case for large crystals as the time required for oxygen diffusion increases like $R^2$, implying that the time required for single crystals in $10^4$ to $10^5$ longer than for usual decoupled grain samples) it will present a gradient in oxygen concentration which can be defined by $YBa_2Cu_3O_{6+\delta(r)}$ with $\delta(r) \approx 1$ in some spatial region near the surface defined by $(R - \Delta r \leqslant r \leqslant R)$ and $\delta(r) \approx 0$ for $r \leqslant R - \Delta r$ ($\Delta r$ is the oxygen diffusion distance). Consequently :

(1) If $\Delta R \ll R$ this will simulate surface effects since there will be no critical current in the region $r < R - \Delta R$ (see Sect. 16 on surface currents for more details).

(2) Secondly, with this simple picture, in the transition region between $\delta(r) \approx 0$ and $\delta(r) \approx 1$ the transition temperature $T_c(r)$ will vary continuously from zero (presumably from some low but not zero value in real systems) to $T_c \approx 92$ K near the surface. Then, since $H_{c_2}$ will also go to zero in these regions of $T$ and $r$ we would expect that the pinning potential, $U(r, T, H)$, will go to a maximum in the sample regions where $H$ is very close to $r$ (due to the local softening of the VLL which must occurs just below $H_{c_2}$). This can explain the appearance of the butterfly peak in the magnetic loop as well as surface like pinning (if $\Delta r \ll R$).

**10.6** DISCUSSION AND CONCLUSION CONCERNING INTRAGRANULAR CURRENTS IN SINGLE CRYSTALS. — The calculated hysteresis cycles exhibit many of the characteristic features of the experimental data. The characteristic radii $R_{olr}$ and $R_{osr}$ (defined by Eq. (16), and ascribed to long and short range vortex interactions respectively) associated with $J_{olr}$ and $J_{osr}$ (Eq. (38)) are of the order of 5 to 20 $\mu$m and 2 to 5 mm respectively at 4.2 K. This means that Bean's formula (Eq. (4)) relating $M$ and these currents become incorrect at larger radii. In particular, this implies that the critical current density $J_{mag}$ deduced from the magnetization of single crystals at low $H$ (peak region) is systematically lower than that of intragranular current of granular systems by a factor of about two to three. This size effect has already been sketched in figure 19b of section 6.

Another important condition for the validity of the calculation of the hysteresis cycle concerns the way the contribution of $M_{eq}$ to the total magnetization is taken into account : we have already emphasized that in addition to its direct contribution, $M_{eq}(H)$ changes the effective field seen by the bulk of the sample and as a consequence changes the apparent field dependence of $J$. This result exists independently of any usual demagnetizing field (neglected here). The present model can probably be improved by choosing a more suitable $J(T, H)$ relationship especially close to the irreversibility lines where the phenomena vary strongly with $T$ and $H$. This is also true for a better description of the low-$H$ peak region which requires a more exact calculation of $M_{eq}$ of HTSC in the $H_{c_1}$ region. We are presently

carrying out further calculations using a Kim-like model [200]. We stress that by comparing many different samples with different demagnetizing factors we found that the main effect of the demagnetizing field is to move the centre of the peak towards the origin. Lastly, it is important from both practical and fundamental point of views to identify the microscopic mechanisms (either intrinsic or extrinsic and defect-dependent) which govern the $H$ and $T$ dependences of $J$. To achieve this goal, it is necessary to carry out both microscopic observations (for instance, using transmission electron microscopy) and macroscopic investigations as those described above. It is also of fundamental interest to know how to correct the experimental data for size and other spurious effects in order to deduce the right $J$ entering the flux creep equations. Finally, it is also important to recall that the reversible magnetization given by equation (5) coincides with the equilibrium magnetization only in the limit where $M_{ir}$ (in Eq. (4)) is not very large compared to $M_{eq}$ which is generally not the case for single crystals at low $T$. For the same reasons the error in the derivation of the first critical field $H_{c_1}$ is often gigantic at low temperatures. This is illustrated in figure 50 (for various sample sizes $r_g$) which shows the effective $H^*_{c_1}(T)$ obtained by computer simulation using the present model and the experimental constraints and conditions encountered in real experiments (more explanations on these computer simulated experiments are presented in [358]). It is clear that the result of the simulated experiment differs considerably from the actual (BCS) $H_{c_1}(T)$ used in the starting calculations. The simulated $H_{c_1}(T)$ is very similar to those reported in the literature. To plot these curves we neglected the low-$H$ peak effect and we only used the « short range current » $J_{sr}$ in the calculations. The fit with experimental effective field can be further improved if we take into account $J_{lr}$.

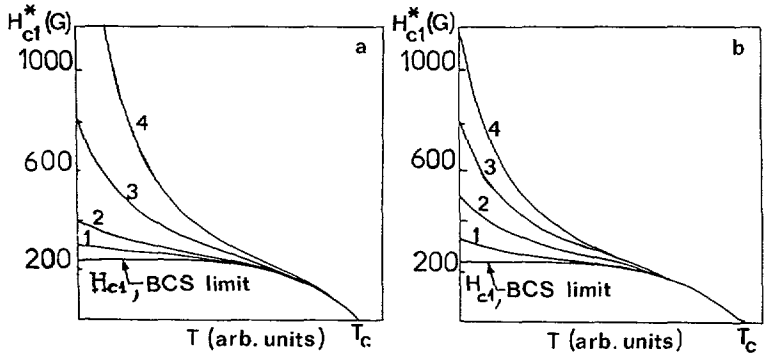


Fig. 50. — $H^*_{c_1}(T)$ calculated from the simulated magnetization curves ($M$ *versus* $H$) with several values of the grain radius (1, 10, 100, 500 μm) and $J_c$ : a) $J_c = 2 \times 10^6$ A/cm$^2$ ; b) $J_c = 5 \times 10^6$ A/cm$^2$ for 1 and 2 ; $J_c = 2 \times 10^6$ A/cm$^2$ for 3 and $J_c = 8 \times 10^6$ A/cm$^2$ for 4 (from Aguillon and Senoussi [358]). The same discrepancy is found for the calculated « reversible magnetization ».

### 11. Calculation of the low-$H$ hysteresis cycle of weakly coupled grains.

Since the discovery of high $T_c$ ceramics, the magnetization of granular materials has been the object of many theoretical and experimental studies [285-298, 303-305, 353-356]. However, up to very recently there has been no quantitative model relating the magnetization to the intergrain critical current and to the microstructure of sintered materials. Here, we would like to recall briefly the results of a recent calculation of the hysteresis cycle of granular superconductors (weakly coupled grains through Josephson interactions) [77, 104]. Since the hysteresis cycle induced by intragrain currents has been treated in the previous paragraph, we

shall restrict the present investigation to the low field domain where the applied field is smaller than the first critical field $H_{c_1}$ of the grains of mean radius $r_g$. In particular, we shall compare the calculated and the measured hysteresis cycles and emphasize their connection with the intergrains critical current as well as the influence of both the radius $R$ of the bulk sample and the radius $r_g$ of the grains.

As discussed previously, the intergrains magnetic current $J_{wl,\,mag}$ is related to the magnetization $M_{wl,\,ir}$. However, $M_{wl,\,ir}$ cannot be probed directly by classical measurements and must be extracted from the total magnetization $M_{tot}$ which is the only measurable quantity. The relationship between $J_{wl,\,mag}$ and the low-$H$ cycle of the weak links will be clarified later.

We wish now to use the same kind of model as above to calculate the low field magnetic loop exhibited by weakly coupled granular systems. At first, by analogy with the procedure outlined previously for single rystals, we consider the contribution of the reversible Josephson currents associated with the magnetization $M_{wl,\,eq}$ of the weak links [18, 341] (i.e. the analogous of the London-Abrikosov magnetization in homogeneous materials) to the total magnetization (see Ref. [97] for more details on this point). This magnetization is induced by currents flowing at the edge of the junction in the penetration depth $\lambda_J$ (as depicted schematically in Figs. 42b and 42c). Apart from this equilibrium Josephson term, the measured magnetization also includes two extra contributions $M_{wl,\,irr}$ and $M_{gr}$ associated respectively with the macroscopic current loops threading the weak links and extending over the whole sample and the « microscopic » current loops circulating inside the individual grains. Here, for simplicity we shall assume that $H < H_{c_1}$ so that the intragranular currents are restricted to the London penetration depth $\lambda$, though the calculation can be easily performed without this restriction (note that these small loops do not contribute to the measured transport currents). The currents associated with these various magnetizations are displayed in figure 33.

To calculate the hysteresis cycle we shall again neglect demagnetizing fields (which are deferred to Sect. 16) and assume that the total magnetization is the sum of the three contributions, $M_{tot} = M_{wl,\,eq} + M_{wl,\,irr} + M_{gr}$ just introduced. For axial symmetry we can write the total magnetization (in practical units in which $J$ is in A/cm$^2$ and M in emu/cm$^3$) (*)

$$M_{tot} = M_{wl,\,eq} + M_{wl,\,irr} + M_{gr} = \frac{-1}{10\,R^2}\int_0^R (J_{wl,\,eq}(r) + J_{wl,\,irr}(r) + J_{gr}(r))\, r^2\,dr \qquad (45)$$

and calculate the associated apparent magnetic current related directly to $M_{wl,\,irr}(H)$ (but not related directly to $M_{tot}$) by :

$$J_{wl,\,mag}(H) = 15\,\frac{M^+_{wl,\,irr} - M^-_{wl,\,irr}}{R} \qquad (46)$$

For the numerical calculation below we will take for $J_{wl}(B/B_0)$ the same exponential relationship as in equation (25). Moreover, from magnetic measurements on samples with different grain sizes, it is found that the hysteresis cycle depends strongly on $r_g$ not only for HTSC [287, 288] but also for classical superconductors [289]. Comparison with theoretical

(*) However, this formula does not mean that all of the three contributions are independent. This is because the effective field seen by a given filament includes both the external applied field $H$ and the field generated by the surrounding macroscopic current loops. The influence of the intrafilament currents on the macroscopic current loops is less important if the length of the filament is much larger than the sample radius $R$ (as assumed to be the case here).

calculations shows [77, 104] that this is consistent with the fact that $B_0$ varies as the inverse of $r_g$ :

$$B_0 = \frac{\alpha}{2} \left\langle \frac{\Phi_0}{(2\lambda + d) r_g} \right\rangle. \tag{47}$$

Here $\alpha$ is a prefactor of order unity at $T \ll T_c$. Comparison between calculated and experimental cycles are presented below for the following numerical values of the microscopic parameters of the junctions and the grains : $\langle \lambda(T = 0) \rangle \approx 0.5$ μm in average and $J_{wJ}(H = 0) \approx J_0 = 2\,000$ A/cm$^2$, $d = 0$ and $\alpha \approx 2$.

**11.1** THE HYSTERESIS CYCLE, THE INTERGRANULAR CRITICAL CURRENT AND THE CONNECTION WITH THE MICRO AND MACRO STRUCTURES.

**11.1.1** *Comparison with experimental data.* — Shown in figure 51a and figure 51b are the evolutions of the measured and the calculated [77, 104] hysteresis loops as a function of the maximum cycling applied field $H_{max}$. In this example, we took $R = 3$ mm, and $r_g = 1.5$ μm. We note a strong similarity between the calculated and the measured cycles. We also find that changing either $R$, $r_g$ or $J_0 = J_{wJ}(H = 0)$ only changes the amplitude of the cycle but not its shape.

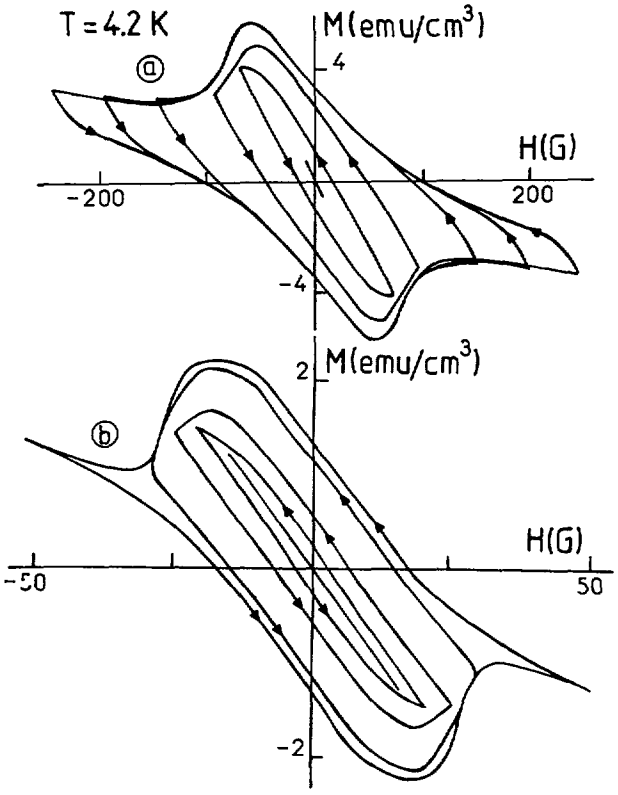


Fig. 51. — Development of the low $-H$ cycle of a sintered pellet of $YBa_2Cu_3O_7$ as a function of the maximum applied field $H_{max}$ for $R = 3$ mm, $r_g = 1.5$ μm, a) experimental ; b) calculated taking $J_0 = 2\,000$ A/cm$^2$ and $H_{c1}^{w} = 1.5$ G.

It is to be stressed that the linear and reversible region of the initial curves seems to extend over nearly 10 œ. This is much more than the value $H_{c_1}^{w} = 1.5$ œ used in the initial equations as the Josephson first critical field of the weak links. In other words, this shows that it is extremely difficult to determine the exact $H_{c_1}^{w}$ from the measured hysteresis cycle because of irreversibility effects which hinder the propagation of Josephson vortices within the interior of the weak links and increase the apparent $H_J$. The same source of errors has been discussed before (in Sect. 10) for $H_{c_1}$ and $M_{eq}$ of decoupled grains and single crystals (see Fig. 50).

**11.1.2** *Evolution of the intergranular hysteresis cycle with R.* — The influence of the macroscopic radius ($R$) on the low-$H$ cycle is illustrated in figure 52a (measured) and 52b (calculated). It is clear that in the two cases the hysteresis cycles are quite similar and stay almost the same upon increasing $R$ by a factor of 2.5. From these figures we conclude that : (i) Near $H = 0$, $M_{tot}$ increases only very slowly ($\approx$ logarithmically) with $R$. This is in contradiction with the usual Bean model which states that the irreversible magnetization is proportional to $R$, but in agreement with the conclusion of section 6 and figure 19 concerning size effects in the limit $H \approx 0$. (ii) The initial branch of the total magnetization exhibits almost perfect shielding in the limit where $H$ tends to 0 (i.e. $M \approx -H/4\pi$), in agreement with experimental data, assuming $R \gg \lambda_{eff}$. Here $\lambda_{eff}$ is an effective penetration depth (estimated in Ref. [357]) which is a combination of both $\lambda$ and $\lambda_J$ ; see also figure 33a. (iii) At high

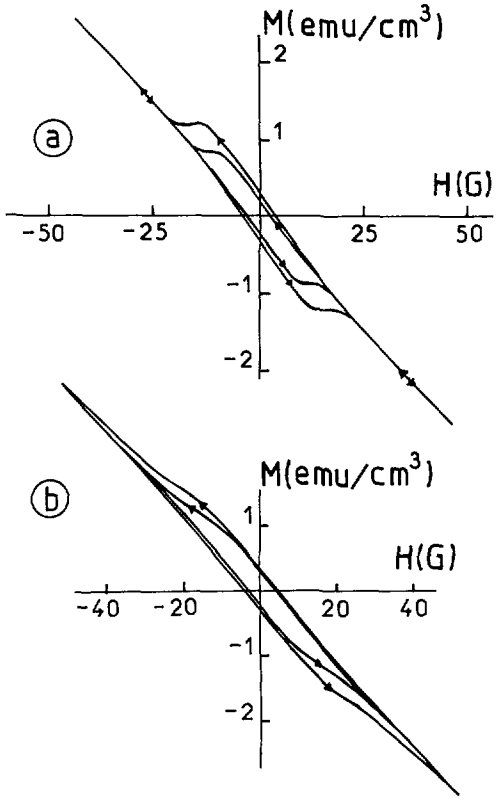


Fig. 52. — Influence of the radius $R$ of the pellet on the low-$H$ cycle, a) experimental [198], b) calculated. Inner cycle $R = 2$ mm, outer cycle $R = 5$ mm.

enough fields, $M_{wl,\,irr}$ vanishes and the total magnetization reduces to that of a collection of independent grains or filaments ; see also figure 33c. In addition, in this field domain the magnetization becomes again linear and reversible and scales with the inverse of the grain radii, again in good agreement with experiments [198, 287].

**11.1.3** *Variation of $M_{tot}$ with $r_g$, microscopic size effect.* — The influence of the size of the grains ($\langle r_g \rangle$ = 1, 3.5 and 5 μm) is presented in figure 53a for the experimental cycles [198, 287] and in figure 53b for the calculated ones. The agreement is still very good except for the persistence (Fig. 53a) of some hysteresis at relatively high field in the experimental case. This effect can be easily accounted for by adding a further but small current term to equation (45). In addition, since this term persists at higher fields it should be slowly varying with $H$. Again, the exact shape of the loops depends on both $R$ (the radius of the macroscopic pellet) and $r_g$ but the agreement between the experimental and the calculated cycles (Figs. 53a, 53b) is once again excellent. This is especially true if one remembers that the cycle does not in fact depend on $1/\langle r_g \rangle$ but rather on the average $\langle 1/r_g \rangle$ of the inverse (the averaging of $r_g$ is more complicated when $\lambda/r_g$ is not very small), which is larger (Jenssen inequality). Lastly, we observe that the slope of the linear domain for $H \gg H_0$ (or $H > H_{c_2}^{w}$) decreases as $1/r_g$.

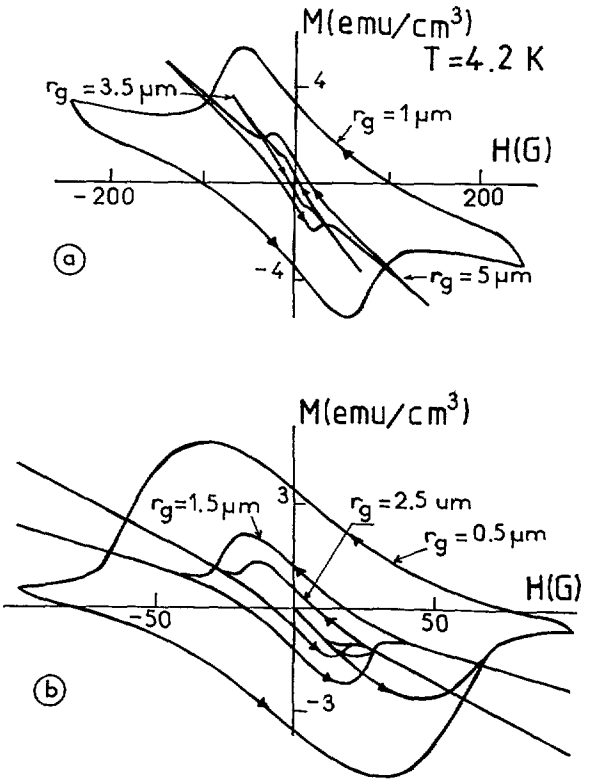


Fig. 53. — Influence of the radius $r_g$ of the grains on the low-$H$ cycle for different macroscopic radii $R$, a) experimental [198] ; b) calculated. Note that the radii $r_g$ are not the same in the two cases. The agreement should be improved if we took into account the fact that $(\langle 1/r_g \rangle)^{-1}$ is necessarily smaller than $\langle r_g \rangle$ ; $J_0$ = 2 000 A/cm².

**11.1.4** *Variation of the apparent magnetic critical current with R.* — The critical current density deduced from formula 40 is plotted in figure 54a for $H = 0$ and in figure 54b for $H = 10$ G as a function of the radius $R$ of the specimen for different fixed $r_g$. In agreement with experimental data in figure 36 we see that the apparent current density decreases approximately as $1/R$ at large $R$ ($R \gg R_0$ where we recall that $R_0$ is a characteristic length related to $B_0$ by Eq. (16)) and approaches a maximum value as $R$ tends towards $R_0$ ($R \leq R_0$). This is to be compared with the measured transport critical current as a function of $R$ for $H = 0$ which is found [284-286, 291, 328] to decrease as $1/R$. (Compare also with Fig. 36 and with Fig. 19 of Sect. 6 valid for zero applied field, i.e. in the remanent state). It is clear that the agreement between the experimental and the computed currents is again reasonable. It is also interesting to emphasize that the size effect (i.e. the fact that the effective experimental currents decrease as $1/R$ for $R \leq R_0$) reported in figure 19 at $H = 0$ and ascribed to the self-field $H_{sf}$, disappears when the applied field is much higher than $H_{sf}$.

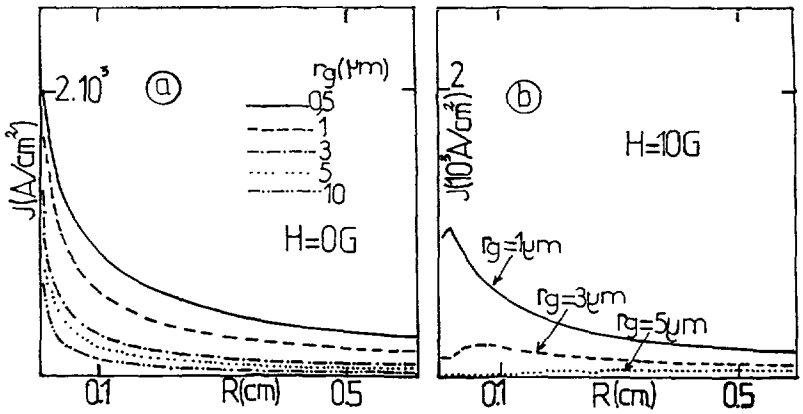


Fig. 54. — Calculated critical current density as a function of the radius $R$ of the pellet at $H = 0$ and $H = 10$ œ and for the indicated grain radius $r_g$.

**11.1.5** *Variation of the apparent magnetic current with $r_g$.* — We have seen that the experimental data of Maury [198] suggest that the characteristic field $B_0$ controlling the field variation of $J_{wl}$ is inversely proportional to $r_g$. To illustrate this effect we show in figure 55a the calculated variation of $J_{wl,\,mag}$ with $r_g$ for four different but fixed radii $R$ ($10^{-3}$, $10^{-2}$, $10^{-1}$, and 1 cm) and for $H = 0$. As we can see the current is considerably enhanced as $r_g$ is decreased. Moreover, here too the influence of $H$ is very strong for $H = 10$ G and $R = 10^{-2}$, $10^{-1}$, and 1 cm.

**11.1.6** *Discussion.* — We expect that Bean's model should be severely modified by the weak link network. Moreover, the Bean model assumes implicitly that $J$ is independent of the radius $R$ of the specimen. However, we have seen that this assumption is not always realized particularly in granular materials. The various limits are summarized below.

From equations (16) and (47), it turns out that for the present examples the characteristic length $R_0$ (for the intergrain currents) is related to $r_g$ and to $J_0$ by $R_0$ (cm) $\approx \alpha \Phi_0/(2 \lambda J_0 . r_g)$ with $\alpha \approx 1$. This implies that for $r_g \approx 0.5$ μm and $J_0 \approx 2\,000$ A/cm$^2$ $R_0 \approx 50$ μm. In general $r_g > 1$ μm and $J_0 \geq 2\,000$ A/cm$^2$ so that $R_0$ is expected to be lower than this value in most

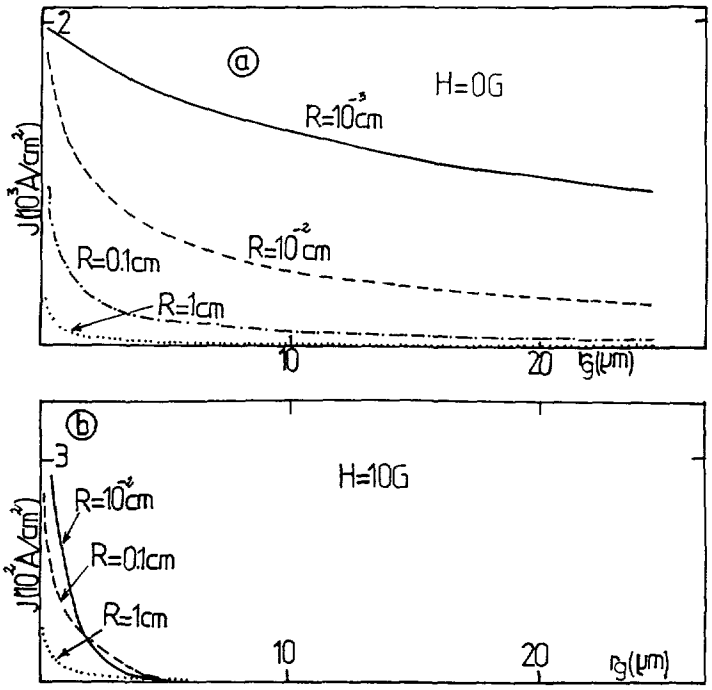


Fig. 55. — a) Shows the variation of $J_{mag}$ with $r_g$ for the different but fixed radius $R$ ($10^{-3}$, $10^{-2}$, $10^{-1}$, 1 cm) and for $H = 0$ and $J_0 = 2\,000$ A/cm$^2$. It is seen that the current is enhanced considerably as $r_g$ is decreased. The influence of $H$ is illustrated in figure b for the same parameters as in a.

cases. We recall however that $R_0$ depends in fact on $H$ and increases notably for $H \gg H_0$.

For $H < H_0$ the real $J_0$ would be proportional to the maximum critical current density of the Josephson junction and would probably be given by the Ambegaokar-Baratoff formula [33]. Finally, it is found that as $T$ increases the characteristic field $B_0$ decreases roughly linearly with temperature and this is not quite consistent with BCS temperature variation of $\lambda$ if one accepts the validity of Fraunhofer's equation (47).

### 11.2 Generalization of the Bean model.

**11.2.1** *The relationship between the intergranular current density and the hysteresis cycle.* — We have seen that in the case of YBaCuO intragranular current density depends rather slowly on $H$. Then, for homogenous superconductors having a critical current density obeying a single exponential law as given by equation (25) we find the following results between the hysteresis cycle on the one hand and $J_{mag}(H)$ and $M_{eq}(H)$ on the other hand

$$J_{mag} = 30 \frac{M_{irr}}{R} \left[ 1 - \frac{1}{10} \left( \frac{R}{R_0} \right)^2 e^{-2\frac{B_{eff}}{B_0}} \right]; \quad \left( R \ll R_0 e^{+\frac{B_{eff}}{B_0}} \right) \tag{48}$$

$$M_{eq}(H) = M_{rev}(H) + M_{irr}(H) \frac{R}{4 R_0} e^{-\frac{B_{eff}}{B_0}} \tag{49}$$

We recall that $M_{ir}$ and $M_{rev}$ are defined from the hysteresis loop by equations (4, 5) whereas $B_{eff}$ which depends on $M_{eq}(H)$ is given by equation (39). It is interesting to note that the Bean model is always more easily satisfied at high fields such that $B_{eff} \gg B_0$, in particular close to the irreversibility line. The same remark is valid for the relation between $M_{eq}$ and $M_{rev}$. Concerning this relation, however, we can easily see that at very low $T$ and $H$ we have $\exp(-B_{eff}/B_0) \approx 1$. Then assuming $J_0 = 6 \times 10^6$ A cm$^{-2}$, $H_{c_1} = 250$ G, $R = 1$ mm and $R/R_0 = 1$, putting in equations (48, 49) and taking $|M_{eq}| \ll H_{c_1}/4\pi$ yields $M_{eq}/M_{rev} \approx 5 \times 10^{-3}$ and consequently two orders of magnitude errors in equation (5) which is often applied to derive $M_{eq}(T, H)$ from the experimental hysteresis cycle assuming $M_{eq} = M_{rev}$. The situation is even more dramatic if one takes into account of the low-$H$ peak (in the cycle) the effect of which is to lower the apparent $R_0$ to be put in equation (49). Nevertheless, the error diminishes very rapidly with $T$, $H$ and $R$, particularly for Bi oxides, because of the exponential drop with $T$ and $H$ entering $M_{irr}$ and equation (49). This is in fact reflected indirectly in figure 50 which compares the apparent critical field $H_{c_1}^*$ (obtained by numerical simulation of the experiment) and the theoretical BCS value of $H_{c_1}$ used in the calculation (represented by the lowest curves of the figure). See also references [77, 358]. The same kind of curves are encountered when $H_{c_1}$ is extracted directly from the experimental curves. Consequently, we conclude that the higher the irreversible magnetization the larger the uncertainties in the equilibrium quantities $H_{c_1}$ and $M_{eq}$. Note that we have performed the same calculations as above using other $J(H)$ models (Koppé and Kim models, Sect. 6) and found very similar results as equations (48) and (49).

**11**.2.2 *The relationship between the intergranular current and the low-H cycle.* — Quite generally we find [77, 104] that the irreversible magnetization $M_{wl,\,irr}$ induced by intergrain currents is proportional to the total magnetization $M_{tot}$ and that the relationship between the low field hysteresis cycle and the apparent current is given (to a good approximation) by :

$$J_{wl,\,mag} = 15 \frac{M_{tot}^{+} - M_{tot}^{-}}{R} \frac{\chi(H < H_{c_1}^{w})}{\chi(H < H_{c_1}^{w}) - \chi(H > H_{c_2}^{w})} = 15 \frac{\Delta M}{R} \frac{p}{\Delta p} \tag{50}$$

Here $\chi(H < H_{c_1}^{w}) \approx [\partial M/\partial H]_{H \approx 0}$ is the slope of the initial or virgin magnetization in the linear region near $H \approx 0$ whereas $\chi(H \geqslant H_{c_2}^{w})$ is the slope of the magnetization in the linear region above $H_{c_2}^{w}$ (but below $H_{c_1}$). The quantities $\Delta M$, $\Delta P$ and $p$ in equation (50) are defined in figure 56. In addition, the proportionality factor $p/\Delta p$ is related to the microstructure of the sample and has been calculated [77, 104] in various approximations. In the limit of a long cylinder where demagnetizing effects are negligible and the grains sufficiently large ($r_g \gg \lambda$) we have the approximate formula :

$$\frac{p}{\Delta p} = \langle (2\lambda + d)/r_g \rangle \qquad (r_g \gg \lambda_L) . \tag{51}$$

Putting this equation in equation (50) gives :

$$J_{wl,\,mag} = 15 \frac{\Delta M}{R \langle (2\lambda + d)/r_g \rangle} , \qquad (2\lambda + d) \ll r_g . \tag{52}$$

We wish now to recall that the apparent current density (whether magnetic or transport) represents a certain spatial average of the current density over the specimen and that the resulting apparent current depends on the exact $J_{wl}(H)$ relationship as well as on the

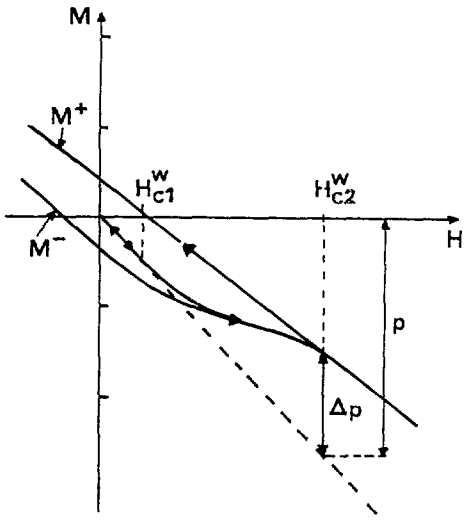


Fig. 56. — Definition of the parameters $\Delta P$ and $P$ used in equation (50) relating the magnetic critical current density of the weak link network to the associated low field hysteresis loop. Note that equivalent parameters will be defined from susceptibility curves in figure 71.

dimension of the sample *via* the self-field (see Sect. 6 and Fig. 19 in this section). It also depends on $r_g$ *via* the characteristic field $B_0$ (Eq. (47)). It is equally important to remember that because of the variation of the self-field through the sample, the apparent current can have almost no thing to do with the real $J_{wl}(H)$ at low $H$ if $R \gg R_0$. Using equation (47) and assuming $H \approx 0$. In the present exponential model we find :

$$J_{\text{wl, mag}} \approx \frac{15\, B_0}{2\, \pi R}\left[\ln\left(\frac{R}{R_0}\right) - \frac{3}{2}\right] \approx \frac{15\, \phi_0}{8\, \pi r_g R \lambda}\left[\ln\left(\frac{8\, \pi J_0 R r_g \lambda}{5\, \phi_0}\right) - \frac{3}{2}\right], \quad (R \gg R_0)\,. \tag{53}$$

What is very interesting to emphasize is the fact that there is no time dependent quantity in this expression. This probably explains why no significant time effect has been seen in the low-$H$ hysteresis cycle of the weak links. The physical meaning of equation (53) is interesting. It means that for a given fixed current the total irreversible magnetization $(M^+_{\text{tot}} - M^-_{\text{tot}})/2$ tends to zero as $1/r_g$ or as the number of weak links by unit length which is proportional to $1/r_g$. In other words, $(M^+_{\text{tot}} - M^-_{\text{tot}})/2$ is proportional not only to the intergrain current but also to the density of weak links. Concerning the above expressions, it is of interest to emphasize again that : (1) The mean value of the ratio $\langle(2\,\lambda + d)/r_g\rangle$ is directly related to the slopes $\chi(H = 0)$ and $\chi(H \gg H_0)$ of the total magnetization in the reversible field domains of the low $-H$ cycle (see Fig. 56). (2) The mean value $\langle 1/r_g\rangle^{-1}$ is always smaller than the mean radius $\langle r_g\rangle$ (Jensen inequality). Owing to the comparison between experimental and theoretical data we find it often reasonable to take $\langle 1/r_g\rangle^{-1} = \langle r_g\rangle/2$ (or $\alpha \approx 2$ in Eq. (47)). (3) It is also important to keep in mind that the London penetration depth $\lambda$ must in principle be averaged over the crystallographic axes of the grains. In addition, this averaging depends on the exact shape of the grains and is in fact extremely difficult to carry out correctly. (4) The physical thickness $d$ of the weak link (i.e. the region where the order parameter is strongly depressed) is difficult to determine as well but it is expected to be much lower than 2 $\lambda$ (which is equal to

the electromagnetic thickness of the junction) and can be neglected in compact specimens (i.e. $d \ll 2\lambda$).

## 12. Magnetic susceptibility of superconducting materials.

12.1 INTRODUCTION. — Magnetic susceptibility measurements represent probably the most common and the most popular technique for the characterization of superconducting materials [84-95], coming perhaps just after resistivity measurements. They can provide very important and very valuable information on the superconducting properties but, contrary to a naive and a wide spread opinion the obtention of quantitative and correct information requires much analysis and a great deal of effort for their interpretation. This interpretation is relatively simple only when we compare samples of the same family with the same shapes, the same dimensions, in the same applied field, and measured at the same temperature with the same time scale.

Usually, one has to distinguish between ac (alternating current) and dc (constant current) susceptibilities. The ac-susceptibility itself includes an in phase (or real) component $\chi'$ and an imaginary out of phase component $\chi''$. Both components depend strongly on the microstructure of the specimen. For this reason and for the sake of simplicity we shall discuss separately the case of single crystals (including decoupled oriented grains) and that of fine grains weakly coupled through Josephson interactions in the limit $H \leq H_{c_1}$ (we recall that $H_{c_1}$ is the first critical field of the grains). It is interesting to note that the theoretical treatment of the more general case (i.e. including both intragranular and intergranular critical currents which appear for $H > H_{c_1}$) is time consuming but presents no difficulty with the present model. Concerning dc-measurements (i.e. measurements in a given static field as a function of temperature) one defines the so called zero field cooled susceptibility ($\chi_{zfc}$) and field cooled susceptibility ($\chi_{fc}$). At this point it is to be emphasized that these terminologies are not connected with any specific feature of HTSC and have been introduced by analogy with experiments on spin glass (S-G) materials. As in these systems, $\chi_{zfc}$ is by definition the susceptibility measured just after cooling the sample in zero applied field down to the lowest temperature, turning on the dc-measuring field and then increasing the temperature in such applied field. The other dc susceptibility, $\chi_{fc}$, is measured during cooling from above $T_c$ to the lowest temperature of interest in a static cooling field $H_{cool}$. At a given field $H$, a given temperature $T$ and for a fixed experimental time scale these two susceptibilities are different from each other whenever the critical current density is different from zero (or equivalently whenever the vortices are subject to pinning forces different from zero). The point of intersection or bifurcation (in the $T$-$H$ plane) of $\chi_{fc}(T, H)$ and $\chi_{zfc}(T, H)$ is sometime taken as defining the irreversibility line, but as we shall see it is not readily a property of the material alone and depends on many experimental conditions in general (see [359]). In addition it is to be noted that close to this line these different susceptibilities are no longer independent of the amplitude $H$ of the measuring field. We will try here to clarify these points.

Considering ac susceptibilities it can be shown that if the time scale of the dc measurement is comparable to the period of the ac field then $\chi'$ and $\chi_{zfc}$ are « almost » identical except in a narrow temperature region around the maximum of $\chi''(T)$ where they are slightly different (we are assuming that the measured sample is the same in both cases). See figure 57 which displays $\chi'$ and $\chi_{zfc}$ calculated (see below) at the same temperatures and fields.

Magnetic and transport properties of conventional superconductors in the presence of applied ac fields were extensively investigated during the sixties and seventies [19]. Bean [72b] was the first to point out the advantages of ac-methods for the investigation of the critical

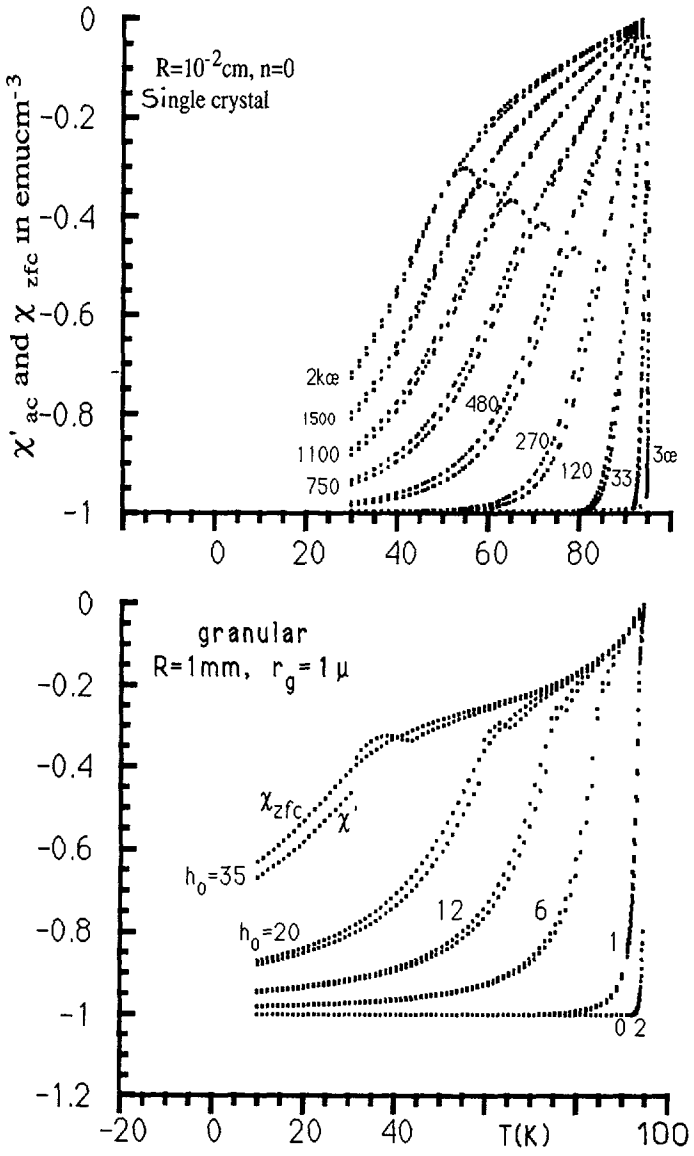


Fig. 57. — Compares the calculated ac-susceptibility $\chi'$ (lower points) and dc-susceptibility $\chi_{zfc}$ (upper points, single crystals) as a function of temperature for several applied fields and for intragrain (upper curve) and intergrain (lower curve) current densities. We do not know the origin of the small anomaly in $\chi'$. It is possibly due to the sharp peak in the calculated hysteresis cycle associated with $\chi'$. In experiments the sharpness of the peak and other anomalies are smoothed out by demagnetizing effects and by inhomogeneities.

current density. The ac-susceptibility considered here is in principle deduced by means of a lock-in amplifier which is assumed to detect only the voltage component at the fundamental frequency $\nu$ of measurement (band-pass mode) [360, 361]. In particular, ac-methods were frequently used to determine the critical current density at and near the surface of the specimen [362-364] in the presence of a superimposed constant field ($H$) much greater than the amplitude $h_0$ of the variable field ($H \gg h_0$). The condition $H \gg h_0$ is intended to linearize

the $J$ *versus* $h_0$ function (or equivalently to minimize the dependence of the measured critical current density on the ac-field $h(t) = h_0 . \sin(\omega t)$ (since it can be developed into $J(H + h(t)) \approx J(H) + h(t) . (dJ/dH)_H$) for $H \gg h_0$. In the ac-method proposed by Bean the critical current can also be deduced from higher harmonics of the imposed frequency and therefore provides more information on $J$ than usual susceptibility measurements. In real applications, this method neglects any effect associated with the equilibrium magnetization $M_{eq}$. For the same arguments as those discussed for the hysteresis cycle, this is probably not justified except in the limit where the total applied field is much larger than $H_{c_1}$ ($H \pm h_0 \gg H_{c_1}$).

Existing theoretical models for the calculation of the susceptibilities $\chi'$ and $\chi''$ can be classified into three main categories related either to the conventional critical state model [365-367] or to spin glass like models [303-305, 308-370], or else to the collective pinning theory in the limit of very low field. The latter approach will be the object of the next section 13 where we will try to find out the threshold field $h_{2,\,th}$ which delimits a line in the $T$-$H$ plane below which the critical state is no longer valid and where the use of collective pinning treatment is necessary. Concerning the S-G like approach it turns out that it is somewhat more general and more appropriate than the critical state to investigate cooperative and transition effects in the vortex lattice [371-373]. However, it seems that the working hypothesis used in S-G like models are generally rather restrictive and only valid in very special conditions rarely satisfied in practice. We believe that the critical state like models as those first developed by Clem [365] and then by Müller [366, 367] are generally easier to handle theoretically and more appropriate from the point of view of the derivation of the critical current density from experimental data (see below). They are also simpler for the investigation of the effects of other experimental parameters such as the size of the grains and the macroscopic radius of the sample. It seems that the latter size effect is hard to investigate in the framework of the S-G like picture. Nonetheless we must keep in mind that the critical state model used in this section can break down either for very low amplitudes $h_0$ of the alternating field or in the TAFF limit. In addition, other problems can arise because of eddy currents (connected with viscous flux flow) especially at high frequencies and low $J$. For the moment we shall ignore these extra effects and we wish now to generalize the above fluw creep phenomenological approach and calculate the susceptibilities of both single crystals and granular materials using the same models as those introduced previously for the computation of the hysteresis cycles (Sect. 10, 11).

Concerning high $T_c$ materials, susceptibility data are currently used to determine the superconducting transition temperature $T_c$, the width $\Delta T$ of this transition, the fractional volume $V_p$ of superconducting material, the critical current density $J(T)$ as well as the energy barriers entering the flux creep theory *via* the frequency dependence of the temperature $T_m$ corresponding to the peak of $\chi''(T, \omega)$ [86, 87, 91]. In addition, we have already mentioned that ac-susceptibility has sometimes been used to derive either the apparent irreversibility line (another spin glass terminology) frequently associated with the peak of $\chi''$ [26, 359, 374]. We shall see however that, apart from the determination of $T_c$, the relation of $\chi''$ and $\chi'$ with the other physical quantities just mentioned is as a rule very complex and sometimes contrary to the most common opinions on the subject. This is why we find it important to pay much attention to susceptibility measurements here.

We begin by considering the case of single crystals (§ 12.2) emphasizing successively the influence of $h_0$, the macrostructure and demagnetizing effects on $\chi'$. In order to help understanding the physical meaning of the peak in $\chi''$ and its relation to the critical current density $J$ on the one hand and to the so called irreversibility (or depinning) line on the other hand we will also discuss in many details the influence of the radius of the sample. Granular

superconductors are examined in section 12.3, where the influence of both the microstructure and macrostructure are illustrated by several numerical examples. The relationship between $\chi''$ and the magnetic intergranular current density $J_{wl,\,mag}$ is investigated in detail and a relationship of the same form as that derived in section 11 from the low-$H$ cycle (Eqs. (50) and (52)) is established in certain conditions. Influence of anisotropy on the magnetization of polycrystalline materials is examined in § 12.4. dc-susceptibilities ($\chi_{zfc}$ and $\chi_{fc}$) are the subject of section 12.5 where we will show that there is a striking analogy with the corresponding quantities in reentrant-ferro-spin-glass materials. Frequency effects on single crystals and polycrystals will be considered in section 12.6 and 12.7 respectively.

As in the preceding sections, we shall again make extensive use of numerical calculations to elucidate the dependence of $\chi'$ and $\chi''$ upon the various parameters $R$, $r_g$, $N$ (the demagnetizing factor) as well as the $J$ *versus* $T$ law.

## 12.2 AC-SUSCEPTIBILITIES OF SINGLE CRYSTALS AND ORIENTED DECOUPLED GRAINS.

12.2.1 *Experimental results.* — Let us now consider the temperature variation of $\chi'$ and $\chi''$ assuming that the applied field varies sinusoidally with time ($h = h(t) = h_0 . \sin(\omega t)$) and includes no steady field term. Figure 58 [376] shows the temperature variation of the ac-

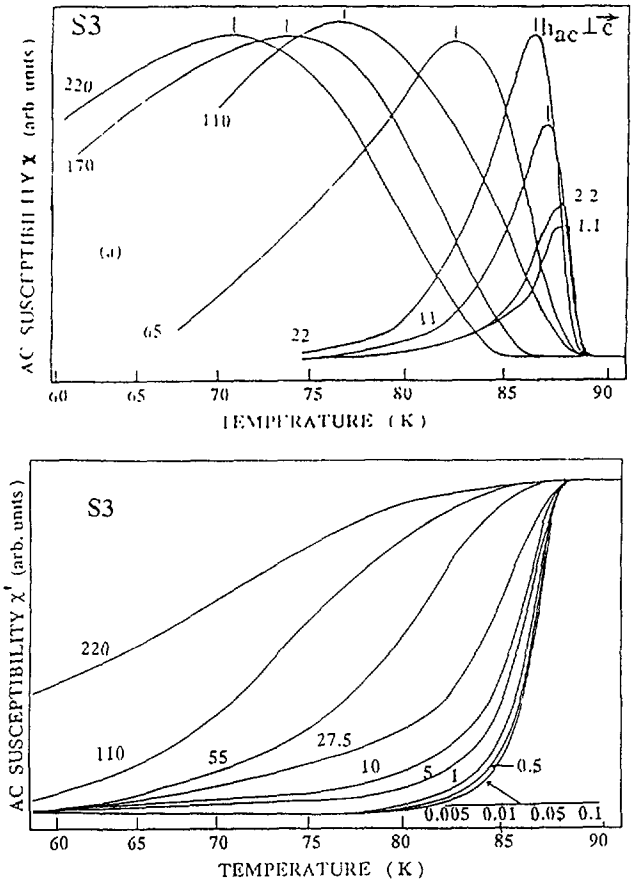


Fig. 58. — Typical examples illustrating the temperature variation of the ac-susceptibilities $\chi'$ (in phase component) and $\chi''$ (out of phase component) for a single crystal of $YBa_2Cu_3O_7$ [376], at the indicated amplitudes $h_0$ of the alternating field (in œ) ; $h$ in the $a$-$b$ planes [376].

susceptibility of a single crystal of $YBa_2Cu_3O_{7-\delta}$ at various amplitudes $h_0$ of the alternating field, for $h$ in the $a$-$b$ planes.

In the extensive published literature on HTSC one encounters a large variety of shapes for $\chi'(T)$ and $\chi''(T)$ curves but presenting no evident correlations with the microstructure nor with the critical current density. In particular, the physical meaning of the peak $\chi''_m(T_m)$ in the $\chi''(T)$ curve is at present controversial. We have already mentioned that such a peak is sometimes ascribed to a melting transition in the vortex lattice. On the other hand, by analogy with spin glass materials and following some theoretical models, the peak has also been often considered as a manifestation of an Almeida-Thouless transition of the kind observed in spin glasses. Finally, it seems that a majority of authors have a rather « conservative » point of view and believe that it is simply due to more classical pinning effects at low enough frequencies (the physical meaning of the term low frequency will be explained later). It is to be noted that in this last case the peak should depend both on the size of the sample and on the measurement frequency. Unfortunately, despite the fundamental as well as practical importance of this question, there is as yet (except in very few cases [377-379]) no systematic investigation of such size effects in the literature on high $T_c$ superconductors. Likewise, it seems that there is not yet any clear cut analysis of the experimental data near the irreversibility line in favour of or against a thermodynamic melting transition (at least in the case of Bi and Tl based compounds). We hope that the following analysis based on the usual critical state picture is sufficient to explain most of the experimental data described above concerning ac-susceptibility.

**12.2.2** *A model for the calculation of the ac-susceptibility of single crystals and decoupled grains.* — For the present calculation we shall assume that the local critical current density follows the expressions given below as a function of $H$ and $T$. These equations are very similar to equations (39-44) used for the calculation of the hysteresis cycle. For the sake of simplicity, we shall only use here the short range current term $J = J_{sr}$ instead of $J = J_{sr} + J_{lr}$ in equation (43). The numerical calculation is based on the following equations (56, 57) the derivation of which will be reported elsewhere :

$$J(T, b) = J_0(1 - T/T_c)^n \exp\left[\frac{-T}{T_0}\right] \exp\left[\frac{-b}{B_0(T)}\right],$$
$$B_0(T) = [1 - (T/T_c)^m]. \tag{54}$$

We recall that $b$ is the local magnetic induction and that the apparent field seen by the vortices at the surface is given (for a long cylinder) not by $h(t)$ alone but by :

$$h_{eff}(T, t) = h(t) + 4\pi M_{eq}(T, h(t)) \tag{55}$$

$$\chi' = \frac{4}{\pi h_0^2} \int_0^{h_0} [M^+(h) + M^-(h)] \frac{h\,dh}{\sqrt{h_0^2 - h^2}} \tag{56}$$

$$\chi'' = \frac{4}{h_0^2} \int_0^{h_0} [M^+(h) - M^-(h)]\,dh. \tag{57}$$

Equations (56) and (57) were derived assuming that the lock-in amplifier is programmed in the narrow band mode, hence detecting only the fundamental frequency of the signal. The functional forms (or the mathematical equations) of the magnetizations $M_{vg}$ (the virgin branch), $M_{rl}$ (the reversal branch) $M^+$ and $M^-$ (the cyclic branches), which are calculated in reference [77] for the whole hysteresis cycle, depend on the relative value of $h_0$ with respect to the full penètration depth field $H_p$ (defined in Fig. 2).

It can be seen from the various equations of reference [77] and from equation (57) that $\chi''$ is related to some spatio-temporal average of the critical current density and gives information on such a quantity (see below). This is because $\chi''$ is proportional to the total area of the hysteresis cycle induced by the applied oscillating field $h_0 \sin \omega t$, divided by $4\, h_0^2$. However, as already noticed the relationship between $\chi''$ and $J$ is in fact very complex and these information are only qualitative and often restricted to a very small region of the $T$-$H$ plane (in particular for single crystals). The examination of equation (56) shows that the in-phase susceptibility $\chi'$ does not exactly represent the average slope of the $(M^+ + M^-)/2$ curve but our numerical calculations show that the difference is generally rather small (as illustrated in Fig. 57). The small anomaly of $\chi'$ in figure 57 is perhaps associated with the sharp peak in the corresponding hysteresis loop and to the absence of smoothing effects due to a demagnetizing field.

12.2.3 *Evolution of the calculated $\chi'(T)$ and $\chi''(T)$ of single crystals with the amplitude $h_0$ of the applied field ; the physical meaning of the maximum in $\chi''(T)$.* — Shown in figure 59a, b, c are the calculated susceptibilities $\chi'(T)$ and $\chi''(T)$ curves for various amplitudes $h_0$. The same calculation has been repeated for three different exponents $n$ ($n = 1/2$, 1 and 3/2) entering equation (54) which defines the $J$ *versus* $T$ function (the exponent $m$ controlling $B_0$ being kept constant and equal to 2.2 as in the calculation of the hysteresis cycles). The values of the other parameters ($J_0$, $\lambda_0$, ...) are given in the figure caption and are roughly the same as for the corresponding hysteresis cycles of section 8. At first, it is clear that the calculated curves resemble strongly the experimental ones except that the peak of $\chi''$ is somewhat sharper and the transition region ($\chi'(T)$ curve) narrower here than in the experimental case, in particular for large radii. This however depends on the value of the exponent $n$. Note also that the fields are larger in our calculations. It is seen that at very low amplitude $h_0$ and for $n = 1/2$ the amplitude $\chi_{max}(T_m)$ of the peak is almost independent of $h_0$. On the other hand, it varies rather rapidly with $h_0$ for $n = 1$ and $n = 3/2$. This reflects the fact that the slope of $J(T)$ at $T = T_c$, as given by equation (54), is infinite in the first case but zero in the last one. Obviously the value $n = 1$ corresponds to intermediate behaviour. These points will be considered later where we shall see that for fine grained samples such that $R/\lambda_0 < 1$ (we recall that $\lambda_0$ is the London depth at $T = 0$) most of the broadening of $\chi'$ reflects the temperature variation of the penetration depth $\lambda$ whereas for large samples ($R/\lambda_0 \gg 1$, $\lambda_0 = \lambda(T = 0)$) this effect is negligible and most of the broadening in these quantities is in general related to demagnetization effects and eventually to inhomogeneities in $T_c$ (**). Shown in figure 60 is the factor $(h_{eff} - H_p(h_0))/H_p(h_0)$ where the effective field is defined by equation (55) and where $H_p(h_0)$ is the field of complete penetration of the magnetic flux down to the centre of the sample assumed to be a long cyclinder with $N \approx 0$. We wish to make two important remarks.

1) Since our calculation shows that the factor $h_{eff} - H_p(h_0)$ crosses zero at $T = T_m$ this means that the maximum in $\chi''$ occurs just when the first vortices arrive at the centre of the specimen upon heating the sample. In other terms, as $T$ increases the flux front (which is generally very close to the surface at low temperature) moves towards the centre $r = 0$ at which we have $H_p(h_0) = h_{eff} = h_0 + 4\pi . M_{eq}(h_0)$. It is striking to find that this result is

(**) It is to be recalled that in the numerical calculations carried out in this paper we assumed that $\lambda$ was independent of $B$. In reality, $\lambda$ varies as $(1 - B/B_{c_2})^{-1/2}$ (Sect. § 2.4). Then, for very fine grains this may lead to a broadening of the superconducting transition because of the factor $\lambda/r_g$ which controls $M$ in this $T$-$H$ domain.

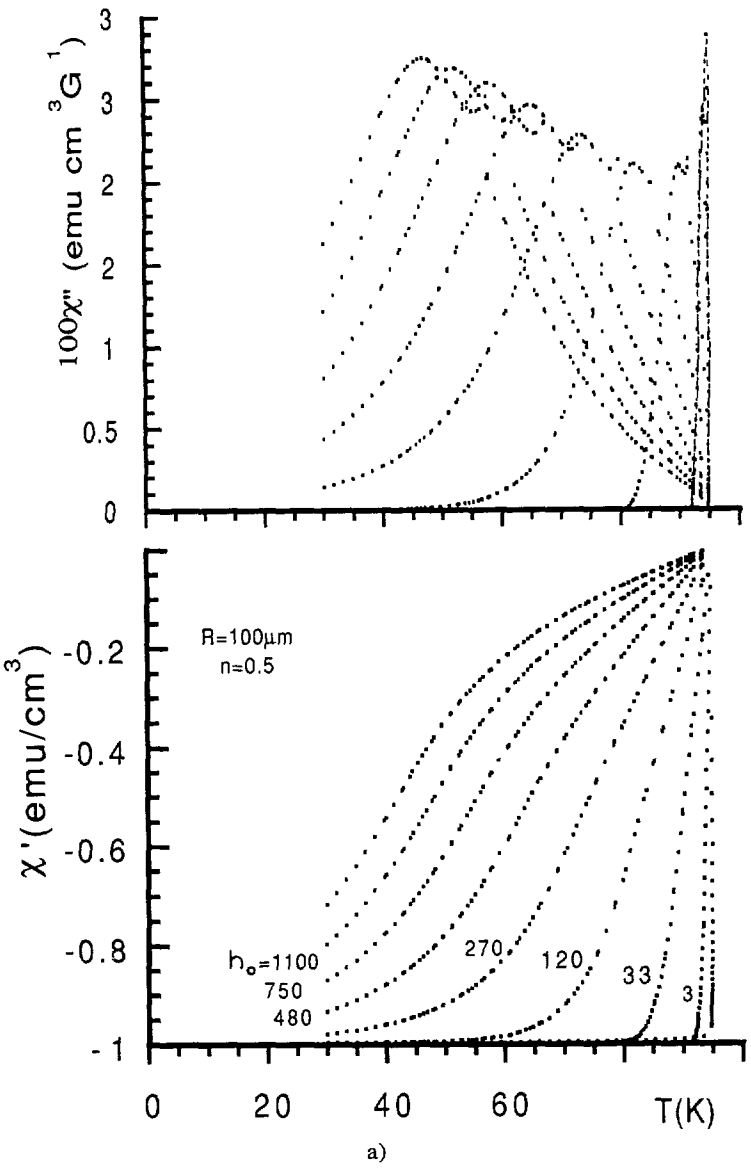


Fig. 59. — Calculated susceptibilities $\chi'(T)$ and $\chi''(T)$ for the indicated field amplitudes $h_0$ (varying from 3 œ to about 2 kœ) and for three distinct $J(T)$ laws, differing by the exponent $n$ entering equation (54). a) $n = 1/2$, $R = 100\ \mu$, b) $n = 1$, $R = 10\ \mu$, and c) $n = 3/2$, $R = 10\ \mu$, $J_0 = 2 \times 10^6$ A/cm$^2$, $\lambda_0 = 0.5\ \mu$, $B_0 = 2 \times 10^5$ G in all cases.

almost independent of the exponent $n$ in equation (54) as well as of the exponential factor in the same equation.

2) We can now easily interpret the line $T_m(h_0)$ in the $T$-$H$ plane deduced experimentally from the maximum $\chi''_{max}(T_m, h_0)$ of $\chi''$. It is indeed clear from the above discussion and from figure 60 that this line is also defined by the implicit equation

$$h_{eff} = h_0 + 4\ \pi\ .\ M_{eq}(h_0) = H_p(T_m, h_0)\ .$$

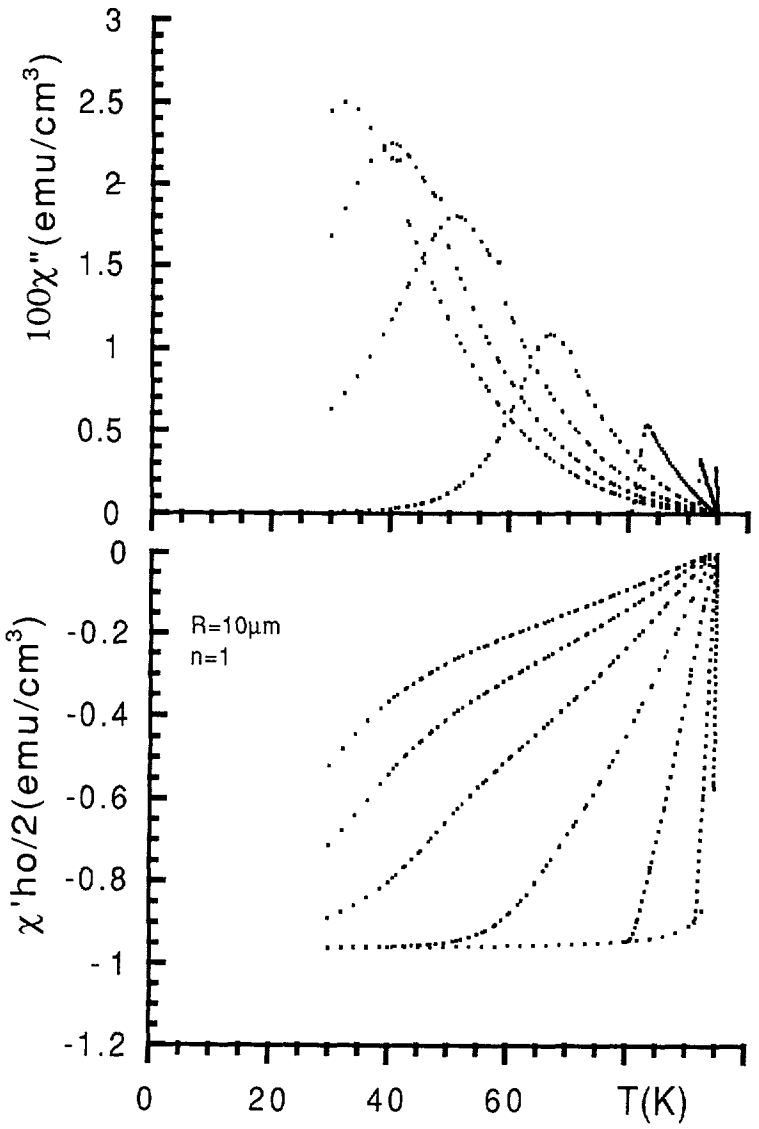


Fig. 59b.

Since $H_p$ depends on the dimension and the shape of the sample (see next sub-section) as well as on the exact variation of the critical current density with $T$ and $H$, it is obvious that this line has no thing to do with the irreversibility line as has been often assumed in the literature on HTSC. In fact, it is more correct to define the irreversibility line by the condition $\chi'' = 0$ which implies $J = 0$ at low frequencies of measurements.

12.2.4 *Influence of the radius R of the single crystal on $\chi'(T)$ and $\chi''(T)$ curves : the behaviour near the irreversibility line.* — Presented in figure 61a, b, c are the evolutions of $\chi'(T)$ and $\chi''(T)$ as a function of the radius $R$ ($R$ = 1, 10, 100 and 500 μm) of the crystal for the same $J(T)$ relationships as in the previous figure 59 ($n$ = 1/2, 1 and 3/2). It is seen from figure 61 that the dependence of the peak of $\chi''$ on $R$ is very weak especially for

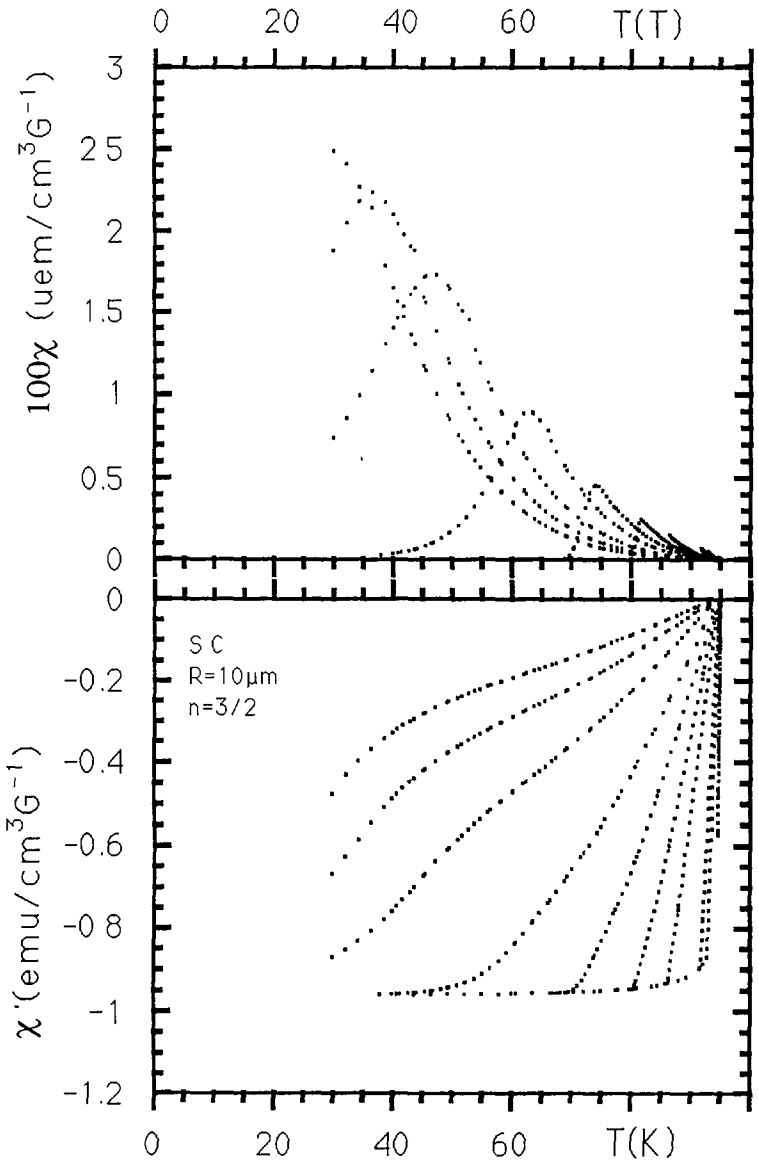


Fig. 59c.

$n = 3/2$. For example in the case $n = 1$ (and $h_0 = 40$ G) we find that $T_m$ varies only between 91.3 and 94.6 K when $R$ increases from 1 μ to 500 μ (about 0.4 K per decade of $R$). It is to be stressed that the small shift of $\chi''_{max}(T_m)$ with $R$ would be difficult to detect experimentally as the $J$ *versus* $T$ relationship could be slightly different from one specimen to another because of the possible differences in their microstructures and in the demagnetizing fields. Therefore, the presence or the absence of any significant size effects in $T_m$ has no evident implication concerning the possible relationship between the apparent irreversibility line and $\chi''_{max}(T_m)$. Moreover, since we have just seen that $\chi''_{max}(T_m)$ depends rather strongly on $h_0$, we expect that the position of the peak will be quite sensitive to demagnetizing effects which are very difficult to correct for rigorously, particularly in the peak region of $\chi''$ (see below).

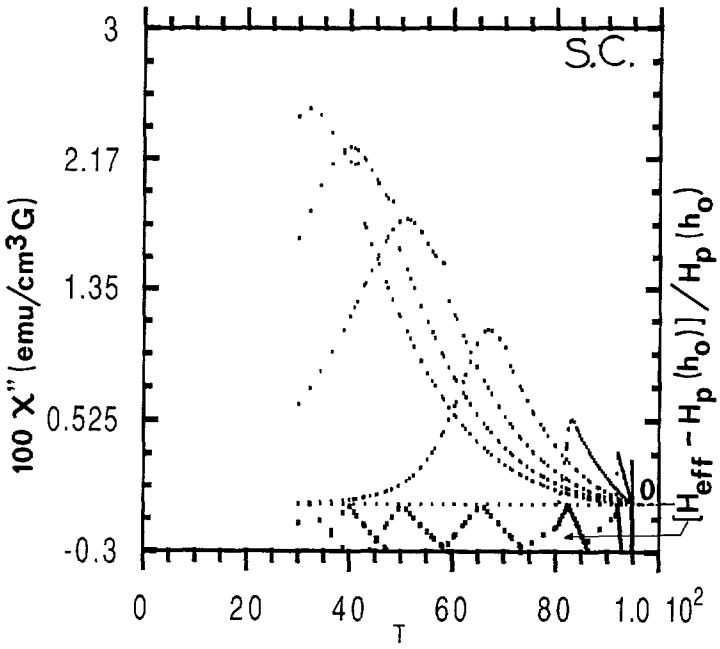


Fig. 60. — Shown together with $\chi''(T)$ is the absolute value of the reduced field $(h_{\text{eff}} - H_p(h_0))/H_p(h_0)$ where $H_p$ is the field of full flux penetration (see inset of Fig. 2). The plotted full penetration field is normalized so as to give zero when the flux just reaches the centre of the sample. It is clear from the figure that this occurs at about $T = T_m$.

A very subtle effect expected to arise near the irreversibility line is the following : in the usual models for the calculation of the intragranular critical current density it is tacitly assumed that the spatial distribution of the pinning barriers is homogeneous on some scale probably smaller than $\lambda$. This condition is always very difficult to satisfy very close to the irreversibility line because in many experimental conditions there is a wide distribution in the pinning energy. Then we expect that in these experimental conditions the number of effective pinning centres (really contributing to the measured $J$) decreases with increasing temperature and tends to zero as one approaches the irreversibility line. It is then possible that very close to this line the effective pinning barriers are so distant from each other that the current loops can no longer be continuous on the scale of the sample. In other words, in this limit we expect a granular-like behaviour for the critical current even for very good single crystals (the granular-like behaviour also means that $M_{\text{irr}}$ is no longer proportional to $R$). This is a very complicated percolation problem which would depend on the distribution of the pinning barriers both in space and in energy (more on this question will be reported elsewhere).

**12.2.5** *The link between $\chi''(T)$ and the intragranular critical current density, $T > T_M$.* — In this section we wish to search for a general relationship between $\chi''(T)$ and the critical current density $J(T)$. For this purpose it is not interesting to compare the $J$ *versus* $T$ curve with the $\chi''(T)$ curve but rather with the product $J(T)\,R/30$ (by analogy with Bean's model). Here we prefer the comparison between the « irreversible magnetization » $h_0\,\chi''(T, h_0)$ (which includes only measurable quantities) with the product $\alpha\,.\,J(T)\,R/30$ where $\alpha$ is a fitting parameter. This is done in figures 62 and 63 for three distinct $J(T)$ laws differing by the

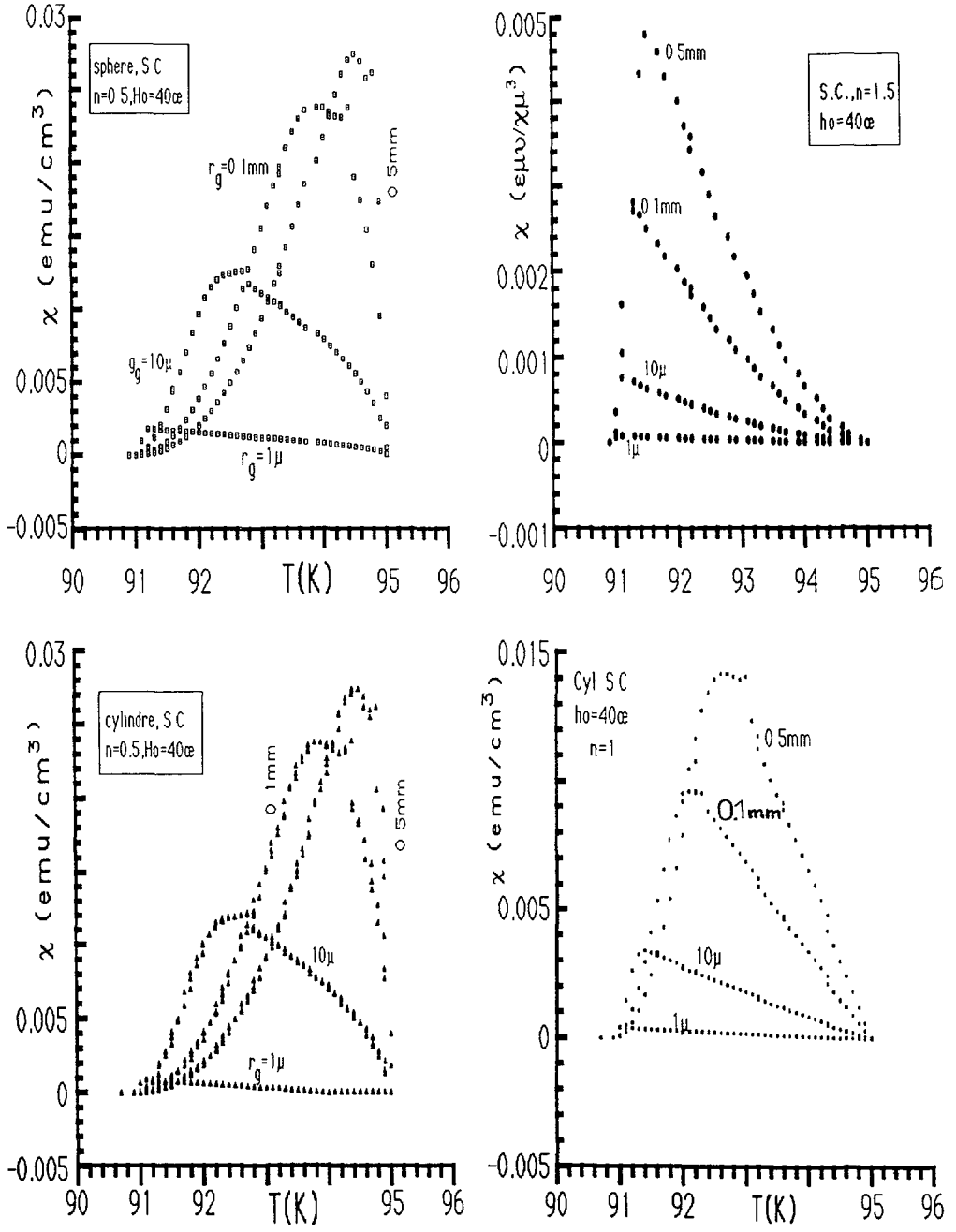


Fig. 61. — Calculated ac-susceptibilities ($\chi''$) for cylindrical samples having the indicated radii (1, 10, 100 and 500 $\mu$) and for three distinct $J$ *versus* $T$ relationships, differing by the exponent $n$ entering equation (54) : $n$ = 1/2, 1 and 3/2 at fixed $h_0$ = 40 G. Also shown is the calculated $\chi''$ for a sphere (top-left fig) assuming that the usual demagnetizing factor calculation applies here.

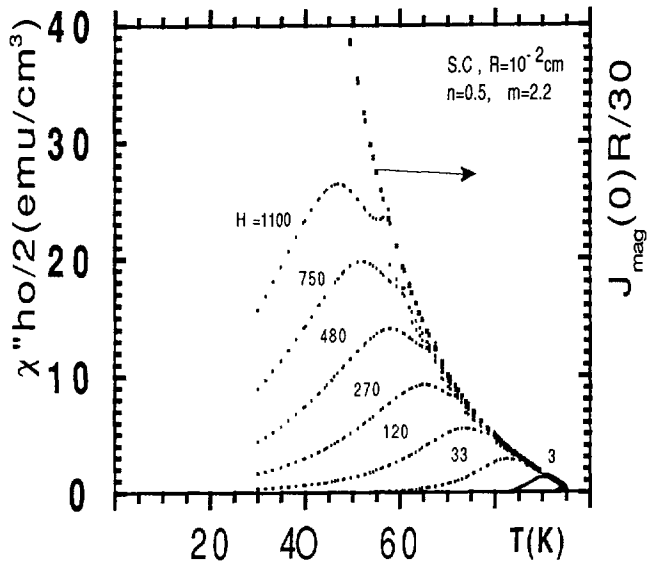


a)

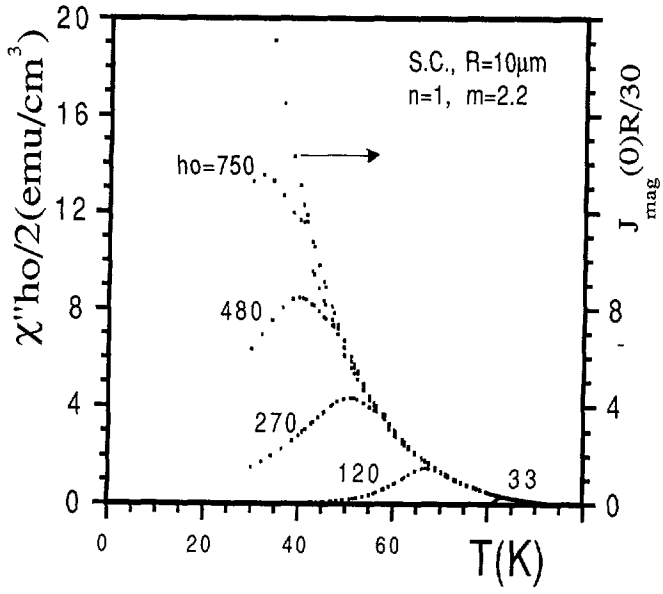


b)

Fig. 62. — Compares the calculated $h_0 \cdot \chi''(T)$ « magnetization » curves as explained in the text with the curve describing the « irreversible magnetization » $\alpha \cdot J(T)\ R/30$ (here $J(T)$ is given by equations (4) and (48) in which $h = 0$) for the three indicated exponent factors $n$. $\alpha$ is a proportionality factor of about 0.5 for the present examples.

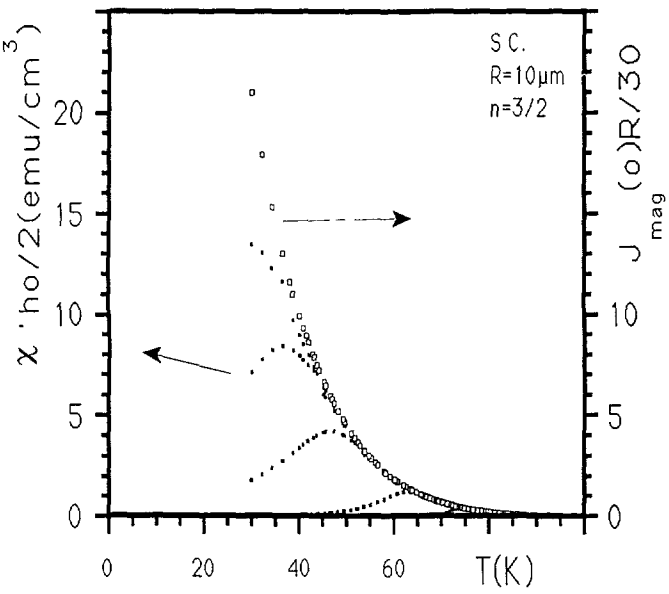


Fig. 62c.

exponent $n$ in equation (54) : $n = 1/2$, $n = 1$ and $n = 3/2$. We find that the best fit is achieved by taking $\alpha \approx 0.5$ and assuming $H = 0$ (i.e. for $J = J(T, 0)$).

The following remarks are of interest here.

(1) The proportionality factor $\alpha$ is found to depend only weakly on the parameters $n$, $m$ and $R$ entering the various equations for the calculation of the susceptibility. Therefore, in the simplest case the apparent current is given approximately by :

$$J_{\text{mag}}(T, H_0) \approx 30\, h_0 \frac{\chi''(T, H_0)}{\alpha R} \qquad (T > T_m) \tag{58a}$$

$$J_{\text{mag}}(H_0, r \approx R) = \frac{\gamma h_0}{R\chi''(H_0)} \qquad (T \ll T_m)\,. \tag{58b}$$

Here $T_m$ is the temperature of the peak of $\chi''$, $H_0$ is a superimposed dc field whereas $\alpha$ and $\gamma$ are numerical factors. It is to be stressed that the critical current density intervening in equation (58a) does not correspond to a fixed field and hence to a well defined critical state as in the Bean formula and is averaged over the variable field $h(t)$. As a consequence, the critical current deduced from susceptibility measurements at a given temperature (larger than $T_m$) is expected to be a complicated function of $h_0$. For this reason equation (58a) is valid only sufficiently above the temperature $T_m$. This is clearly reflected in figure 62 and more strikingly in figure 63 which shows that for $T$ slightly above $T_m$ (the temperature of a given peak of the figure defined by a fixed field $h_0$ of the same figure) the various branches of the curves $h_0 \cdot \chi''(T, h_0)$ which include only measurable quantities (left scale) coincide with the single curve representing the function $\alpha \cdot J(T, H = 0)\, R/30$ (right scale).

(2) It is important to emphasize that despite the fact that the curves $h_0\chi''(T, h_0)$ correspond to various fields $h_0$ the best fit with the magnetic critical current $J_{\text{mag}}$ is realized when we assume $H = 0$ $\{\text{i.e. } J_{\text{mag}} = J_{\text{mag}}(T, H = 0)\}$. This is perhaps due to the fact that $J$ varies very rapidly with $T$ in this high temperature domain. At much lower temperatures the

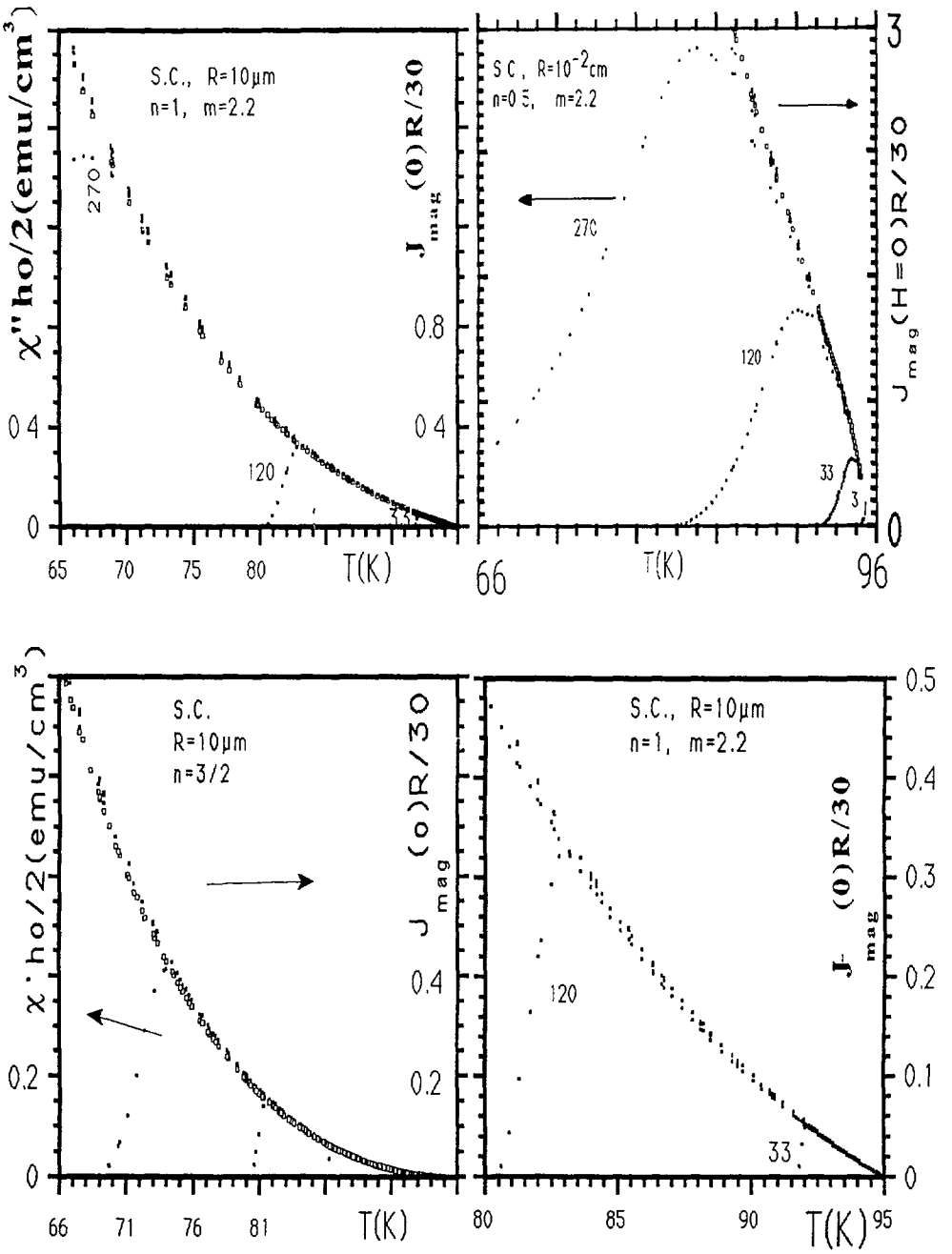


Fig. 63. — The same as figure 62 but the temperature scale is expanded close to $T_c$.

maximum of the $h_0 \cdot \chi''(T, h_0)$ curve is generally significantly below the $\alpha \cdot J(T, H = 0) R/30$ curve for all the cases considered here.

(3) From the examination of the envelope curve it is seen that it can be used to determine the temperature dependence of $J$ near $T_c$ with a very high accuracy.

(4) It is also possible to perform the same calculation for $\chi'$ and $\chi''$ but with a dc-field

$H_0$ superimposed to the ac-field ($H_{tot} = H_0 + h(t)$). Then the relationship between $\chi''(T)$ and the critical current density can be generalized to give the magnetic critical current density at $H = H_0$, as is given in equation (58a). Moreover if $H$ is high enough we can make $J$ vanishingly small and investigate the field and temperature dependences of the apparent irreversibility line in the same way.

(5) In the opposite limit $T \ll T_m$, the out of phase susceptibility is governed by the critical current density and the associated pinning barriers at and near the surface of the specimen in a thin shell of thickness (for $H_0 = 0$) :

$$\Delta r = \lambda + \frac{[h_0 + 4\,\pi M_{eq}(h_0)]}{H_p} R\,, \quad (R \gg \lambda\,,\ h_0 + 4\,\pi M_{eq}(h_0) \ll H_p,\ H_0 = 0) \qquad (59a)$$

$$\Delta r = \lambda + \frac{[h_0 + 4\,\pi (dM_{eq}/dH_0)\, h_0]}{H_p} R\,, \quad (\text{if } H_0 \neq 0)\,.$$

In this case the relationship between $\chi''(T)$ and the critical current density can be generalized to give the magnetic critical current density near the surface and would be given approximately by equation (58b). At this point it is to be emphasized that if $H_0$ is not too large compared to $H_{c_1}$ then $H_0$ in equation (58b) should be replaced by the effective field given by equation (55) for long cylinders.

We note that equation (59a) is equivalent to the condition $T \ll T_m$ which is itself equivalent to the condition $h_{eff}/H_p = \{h_0 + 4\,\pi M_{eq}\}/H_p \ll 1$ as evidenced by figure 60 above. We also recall that the effective field $h(t) + 4\,\pi M_{eq}$ seen by the vortices at the surface is equal to zero as long as $h(t) \leq H_{c_1}$. Consequently, because of the smallness of $\Delta r$ relatively to $R$ the information on $J(T, H)$ from $\chi''$ is in this limit restricted to a surface region of depth $\Delta r$ and concern « surface pinning » (Bean [72b]) if $\Delta r \ll R$. However, as we have already seen, the Bean picture for ac-effects neglects the London-Abrikosov screening currents since $h(t)$ instead of $h_{eff}(t)$ is used as well as the effect of the peak close to $H_{c_1}$ exhibited by the hysteresis cycle reported in section 7 (as $J$ is assumed independent of $h_0$). We recall that this peak is also correlated with $M_{eq}$. Both effects can be safely neglected in the presence of a dc-field $H_0$ very large compared to $H_{c_1}$ or more correctly if $(H_0 \pm h_0) \gg H_{c_1}$ everywhere in the sample. In fact, from the above considerations we can see that for a cylindrical sample with negligible surface imperfections and weak links (the existence of which could reduce the effective field $H_{c_1}$) $\chi''$ is rigorously equal to zero up to $h_{eff} = H_{c_1}(T)$ and proportional to the inverse of $J$ averaged over the variable field above this value. For instance if $H_0 = 0$ we have :

$$\chi'' = \gamma' \frac{h_{eff}}{R\,\langle J\rangle} [1 + 4\,\pi M_{eq}(h_0)/h_0]^2\,, \quad (T \ll T_m)\,, \qquad (59b)$$

with in particular $\chi'' = 0$ for $h_0 \leq H_{c_1}$ since $M_{eq} = -\,h/4\,\pi$ in this limit.

(6) Because in usual ac-measurements $h_0$ is as a rule very low, then $T_m$ is generally very close to $T_c$ so that the corresponding $J_{mag}$ is generally extremely small. Typically, for single crystals of YBaCuO (123), $\chi'' \approx 10^{-3}$ emu cm$^{-3}$ G$^{-1}$ at $h_0 \approx 1$ G and $R \approx 10^{-2}$ cm. The associated critical current density is as low as 1 A cm$^{-2}$, a value to be compared with $J = 10^6$ A cm$^{-2}$ generally deduced from other techniques (at $T \ll T_c$).

**12.2.6** *Oher information that can be extracted from curves* $\chi'(T)$. — In the previous sections, we have pointed out that $\chi'(T)$ depends strongly on the amplitude $h_0$ of the alternating field and to some extent on the effective size of the sample (compare $\chi'$ curves of Fig. 59). Of course, in real experiments, $\chi'(T)$ also depends on the demagnetizing field as well as on any

spatial (physical or chemical) inhomogeneities and thus on any spatial distribution in the transition temperature. The last two effects were ignored up to now. Because of these effects it is very difficult in general to interpret $\chi'(T)$ quantitatively and to characterize the material from this curve alone.

Concerning demagnetizing effects it turns out that the situation is somewhat less complicated in the following two limits (but see Sect. 16 for a more detailed discussion).

(1) The fractional volume $V_p$ of superconducting material is sufficiently small so that both Josephson coupling and multipolar coupling between grains are negligible. In this case one has to a first approximation :

$$\chi'(T) \approx - V_p \frac{1 - f(r_g/\lambda)}{4\pi(1-N)} \quad (\text{if } r_g \gg \lambda,\ h_0 < H_{c_1}) \tag{60a}$$

or

$$\chi'(T) \approx - V_p \frac{1 - f(r_g/\lambda)}{4\pi} \quad (\text{if } r_g \ll \lambda,\ h_0 < H_{c_1}) . \tag{60b}$$

Note that we have neglected the influence of the demagnetizing factor $N$ in the limit $r_g \ll \lambda$ (Eq. (60b)). This will be justified later. The function $f(r_g/\lambda)$ is in principle also negligible in the limit $r_g \gg \lambda$ of equation (60a). We recall that this function has been introduced before for the calculation of the hysteresis cycle and is defined whichever the value of its argument $r_g/\lambda$. It depends on the shape of the grains and can be estimated only if this shape is known. This function is calculated in reference [77] in different approximations. It can be neglected whenever the condition $r_g \gg \lambda(T)$ is satisfied (see Sect. 16 for the use of experimental data to derive both $N$ and $V_p$).

(2) The second limit where demagnetizing effects can be estimated corresponds to a fractional superconducting volume $V_p$ close to one (highly compact pellets) in very low field. It is to be stressed however that even in this case, there are physical situations where the magnetic screening is very low (that is $\chi'(T \approx 0)$ very small) which can lead to the erronous conclusion that $V_p$ is small as well. Now, we wish to point out that in the later situation it is possible to establish a qualitative criterion which could be of great help for the analysis of the data and the characterization of the material.

**12.2.7** *Influence of the ratio $\lambda/r_g$ on $\chi'(T)$ and on the width $\Delta T$ of the superconducting transition.* — From the inspection of the preceding figures (corresponding to single crystals and decoupled grains only) it is clear that most of the broadening of the $\chi'(T)$ curves is related to the size of the specimen *via* the factor $\lambda/r_g$. Therefore, the usual transition width $\Delta T$ referred to in the literature as the point where the measured signal is reduced to half of its maximum value is essentially related to the grain size and, to a lesser extent, to the demagnetizing factor (see below). It is interesting to estimate qualitatively this width.

Let $T'$ the temperature defining the transition width $\Delta T$ just invoked. Of course this temperature is difficult to derive exactly. However, neglecting demagnetization effects for the moment (see below) and any possible inhomogeneities (and hence possible distribution in $T_c$) it can be estimated qualitatively from the function $f(r_g/\lambda(T))$ and the condition $f(r_g/\lambda(T)) = 1/2$. We find that in the limit $h_0 \ll H_{c_{10}}$ and $R \gg \lambda_0$ the temperature $T'$ is related to the ratio $\lambda_0/R$ (here $\lambda_0 = \lambda(T = 0)$) and is of the order

$$T' \approx T_c[1 - (\alpha\lambda_0/R)^2]^{1/4} \tag{61}$$

or

$$\Delta T = T_c - T \approx T_c\left[1 - \frac{(\alpha\lambda_0/R)^2}{4}\right]^{1/4}, \quad (R \gg \lambda_0,\ h_0 \ll H_{c_{10}}) . \tag{62}$$

Here $\alpha$ is a proportionality factor $\approx 4$ for cyclindrical samples and $\approx 6$ for spherical samples. These qualitative equations were derived assuming BCS temperature variation for $\lambda(T)$ and are not valid for small $R/\lambda$ ratio. Nevertheless they show that $\Delta T'$ increases quadratically with the ratio $\lambda_0/R$. Recall also that very close to $H_{c_2}(T)$ $\lambda$ must be replaced by the field dependent penetration depth $\lambda(1 - H/H_{c_2})^{-1/2}$

12.2.8 *Influence of demagnetization effects on the apparent transition width* $\Delta T$. — To interpret an ac-susceptibility measurement reliably it is necessary to estimate the influence of the demagnetizing field. We feel that this is generally a formidable task which is made even more complicated by anisotropy effects. In addition, contrary to the case of conventional ferromagnets the demagnetizing effects depend here not only on the outer shape of the specimen but they also depend explicitly on its dimensions. For instance, in the case of spherical samples the influence of demagnetizing effects will vary with the radius $R$ of the sphere and will therefore be quite different for large single crystals and for finely dispersed grains.

Here we wish to consider some limiting cases from a rather qualitative point of view.

• *Case of decoupled grains but such that* $r_g/\lambda_0 \gg 1$ : Let us assume that the effective field $h_{\text{eff, s}}$ (seen by the vortices at the surface of the specimen) is small compared to the full penetration field $H_p$ (it can be shown that this is approximately equivalent to the condition $\{h_0/(1 - N) + 4\pi M_{eq}(h_{\text{eff, s}})\} \ll H_p$). It is then possible to estimate the demagnetizing field over most of the $\chi(T)$ curves. The principal arguments are as follows :

1) Firstly, as long as $T$ is much lower than $T_m$ the penetration distance $\Delta r$ of magnetic flux within the sample is small ($\Delta r/R \ll 1$ and $\lambda/R \ll 1$, Eq. (59a)). Then the analogy with conventional ferromagnetic materials is reasonably justified. Consequently, in this limit we can correct for demagnetizing effects simply by replacing the applied field $h(t)$ by the effective field

$$h_{\text{eff, s}} = h_d + 4\pi M_{eq}(h_d)$$
$$h_d = h(t)/(1 - N)$$

where $N$ is the usual demagnetizing factor and $h_d$ the associated demagnetizing field. We recall that in the above equation the term $4\pi M_{eq}$ is induced by the London-Abrikosov currents circulating in the penetration depth $\lambda$. It is shown in section 16 that such a factor can be determined from experiments in some conditions.

2) Secondly, for temperatures well above the temperature $T_m$, in particular very close to $T_c$, the demagnetizing field $h_d$ can be neglected compared to the applied field. This is because the strength of $h_d$ never exceeds $4\pi NM(T, h_0) \approx 4\pi N h_0 \chi'(T, h_0)$ and hence goes to zero in the same way as $\chi'(T, h_0)$ when $T$ tends to $T_c$. The interesting point to be emphasized then is that very close to the superconducting transition the shape of $\chi'(T)$ curve is probably independent (to a first approximation) of demagnetizing effects (i.e. once the condition $4\pi N|\chi'(T, h_0)| \ll 1$ is realized).

To illustrate the above points we compare in figure 64 the calculated diamagnetic responses $\chi'(T, h_0)$ of a cylindrical sample and a spherical sample respectively without correcting for the demagnetizing field and neglecting the influence of the critical current density on $\chi'(T, h_0)$. As expected, we find that for $R \gg \lambda(T)$ the signal of the sphere is higher than that of the cylinder by the correct factor $1/(1 - N_{\text{sph}}) = 3/2$ (since $N_{\text{sph}} = 1/3$). However, it is also found that this difference is reduced as the ratio $\lambda/R$ is increased. Qualitatively, the two responses become comparable at about $\lambda(T) = \beta R/(1 - N)$ with $\beta \approx 1$ to 2. Since $\lambda(T)$ diverges as $T$ approaches $H_{c_2}(T)$ or $T_c$, the condition $\lambda(T) \approx 2R/(1 - N)$ can always be realized above a certain temperature $T''$. Since HTSC are frequently granular with grain

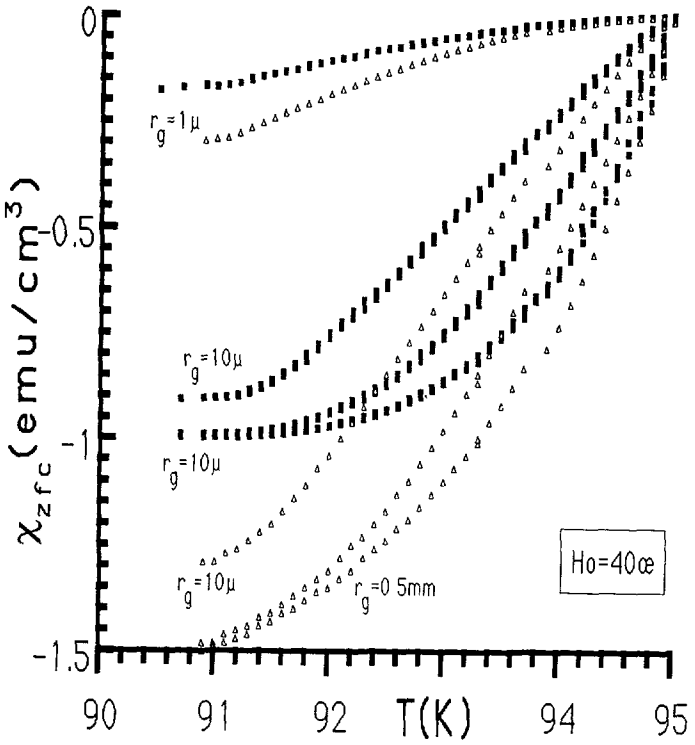


Fig. 64. — Calculated $\chi'$ and $\chi''$ (per unit volume) of a spherical sample (empty triangles) and a cylinder (full rectangles) as a function of temperature, in the London approximation and for four different grain radii : $R$ = 1, 10, 100 and 500 μ. Note that the curves $R$ = 100 μm (not labelled) and $R$ = 500 μm coincide at low temperatures.

radius comparable to $\lambda_0$ the condition $T \geqslant T''$ can be satisfied over a significant temperature interval. However for large samples and for large $N$ this is achieved only very close to $T_c$. A more quantitative estimation of $T''$ requires numerical calculations in this condition. The situation can be considered in a different way as explained below in this case.

• *Case of large single crystals :* In the case of single crystals and very large grains the influence of the demagnetizing field can be limited further by another factor when $h_0 \gg H_{c_1}$, a situation always realized close enough to $T_c$ :

Since very close to $T_c$ the total magnetization is always dominated by the equilibrium term (because $J$ and hence $M_{ir}$ go to zero rapidly there) and that the condition $H_{c_1} \geqslant 4\pi |M_{eq}(h_0)|$ always holds for $h_0 \gg H_{c_1}$ the shape of the measured magnetization depends essentially on the product $[1 - f(r_g/\lambda)]\, M_{eq}(h_0)$ (that is the reduction of $M_{eq}$ due to $\lambda$ effects). At this point it is important to keep in mind that as soon as $h_0 \gg H_{c_1}$ the function $M_{eq}(h_0)$ is no longer linear in $h_0$ which means that $\chi'(T)$ depends now on $h_0$. This introduces a third threshold temperature $T'''$ related to $H_{c_1}$ by $h_{eff,\,s} = H_{c_1}(T''')$. Assuming a two fluid law for the temperature variation of $H_{c_1}$ we obtain :

$$T''' \approx T_c \left[ 1 - \frac{h_0}{(1-N)\, H_{c_{10}}} \right]^{1/4}, \quad R \gg \lambda\,(T''') . \tag{63}$$

Here $H_{c_{10}}$ is the first critical field at $T = 0$. For temperatures lower than $T'''$ the effective field

is given by the usual formula (55) but the demagnetizing field should become negligible at temperatures higher than $T'''$.

**12.3** AC-SUSCEPTIBILITY OF GRANULAR SUPERCONDUCTORS WITH WEAK JOSEPHSON COUPLING. — The ac-susceptibility of weakly coupled and textured granular superconductors has been the object of many theoretical and experimental investigations during the last few years. Here we wish to calculate the ac-susceptibilities of weakly coupled Josephson grains in the framework of the model used for the computation of the low-$H$ hysteresis cycles in section 11 (Eq. (45)). This model assumes that the measured magnetization is the sum of four distinct current contributions which are : the London-Abrikosov reversible currents, the Josephson reversible current and the two irreversible magnetizations due to intergrain and intragrain critical current densities ($J_{wI}$ and $J$ respectively). Since in the case of granular materials the intergranular current density $J_{wI}$ depends strongly on $H$, and as a consequence on the position $r$ inside the sample (see Sect. 6), this makes it more difficult to obtain a direct relationship between $\chi''$ and this critical current density than in the case of single crystals. However, one of the most important results of the present model is to demonstrate that such a relation readily exists and has approximately the same form (about the same dependence on $R$, $r_g$, $\lambda$, $H_0$, ...) as that already deduced for the low $H$ cycle (Eqs. (50, 52)) (this point will be reconsidered later).

**12.3.1** *Experimental $\chi'(T)$ and $\chi''(T)$ curves in granular superconductors.* — Typical examples of experimental $\chi'(T)$ and $\chi''(T)$ curves of YBaCuO ceramics are presented in figure 65 for different amplitudes $h_0$ of the alternating field [376]. The most characteristic features of these curves can be summarized as follows :

1) For very low ac-field ($h_0 \leqslant 1$ œ typically) and for $T \ll T_c$ the degree of magnetic screening is essentially perfect (i.e. $4\pi\chi'(T \approx 0) \approx -1$ after correcting for the macroscopic demagnetizing field). However, it is very important to recall that this property does not really reflect the quality of the material but depends on the macroscopic radius $R$ of the specimen and holds only if the condition $R/\lambda_J \gg 1$ (where $\lambda_J$ is the Josephson penetration depth, Eq. (35)) is satisfied as discussed by Senoussi *et al.* in reference [299, 357]. Strictly speaking, this means that in the limit where $h_0$ tends to zero ($h_0 \ll H_{c_1}^w$) it is always possible to achieve perfect screening provided that the radius of the pellet is sufficiently large, even when the fractional volume $V_p$ of superconducting material is very low. In other terms, there is in general no simple relationship between $V_p$ and $\chi'(T \approx 0, h_0 \approx 0)$. As discussed in reference [299, 357], the incomplete screening (in the limit $h_0 \ll H_{c_1}^w$) is related to some phenomenological penetration depth $\lambda_{s,\,eff}$ which depends on the microstructure of the surface of the specimen ($\lambda_{s,\,eff} \approx \lambda_J$ for very fine grains). According to [357], for large samples one has $\chi'(T \approx 0, h_0 \approx 0) \approx -[h_0/(1-N)](1-\lambda_{eff}/R)$ where $N$ is the macroscopic demagnetizing factor (compare with Eq. (60a)). However this point certainly requires more detailed investigation than done in reference [299, 357].

2) As the temperature is further increased $\chi'(T)$ stays almost constant over a large temperature domain and then exhibits a step like increase at some temperature which we call $T_{wI}$ by analogy with the characteristic field $H_{c_1}^w$ of the low-$H$ cycle reported in sections 8 and 11. The temperature $T_{wI}$ represents some average value of the temperature of Josephson decoupling between grains at the field $h_0$ (note that the smaller $h_0$ the larger $T_{wI}$).

3) The width $\Delta T$ of the superconducting transition increases with $h_0$, as in the case of single crystals (Fig. 58).

4) $\chi''(T)$ exhibits a pronounced peak at approximately the same temperature $T_{wI}$ as the jump in $\chi'(T)$.

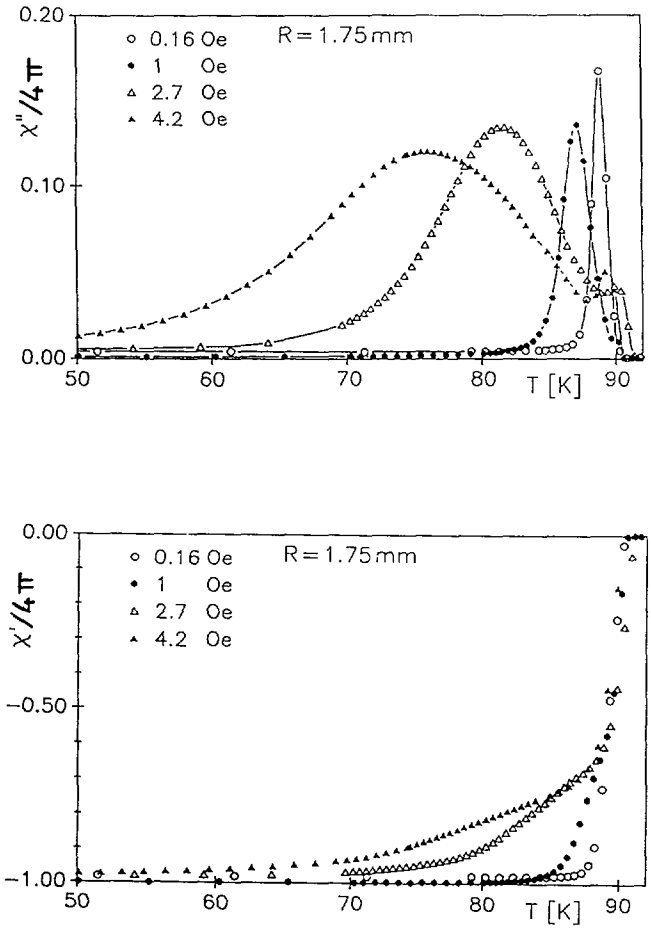


Fig. 65. — Typical experimental examples illustrating the temperature variation of the ac-susceptibilities $\chi'$ (in phase component) and $\chi''$ (out of phase component) of sintered $YBa_2Cu_3O_7$ samples at the indicated amplitudes $h_0$ of the alternating field [375].

5) The temperature $T_m$ of this peak decreases while its width increases upon increasing $h_0$.

6) We shall see later that this width also increases as the inverse $1/r_g$ of the grain radius.

7) More interestingly, we shall also see that for very low field $h_0$, the sharpness of the peak increases considerably with the average radius $r_g$ of the grains.

8) A further important result that will be discussed too concerns the fact that the amplitude $\chi''(T_m)$ of the peak is related to the intergrain critical current density by the scaling function $f(r_g/\lambda)$ introduced before and used for the calculation of the hysteresis cycle (Sect. 11 and Refs. [77, 104]).

**12.3.2** *A model for the calculation of the ac-susceptibility of weakly coupled granular superconductors.* — We have computed the ac-susceptibilities $\chi'$ and $\chi''$ of granular materials taking into account both intra- and inter-granular currents as written in equation (45). The calculation is based on the integral equations (56, 57) in which the magnetization $M^+$ and $M^-$ are the same as those used for the low-$H$ hysteresis cycle [77, 104]. In addition, we neglect frequency effects (for the moment) and assume now that the local intergranular

current density varies as

$$J_{w1}(T, b) = J_0(1 - T/T_c)^n \exp[-b/B_0(T)], \quad B_0(T) = B_0[1 - (T/T_c)^m]. \tag{64}$$

Here, $h_{eff}$ is given by formula (55) in which $M_{eq}$ is replaced by the Josephson equilibrium magnetization $M_{w1,eq}$ (defined in Ref. [77]) whereas $B_0$ is assumed to be given by equation (47). In all the numerical applications reported here we took $J_0 = 2 \times 10^3$ A/cm$^2$ and $m = 2.2$ (as in the preceding examples of the low-$H$ hysteresis cycles in Sect. 11). These formulae are rather phenomenological but this is not a limitation since, according to the literature, intergranular currents of sintered superconductors exhibit various kinds of behaviours as a function of $H$ and $T$ depending on their microstructures. For the sake of simplicity we shall neglect here the intragrain bulk currents $J$ and keep only the reversible London-currents circulating around the individual grains. These questions will be investigated in more detail elsewhere.

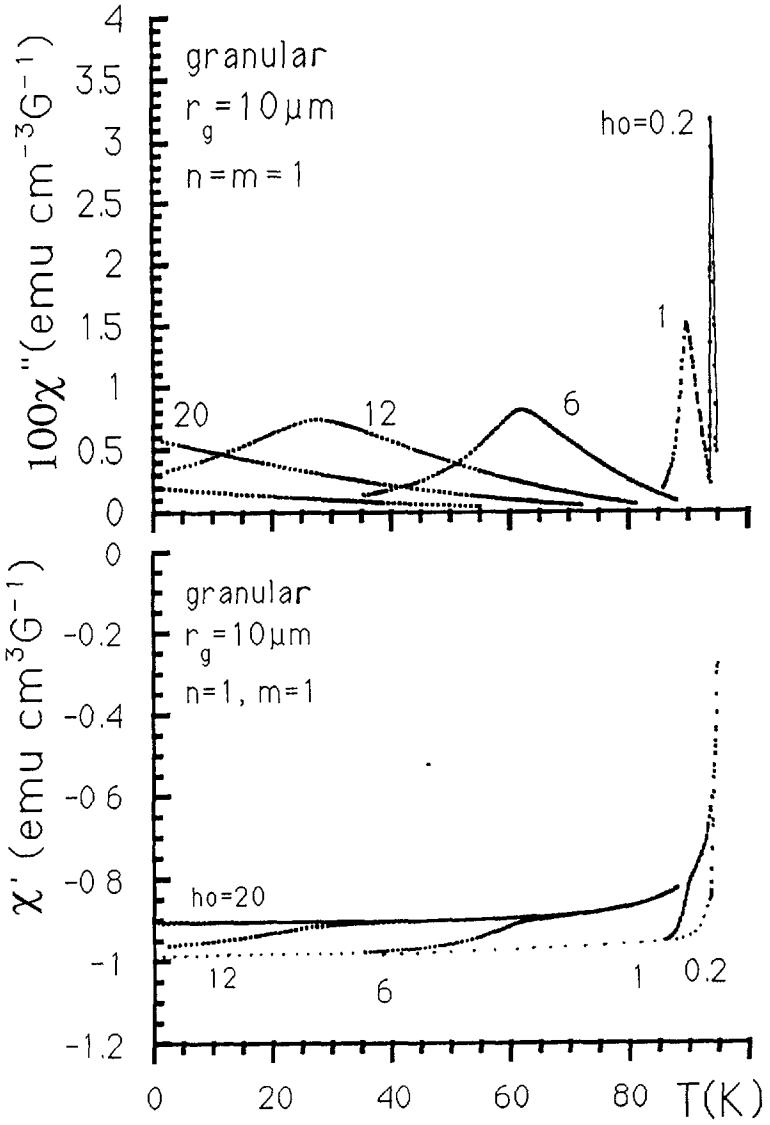


Fig. 66a.

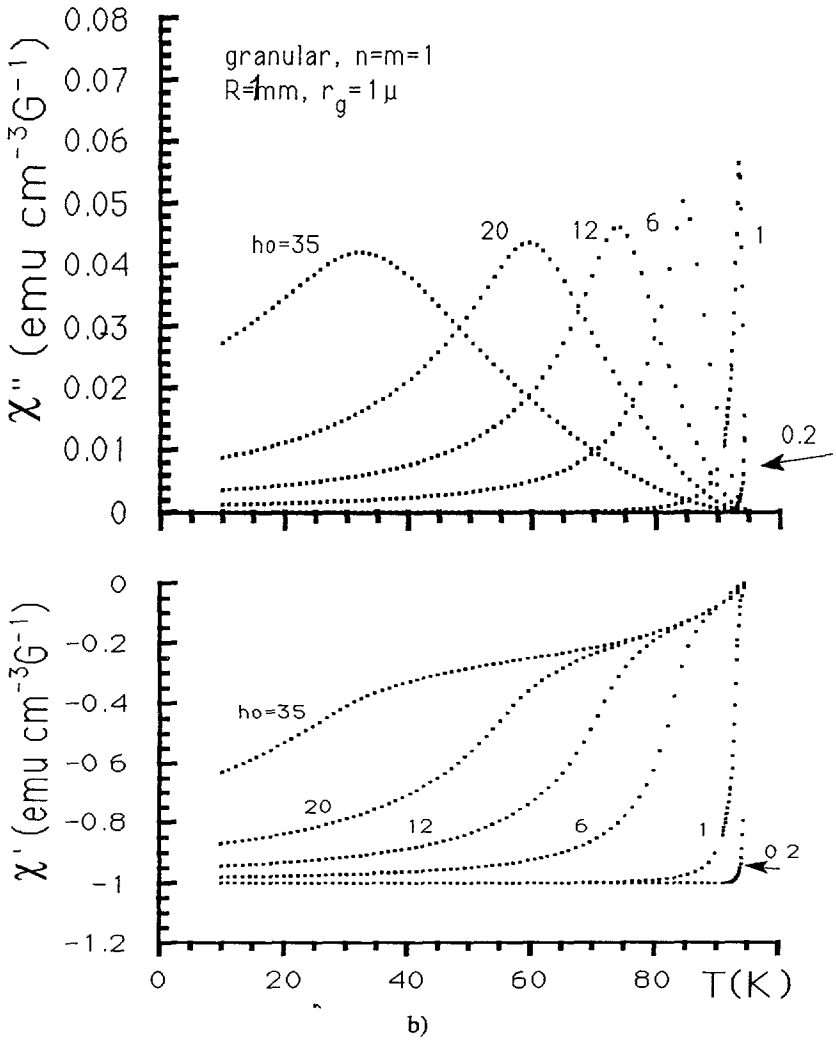


Fig. 66a, b. — Calculated $\chi'$ and $\chi''$ of a polycrystalline material at the indicated values of $n$, $r_g$ and the amplitudes $h_0$ of the alternating field. $R$ = 1 mm in both cases.

**12.3.3** *Behaviour of the calculated $\chi'(T)$ and $\chi''(T)$ as a function of $h_0$ for polycrystalline superconductors.* — Figures 66a, b shows the evolution of the calculated $\chi'$ and $\chi''$ for different amplitudes $h_0$ of the alternating field (varying from 0.2 to 35 G). The comparison with experimental curves shows that even though the results depend on the exact variation of $J$ with $T$ *via* the exponent $n$ (Eq. (66)) the agreement with experiments is good.

Shown in figure 67 is the function $\text{abs}(h_0 + 4\ \pi M_{eq}(h_0) - H_p)/h_0$ where $H_p$ is the threshold field at which magnetic flux just penetrates at the centre of the specimen (see Fig. 2 and Sect. 6 for more precision on $H_p$). It is found that, to a very good approximation, this factor goes to zero at the temperature $T_m$ of the peak of $\chi''$. We have tested that this behaviour is obtained for other values of $R$, $r_g$ and for different $J_{w1}(T)$ relationships differing by the exponent $n$ entering equation (64) ($n$ = 1/2, 1 and 3/2). We recall that the same result was obtained for intragranular currents in single crystals and decoupled grains (Figs. 58, 59).

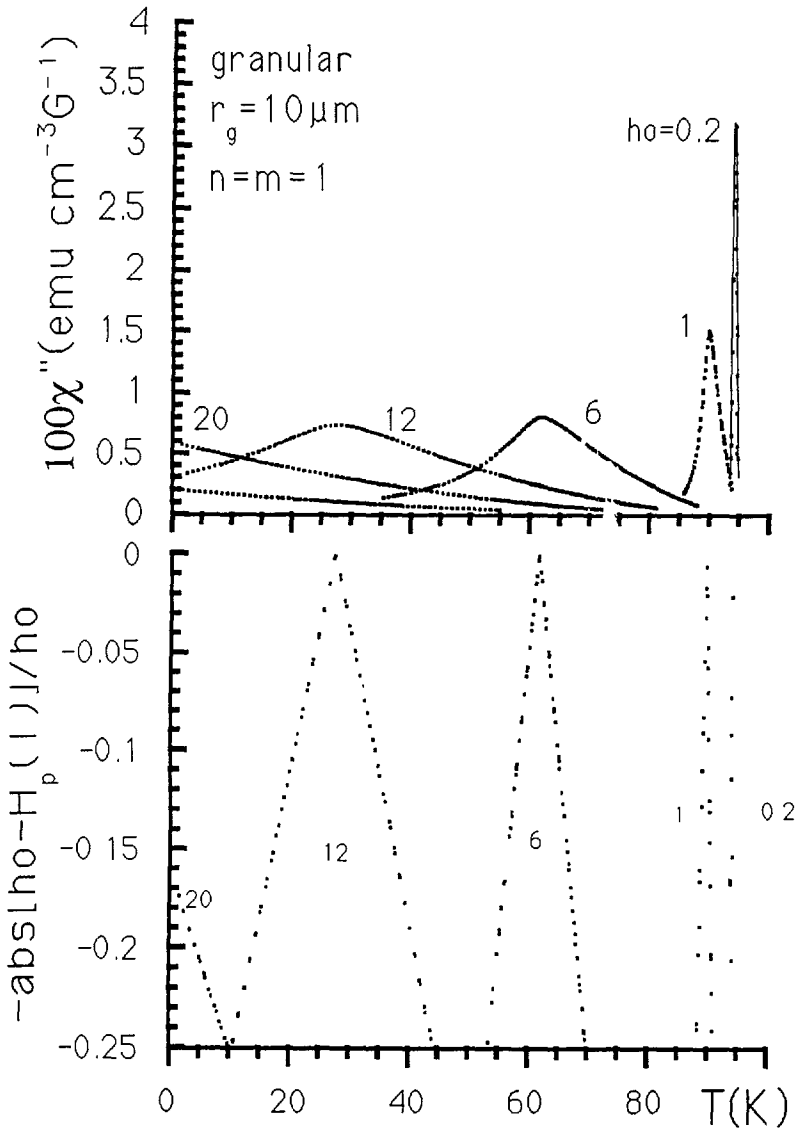


Fig. 67. — The same as figure 60 for single crystals. It shows that the flux penetrates the centre of the granular sample just at $T = T_m$. $R = 1$ mm. Recall that flux penetrates through the weak link network here.

**12.3.4** *Evolution of the calculated $\chi'$ and $\chi''$ with the macroscopic radius R of the granular sample.* — Shown in figure 68 is the evolution of calculated $\chi'(T)$ and $\chi''(T)$ with the macroscopic radius $R$ of the granular sample over the range ($R = 10^{-2}$ to 1 cm). The average radius of the grains is assumed to be the same ($r_g = 5\ \mu m$) for the three examples. As in the case of the low-$H$ hysteresis cycle the effect of $R$ on the calculated curves is rather small. We observe that as for single crystals (see Fig. 61) the effect of $R$ on the shift of the temperature $T_m$ of the maximum of $\chi''$ is rather small. Note that the numerical calculation was carried out point by point using equations (56), (57) together with the analytical expressions of $M^+$ and $M^-$ given in [77].

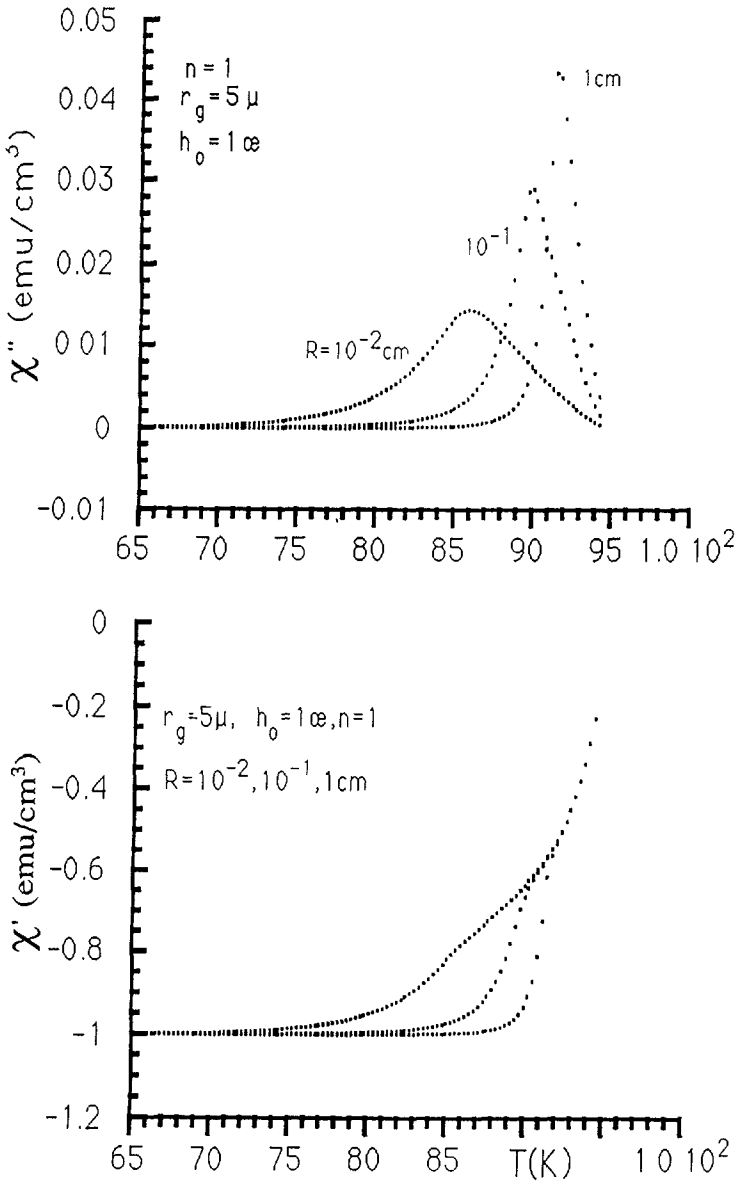


Fig. 68. — Compares the influence of the macroscopic radius $R$ of the specimen on the calculated $\chi'(T)$ and $\chi''(T)$ for $R$ varying from 100 μ to 1 cm and for $r_g = 5$ μ and $n = 1$. The other parameters are the same as in figure 67.

**12.3.5** *Variation of $\chi'$ and $\chi''$ as a function of the radius $r_g$ of the grains.* — The influence of $r_g$, the average radius of the grains, on $\chi'(T)$ and $\chi''(T)$ curves is illustrated in figure 69. The effect of $r_g$ is rather complex in general because it enters into the intergrain currents (at $H < H_{c_2}^{w}$) and in the reversible London magnetization (at higher $H$), but with very different dependences.

Turning back to the previous figures the most striking result is probably the evolution of the

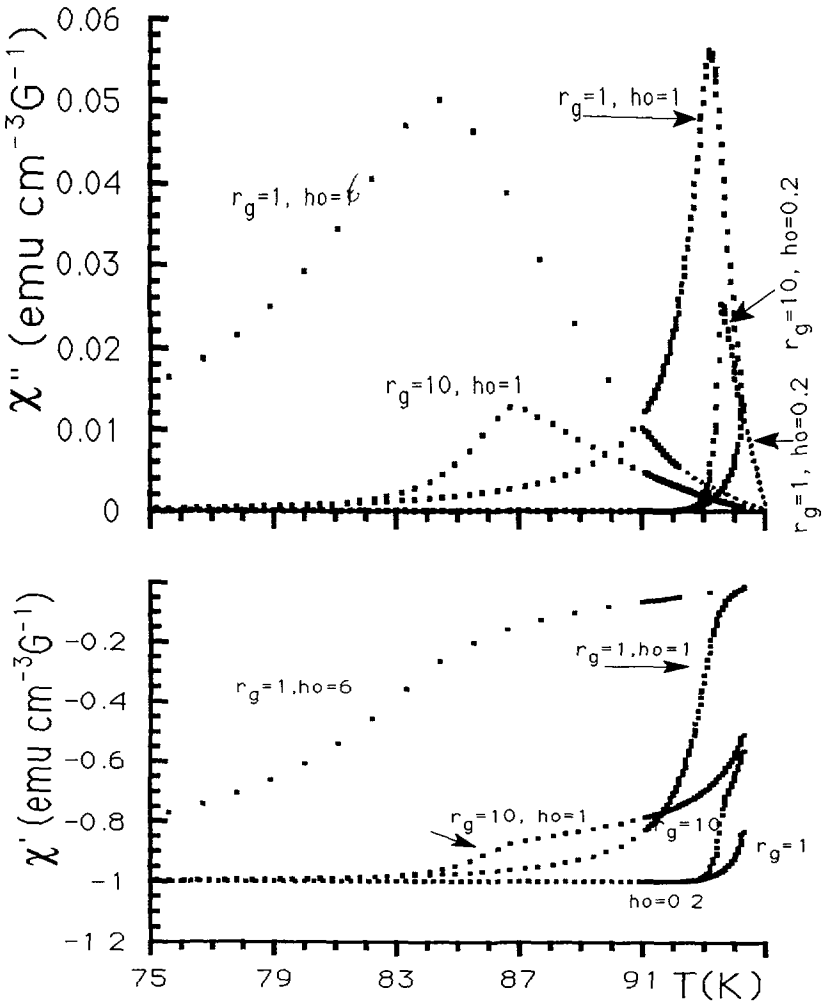


Fig. 69. — Illustrates the influence of the grains radius $r_g$ on the calculated curves $\chi'(T)$ and $\chi''(T)$ at the indicated $R$, $r_g$ and the amplitudes $h_0$ of the alternating field ; $n = 1$.

peak of $\chi''$ with the grain dimensions : it becomes very sharp for very large grains ($r_g \gg \lambda$) and for very low values of $h_0$. The second interesting result connected with $r_g$ concerns the broadening of the superconducting transition (as measured by $\chi'$) with decreasing $r_g$.

**12.3.6** *Why the peak of $\chi''$ does become so sharp as $r_g$ is increased.* — Let us again consider figures 66 and 69 and study the evolution of the peak of $\chi''$ as a function of $r_g$. We know from the preceding discussions that $\chi''$ is proportional to the total area of the low-$H$ hysteresis cycle which is itself proportional to the effective (transverse) surface $S_{wl}$ occupied by the whole weak link network. We have also seen in sections 8 and 11 that for large grains ($r_g \gg \lambda$) this surface is of the order of $S_{wl} \approx [2\,\lambda(T)/r_g]\,S_s$ where $S_s$ is the macroscopic transverse area of the sample (see Fig. 33). Then, we can consider two limiting behaviours as a function of $r_g$. On the one hand, for very large grains the relative surface occupied by the weak link network is negligible, that is the ratio $(S_{wl}/S_s) \approx \{2\,\lambda(T) + d\}/r_g$ is negligible at low

temperature (we recall that $d$ is the physical thickness of the junction where the order parameter is about zero and is generally negligible compared to the electromagnetic thickness $2\lambda$). However, this is only valid far enough below $T_c$ since $\lambda(T, B)$ tends to diverge at $H_{c_2}$ and $T_c$ so that the whole surface of the sample will be unavoidably covered by the weak link network (in other words $S_{wl}/S_s \to 1$). This leads to a sharp change in $\chi''(T)$ and thus to a sharp peak in this function if $h_0$ is sufficiently low (see below why). On the other hand, when the number of weak links is very large (or equivalently when the ratio $2\lambda/r_g$ is already large at low $T$, of the order of one) the relative change in the total area covered by the weak link network will be small when $T$ approaches $T_c$ (since it cannot exceed $S_s$ anyway) and as a consequence the peak in $\chi''(T)$ which reflects this change would be not very sharp.

Concerning the influence of the amplitude $h_0$ of the alternating field on the sharpness of the peak, it is obvious that the above arguments which are based on the divergence of $\lambda(T, B)$ will stay valid only if the temperature $T_m$ of the sharp peak of $\chi''$ occurs in a temperature region close enough to $T_c$ where $\lambda(T, B)$ increases rapidly. This implies that $h_0$ must be very small since we know that $T_m$ decreases rapidly with $h_0$ (see Figs. 65, 66) and becomes zero for $h_0$ larger than the Josephson decoupling field $H^w_{c_2}$.

From the examination of the $\chi'(T)$ curves (Fig. 66) we also see that the width $\Delta T$ of the superconducting transition is considerably enlarged as $r_g$ is decreased. This is consistent with the case of single crystals and decoupled grains (Fig. 52) and has the same physical origin since it happens above the Josephson decoupling temperature $T_{wl}$. In addition, in agreement with experimental results we find that at very low $T$ and $H$ the magnetic screening is quasi-perfect. As for the low-$H$ hysteresis cycle (Figs. 32, 37) the stepe like change in the $\chi'(T)$ curves reflects the transition (as $T$ is increased) from a regime where this function is to a large extent governed by intergrain currents circulating around the whole sample ($h_0 < H^w_{c_1}$) towards a regime where the grains cease to be coupled through Josephson junctions ($h_0 > H^w_{c_2}$).

12.3.7 *The relationship between $\chi''(T)$, the intergranular critical current density and the micro and macro structures.* — We wish now to concentrate on the relationship between $\chi''(T)$ and the apparent intergrain critical current density. First, we recall again that the apparent critical current density $J_{wl,\,mag}$ reflects some space-time average of the critical currents induced by the time varying field $h(t) = h_0 \cdot \sin \omega t$. For this reason the situation is expected to be extremely complicated here. Firstly, we know that the local current $J_{wl}(h)$ varies strongly with the field $h(t)$. As we have seen this invalidates the Bean model if $R/R_0 > 1$ where $R_0$ is the characteristic field defined by equation (16) of equation (6). Secondly, at a given fixed $h(t)$ (or at a given instant $t$) the direction of the current within the sample changes from positive to negative and *vice versa* (or from clockwise to anticlockwise direction). In particular, we know from the study of the hysteresis loops (Section 11) that if the maximum applied field (equal to the amplitude $h_0$ here) is smaller than the full penetration field $H_p$ ($h_0 \leq H_p$ ; see for instance Eqs. (6) and (8) of Ref. [77a] and the coming Sect. 14 on anisotropy) the sample is always in the reversal magnetic state defined for example in figure 3 by $M(h(t)) = M_{rl}(h(t))$ of equation 24 of reference [77a]. We recall that the term « reversal » refers to the portion of the returning branch of the hysteresis cycle with clockwise and anticlockwise currents within the sample (Fig. 3).

The examination of formulae (50) and (52) connecting the irreversible magnetization $(M^+ - M^-)/2$ of the low-$H$ cycle and the apparent magnetic critical current density $J_{wl,\,mag}$ suggests that the relationship relating this current and $\chi''$ should be of the same form but with $(M^+ - M^-)/2$ replaced by the irreversible magnetization defined by $h_0 \cdot \chi''$. In addition, since in the reversal region of the cycle the sign of the local current $J_{wl}(h(t), r)$ varies

with $r$ we expect that the numerical factor entering formulae (50) and (52) should actually be higher than 30. Figure 70 shows the irreversible magnetization $\chi''(T)\, h_0$ (left scale) together with the product $\beta R\,[1 - f(r_g/\lambda)]\, J_{wl,\,mag}(T,\, h = 0)/30$ (right scale) for three different $J_{wl}(T)$ relationships $n = 1/2,\ 1,\ 3/2$ in equation (64). Here, the function $f(r_g/\lambda)$ is again the one used for the calculation of the low-$H$ cycle [77b] whereas $\beta$ is a numerical factor of the order of one. The most remarkable result of figure 70 is that, after taking into account of the scaling factor $\beta\,.\,(1 - f(r_g/\lambda))$, the envelope curve passing through the peak of $h_0\,\chi''(T)$ is, to a very good approximation, the same as that defined above from the magnetic current $J_{wl,\,mag}(T)$ curve at zero applied field ($h = 0$).

Therefore, in all the above cases we find that the relationship between $J_{wl,\,mag}$ and $h_0\,\chi''(T)$ is the same (within a numerical normalization factor) as equation (50) (for the low-$H$ hysteresis cycle). The proportionality factor $\beta$ is found to be approximately constant within a few percent. We have tested that this factor depends only weakly on the other parameters $r_g$, $R$, $J_0$, $H_0$.

In summary, we can write the following relationship between $J_{wl,\,mag}$ and $\chi''(T_m)$ :

$$J_{wl,\,mag}(T,\,0) = 30\,\frac{h_0\,\chi''(T_m)}{\beta R\,[1 - f(r_g/\lambda(T_m))\,]} = 30\,\frac{h_0\,\chi''(T_m)}{\beta R}\,\frac{p}{\Delta p} \tag{65a}$$

with the ratio $p/\Delta P$ completely defined from the $\chi'(T)$ curve alone as shown in figure 71 and as follows :

$$\frac{p}{\Delta p} = \frac{\chi''(T_m,\, h_0 < H^{w}_{c_1})}{\chi'(T_m,\, h_0 < H^{w}_{c_1}) - \chi'(T_m,\, h_0 > H^{w}_{c_2})} \tag{65b}$$

For large grains (such as $r_g \gg \lambda(T = T_m)$ (see also Sect. 11) we can rewrite (65a) as :

$$J_{wl,\,mag}(T,\,0) \approx 30\,\frac{h_0\,\chi''(T_m)}{\beta R\,\langle 2\,\lambda(T_m)/r_g\rangle}\,, \qquad (r_g \gg \lambda(T_m))\,. \tag{65c}$$

Note that the scaling factor is related to the jump width of the $\chi'(T)$ curve at $T = T_m$ as illustrated qualitatively in figure 71. This figure is analogous to figure 56 relating the same factor to the low-$H$ hysteresis cycle. However, it is to be recalled that in the $R \gg R_0$ limit (where $R_0$ is the characteristic radius defined by Eq. (16) the critical current density deduced from the envelope curve and from equations (65) above is essentially connected with the characteristic field $B_0(T)$ (Eq. (64)) controlling the field variation of intergrain current. Therefore, like the current deduced from the low field hysteresis cycle (see Eqs. (24b, 27b, 30a) of Sect. 6) the critical current deduced from the envelope curves of figure 70a, b has little thing to do with the local current itself.

12.3.8 *The connection between the maximum of $\chi''(T)$ and the full penetration field $H_p(T)$.* — Let us turn back to figures 67 and 70 where it is seen that the maxima in $\chi''(T)$ occurs just at $h_0 = H_p$, that is just when the flux front produced by the maximum applied field $h(t) = h_0$ reaches the centre of the specimen. Since the amplitude $\chi''_{max} = \chi''(T_m)$ of the peak of $\chi''(T)$ is proportional to the critical current density $J_{wl,\,mag}(T,\,0)$ at $h = 0$ (see envelope curves of Fig. 70), this implies that $H_p$ is also proportional to $J_{wl,\,mag}(T,\,0)$. This can be easily justified from the comparison between the formulae (23b) and (24b) (Koppé model) or (26b) and (27b) (exponential model) or (29b) and (30a) (Kim model) of section 6 ; in the limit $R \gg R_0$. Let us indeed expand any of the formulae (23b) or (26b) or (29b) in Taylor series and assume that $R \gg R_0$. For example, in this limit equation (26b) gives $H_p \approx H_0\,.\,\ln(R/R_0)$. Comparing with formula (50) of section 11 which g ves $J_{mag}(T,\,0)$ in the

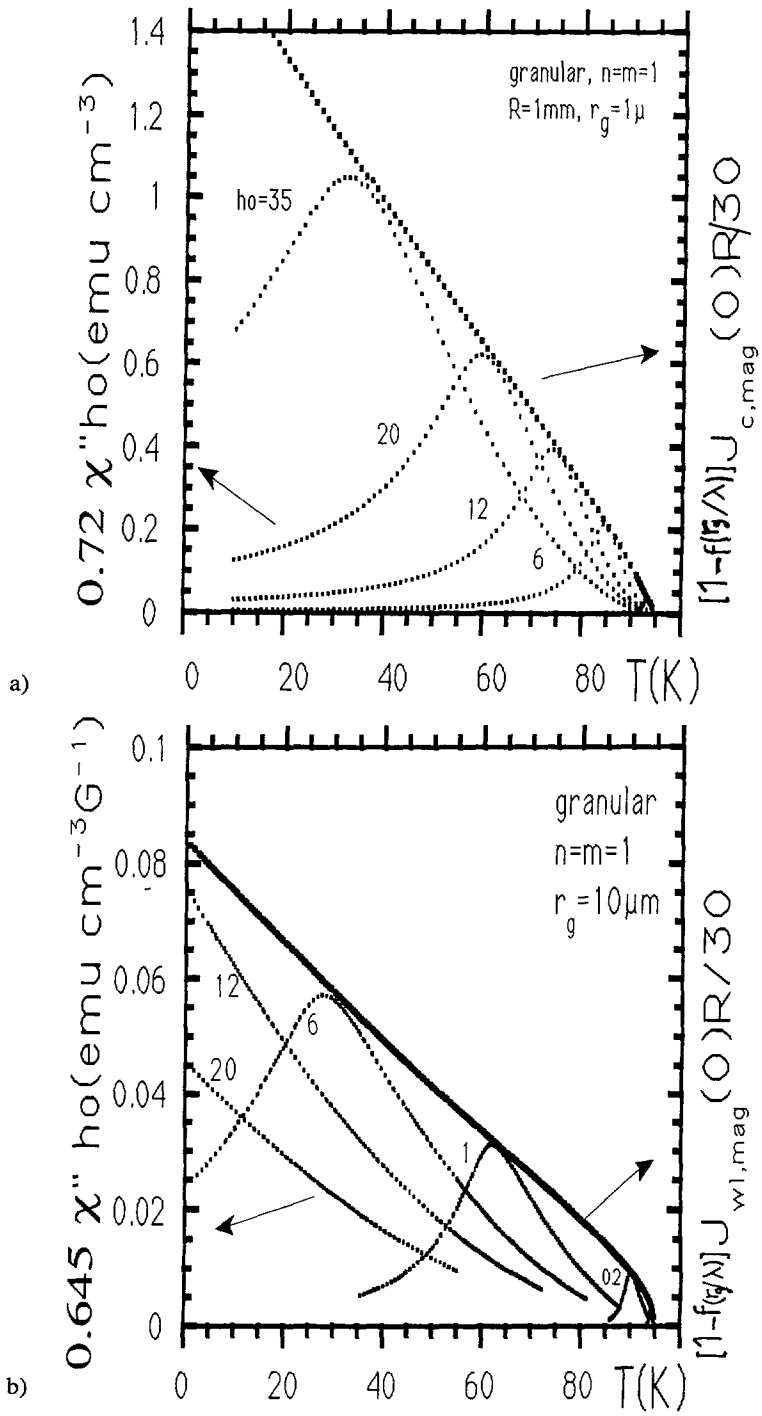


Fig. 70a, b. — Compare the calculated curves defined by « the irreversible magnetization » $h_0 \chi''$ as explained in the text with the product $\beta\ (1 - f(r_g/\lambda))\ J_{wl,\,mag}(T)\ R/30$ (here $J_{wl,\,mag}(T)$ is the intergrain magnetic current at $h = 0$ defined as for Eqs. (50-52)). $\beta$ is a proportionality factor. It is seen that the curve associated with the magnetic current at $H = 0$ coincides almost rigorously with a single envelope curve passing by the maxima (naturally when these maxima exist) associated with $h_0 \chi''(T)$ curves.

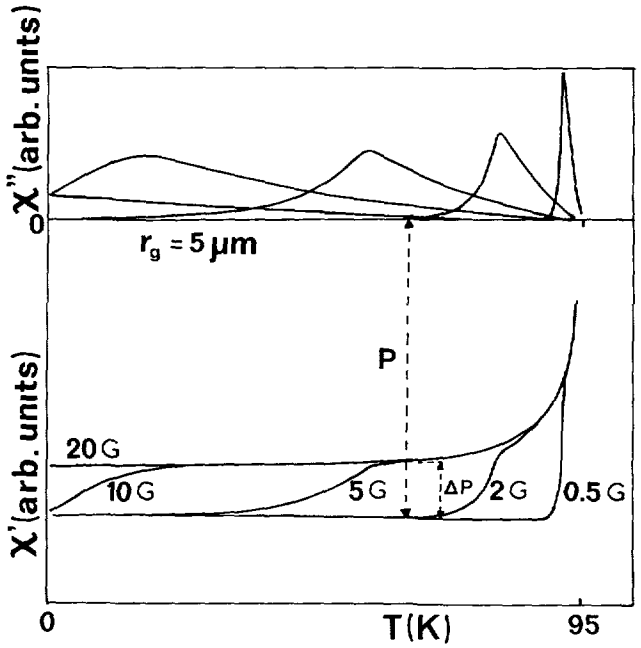


Fig. 71. — Qualitative definition, from a calculated $\chi'(T)$, of the scaling factor $(1 - f(r_g/\lambda)) \approx \Delta P/P$ entering equation (69) and relating $J_{wl,\,mag}$ and the peak of $\chi''$. This figure is the analogous of figure 56 defining the same factor from the low-$H$ hysteresis loop of granular samples.

same limit we find that the two quantities $H_p(T)$ and $J_{wl,\,mag}(T, 0)$ obey approximately the same law as a function of $R$, $J_0$ and $H_0$. Again, this confirms that the occurrence of the peak of $\chi''$ has little connection with the irreversibility line, but depends primarily on $B_0$ and $R/R_0$.

12.4 INFLUENCE OF ANISOTROPY ON THE MAGNETIZATION OF POLYCRISTALLINE MATERIALS. — Up to now we ignored the influence of anisotropy on the ac-susceptibility. Concerning single crystals this question will be treated in section 14. This paragraph is devoted to polycrystals. We would like to emphasize that the influence of anisotropy on polycrystalline or granular materials is always important when the inequality $r_g > \lambda(B, T)$ is fulfilled. This is particularly true close enough to $T_c$ or to $H_{c_2}$ since $\lambda(B, T)$ diverges in these limits. This leads to a further source of broadening of the superconducting transition.

The problem has first been investigated by Kogan and Clem [62] who considered a polycrystal formed of randomly oriented anisotropic grains. They showed that each grain (whose $c$-axis is not parallel to the field) has a transverse magnetic component ($\Delta M_\perp$). However, when averaged over the macroscopic sample the transverse magnetization vanishes. For large grains ($r_g \gg \lambda(H, T)$) this makes no significant difference with respect to the isotropic case in the Meissner domain ($H < H_{c_1}$). However, for large anisotropy ($m_c \gg m_{ab}$) and large $\lambda$ (limit $\lambda(H, T) \gg r_g$) the magnetization is distributed almost uniformly within a solid angle 2 $\pi$ and it is only 1/3 (in the longitudinal direction) of that of a collection of isotropic spheres. Another important limit investigated by Kogan and Clem is the behaviour of the reversible magnetization in the mixed state at $H \gg H_{c_1}$. Here, it turns out that the reduction in $M_{rev}$ of a polycrystal is always important (i.e. even when $r_g > \lambda(H, T)$). In particular, this situation deserves more attention near $H_{c_2}$. The reason is that when $H$ is

increased the grains whose $c$-axes are nearest to the direction of the applied field are the first to undergo a transition to the normal state (this is because in the London approximation $H_{c_2} = H_{c_2}(\theta = 0)\,[\cos^2\theta + (m_{ab}/m_c)\sin^2\theta]^{-1/2}$ where $\theta$ is the angle between the effective applied field and the $c$-axis). One direct consequence of this is that, contrary to the isotropic materials where the slope $dM_{rev}/dH$ is constant near $H_{c_2}$, this slope vanishes here. This means that $\chi'$ as well as $\chi_{zfc}$ and $\chi_{fc}$ are equal to zero (at $H$ just below $H_{c_2}$) rather than to $-(\xi/\lambda)^2/(8\pi\beta)$ ($\beta = 1.16$ for a triangular FLL) as it is the case for isotropic materials in the London limit. Of course all of these anisotropic effects lead to further smearing of the superconducting transition.

12.5 FIELD COOLED AND ZERO FIELD COOLED SUSCEPTIBILITIES. — At present, it is well established that both single crystals and sintered granular pellets of the new high $T_c$ materials exhibit rather reduced expulsion of magnetic flux as the sample is cooled in an external field ($H_{cool}$) through the superconducting transition.

The field cooled magnetization and the associated susceptibility $\chi_{fc}$ have often been used to estimate quantitatively the fractional superconducting volume ($V_p$) which is thought to be of the order of $-4\pi\chi_{fc}$. However, it turns out that the smallness of the Meissner signal might have two different and opposite origins :

(i) At first, a poor Meissner effect could readily indicate that the proportion of superconducting material is small. However, despite the case of $\chi'$ measurements discussed above, there is no reliable relationship between $\chi_{fc}$ and the fractional superconducting volume $V_p$.

(ii) Secondly and perhaps more importantly, a large departure from perfect Meissner effect could also imply that the critical current density of the material is high. In other words, it might mean that the pinnig forces acting on the vortex lines are exceptionnally large so that the superconducting material is not able to expell the magnetic flux introduced at higher temperatures : from this point of view it is expected that the higher the irreversibility line in the $T$-$H$ diagram the lower the absolute value of $\chi_{fc}$. In fact, $H_{cool}\,\chi_{fc}(H_{cool})$ is approximately equal to the value of the equilibrium magnetization $M_{eq}(T_{irr}(H_{cool}))$ just at the point where the irreversibility line is crossed during the field cooling process, assuming extremely rapid cooling through this line. The departure from this value of $M_{eq}$ decreases with the size of the sample as sketched in section 4 (Fig. 13). It is then obvious that in this case the smallness of the Meissner signal has nothing to do with the actual superconducting volume of the material but reflects the apparent irreversibility line and to some extent the characteristic dimension of the specimen as well (see § 12.2.3 and 12.2.4).

It is now interesting to add that the field cooled susceptibility $\chi_{fc} = M_{fc}/H_{cool}$, the zero field cooled susceptibility $\chi_{zfc} = M_{zfc}/H_{cool}$ as well as the remanent susceptibility $\chi_r = M_r/H_{cool}$ are not independent but indeed related by a remarkable relationship discussed below (recall that $M_r$ is obtained after field cooling and then immediately withdrawing the cooling field). It is striking that this property relating the three susceptibilities above is also exhibited by ferromagnetic-spin-glass alloys (also called reentrant-spin-glass-magnets) as established by Senoussi [383] and Senoussi and Öner [384]. This relationship (represented by the experimental diagram of figure 73a [378, 382, 386]) can be understood as follows : since the local magnetic induction $B(r)$ is equal to the vortex density, then the statement that the pinning forces (acting on the vortex structure) are very high means that $B(r)$ (and hence the total number of vortex lines inside the sample) will stay approximately constant after removing the cooling field $H_{cool}$ assumed to be much lower than the penetration field $H_p$. We recall that the conditions $H_{cool} \ll H_p$ and $\Delta r \ll R$ are equivalent ($\Delta r \approx H_{cool}/H_p)/R$ and are more easily satisfied for large critical currents. For the following discussion it is however

important to emphasize that the condition $B(r) = Cst$ is not true within the region of depth $\Delta r$ related to $H_{cool}$ and to $J$ by equation (59) (see Fig. 13 for a qualitative illustration of this). Therefore, we expect that in this limit (in particular for $\Delta r \ll R$) the total induction will stay constant as the cooling field is removed, except within the thickness $\Delta r$. This is exactly what is observed for small cooling fields for both sintered materials (see Fig. 72 from [380]) and single crystals [382]. Applying the above considerations (i.e. $B$ remains constant inside the sample) to the two limiting cases $H = H_{cool}$ and $H = 0$ ($H = 0$ means that $H_{cool}$ is removed) and using the usual Gauss equation ($B = H + 4\pi M$) which relates these magnetic vectors in any condition, we obtain :

$$B_{fc}(H_{cool}) = B_{fc}(0) = H_{cool} + 4\pi M_{fc}(H_{cool}) = 0 + 4\pi M_r . \tag{66a}$$

Moreover, in the field region where $M_{zfc}(H)$ is linear in $H$ and assuming perfect screening (i.e. $\Delta r \ll R$) we get $H_{cool} = -M_{zfc}/\chi_{zfc}$ and $4\pi\chi_{zfc} = -1$. Putting in the above equation gives the experimentally verified relationships :

$$M_{fc}(H_{coll}) = \frac{M_{zfc}(H_{cool})}{4\pi\chi_{zfc}(H_{coll})} + M_r = M_{zfc}(H_{cool}) + M_r = |M_r| - |M_{zfc}|. \tag{66b}$$

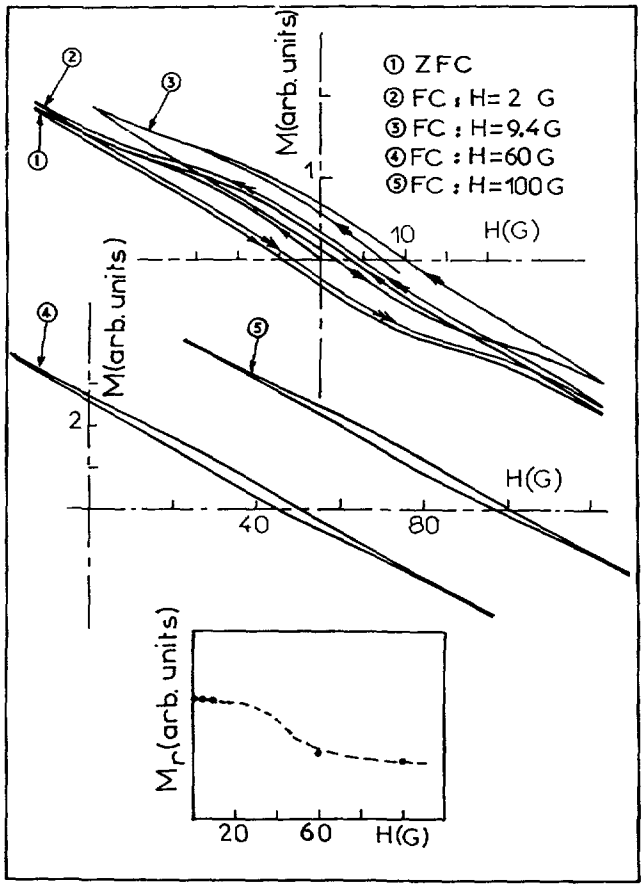


Fig. 72. — Displays several low field $M(H)$ curves plotted after the sample had been cooled through $T_c$ in the indicated fields (from Oussena thesis [380]). The inset shows the variation of the remanent magnetization (obtained after suppressing the cooling field) as a function of $H_{cool}$.

It is to be recalled that the assumption that $B$ remains constant in fc experiments should be valid only for large samples, for negligible relaxation effects and for $J$ not significantly dependent on $H$.

12.5.1 *The connection with usual spin-glasses and reentrant magnets.* — Magnetic irreversibilities and the associated after-effects which characterize high $T_c$ ceramics have been often interpreted within the framework of a spin-glass formalism based on the Josephson Hamiltonian (see for instance discussion in Ref. [13]). At this point, we emphasize that this formalism has nothing to do with the « vortex glass » concept introduced in the collective pinning theory and which will be discussed briefly in sections 13 and 17.

It has been shown by Senoussi *et al.* [383-384] that ferromagnetic-spin-glass materials obey exactly the same relationship as equation (66b) above which, in algebraic terms, reads :

$$M_{fc}^{sg} = M_{zfc}^{sg}(H_{cool}) + M_r^{sg}. \tag{66c}$$

This is shown in figure 73b. Formally, the physical origins of the two equations (66b) and (66c) are very much the same and can be understood as follows :

(i) On the one hand the vortices created in the reversible region of the $T$-$H$ phase diagram are quenched-in by the pinning forces produced during cooling through the crossover irreversibility line of that diagram. As we have already noted this line delimitates also the $H$-$T$ area where the bulk critical current density is not zero.

(ii) On the other hand, the domains in a ferro-spin-glass — reentrant magnet existing initially in the ferromagnetic reversible phase are quenched-in along their initial directions [383] by the strong unidirectional Dzyaloshinsky-Morya anisotropy (pinning-like) forces created during cooling through the ferromagnetic spin-glass transition (or the Almeida-Thouless irreversibility line). Moreover, we know that in both cases the irreversible (i.e. the non-equilibrium) magnetizations vary with time following a logarithmic law, to a first approximation. This shows that the similarities between the above relationships (66b and 66c) hold as a function of time as well. Nevertheless, we conclude from the present discussion and from earlier data [13] that despite the strong analogy with conventional ferro-spin glasses the observed superconducting irreversibilities can be explained very simply in the framework of the critical state picture and the related flux creep mechanism.

The spin glass-like picture would be more appropriate only in the limit where the dimensions of the grains composing the ceramic material are small compared both with the London penetration depth $\lambda$ and the Josephson penetration depth $\lambda_J$ characterising the junctions between adjacent grains (such conditions are in fact generally assumed in these models). In addition, to resolve theoretically the very complex Josephson Hamiltonian of a junction network it is generally assumed that the distance $d$ between neighbouring grains is much larger than their diameters $2R$ (see Fig. 33c). The latter condition is equivalent to the condition that the packing factor $V_p$ of superconducting matter is very small ($V_p \ll 1$).

At first sight there seems to be not much difference between the spin-glass and the critical state approaches. However, we believe that for currently investigated ceramics the critical state picture is not only much simpler to handle than the spin-glass one but it is also much more reliable for quantitative analysis. Finally, the discussion confirms that the Meissner effect (connected with $M_{fc}$) considered alone has not much meaning in the irreversible region of the $T$-$H$ plane. Though not always easy to interpret too (see previous discussions of this section), the zero field cooled magnetization is a good probe for characterizing the material and determining the fractional superconducting volume.

12.6 FREQUENCY AND VISCOSITY EFFECTS. — In the previous sections we ignored frequency effects particularly concerning the position $T_m$ of the peak of $\chi''$ which is generally found to

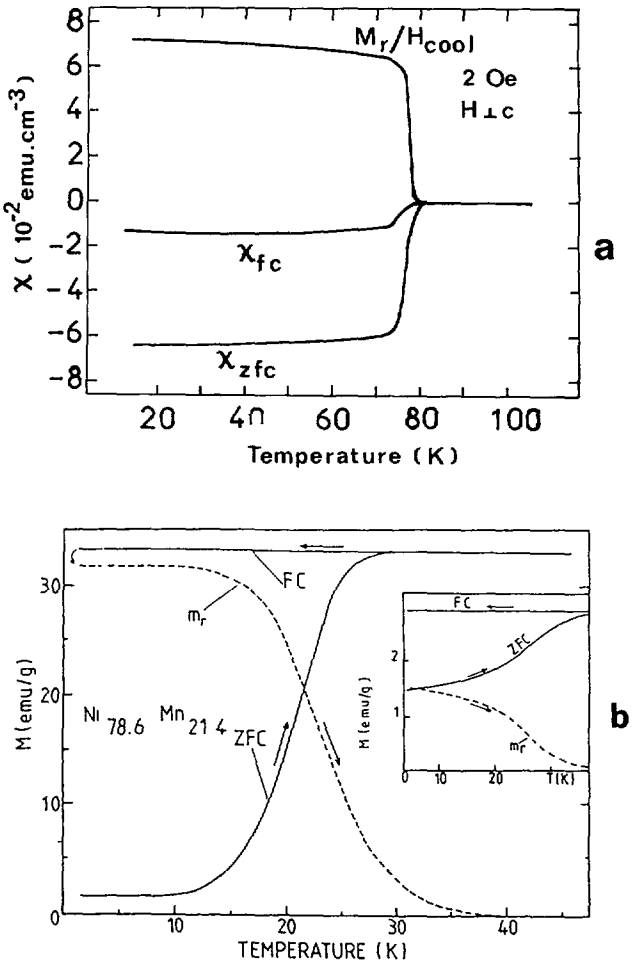


Fig. 73. — The upper figure compares zero field cooled, field cooled susceptibilities and remanent magnetizations in HTSC [382]. Lower figure, the same in a reentrant-spin-glass [383, 384] for two different shapes of the NiMn-S.G. sample : a needle and a sphere (inset). It is indeed found that for spin glasses the general curve shapes depend strongly on the shape of the sample as well as on the material itself but equation (66b) relating $\chi_{fc}$, $\chi_{zfc}$ and $M_r$ is conserved.

depend experimentally on frequency [84-95, 385-388] (see also next section). A second aspect also completely neglected in the preceding sections (for the sake of simplicity) concerns the usual viscous flux flow (particularly important in the mixed state) which by itself can give rise to a large frequency dependence and eventually to a maximum in the experimental $\chi''(T)$ [393], when the skin depth $\delta_{ff}(\omega, T, H)$, which increases with $T$ becomes comparable to the radius of the sample. This has the same physical origin as the flux flow resistivity and is connected with the normal current density $J_n$ of the normal electrons in the cores of the vortices (see subsection 5.1). Viscous flow and flux creep relaxation phenomena are generally present at the same time in experimental data. In some frequency regions, as in the TAFF limit and close to the depinning line, the interplay between the two is very severe. These effects have been discussed in section 5 and further information is available in the literature [390-395].

From the many measurements reported in the literature it appears that frequency effects are radically different in single crystals and decoupled grains on the one hand and in sintered granular materials (but for $H < H_{c_2}^{w}$ in this case) on the other hand. In other words, frequency effects are very different for intergranular and intragranular currents. As discussed in section 5 we believe that this is because the usual flux creep picture concerning relaxation effects is generally not valid in the case of intergranular currents. More arguments supporting this will be given later (subsection 12.7).

12.6.1 *Frequency effects in single crystals and decoupled grains in the Meissner state, $h_0 < H_{c_1}$.* — Let us first consider the Meissner state at $h_0 < H_{c_1}$ and zfc state (with no vortices in the sample and thus no critical current ; $J = 0$). It is interesting to recall that in the limit $h(t) \leqslant H_{c_1}$ and in the presence of an applied alternating field of frequency $\nu = \omega/2\pi$ the total current includes in principle three contributions $J_s$, $J_n$ and $J_d$ corresponding respectively to the superconducting electrons (Cooper pairs), the normal electrons (depaired by thermal fluctuations for $T > 0$) and the displacement current. According to London [396] the contributions of these currents ($h_0 < H_{c_1}$) are in the proportion :

$$[|J_s| : |J_n| : |J_d|] = \left[\omega : \frac{4\pi\sigma\lambda^2\omega^2}{c^2} \quad \frac{\lambda^2\omega^3}{c^2}\right], \tag{67}$$

where $\sigma$ is the normal state conductivity and $c$ is the velocity of light (Gauss units). Also according to London [396], this defines a threshold frequency $\nu_0 = 1/\sigma\lambda^2$ which is of the order of $\nu_0 \approx 10^{12}$ Hz for conventional superconductors. Concerning the physical meaning of $\nu_0$ we note that it is the frequency value at which the usual normal state skin depth $\delta_n$ is exactly equal to $\lambda$. Since the conductivity of the new high $T_c$ materials is rather low, one expects $\nu_0$ to be very large for these compounds as well. Therefore, in usual susceptibility measurements considered here the frequency $\nu_0$ is probably so large that the signal is dominated by the reversible supercurrents at least before the nucleation of any quantized vortex ($H \leqslant H_{c_1}$). In addition, in real experiments surface imperfections which are unavoidable are thought to give significant frequency dependent hysteresis whichever the applied field (see Sect. 16). Further frequency effects appear in the mixed state because of the extra normal current introduced by the cores of moving vortices and because of flux creep (in the presence of pinning defects). Finally, it is to be noted that the displacement current is certainly always negligible in susceptibility measurements. However, it might be easier to encounter in HTSC than in conventional superconductors, at least for $H$ parallel to the $a$-$b$ planes because of the possible capacitance effect of the $a$-$b$ sheets. Also, we feel that this current is connected with the inertial mass of the vortices and it seems that in usual magnetic measurements vortices behave like massless particles.

12.6.2 *Frequency effects in single crystals and decoupled grains in the mixed state, $H_0 > H_{c_1}$.* — It was first shown by de Gennes and Matricon [119] that the response of the vortex lattice to a time varying field $h(t)$ in the mixed state ($H \geqslant H_{c_1}$) is dominated by thermal activated depinning at low frequencies and by viscosity effects above a depinning frequency $\nu_p$. Accordingly, below this depinning frequency the system would be better described by the flux creep theory. Intuitively, above $\nu_p$ the energy losses are mainly induced by the usual viscous forces (flux flow) acting against the normal electrons of the vortex cores (i.e. by the scattering of these electrons by all kinds of defects). Recall that this important question was already discussed in section 4 in relation with the flux creep theory and with magnetic relaxation measurements.

12.6.3 *The influence of flux flow and the associated frequency effects.* — A more quantitative

way to account for the viscous forces is to rewrite Maxwell's equation curl $\mathbf{H} = 4\pi\mathbf{J}/c$ in the most general case and replace the critical current density $J$ (associated with the usual pinning forces) by the total current density $J_{tot} = J + J_n$ where $J_n$ is the flux flow normal current induced principally by the normal electrons of the vortex cores. This approach was applied by Melville [397] who calculated the hysteresis losses in the limit where the viscous forces are small compared with the usual pinning forces (or equivalently in the limit $J \gg J_n$) and $J$ independent of the applied field (usual Bean's approximation). More recently, Tacacs and Gömöry [390] and Geshkenbein *et al.* [393] considered the opposite limit ($J_n \gg J$) and concluded that energy losses due to viscous forces are considerably higher in HTSC than in classical superconductors. Naturally the influence of the normal current $J_n$ always becomes preponderant close enough to the irreversibility line when the critical current $J \to 0$. Viscous effects are also treated extensively by Van den Berg *et al.* [388] and by Brandt [110].

The maximum (at $T = T_m$) as well as frequency and field dependences of the complex flux flow susceptibility $\chi''_{ff}$ are discussed in detail in references [110, 390, 393]. From such studies it is deduced that this maximum occurs when the « skin depth » $\delta = (D/4\pi\nu)^{1/2}$ (here $D$ is the diffusion coefficient of flux lines) is of the order of the sample dimension, that is for $\delta \approx R$. The maximum occurs because $D$ and consequently $\delta$ increases with $T$. As in our preceding study the maximum occurs when $\delta$ becomes comparable to the dimension of the specimen. Below the fluw flow temperature maximum, $T_m$, the *energy losses per cycle* are approximately proportional to the skin depth $\delta$ implying that they vary as $\nu^{-1/2}$ in the corresponding $T$ and $H$ domains. At much higher temperature they would vary like $\nu^{1/2}$. In terms of power dissipation (i.e. *energy losses per second*), the frequency terms must be multiplied by $\nu$ (i.e. replaced by $\nu^{-1/2}$ and $\nu^{-3/2}$ respectively) for $\chi''$. This is because $\chi''$ is given not per cycle but per second.

By combining the results of the above authors, in particular those of Tacacs and Gömöry [390], with our present analysis (see below for more details) and defining the depinning frequency $\nu_{dep}$ by the condition $J = J_n$, we propose the following relationship for this frequency :

$$\nu_{dep} \approx \frac{\rho_n(T)\,[J(T, h_0, t_0)]^2}{\pi A \mu_0 h_0 H_{c_2}(T)} \left[1 + \frac{kT}{U_0^*(T, H)} \ln(\tau\nu_{dep})\right] \qquad \text{(in SI units)} \qquad (68)$$

where, $\mu_0 = 4\pi \times 10^{-7}$ is the permeability of vacuum, $A$ is a geometrical factor of the order of one [390], $\rho_n$ is the normal state resistivity extrapolated to the measurement temperature, $U_0^*$ is the apparent pinning potential defined in sections 4.2 and 4.3, $J$ is the critical current density for measurements performed at $T$ and $h_0$ and at some reference time $t_0$.

It is worth noticing that this formula can be generalized to take into account TAFF effects as well as any static field $H_0$ superimposed to the field $h_0 \sin(\omega t)$. This can be achieved simply by equating equation (14g) giving the penetration depth in the critical state model with the skin depth $\delta_{taff}$ or $\delta_{ff}$ depending on $T$ and $H$. The result is straightforward :

$$\nu_{dep} \approx \frac{\rho(T, H)\,[J(T, H, t_0)]^2}{\pi A \mu_0 h_0^2} \left[1 + \frac{kT}{U_0^*(T, H)} \ln(\tau\nu_{dep})\right] \qquad \text{(in SI units)}\,. \qquad (68b)$$

Here $\rho = \rho_{taff}$ (Eq. (14e)) or $\rho = \rho_{ff}$ (Eq. (14f)) depending on $T$ and $H$.

The following remarks are now of interest.

(i) Since in the flux flow regime we have $\rho_{ff} = \rho_n H/H_{c_2} \approx \rho_n h_0/H_{c_2}$ (if $H_0 = 0$) we easily recover equation (68) from equation (68b) in which we replace $\rho$ by $\rho_n h_0/H_{c_2}$.

(ii) Because of the very rapid drop of $J(T)$ with $T$ in HTSC and because the quadratic form of $J$ in equations (68) and (68b) we expect that $\nu_{dep}$ will drop very rapidly with $T$ as well, particularly for Bi and Tl ceramics.

(iii) The above equation do not imply that $\nu_{dep}$ marks an abrupt change from the flux creep to the flux flow or the TAFF regimes. It would correspond to a wide cross-over domain where both phenomena are comparable in magnitude. Because of the logarithmic frequency dependence in the creep regime the width of the cross over region would be imposed by the power law variation of $\chi''_{ff}$ or $\chi''_{taff}$. Considering the FF regime, it can be shown that the frequency dependence of the apparent normal current (i.e. $J_n$ averaged over the whole sample) and the associated $\chi''_{ff}$ depend on the value of $h_0$ compared to the full penetration field $H_p$. As a consequence, $\nu_{dep}$ would also depend on this condition. Since from the previous studies we know that $H_p$ increases with the radius $R$ of the sample and decreases with $T$, this implies that the exact equation defining $\nu_{dep}$ would depend on $R$ and would be different for $T \ll T_m$ and $T \gg T_m$ where $T_m$ is again the temperature of the peak of the experimental $\chi''$. Equations (68 and 68b) were deduced under the assumption that $J$ is independent of the applied field and uniform within the sample (usual assumption of the Bean model). The last condition implies that the reversal field domain of the hysteresis cycle is very small compared to the whole cycle itself or equivalently the amplitude $h_0$ of the oscillating field is much larger than the penetration field $H_p$ or else the temperature $T$ of measurements is well above $T_m$. We know from the preceding study of $\chi''(T)$ that this condition is realized only if $h_0 \gg H_p$ or equivalently if $T \gg T_m$. However, these questions are not quite clear for us at present and we feel that they need more experimental as well as theoretical considerations.

It is also interesting to address the problem of whether or not the frequency effects and other formulae calculated in the flux flow limit [390, 393, 394] apply to intergranular currents as they stand ? We believe that this is not the case because of the following arguments.

As far as flux flow effects are concerned, the upper critical field $H_{c_2}$ intervening in the equations defining $\chi''_{ff}$ in various limits is introduced in these equations because the number of conduction electrons carrying the normal current $J_n$ is proportional to the volume of the core of the vortex and hence to $\xi^2$ related to $H_{c_2}$ by $H_{c_2} \approx \Phi_0/2\,\pi\xi^2$. Of course, this condition does not hold for intergrain vortices, especially for Josephson vortices which have no core at all and *a fortiori* no defined core radius $\xi$. Nonetheless if one wants to use these equations for granular samples we should replace the order parameter $\xi$ by some appropriate Josephson parameter $\xi_J$. Likewise, one should also use the appropriate normal resistivity $\rho_{J,n}$ of the junction which is different from the measured resistivity, since the latter includes scattering of the conduction electrons by intragrain defects (see Sect. 9).

Hereafter, we shall neglect viscosity effects and assume that the measuring frequency $\nu$ is much lower than the depinning frequency $\nu_{dep}$ and ignore these effects in discussing the frequency dependence of the *ac*-susceptibilities.

12.6.4 *Frequency effects in the approximation of à Debye distribution for the relaxation times.* — We have noted that $\chi''$ is proportional to the area of the hysteresis cycle (generated by $h(t)$) times the number these cycles are swept per second, that is times the frequency $\nu$. Then, we know from figure 17 of section 5 that the area of the cycle depends on the time scale of the experiment and thus on the measuring frequency $\nu$. For this reason we expect that $\chi''$ (or more correctly the complex susceptibility per cycle $\chi''/\nu$) as well as the temperature $T_m$ of its peak will increase with frequency. The question is then how to calculate quantitatively such a frequency effect at fixed $T$ and $h_0$.

Before applying the critical state approach we have previously used to derive the hysteresis cycle we now present two phenomenological models suggested independently by Nikolo and

Goldfarb [86] and by Palstra *et al.* [87] to explain frequency effects in granular materials (more quantitative models will be presented in the next section 13). Firstly, using flux creep arguments, Nikolo and Goldfarb [86] suggested that the temperature $T_m$ should be related to the measurement frequency by a formula of the form :

$$T_m = \frac{U_0/k}{\ln(\nu_m/\nu)} \tag{69}$$

where $U_0$ is a field dependent value of the activation energy. From this equation the frequency shift in the peak position $T_m$ can be derived as : $[\partial(1/T_m)/\partial \ln \nu] = -k/U_0$. On the other hand, Palstra *et al.* [87] suggested that the complex *ac*-response is given by a Debye relaxation approximation :

$$\chi(\omega) = \frac{\chi(0)}{1 + i\omega\tau} \tag{70}$$

and concluded that a transition in $\chi'$ accompanied by a peak in $\chi''$ should occur if the measuring frequency $\nu$ couples to the dynamics of the vortex system at some resonance frequency $\nu_m$ such that $\nu_m \tau \approx 1$. Here, $\tau$ would be some relaxation time of the vortex lattice. After some mathematical transformations we indeed find that the temperature $T_m$ of the peak of $\chi''$ deduced from these considerations is given by the same formula (69) as that proposed by Nikolo and Goldfarb [86]. Almost the same analysis has been carried out in references [378, 386].

As far as flux creep is concerned, it however seems to us that these formulae neglect two important effects. The first one is the influence of the shape of the sample which comes into play quite naturally if one accepts that $\chi''$ is related to the area of the hysteresis cycle. We have indeed seen that the peak in $\chi''$ is related to the full penetration field $H_p$ which increases with $R$. Furthermore, we have seen that, even for a long cyclinder with negligible demagnetizing factor $N$, the field seen by the vortex lattice is not the applied field $h(t)$ but more correctly the effective field $h_{eff}(t) = h(t) + 4\pi M_{eq}(h(t))$. As a result for single crystals with $R \gg \lambda$ (the London depth) this field is equal to zero up to $h_0 = H_{c_1}(T)$ and $\chi''(T)$ is rigorously zero up to some temperature $T'''$ (Eq. (63)) at which this condition is just realized. Of course, we know that in real experiments $\chi''(T)$ is never rigorously equal to zero either because of the presence of some weak links at the surface of the specimen or because of the existence of singular demagnetizing effects at the corners (or any sharp feature) of the sample. However, these effects could be corrected for approximately at least in the case of large single crystals and do not change the present qualitative conclusions. See also sections 41 and 17.

**12.6.5** *Frequency effects in the flux creep regime.* — To discuss frequency effects in $\chi''(T)$ it is in principle necessary to resolve the flux creep equation taking into account of the various magnetizations ($M_{eq}$, $M_{vg}$, $M^+$, $M^-$, $M_{rl}$) describing the whole hysteresis cycle. besides, since in some *T-H* regions $J$ depends strongly on the field it is also recommended to include this dependence. Formally, this can be done numerically at any temperature and field. Lastly, for reliable comparison with experiments we should use the real pinning potential $U(r)$ and not necessarily the one which linearize the flux creep equations. In practice, there are at least two difficulties to overcome in order to obtain quantitative data. The first difficulty concerns the fact that in the temperature region of most interest (particularly near the peak of $\chi''$) we are most of the time in the field reversal condition (i.e. there exists in the sample both clockwise and anti-clockwise circulating currents and $M(t) \approx M_{rl}(h(t))$. In principle, there is no reason that the reversal magnetization $M_{rl}(h(t))$ exhibits the same

relaxation as in the cyclic critical state defined by $M^+(t)$ or $M^-(t)$. A second difficulty concerns the question of how to incorporate time effects explicitely in the magnetization $M(t)$ entering the calculation of the hysteresis cycle. On the one hand, this magnetization is necessarily a periodic function of time. On the other hand, it must somehow incorporate relaxation effects induced by flux creep : it is not clear how to account for this last effect. The linear case is resolved in reference [388] but only in some limit and when the contribution of $M_{eq}$, $M_{vg}$ and $M_{rl}$, are all negligible compared to those of $M^+$ and $M^-$ The latter approximation amounts to assume that $T \gg T_m$. For the general case, particularly for HTSC, one of the difficulties comes from the fact that the flux creep equation (11) which gives the usual logarithmic relaxation : indeed, this equation includes the magnetization at some starting time $t = t_0$ ($M_{ir}(T, H, t_0)$) which has no physical justification for periodic signals and for general $U(r)$ laws. This means that the distribution of currents within the sample at a given field $h(t)$ depends not only on the instantaneous value of this field but also on the whole previous history during some correlation time $\tau_c(h_0, \omega)$. From equations (12a-c) (especially Eq. (12c)) of section 4.3 we suggest that $\tau_c = 1/\alpha\nu$ and that the time dependent magnetization obtained from the flux creep model (Eq. (12)) transforms into the equation below. According to section 4.3 as well as to the discussion of section 4.7 and figure 15, $\alpha$ is a factor (see below far an approximate value of this factor) which is expected to depend on $T$, the dimension of the sample $R$ (*via* the penetration fields), and $h_0$.

$$M = M(T, h(t), t_0)\left[1 - \frac{kT}{U_0^*(T, H)} \ln(\tau_c/\tau_0)\right] \quad (\tau_c \gg \tau_0). \tag{71a}$$

If we assume for simplicity that the above equation is valid for all the branches of the hysteresis cycle then we can put into the equations (55-57) we have used for the numerical calculation of the susceptibility and deduce that $\chi''$ would have the following form :

$$\chi''(T, h_0, \nu) = \chi_0^*(T, h_0, \nu_0)\left[1 + \frac{kT}{U_0^*(T, H)} \ln(\alpha\nu\tau_0)\right] \quad (\nu\tau \gg 1) \tag{71b}$$

with

$$\chi''(T, h_0, \nu_0) = \chi_0''(T, h_0, \nu_1) \frac{1}{1 + \frac{kT}{U_0^*} \ln(\alpha\nu_1\tau_0)} \tag{71c}$$

Note that we have included $h_0$ in the prefactors of the above equation to recall that in general $\chi''$ depends on the applied field. It is interesting to add that if $\nu_1$ is the lowest frequency of measurement we can rewrite the term $\chi''(T, h_0, \nu_0)$ of the right hand side of equation (71b) as given by equation (71c) and normalize the measurement with respect to the lowest frequency data. The very qualitative reasoning carried out in section 4.7 suggests that the parameter $\alpha$ in the above equation would be of the form

$$\alpha \approx h_0/\beta(T)\, R$$

where $\beta$ is an increasing function of $T$, probably of the order of $J_{max}(T) - J(T)$ where we recall that $J_{max}(T)$ is the maximum possible critical current which can exist only before flux commence to creep (see Eq. (12c) and § 4.7). However, it is to be emphasized that this qualitative result would be more justified in the limit $T \gg T_m$. Recall also that the working frequency $\nu$ is assumed to be such that $\nu \ll \nu_{dep}$ where $\nu_{dep}$ is given by equation (68).

Finally, it is also possible to show that equation (71a, b) leads approximately to the same frequency shift in the temperature $T_m$ as equation (69) of Nikolo and Goldfarb [86] and

Palstra *et al.* [87]. However the physical meaning of this shift is completely different and less fundamental here as it depends on several experimental conditions. It is also important to recall that in the equations (71a, b, c) $U_0^*$ is an apparent energy barrier which is related to the derivative of the true barrier by equations (9b) and (10).

12.7 FREQUENCY EFFECTS IN WEAKLY COUPLED GRANULAR MATERIALS, $h_0 < H_{c_1}$. — Equations (69, 70) have been applied in the literature mostly to granular materials [86, 87]. However, we believe that these formulae as well as equation (71) derived above are probably not valid for intergrain currents. We know indeed from previous results (particularly Sect. 6) that the measured intergranular current $J_{wl,\,mag}$ is very different from the local current $J_{wl}$ which is highly inhomogeneous within the material because of the self fields. It is clear that it is the macroscopic apparent current $J_{wl,\,mag}$ (and not the local $j_{wl}(r)$) which must enter flux creep equations (71) somehow when comparing with experimental data. The contradiction is that the derivation of equations (71) is based on the flux creep equations (11 or 12) which assume implicitly that the current is homogeneous in the material.

We have mentioned in section 5 that the low $H$-cycle of granular materials generally depends very little on the sweeping rate of the applied field at least at low $T$ (Fig. 17b and Ref. [198]). Similarly, we have also mentioned that frequency effects in ac susceptibility measurements are extremely weak in granular materials and that this has led several groups to the conclusion that intergrain pinning barriers (responsable for $J_{wl}$) are extremely large, up to 35 eV. These erroneous conclusions were often based on the assumption that equation (69) relating $T_m$ and applies for granular materials as well.

We suggest that the almost complet absence of time and frequency effects (in the range 0.02 to $2 \times 10^3$ Hz at low $T$) in granular materials is connected with the fact that for $R \gg R_0$ the magnetization as well as $\chi''$ are essentially proportional to the characteristic field $B_0$ (see Sect. 6). We recall here that the characteristic length $R_0$ is defined by equation (16) whereas $B_0$ is a field parameter governing the field variation of $J_{wl}$. We also recall that $B_0$ is approximately independent of time ($B_0 \approx \Phi_0/(2\,\lambda\, r_g)$ to a first approximation ; Eq. (47)) and is generally little sensitive to the local current $J_{wl}$ which is the most relevant time dependent parameter. Quantitatively speaking, this depends on the exact model for the $J$ *versus* $H$ relationship. For example the Kim model should lead to stronger time effects for $R \gg R_0$ than the other models considered in section 6.

From the literature on sintered HTSC there are numerous experiments [398-403] which show that persistent « transport currents » induced either in macroscopic rings or in hollow cylinders by a field pulse often decay notably with time in apparent contradiction with the absence of any significant time effects in magnetic relaxation at relatively low fields. It is possible that this is principally due to the fact that in persistent current experiments the excitation field (which was applied for a short time and then removed to induce the remanent current) is generally relatively high (several hundered Gauss) compared with $H_{c_1}$ of the individual grains. Consequently this creates intragrain vortices. It is then tempting to associate the decay of the remanent current with the creep of these intragrain vortices. This analysis is consistent with the fact that in some experiments the remanent or persistent current is found to decrease by more than 25 % within about one hour [398] whereas under other conditions after a few minutes the current is found to stay constant within about 10 % over a period of almost one year [401].

## 13. Very low amplitude of the variable field and breakdown of the critical state.

In most of the preceding sections our analysis was based on the critical state which assumes that any electromotive force ($e = -\,\mathrm{d}\Phi/\mathrm{d}t = -\,\alpha\,\mathrm{d}h/\mathrm{d}t$) however small, induces the full

critical current $J$ to flow locally with its direction imposed by that of the last electromotive force ($-\alpha\, dh/dt$) applied at the same point of the specimen. It is the critical state assumption which yields the well defined field and current profiles presented in figure 3 (Sect. 2) for example. It is clear from these figures that in this theory only three critical current states ($+J$, $-J$ or zero) are possible depending on the sign of the last variation of the field $h(r, t)$. However, it was pointed out some time ago by Campbell [404] that if the ac-field is too small, it is not able to depin a significant number of vortex lines (or to overcome the critical pinning force) and to build up the full critical state. Therefore this makes such a picture inadequate to describe the experimental results. In fact, in this case the local current density can take any value between the « true » critical current density $+J$ and $-J$ (instead of only three possible states $+J$, $-J$ or zero). This is based on the experimental observations [405] that at sufficiently small amplitude of the varying field the displacement of the vortices is reversible within their potential wells in the sense that there is no frictional dissipation produced by the pinning centres (in the Bean model the deformation of the vortices is always irreversible and always costs energy). This changes the process of field penetration within the superconductor and introduces a new penetration (or screening) depth $\lambda_{el}$, independent of the excitation field in a first approximation. Hereafter, we shall discuss the current and field profiles induced by a small variable field ($h_0 \sin \omega t$) superimposed on a large static field $H$ ($H \gg h_0$ and $H \gg H_{c_1}$). The conclusion will be also valid for the initial portion of the reversal curve (e.g. very close to points A or B of the hysteresis cycle of Fig. 3). We shall also examine briefly the same question for resistivity measurements.

It is to be emphasized that here as well we shall take a rather qualitative point of view allowing us to compare the experimental results with relatively simple though realistic theoretical formulae. In order to facilitate further these comparisons we shall try (when possible) to express the calculated quantities in terms of known parameters commonly used by experimentalists. Of course, all of these simplifications limit the generality of the present treatment.

Here, we shall give the approximate equations of $\lambda_{el}$ in several field-limits and for various geometrical configurations of the static field **H** (or **B**), the excitation field **h**, the surface of the specimen and the crystalline axes (the field penetration depends indeed on all these factors). We shall also determine the corresponding magnetization $\Delta M(h)$ in some cases.

### 13.1 Breakdown of the critical state, the elastic limit of the vortex line lattice.

**13.1.1** *A small longitudinal field superimposed to a large longitudinal field.* — To illustrate the above claim let us temporarily assume the validity of Bean's model and calculate approximately the distance over which the flux density is disturbed by $h$ : $\Delta r = R - r = 5\, h/2\, \pi J$ (see Eq. (59a) for a more accurate expression). Intuitively, we feel that a necessary though not sufficient condition for this equation to be meaningful is that the disturbed distance $\Delta r$ must be much larger than some depinning distance $r_p$ (the average radius of the pinning potential) of the vortex lines. This allows us to define a threshold field $h_{1,\,th}$ by the equation $\Delta r \approx r_p$ .

$$h_{1,\,th} \approx \frac{2\,\pi}{5} J r_p \,. \tag{72}$$

In general $r_p$ is equal to few coherence lengths $\xi$. Taking $r_p = 20$ Å and $J = 10^7$ A/cm$^2$ yields $h_{1,\,th} \approx 4$ œ defined from the condition $\Delta r \approx r_p$ above. This threshold field can therefore be quite large for high critical current density $J$ and shows that this kind of situation often happens in ac-susceptibility measurements where the amplitude $h_0$ of the ripple field is

sometimes as low as $10^{-3}$ œ. Equation (72) shows also that deviations from the critical state are more important at low temperature where $J$ is generally very large. As will be seen below the true threshold field is in fact much larger than $h_{1,\,th}$.

13.1.2 *A small transverse field superimposed to a large longitudinal field.* — Now, it is interesting to mention that the low field situation above is probably more easily satisfied when the excitation field is perpendicular to the steady field $H \gg h$, since in this case the amplitude of the total field stays unchanged to the first order in $h$ (it is equal to $H + h^2/2\,H$). Typical examples of transverse field geometry of this kind are torque [406], EPR, NMR and vibrating reed experiments.

At this point, we recall that in NMR, vibrating reed and more particularly in EPR measurements the operating frequencies are extremely high (compared to those intervening in ordinary ac-susceptibility) and lead to a considerable increase of the contribution of the flux flow viscous forces (not included here) to the measured signal. Of course as we know the relative weight of this contribution tends to 100 % above the depinning (or irreversibility) line.

In the transverse configuration the effective displacement of the vortex lines due to the transverse oscillating field as well as the threshold field equivalent to $h_{1,\,th}$ are more difficult to calculate accurately. The question of field and current penetrations and profiles in the perpendicular geometry are of great importance for the correct interpretation of torque, EPR, NMR and vibrating reed experiments. For instance, as it is well known the NMR line width is extremely sensitive to the homogeneity of the radio frequency field within the material. It is certainly very important to pay more attention to these effects than is done at present in the litterature on HTSC. A quantitative examination of this very complex topic requires accounting for the anisotropy of the critical current density of HTSC together with all the elastic constants, $C_{ij}$, of the flux lattice. For the sake of clarity we shall first restrict our analysis to the longitudinal ($H$ and $h$ parallel to each other and to the surface of the specimen) and isotropic case first considered by Campbell [404]. The generalization of Campbell's theory to take into account the anisotropy of $J$ and $C_{ij}$, transverse geometry, frequency effects and non local effects (i.e. dispersion, or $k$ dependence of the $C_{ij}$) will be examined subsequently in § 13.4 using a more complex approach.

13.2 FIELD AND CURRENT PENETRATIONS AT VERY LOW TEMPERATURE $h_0$ OF THE EXCITATIONS FIELD, ISOTROPIC MATERIALS. — According to Campbell [404], if the amplitude $h_0$ of the excitation field is small enough, the distribution of the variable fields and currents within the sample are better described by assuming that the vortices should oscillate reversibly (with the same frequency as $h(t)$). These oscillations take place either between (for unpinned lines) or within (for pinned lines) the potential pinning wells ; rather than jumping irreversibly over the potential barriers as in the critical state. This is in agreement with the more general theory of Labush [126] concerning the elasticity of the vortex lattice and with more recent theories of collective thermal fluctuations and collective pinning [110, 172-175].

Accordingly, for very small field variations $h(t)$ superimposed on a large static field $H$, a given vortex line is submitted to a restoring force ($F_r$) proportional to the line displacement, $u(r)$, within the potential well and to an extra Lorentz force equal to $B\ \delta J/10$. To a first approximation such an elastic force is proportional to the displacement distance $u(r)$ of the line and can be written as (in practical units) :

$$F_{r(r)} = \frac{F_0}{r_p}\,u(r) = \frac{B}{4\,\pi}\,\frac{\mathrm{d}h}{\mathrm{d}r} = \frac{B\ \delta J(r)}{10} \tag{73}$$

Note that since our approach is rather qualitative we shall neglect numerical factors of the order of 1 to 2. With this caution in mind, $F_0/r_p = \sigma$ is an elastic constant in the presence of

pinning forces of maximum value of the order of the critical pinning force $\sim F_0$, $\delta J(r)$ is the change in the current density at site $r$, produced by the local variable field at the same point. In such a limit where the displacement $u$ is small compared to the depinning range $r_p$ the penetration distance $\Delta r = R - r$ is no longer given by the usual critical state model. Then, the penetration distance is replaced by a unique characteristic penetration length $\lambda_{el}$ independent of both $r$ and the variable field $h$ (in the linear approximation assumed above). This length can be determined approximately by supplementing equation (73) by the flux conservation condition below (in order to take into account of demagnetizing effects we will replace the field $h$ by an effective field $h_{eff}$ in the following equations). In the simple case of cylindrical symmetry the flux conservation condition is given by :

$$B\, 2\, \pi\, [(r_2)^2 - (r_1)^2] = [B + b_{eff}(r)]\, 2\, \pi\, [\{r_2 - u(r_2)\}^2 - \{r_1 - u(r_1)\}^2]\,. \tag{74a}$$

After some rearrangements and simplifications we get

$$h_{eff}(r) = H \frac{\partial u}{\partial r} \quad (\text{with } r = (r_2 + r_1)/2 \text{ and } \partial r = r_2 - r_1 \ll r)\,. \tag{74b}$$

Deriving this equation once again with respect to the variable $r$ and putting in equation (73) gives

$$\lambda_{el} \approx \left[ \frac{10}{4\,\pi} \frac{H r_p}{J} \right]^{1/2} \quad (H \gg h_{eff} \text{ and } \lambda_{el} \gg \lambda)\,. \tag{75}$$

It is interesting to note that if one replaces the field $H$ in equation (75) by $h_{1,\,th}$ (right hand side of Eq. (72)) we find that $\lambda_{el}(h_{1,\,th}) = \Delta r(h_{1,\,th}) = r_p$ where $\Delta r$ is the Bean partial penetration depth. The induced local field associated with the applied ripple $h(t)$ is given by :

$$h_{eff}(r) = h_{eff}(r = R) \exp\left[ - \frac{R - r}{\lambda_{el}} \right] \quad (H \gg h_{eff}) \tag{76a}$$

$$h_{eff}(r = R) = \frac{h(r = R)}{1 - N_{eff}} \tag{76b}$$

Here $N_{eff}$ is an effective demagnetizing factor which coincides with the conventional one in the limit $R \gg \lambda_{el}$.

It is now interesting to make the following remarks :

(1) The magnetizations associated with the above field distribution (Eq. (76a)) are purely reversible (we shall consider irreversible effects later).

(2) These equations neglect the contribution of $M_{eq}(H + h(t))$ to $\Delta M$ and are thus not valid very close to $H_{c_1}$.

(3) We shall see later that $\lambda_{el}$ is the lowest possible penetration depth, implying that the usual critical state penetration depth $\Delta r$ is necessarily larger than or at least equal to $\lambda_{el}$ (otherwise it has no physical meaning).

(4) Moreover, it is probable that $\lambda_{el}$ is also a measure of the region around the singularity at the reversal point $r_1$ (such as in Fig. 3, Sect. 2) where $J$ changes discontinuously from $-J$ to $+J$ in Bean's model. Of course such a discontinuity cannot be justified physically.

(5) Now, we can use the above results to define a second characteristic field $h_{2,\,th}$ beyond which the present linear treatment ceases to be valid. We assume that this occurs just when the reversible displacement of the vortex lines located near the surface of the specimen becomes comparable to $r_p$. In terms of a maximum admissible ripple field the result is :

$$h_{2,\,th} \approx \left[ \frac{4\,\pi}{10} H J r_p \right]^{1/2} \tag{77}$$

From the comparison with equation (72) we deduce that $h_{2,\,th} = [H/h_{2,\,th}]\, h_{1,\,th}$ and thus $(h_{2,\,th} \gg h_{1,\,th})$ in general.

(6) It is interesting to calculate the critical state penetration depth $\Delta r(\Delta H)$ corresponding to a variation $\Delta H = h_{2,\,th}$. The remarkable result is that $\Delta r = \lambda_{el}$ at this limit. In other words, one goes from the elastic limit to the critical state limit just when the penetrations depths calculated within the two approximations become equal.

(7) It is now time to note that equation (76a) has a form similar to the well known London equation giving the field distribution inside the material. Therefore, the variation $\Delta M$ of the « elastic » magnetization induced by the applied field $h(t)$ is probably also very similar to that derived from the London calculation except that the London penetration depth $\lambda$ should be replaced by the elastic distance $\lambda_{el}$. We propose the approximate expressions below, valid in the case of isotropic and independent grains (negligible Josephson and dipolar couplings)

$$\Delta M = -\frac{3}{8\pi} h\left[1 - 3\frac{\lambda_{el}}{r_g}\coth\left(\frac{r_g}{\lambda_{el}}\right) + 3\left(\frac{\lambda_{el}}{r_g}\right)^2\right] \quad \text{(for spherical particles)} \tag{78a}$$

$$\Delta M = -\frac{h}{4\pi}\left[1 - \exp\left(-\frac{e}{\lambda_{el}}\right)\right] \quad \text{(for a thin slab of thickness } 2e\text{)} \tag{78b}$$

with both $H$ and $h$ parallel to the surfaces of the slab

$$\Delta M = -\frac{h}{4\pi}\,[1 - f(r_g/\lambda_{el})] \quad \text{(for a long cylinder with } N = 0)\,. \tag{78c}$$

Here the field is parallel to the cylinder axis and $f(x)$ $(= I_0(x))$ is a modified Bessel function of the first kind of order zero. If the cylinder is thick enough so that $r_g \gg \lambda_{el}$ then the above equation reduces to

$$\Delta M \approx -\frac{h}{4\pi}\left[1 - \frac{2\lambda_{el}}{r_g}\right] \qquad (r_g \gg \lambda_{el})\,. \tag{78d}$$

The modification of fields and currents (induced by the ripple field $h(t)$) should be as schematized in figure 74b, which is to be compared with figure 74a valid in the critical state conditions.

From the above discussion it seems that for the critical state picture to be valid the field $h$ must be much larger than $h_{2,\,th}$. We believe that this will be reflected not only in the ac-susceptibility $\chi' = \Delta M/h$ but also in the reversal branches of the hysteresis cycle. Because of the ratio $\lambda_{el}/r_g$ in equation (77d) the effect would be more pronounced in granular materials which would exhibit a more extended linear $\Delta M_{rl}$ *versus* $\Delta H$ region with a reduced slope (i.e. smaller magnetic sheilding) as compared to the slope measured just below the first critical field $H_{c_1}$ (that is to say $-\partial M\,(M < H_{c_1})/\partial H \geqslant -\Delta M_{rl}/\Delta H$). We indeed expect that above $H_{c_1}$ the magnetic screening (i.e. the slope of $\Delta M$) would be given by equation (77) in which $\lambda_{el}$ must replace the usual London depth $\lambda$.

**13.3** AC-RESISTIVITY IN THE PRESENCE OF A SUPERIMPOSED LARGE DC CURRENT. — It is important to know that ac-resistivity behaviour is also expected to be quite different depending on the amplitude $i_0$ of the applied excitation current $(= i_0 \sin \omega t)$ assumed to be superimposed on a dc current. Neglecting again viscous flux-flow forces, it is found [407] that below some threshold current density $(i_{0,\,th})$ there is a finite electric field $E_{qu}(t) = \alpha\omega i_0 \sin(\omega t + \pi/2)$ in quadrature with the excitation current (thus producing no dissipation) proportional to this current and as well as to the measurement frequency $\omega$. It is to be

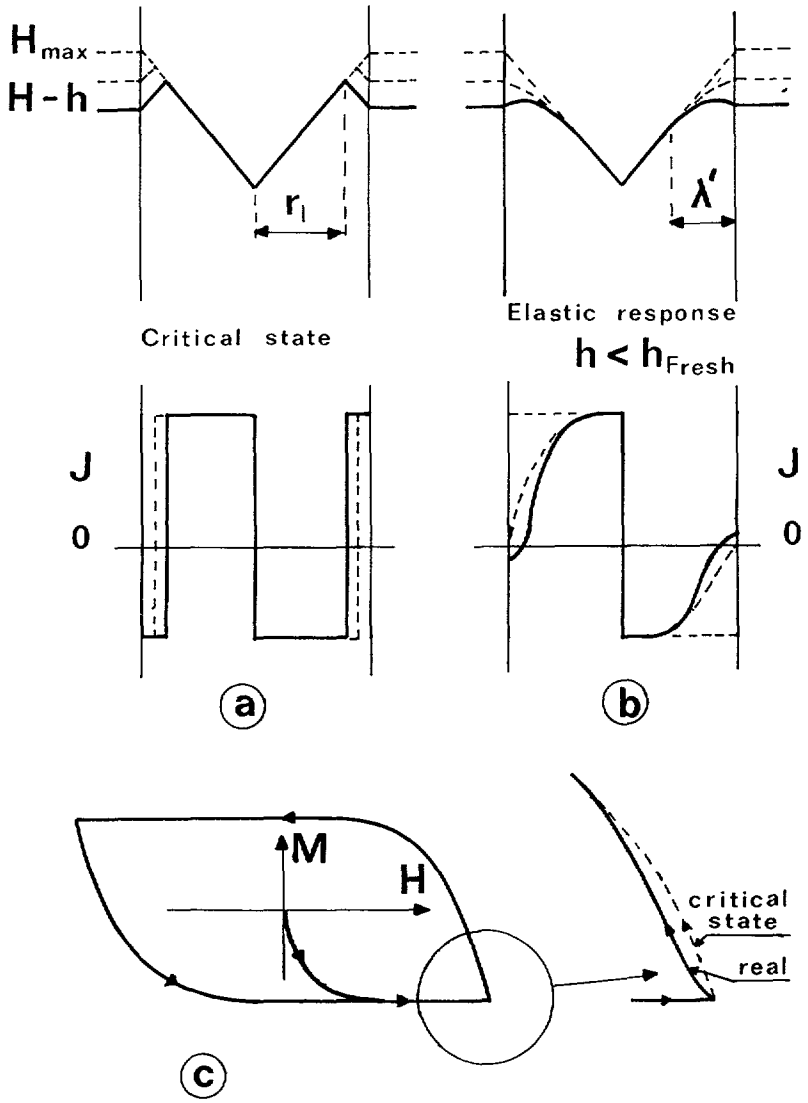


Fig. 74. — Intended to compare schematically the flux and current profiles across the sample (assumed to be a long cylinder) in the limit of Bean's model (a) and in the elastic regime when the excitation field is too small to depin the vortices (b). (c) The initial slope of the reversal curve is reduced by this elastic force and is divided by a factor of the order of $[R - \lambda_{el}(T, H)]/[R - \lambda(T, H)]$. However, it is possible that the vortex glass effect which appears in the more elaborated collective pinning theory suppresses this elastic effect, but the existence of this vortex glass phase is not yet established (see text).

emphasized that if the viscous forces are not negligible the total electric field $E$ will also present an in phase component $E_{ff}$ of flux flow type which varies as $\omega^2$ (see Sect. 12 and Eq. (68) for the conditions under which this field can be neglected). Above the threshold current the total electric field $E$ is nonlinear in $i_0$ and presents an in phase dissipative component $E_p$, directly related to the critical current density $J$ (remember that $J$ is assumed to be large enough and far away from the TAFF regime for which $E$ is also linear in $J$). An example of

$V(I)$ characteristic is illustrated in figure 75 from Lowell [407]. Note that $V$ is given in $\mu$V per kHz to recall that $E_{qu}$ is proportional to the frequency. As in the case of magnetic measurements considered above, the threshold current below which the critical state picture becomes inadequate depends on the effective dc-field $H$ (which generally includes the self field generated by the dc-current as well as any external constant field assumed to be perpendicular to the current direction). It goes to zero for $H = 0$ but is proportional to $r_p$ and, according to [407], almost constant at high $H$.

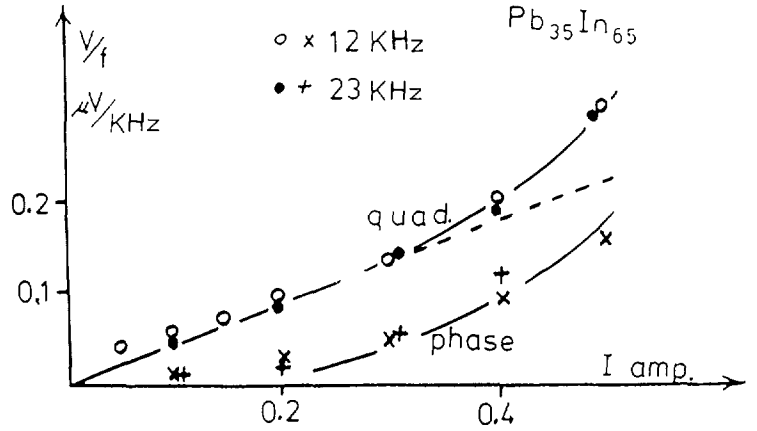


Fig. 75. — Example of ac-voltage induced by an ac-current. At very small currents $V$ is linear with frequency and current and is in quadrature with the latter, from Lowell [407].

Therefore, it turns out that Campbell's picture can be put in a more general form using the collective pinning theory which accounts naturally for the elastic response of the VLL medium as well as for time (or frequency) effects. In the limit of our understanding of the collective theory, it seems that this question is intimately related to the « vortex glass » problem (discussed briefly later in this section and more extensively in Sect. 17). Indeed, if the « vortex glass » phase readily exists it should modify considerably the elastic response of the VLL (as the pinning barriers tend to diverge in this phase). Clearly, this fascinating question deserves more experimental as well as theoretical development.

**13.4** FIELD AND CURRENT PENETRATIONS IN ANISOTROPIC MATERIALS. — This subject is rapidly developing at present and have been recently the object of a number of very nice papers [408-414]. The basic equations used in most of these papers are summarized below.

(i) The equation of motion of the VLL which represents the fact that the vortices are submitted to four different kinds of forces (per unit length) which are : (1) the viscous force $\eta\ \partial u/\partial t$, (2) the pinning force per vortex $K_p\ u(r, t)$ (note that in the elastic limit this force is proportional to the vortex displacement $u$), (3) the Lorentz force per vortex $J(r, t)\, x\phi_0$ and (4) the so-called Langevin thermal force, $F(\omega)$ assumed to be a Gaussian white noise with zero mean [123]. Here, $K_p$ is the Labush parameter per unit length and per single vortex line (to be distinguished from the Labush parameter per unit volume $\alpha_1$). The final result is

$$\eta\ \partial \mathbf{u}/\partial t + K_p\, \mathbf{u}(r, t) = \mathbf{J}(r, t)\, x\phi_0 + \mathbf{F}(\omega)\,. \tag{79a}$$

This equation must be completed by Maxwell and London equations connecting the fields and currents within the specimen and by the boundary condition that the field at the surface

must be equal to the applied field (if the demagnetizing factor is negligible). The interesting results which are common to most of these papers [123, 408-414] are the generalization of Campbell's penetration depth to include the London penetration depth $\lambda$ and the introduction of frequency and time effects in the expression of $\lambda_{el}$. As a consequence the latter becomes a complex quantity the imaginary part of which accounts for irreversible effects and energy losses.

(ii) Koshelev and Vinokur [408] calculated $\lambda_{el}$ and other quantities in various approximations corresponding to different regions of the *T-H* phase diagram. These regions are in fact associated with different $J(T, H)$ relationships as deduced from the collective pinning theory in presence of « phonon like » thermal fluctuations [174]. Among other results, they derived three frequency regimes : (1) At very high frequencies, energy losses are caused by viscous motion of the VLL. (2) At intermediate frequencies the ac-absorption is dominated by the oscillation of the lattice near equilibrium regime (or « Campbell's regime »). At extremely low frequencies irreversible jumps of large lattice regions (bundles of lines) between different metastable states would come into play and would give the main contribution to the absorption. This last behaviour is called the « two levels » regime and would correspond to the vortex glass phase (SG).

(iii) Noting that in the above collective theory the pinning potential diverges as $U = U_0[J_{max}/J]^y$ ($y > 0$), Van der Beek and Kes [414] argued that at sufficiently low $J$ (or low ripple field $h_0$) these collective depinning mechanisms should be frozen. Nevertheless, flux creep would proceed *via* interstitial defects and vacancies in the VLL. If these VLL defects were free to move across the material the critical current would be zero. However, these defects are thought to be impeded by oxygen vacancies giving rise to a non zero critical current density. Such VLL defects are modeled by small pairs of edge dislocations the distance between which is approximately equal to the vortex spacing. This leads to a further creep mechanism called « plastic creep » because the border limit (i.e. the contour) of the associated correlation volume $V_c$ (in the VLL) remains finite and is defined by the inter dislocation distance. By contrast, in the usual collective pinning theory $V_c$ is exclusively determined by the elastic properties of the VLL and tends to diverge as $J$ approaches zero (vortex glass limit). In fact, in the collective pinning theory $V_c$ is defined (more or less arbitrarily) when the elastic deformation between the centre ($r = 0$) and the periphery ($R_c$) of $V_c$ is of the order of $\xi$; i.e. $u(R_c) - u(0) \approx \xi$.

The limited validity of collective pinning theory, particularly for 2D VLL, seems also to be inferred from numerical simulation [410, 411] as well which demonstrates that the nature and size of the pinning force is determined by plastic deformations of the VLL generated by the random potential whatever small. The interplay between « plastic flux creep » occurring *via* dislocation in the VLL and the elastic creep (typical of the vortex glass) state is also discussed by Feigel'man *et al.* [174b] who incorporate temperature effects, particularly thermally induced dislocations. This question is also the object of a nice paper by Vinokur *et al.* [415].

From the quantitative aspect, the treatment of van der Beek and Kes [414] seems to be more appropriate to the TAFF domain of the *T-H* plane.

(iv) Coffey and Clem [123] were able to determine both $\lambda_{el}$ and the frequency dependent complex resistivity $\rho_{el}(\omega)$ taking into account viscous flow, thermally activated flux flow (TAFF) and flux creep simultaneously. They also considered several frequency regimes defined by a dimensionless parameter $\omega\tau$ where $\tau$ is now a characteristic relaxation time equal to $\eta\,[I_0^2(\nu) - 1]/[K_p\, I_0(\upsilon)\, I_1(\upsilon)]$ with $\upsilon = U_p/2\,kT$. We recall that $U_p$ is the height of the pinning potential whereas $I_0$ and $I_1$ are modified Bessel functions of the first kind (see [123] for other details).

(v) Brandt [412] included explicitly in the calculation of $\lambda_{el}$ the elastic constants

$C_{ij}$ and non local effects (i.e. the dependence of $C_{ij}$ as well as $K_p$ on the wave vector **k** associated with the elastic deformations). He also considered several geometrical configurations of the vectors **H** and **h** with respect to the surface of the specimen.

Other penetration depths associated with the vortex glass (VG) phase [413] are discussed in reference [106] where it is found that the dc-skin depth in the limit of a static field ($\omega = 0$) is different from that obtained by taking the limit $\omega \to 0$ (in ac-measurements). Accordingly, in this last case $\lambda_{ac}$ would diverge as $[\ln \omega]^{1/\psi}$ near the VG line in the $H$-$T$ phase diagram of the VLL. This means that the limits $\delta H \to 0$ and $\omega \to 0$ are noncommuting (or not interchangeable). However, we believe that the SG picture within which these arguments would be valid is not yet well established (see [410-414] and Sect. 17). Finally, it is worth noticing that field penetration in relation to intrinsic pinning is considered in [420].

Most of the above theoretical calculations have used the Labush parameter $\alpha_p$ (per unit volume) which is related to $F_0$ and $r_p$ of our equation (73) by the approximate but useful equation (in practical units)

$$\alpha_p \approx \langle d^2U/dr^2 \rangle \approx (\Delta U/r_p)/r_p \approx F_0/r_p \approx BJ/10\, r_p\,. \tag{79b}$$

We recall that $U(r)$ is the real pinning energy per unit volume acting on the VLL and incorporating the elastic interactions within this lattice.

To allow qualitative comparison with experimental data in presence of uniaxial anisotropy (HTSC materials) we propose the following expressions for the elastic penetration depths $\lambda_{el}$. For this purpose we also need, in addition to the elastic modulii $C_{ij}$, the two London penetration depths $\lambda_c$ and $\lambda_{ab}$ together with the three critical current densities $J_{c,ab}$, $J_{ab,c}$, $J_{ab,ab}$ introduced previously (Sect. 2) and which will be defined more rigorously in the next section.

In view of the complexity of the problem we will also make us of the following approximations.

(1) First of all, when possible we shall first give the general expression (involving the elastic constants) of $\lambda_{el}$ and then a simplified formula. The latter is generally roughly valid in the limit of high field ($H_{c_1} \ll H \ll H_{c_2}$) and large elastic depth ($\lambda_{el} \gg \lambda$).

(2) In some cases the exact London penetration depth entering the equation of $\lambda_{el}$ is not well defined and includes a combination of both $\lambda_c$ and $\lambda_{ab}$. In such cases we shall use the notation $\lambda$ rather than $\lambda_c$ or $\lambda_{ab}$.

(3) For the sake of simplicity we shall generally neglect the anisotropy of both $\alpha_1$ and $r_p$ in the expression of $\lambda_{el}$. Of course this is difficult to justify in some geometrical configurations where we are forced to take into account the anisotropy of these parameters.

(4) We shall neglect frequency and time effects and assume that the sample is very thin in the direction perpendicular to **h** (this is to avoid demagnetizing effects associated with this field).

(5) However, the way how the elastic constants presented below enter the measured magnetic signals $\Delta M$ together with the influences of time, frequency and demagnetization effects will be discussed briefly at the end of this section.

(6) Finally, we emphasize again that due to the extreme complexity of the problem the derivation of the following elastic penetration depths is not rigorous but rather intuitive. It is also an attempt to generalize some of the results of references [123, 404, 410-414]. Therefore, waiting for new progress in this topic, our aim is to allow some qualitative comparisons with experimental data and, at the same time, illustrate some of the situations that can be encountered in experiments.

We now want to consider several possible geometrical configurations of the field vectors **H**

and **h**, the crystalline axes and the surface of the specimen and give the corresponding $\lambda_{el}$.

**(1) h // H // c //** to the surface of the specimen

$$\lambda_{el} = \left[\lambda_{ab}^2 + \frac{C_{11}}{\alpha_1}\right]^{1/2} \approx \left[\lambda_{ab}^2 + \left(\frac{10}{4\pi}\frac{Hr_p}{J_{ab,c}}\right)^2\right]^{1/2} \quad (\text{if } H \gg H_{c_1}) . \tag{79c}$$

Note that here the ratio $C_{11}/\alpha_1$ tends to zero as $H$ approaches $H_{c_1}$ and thus $\lambda_{el}$ tends to $\lambda$. The second term of (79c) is valid in the limit $H \gg H_{c_1}$.

**(2) h ⊥ H // c //** to the surface of the specimen

$$\lambda_{el} = \left[\lambda^2 + \frac{C_{44}^2}{\alpha_1}\right]^{1/2} \approx \left[\lambda^2 + \left(\frac{10}{4\pi}\frac{Hr_p}{J_{ab,c}}\right)^2\right]^{1/2} \quad (\text{if } H \gg H_{c_1}) . \tag{79d}$$

Now $C_{44}$ is the tilt modulus around the $c$-axis. It is equal to $C_{11} \approx \alpha B^2$ at high field, but tends to the so called single vortex term (linear in $B$) as $B$ approaches zero. Since the Labush parameter $\alpha_1$ is also linear in $B$ at low $B$ this implies that this « tilt » elastic depth remains larger than $\lambda$ when $H \to H_{c_1}$. This adds more supports to our previous claim (subsection 13.1.1) that elastic effects are more important in the case of transverse geometries, and as a consequence in torque, EPR, NMR and vibriting reed experiments, than in ordinary susceptibility measurements.

**(3) H // h //** ($a$-$b$ planes) // to the surface of the specimen : by analogy with the reversible London case this geometry is probably characterized by two different elastic penetrations :

$$\lambda_{el} \approx \left[\lambda_{ab}^2 + \left(\frac{10}{4\pi}\frac{Hr_p}{J_{ab,ab}}\right)^2\right]^{1/2} \quad (\text{penetration parallel to } \mathbf{c}) \tag{79e}$$

$$\lambda_{el} \approx \left[\lambda_c^2 + \left(\frac{10}{4\pi}\frac{Hr_p}{J_{c,ab}}\right)^2\right]^{1/2} \quad (\text{penetration perpendicular to } \mathbf{c}) . \tag{79f}$$

Note that at low $H$ these penetration depths are expected to be controlled by the compressional moduli $C_{11\parallel}$ and $C_{11\perp}$ along the $c$-axis and parallel to the $ab$ planes respectively (for **h** in the $ab$ planes).

**(4) H ⊥ h** and both fields are parallel to the ($a$-$b$) planes and to the surface of the specimen. Here too, the magnetic response involves two elastic penetration depths which depend on the in plane elastic constant ($C_{44\parallel}$, see Ref. [110]) and which we approximate here as :

$$\lambda_{ab,ab\parallel} = \left[\lambda_{ab}^2 + \frac{C_{44,\parallel}^2}{\alpha_{ab,ab}}\right]^{1/2} \approx \left[\lambda_{ab}^2 + \left(\frac{10}{4\pi}\frac{Hr_p}{J_{ab,ab}}\right)^2\right]^{1/2} \tag{79g}$$

and

$$\lambda_{c,ab\parallel} = \left[\lambda_c^2 + \frac{C_{44,\parallel}^2}{\alpha_{c,ab}}\right]^{1/2} \approx \left[\lambda_c^2 + \left(\frac{10}{4\pi}\frac{Hr_p}{J_{c,ab}}\right)^2\right]^{1/2} \tag{79h}$$

(The right hand side of Eqs. (79g and 79h) are valid for $H \gg H_{c_1}$.)

For several reasons that will become clear in the next section on anisotropy effects, the relative contribution of each of the above penetration depths to the measured magnetic signal is expected to depend on the ratio $(eJ_{ab,ab})/(wJ_{c,ab})$ where $2e$ and $2w$ refer to the thickness (in the $c$-direction) and the width of the sample. In many circumstances this ratio is much

greater than one, because of the high anisotropy of the critical current density. Then $\Delta M$ is imposed by $\lambda_{c,\,ab\,\parallel}$ alone. The inverse is true in the opposite limit realized sometimes in very thin films of YBaCuO.

(5) $\mathbf{H} \perp \mathbf{h} \,/\!/\, \mathbf{c}$ and the sample is very thin in the direction of the field **h**. Here too the magnetic response is thought to involve two elastic penetration depths which depend on the in plane elastic constant $C_{44\,\parallel}$ (see Ref. [414]) and which we approximate as :

$$\lambda_{ab,\,ab\,\perp} = \left[\lambda_c^2 + \frac{C_{44,\,\perp}^2}{\alpha_{ab,\,ab}}\right]^{1/2} \approx \left[\lambda_c^2 + \left(\frac{10}{4\,\pi}\frac{Hr_p}{J_{ab,\,ab}}\right)^2\right]^{1/2} \tag{79i}$$

**13.5** ON THE RELATIONSHIP BETWEEN THE MAGNETIZATION, THE AC-SUSCEPTIBILITY AND THE ELASTIC PENETRATION DEPTHS. — In this paper we are more interested in direct magnetic measurements ($\Delta M$ and $\chi$) than in the elastic penetration depths themselves. Therefore, the important question we are readily concerned with is that of the magnetic response of the material in the various elastic limits and geometrical configurations just considered. We have seen that a partial answer to this question can be found if one proceeds by analogy with the London reversible magnetization (Eqs. (78a) to (78d)). Naturally, there is probably no general answer to this problem. A first difficulty comes from the fact that, except in the case of cylindrical symmetry ($\mathbf{H} \,/\!/\, \mathbf{h} \,/\!/\, \mathbf{c}$) with negligible demagnetizing effect, the calculation of $\Delta M$ or $\chi$ involves not one but two of the eleastic penetration depths derived before. Secondly, for real specimens we must include demagnetizing effects which are expected to be especially important in the limit where $\lambda_{el}$ is short compared to the effective dimensions of the specimen. Nevertheless, in the absence of concrete theories accounting for these effects, we suggest to proceed by analogy with the anisotropic reversible London problem, at least in the very few cases of the literature where the latter has been resolved. The London's magnetization of uniaxial anisotropic superconductors has been calculated by Kogan and Clem [62] in several limits equivalent to the configurations $\mathbf{H} \,/\!/\, \mathbf{h}$ considered previously. These calculations will be summarized in the next section 15. Also, the configurations $\mathbf{H} \perp \mathbf{h}$, can probably be treated by analogy with existing calculations of the reversible torque.

Another important question concerns the manifestation of frequency and time effects of flux creep origin in magnetic measurements. We have seen that this problem was investigated extensively in references [408-412]. However, in our opinion, it is not certain that the conclusions of these papers can always be applied to experimental data. There is several good reasons for this. (1) First of all, many experiments are performed by means of a lock-in-amplifier and hence involve two characteristic time scales. One is the inverse of the angular measurements frequency ($\omega^{-1}$) and the other one is the time integration constant ($\tau_{ap}$) of the whole apparatus. Since the latter is generally very long ($\omega\,\tau_{ap} \gg 1$) we expect that, due to flux creep effects, the data will generally depend on $\tau_{ap}$ logarithmically (in a first approximation) as in ordinary magnetic relaxation experiments. (2) A second difficulty concerns the domain of validity of the above elastic linear theories. We believe that if the alternating field is much higher than the threshold field $h_{2,\,th}$ (Eq. (77)), the notion of an elastic penetration depth independent of $h$ is no longer valid and more general treatments such as collective pinning are required. The easist way to overcome this difficulty is to come back to the critical state model (treated in Sect. 12) when $h_{2,\,th} > h_0$.

A relatively simple way to investigate frequency effects of flux creep origin and to test the above predictions is to look to the evolution of the magnetic signal as a function of the critical currents density $J$. This can be achieved quite simply by performing the following cycles in the ($H$-$T$) plane : (1) Prepare the sample in the critical state at the measuring temperature and

field. (2) Measure the magnetic signal and eventually record it as a function of time in these experimental conditions. (3) Heat the sample quickly (starting from the same current state ($\sim J$) to a higher temperature $T_1$ and then cool it down to the initial temperature of measurement $T$.

Since we know that $J$ drops more or less exponentially with $T$ we expect that the new value $J_1$ of $J$ will be reduced by a factor of about $\exp[-(T_1 - T)/T_0]$ where $T_0$ is of the order of 15 to 20 K for YbaCuO and 4 to 6 K for BSCCO (for high enough applied field $H$). The magnetization is then measured as in the first case. The same procedure can be repeated with a higher temperature $T_2$ corresponding to a lower current $J_2(\approx J(T_2))$ and so on. At this point we must keep in mind that by doing so we change the values of both $\lambda_{el}$ and $h_{2,th}$ (and as a consequence the associated magnetic signal), since they both depend directly on the critical current density : $J_i = J(T_i)$. By the way we can use this method in conjunction with equations (78a-78d) to test equations (75 to 77) and thus the present predictions on time effects. However, the time drift of the signal should decrease exponentially with $T_i$. The effects are expected to be stronger in granular materials as they depend on the ratio $\lambda_{el}/R$ where $R$ is the effective radius of the sample.

## 14. On the shape and intrinsic anisotropies in high-$T_c$ superconductors.

14.1 INTRODUCTION. — Because of their quasi bidimensional nature high $T_c$ superconductors are highly anisotropic materials. Until recently the magnetic and transport properties of anisotropic ideal type II superconductors were (except in few cases, see [65] and [80-83]) described in the so called London approximation which neglects the core energy of the vortices [66-70] and ascribes all the anisotropic behaviour to their electromagnetic energy. In the London approach the vortices are straight lines and their energy is invariant by translation along any direction. Because of the layered structure these two properties are lost in HTSC and this has enormous consequences on the magnetic and transport properties of HTSC materials. On the one hand, the energy of an isolated vortex parallel to the $a$-$b$ planes is now lower when its core lies between the Cu-O sheets than within these sheets [417-422, 423-425]. On the other hand, according to some of these theoretical calculations there is a certain threshold angle $\theta_C = \theta$ between $H$ and the $c$-axis beyond which the vortex enters the sample parallel to the $a$-$b$ planes. This idea was in fact suggested earlier [43, 358, 380] from magnetic measurements, especially some anomalies in the hysteresis cycle of YBaCuO. For $\theta < \theta_C$ (and $\theta$ not too close to zero) the vortex ceases to be a straight line but acquires a « staircase » shape formed by a periodic succession of kinks. According to the latest theories [426, 427] the vortex segments lying between the $a$-$b$ basal planes would resemble Josephson vortices while those parallel to the $c$-direction would have Abrikosov's character. However, the average direction of the vortex is still imposed principally by the electromagnetic energy. It is likely that at very low $T$ and $H$ far from the irreversibility lines, the vortex lines form a solid lattice which follows the above description. Because of thermal fluctuations, the situation is probably different above the apparent irreversibility line and depends on the real nature of this line.

There is indeed a large consensus among theoreticians (though this is not yet clear experimentally) that at sufficiently high temperatures the vortex lattice undergoes a melting transition [106, 110]. At still higher $T$, the lines should be broken by thermal fluctuations into thin slices particles (or pancakes [431]) of thickness comparable to the crystal spacing in the $c$-direction. This would lead to a new kind of flux particles and should have important consequences on the very debated question concerning the possibility of a thermodynamic transition at or above the irreversibility (or depinning) line.

Turning to the low temperature side below the irreversibility line, we note that the lack of translation invariance of the vortices along the *c*-direction gives rise to a new kind of intrinsic pinning force [52, 53-58-61, 107, 417-428] of considerable interest for the transport and magnetic properties of HTSC. Moreover, because of the imperfect structure of the materials we generally encounter further sources of anisotropy that influence simultaneously both magnetic and transport currents. These anisotropies can be roughly divided into the following four classes :

i) The anisotropy of the microscopic pinning forces either intrinsic or extrinsic due to pinning of the vortex lines by defects, in particular by twin boundaries [63, 64].

ii) The shape anisotropy connected with the spatial distribution and configuration of the current loops (current pathways) generally imposed by the external shape of the specimen.

iii) The more conventional shape anisotropy related to demagnetizing fields associated with the spatial distribution of the self fields (i.e. generated by the currents in the sample).

iv) The anisotropy of the equilibrium magnetization and the associated critical fields $H_{c_1}$, $H_{c_2}$ which have been the object of many theoretical [65, 70] as well as experimental studies [54, 56] during the past few years.

We shall discuss the first two anisotropy effects in detail in this section, as they are almost always present in critical current measurements. The third one will be considered briefly in the section devoted to demagnetizing effects. The anisotropy of $M_{eq}$ will be invoked also briefly at the end of this section. In principle, the four anisotropies just quoted are not totally independent of each other and should be treated simultaneously in a rigorous model, but this is not possible in the framework of this paper. It is to be emphasized however that the two shape anisotropies (ii and iii), though not totally independent, are clearly distinguishable. The first one is related to the spatial shapes of the current loops. The second one is a dipolar effect related to the distribution of magnetic charges in the specimen. For instance, the magnetization (per unit volume) of a thin « isotropic » film with $H$ parallel to its surface depends on the shape of such a surface even though the corresponding demagnetizing factor is zero.

**14.1.1** *Some characteristic manifestations of anisotropy in magnetic and transport data.* — A striking manifestation of the anisotropy in high-$T_c$ oxides is illustrated in figure 76 which compares the variation of the transport critical current $J_{tr}$ of thin films [58-61, 432] and the magnetic current $J_{mag}$ of a single crystal [104, 380] as a function of the angle $\theta$ between the *c*-direction and the field direction. These curves will be discussed later.

A second very unusual manifestation of anisotropy is sketched in figure 77 which shows the longitudinal components $M_L$ (parallel to the applied field) and the transverse component $M_T$ (perpendicular to the applied field) of the measured signal as a function of the strength $H$ of the applied field at fixed direction $\theta$ [52]. This figure shows cearly that the direction of the magnetization is far from that of the vector **H** and is closer to the *c*-direction. It can be proved that in the limit of a real two dimensional system the magnetization is strictly perpendicular to the *a-b* planes except for the trivial case when **H** is rigorously parallel to these planes for which $M$ equals zero anyway. This is simply because the currents are necessarily confined to the *a-b* planes. For instance, this limit of a two dimensional behaviour is almost realized in the case of Bi based HTSC materials.

A third very characteristic feature of HTSC single crystals [380] and oriented grains [50, 358] is displayed in figure 78 which shows how the hysteresis cycle (only the first branches are presented here) of these materials evolve with the angle $\theta$. It is seen that when $H$ is parallel to a symmetry direction (*c* or *a-b*) the cycle presents the usual low-$H$ peak discussed at length in sections 6 and 10. However, out of these directions, especially sufficiently far from the *c*-axis, one observes two distinct anomalies in the curves. These cycles are explained quite

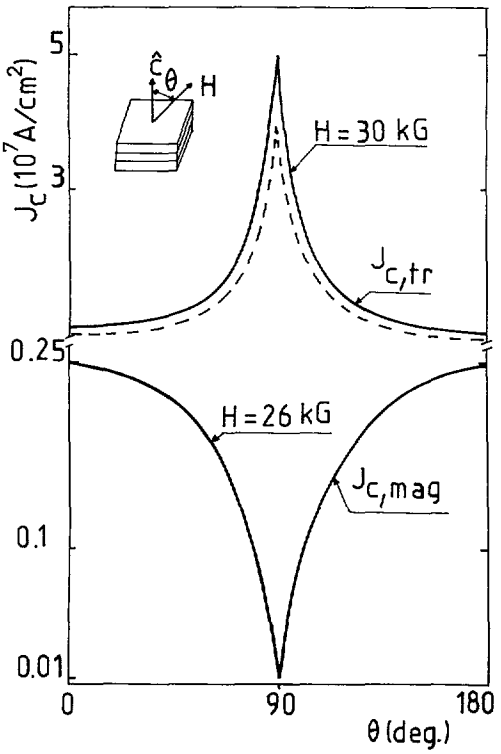


Fig. 76.

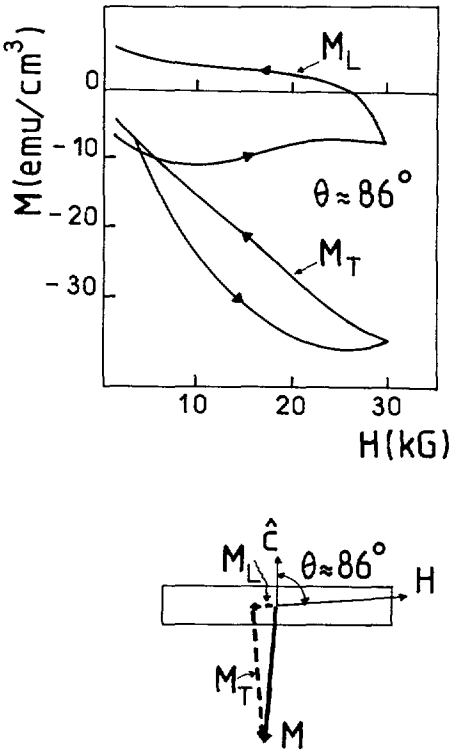


Fig. 77.

Fig. 76. — The anisotropy of the apparent critical current density, as a function of the angle $\theta$ of $H$ with the $c$-axis. The lower curve, $J_{mag}$, is deduced from magnetic measurements on « thick » single crystals (from [380]) whereas the upper curve (heavy line) is representative of transport data on thin films (see for example [58-60] and text for other details). The dashed curve is expected to represent $J_{c,\,mag}$ for a very thin film.

Fig. 77. — Upper graph : hysteresis cycles associated with the longitudinal $M_L$ and the transverse $M_T$ magnetizations as deduced from torque and conventional magnetometer measurements on the same single crystal of $YBa_2Cu_3O_7$ [52] ; lower graph : schematic decomposition of $M$ into $M_L$ and $M_T$.

satisfactorily by a decomposition model developed in references [50, 358, 380] and also later in this section.

The amplitudes and directions of the vectors **M** and **B** represented in figure 79 are qualitative and were deduced from comparing torque and ordinary magnetic measurements (which give the equivalent longitudinal and transverse components of $M$) of the same single crystal of approximately spherical shape (to reduce conventional demagnetizing effects). The sketch shows that when the applied field **H** is oriented out of the high symmetry directions ($\theta \neq 0$ and $\theta \neq \pi/2$) all of the three magnetic vectors **H**, **M** and **B** are not aligned. For instance, in the case of a two dimensional superconductor (very high anisotropy as in bismuth based ceramics) the vector **M** is expected to be essentially parallel to the $c$-axis. This is vhatever may be the angle $\theta$ except when **H** is oriented very close to the $a$-$b$ plane with $\Delta\theta < m_{ab}/m_c$, but $M$ tends to zero in this limit. Here $m_{ab}/m_c$ is the mass anisotropy ratio whereas $\Delta\theta$ is the deviation from the $a$-$b$ planes).

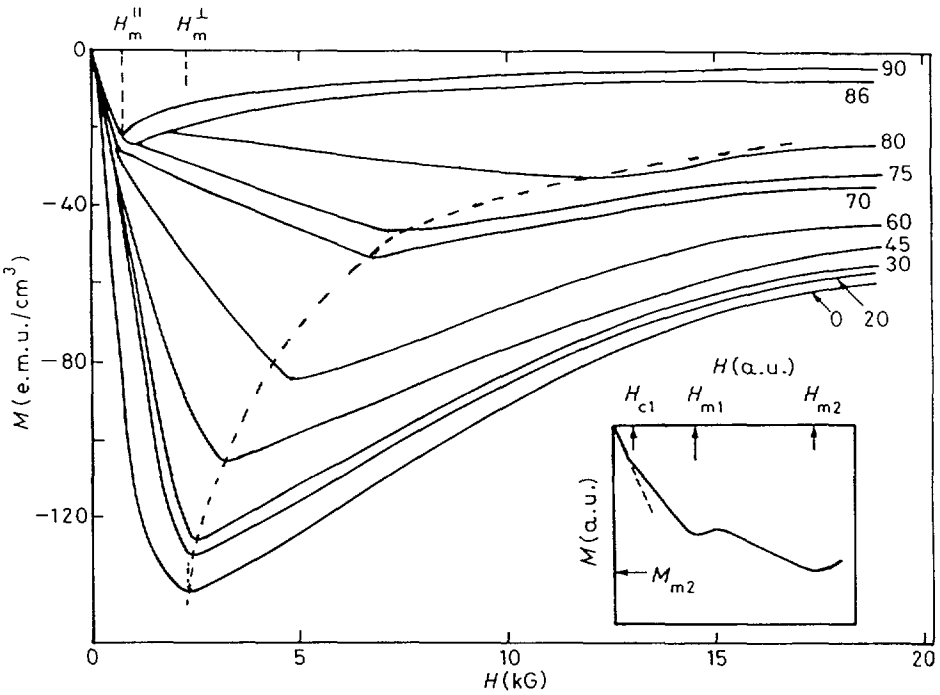


Fig. 78. — $M$ *vs.* $H$ for different angles $\theta$ between the applied field and the $c$-axis [43, 358]. Defined in the inset are the singular points of the $M(H, \theta)$ curves for a fixed $\theta$. The sample consists of an oriented powder of YBaCuO (1 : 2 : 3 phase).

Sketched in figure 80 is the expected variation across the sample of the vortex spacing d($r$), together with the amplitude and the direction of the angle $\theta_v$ of the local induction $B(r)$ for $H$ directed not very close to the symmetry directions ($c$-axis or $a$-$b$ planes).

It should be noted that the orientational variation of the vortex lines of figure 80 is different from the so called « orientational disorder » which is thought [429] to be induced by arbitrarily small pinning disorder. As a matter of fact, according to some theories this « Orientational disorder » would exist even in the case of isotropic materials or for $H$ parallel to the $c$-axis in the case of HTSC. However, this is in strong contradiction with other theoretical predictions [430].

Our point of view is that « Orientational disorder » is very difficult to justify experimentally. The argument is that once the radius of the sample exceeds the « Orientational disorder » correlation range (expected to be of the order of the vortex spacing) the local magnetic induction **B** would be distributed practically uniformly within a solid angle of about 2 $\pi$. At first, this would result in a strong reduction of the anisotropy of the magnetization. Perhaps more importantly, this would lead to the complete disappearance of the macroscopic Lorentz force in transport measurements (since « Orientational disorder » implies $\langle B_{\parallel} \rangle \approx \langle B_{\perp} \rangle$).

**14.2** DESCRIPTION OF THE VARIOUS CRITICAL CURRENT DENSITIES ENCOUNTERED IN LAYERED SINGLE CRYSTALS. — Let us for the moment limit our attention to the configuration where the vectors **J** and **H** are parallel to symmetry directions (**c** axis or $a$-$b$ planes) as is frequently the case in experiments on single crystals. Then, we can identify three different critical current densities ($\mathbf{J}_{c,ab}$, $\mathbf{J}_{ab,c}$ and $\mathbf{J}_{ab,ab}$) defined according to the directions of the Lorentz forces $\mathbf{F}_L = F_{i,j}$ as illustrated in figure 81. We recall that in the above notations the

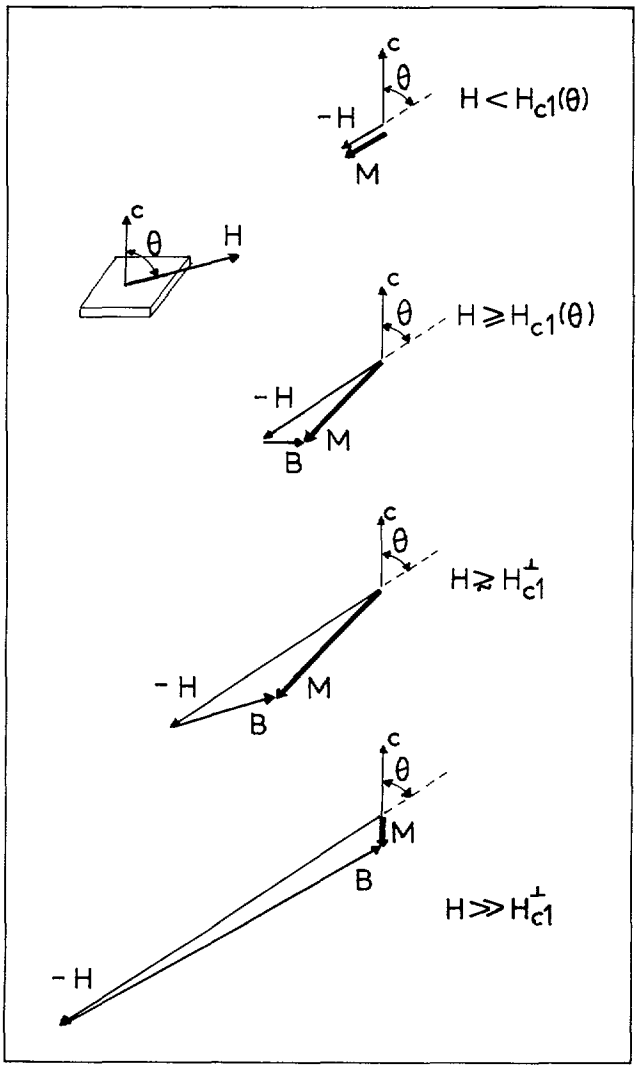


Fig. 79. — Schematic evolution of the direction of the average magnetic vectors $M$, and $B$ as a function of the amplitude of the applied field the direction of which is being kept constant. It is seen that only for $H \leqslant H_{c_1}$ (and for negligible or isotropic demagnetizing field) $M$ is colinear with $H$.

first index ($ab$ or $c$) defines the direction of **J** whereas the second index ($c$ or $ab$) refers to the **B**-direction.

(i) $\mathbf{J}_{c,\,ab}$. It is the critical current density along the **c**-direction with both **B** and $\mathbf{F}_L = \mathbf{F}_{ab,\,ab}$ in the $a$-$b$ plane. At low enough $T$ and $H$, this is expected to be the lowest critical current density value since in this configuration the vortices always stay (and eventually move) between the $a$-$b$ planes where their energy is the lowest possible (but for $H$ much lower than the critical field $H_{c_2,\,c}$, see below the reason of this restriction).

(ii) $\mathbf{J}_{ab,\,ab}$. The current and the field are parallel to the $a$-$b$ planes whereas the Lorentz force ($\mathbf{F}_{c,\,ab}$) is perpendicular to these planes. The current density is expected to be higher here than in any other direction since in this case the vortices have to move in the $c$-direction

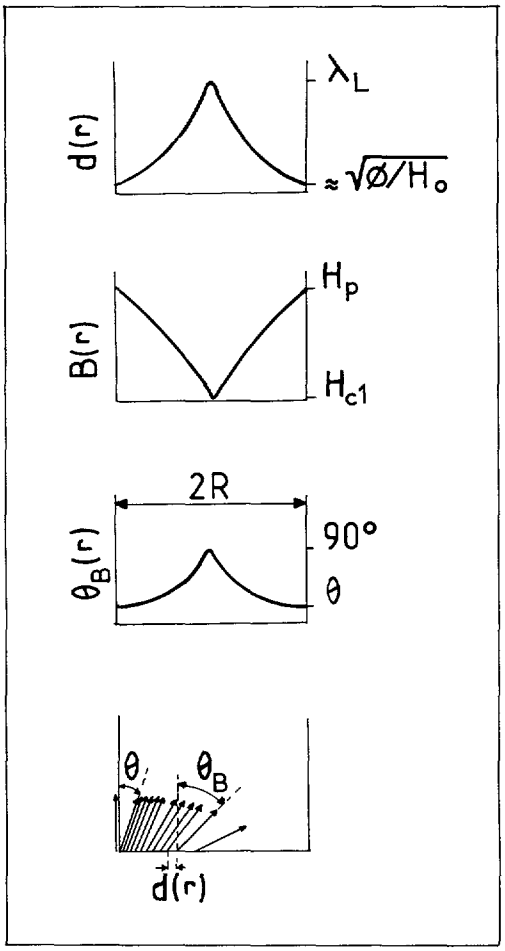


Fig. 80. — Schematic variation across the sample of the vortex spacing $d(r)$, the intensity of the local field $B(r)$ and the direction of this $B(r)$ (the direction $\theta$ of the applied field is still constant, the same as in Fig. 79).

and to overcome the energy gaps between the CuO sheets, thus experiencing some intrinsic pinnig forces.

(iii) $J_{ab,\,c}$. The current and the Lorentz force ($F_{ab,\,c}$) are parallel to the *a-b* planes whereas the field is parallel to the *c*-axis. At first sight it appears that this current should have an intermediate value, lying between the two above extreme cases. However, it is to be noted that because of the anisotropy of the upper critical field ($H_{c_2}^{ab} > H_{c_2}^{c}$) this property would be not true at very high fields and high temperatures. It is indeed expected that in the region $H_{c_2}^{c} < H < H_{c_2}^{ab}$ one has $J_{ab,\,c} = 0$ whereas $J_{c,\,ab}$ is not necessarily zero (from different sources in the literature [433] $H_{c_2}^{ab}$ and $H_{c_2}^{c}$ are estimated to be of order 6 MG and 1 MG respectively, for $YBa_2Cu_3O_7$ at $T \approx 0$). This would lead to the intersection (in the *T-H* plane) of the irreversibility lines associated with these two current densities respectively. It is to be recalled that at present, we know very little about the irreversibility lines and absolutely nothing concerning that associated with $J_{ab,\,ab}$. This is because of the great difficulties to analyse the experimental data correctly and because of the high fields required to investigate a significant

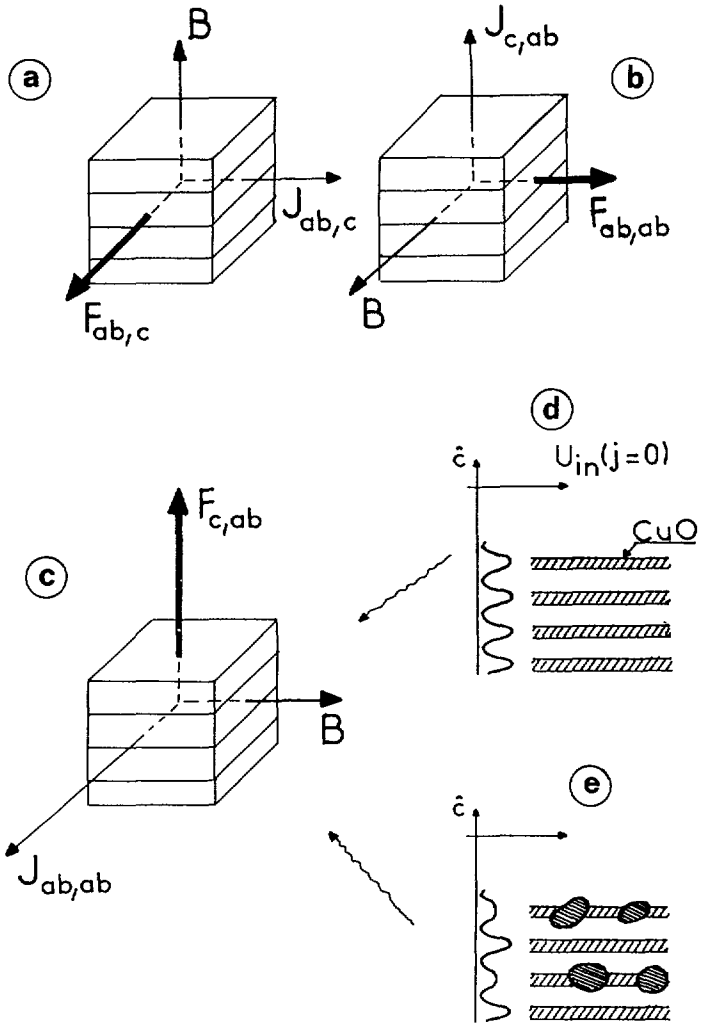


Fig. 81. — Schematic representation of the magnetic induction $B$, the critical currents $J$ and the Lorentz forces $F_L = F_{i,j}$ inside a single crystal. The first index *ab* or *c* gives the direction of the concerned vector ($J_{i,j}$ or $F_{i,j}$) while the second one refers to the direction of $B$, i.e. that of the vortex lines. Also shown in (d) is the intrinsic pinning energy $U_{in}$ (schematic) of the vortex as a function of the variable z (in the *c*-direction) when the flux line is parallel to the *a-b* planes. When both the Lorentz force and the vortices lie parallel to the basal planes the driving force is the lowest, at least far below the irreversibility lines, since the vortex does not need to cross the energy gap in this case. If the vortex is still parallel to the basal planes but the Lorentz force perpendicular to these planes the driving force is the largest because of the energy gaps that the vortex has to overcome in this geometry. Finally, the case where the line is parallel to the *c*-axis would correspond to an intermediate situation (see text however). (e) Defects depress the order parameters in the *a-b* sheets, thus decrease the gap and the intrinsic current. This effect is not easy to detect by magnetic measurements.

portion of such lines. From the above discussion, the three critical current densities should satisfy the inequalities :

$$J_{ab,\,ab} \geq J_{ab,\,c} \geq J_{c,\,ab} \qquad (T < T^*,\ H < H^*) \tag{80a}$$

$$J_{ab,\,ab} \geq J_{c,\,ab} \geq J_{ab,\,c} \qquad (T > T^*,\ H > H^*)\ . \tag{80b}$$

The irreversibility lines associated with these currents should look as sketched in figure 2 (Sect. 1). We can use now these considerations to interpret approximately the $J_{tr}(\theta)$ and $J_{mag}(\theta)$ curves of figure 76.

**14.3** ANISOTROPY OF THE TRANSPORT CURRENT $\mathbf{J}_{tr}(\theta)$. — The critical current densities $J_{c,\,ab}$, $J_{ab,\,c}$ and $J_{ab,\,ab}$ just introduced can be determined directly from transport measurements by choosing the field and current directions accordingly to figure 81. However, due to the very high values of the critical currents (and the resulting heating problems) this is in general only easy to realize for very thin films. Unfortunately, another difficulty appears in this case as the contribution of the reversible London-Abrikosov currents ($J_s$) to the measured current is no longer negligible, especially for $H < H_{c_1}$. In addition, the relative contribution (not the absolute one) of this reversible term should increase considerably with temperature. This is because the bulk critical currents (i.e. $J_{ab,\,c}$ and $J_{c,\,ab}$) of single crystals drop rapidly with $T$ (see Sect. 7) while $J_s$ varies rather slowly except very close to $T_c$. The situation can be described phenomenologically as follows.

*Highly textured thin films.*

1) Let us assume that $J(\theta)$ can always be expressed as a combination of the various current densities $J_{i,\,j}$ of figure 81. Then the first difficulty encountered in analysing the transport current in thin films is related to the question of which among the four currents defined above is really relevant, especially in zero applied field ? Figure 82a shows qualitatively that the pinning force in zero applied field is principally of intrinsic character and that the contribution of $J_{ab,\,ab}$ is expected to be about $(w\,.\,J_{ab,\,ab})/(e\,.\,J_{ab,\,c})$ larger than that of $J_{ab,\,c}$ (here $2\,w$ is the width of the sample parallel to the $a$-$b$ planes and $2\,e$ is its thickness in the $c$-direction (Fig. 83)). For thin films the aspect ratio $w/e$ is generally of the order of $10^3$ so that the factor $(w\,.\,J_{ab,\,ab})/(e\,.\,J_{ab,\,c})$ can be as high as $10^5$ in YBaCuO and even more in Bi based materials. More generally, whenever $w$ exceeds $e$ the contribution of $J_{ab,\,ab}$ to the measured transport current in zero field should be preponderant compared to that of $J_{ab,\,c}$ and or $J_{c,\,ab}$.

2) Secondly, when $e$ becomes comparable to the London penetration depth $\lambda$ the contribution of the equilibrium current $J_s$ to the total current can be preponderant or comparable to $J_{ab,\,ab}$. In addition, as noted before, the contribution of the equilibrium current should decrease rather slowly with $T$ and $H$ and, hence, would play a more important role at high temperatures. Indeed, at zero applied field, the ratio of the equilibrium current to the critical current is probably of the order of $H_{c_1}/Je$, in the limit $e \geq \lambda$ (see Sect. 7 comparing the temperature dependence of some critical currents and also appendix A). Even though the above results are not rigorous they show that the understanding of the critical current density of thin films requires more investigations and cannot be simply compared to the critical current of bulk single crystals, especially when the latter is deduced from magnetic measurements. It is interesting to add that we shall see in section 15 about demagnetizing field effects that the magnetic critical current density in thin crystalline films is also expected to be strongly dominated by intrinsic pinning at relatively low applied field.

*A long single crystal or a highly textured wire.* — We wish now to address the problem concerning the nature of the transport current and the associated pinning in thick ($w \approx e \ll L$) anisotropic samples. It is generally not appreciated that because of the layered

structure the distribution of the current within an anisotropic wire, as that sketched in figure 82c (i.e. melt textured samples), is necessarily inhomogeneous, even when the material itself is highly homogeneous (no weak links). This complicated problem is of course not easy to elucidate in the framework of this paper. Nonetheless, qualitative arguments suggest that the distribution of currents within this wire would be concentrated near the surfaces parallel to the *a-b* planes and in regions far from the surfaces parallel to the *c*-axis. The real distribution depends on the exact shape of the specimen and on the values of the various currents $J_{ij}$. For instance, qualitative arguments suggest that for extremely anisotropic wires the repartition of currents should resemble the tube drawn in figure 82c.

The analysis of this paragraph as well as that of figures (81, 82) suggest that any kind of defects within the material (for example those induced by irradiations) could deteriorate the transport current rather than improve it in highly anisotropic materials. This is because defects are expected to lower the intrinsic pinning barriers as sketched in figure 81e. Therefore, this will result in a decrease of the critical current when the latter is dominated by $J_{ab,\,ab}$. In practice, this is rarely observed in magnetic measurements (which are almost insensitive to $J_{ab,\,ab}$, see figure 83 and § 14.4.2) but may occur in transport data (which are of more interest as technical applications are concerned). However, in real materials the situation can be more subtle and more complicated if $J_{tr}$ is primarily limited by weak links (as sketched in Fig. 43), since in this case the current paths are ill defined. In fact, we know that in this cas $J_{tr}$ depends also on $J_{c,\,ab}$ (see Eq. (37)) and can be, for this reason, increased by defects. Another way to view this is that the diminution of the current anisotropy ratio $J_{ab,\,ab}/J_{c,\,ab}$ limits the negative effect of the weak links.

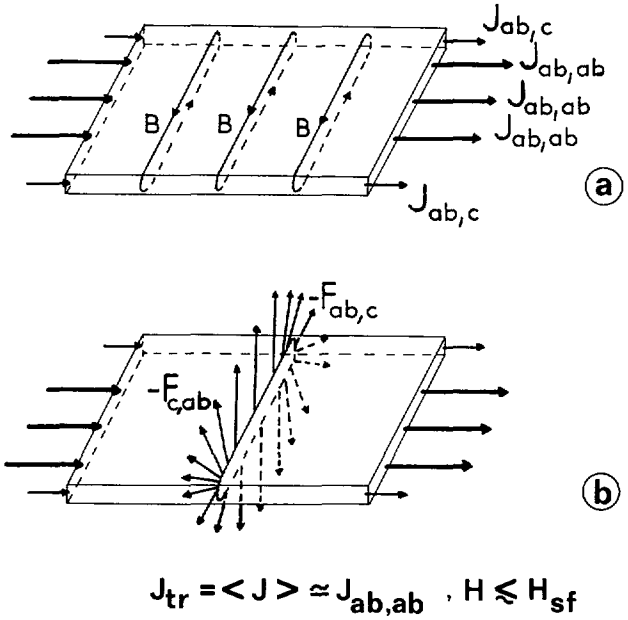


Fig. 82a, b. — Qualitative representation of the vortex rings (a) and the Lorentz forces (b) induced by the applied current feeding a very thin monocrystalline film and their self fields (negligible applied field). It is clear that, in this case, the resulting critical current is dominated by $J_{ab,\,ab}$ compared to $J_{ab,\,c}$. If this is the case it should be decreased by any kind of defects as discussed in the text (here, for simplicity we have not represented the equilibrium current density $J_s$). Intuitively, we expect that defects will decrease $J_{ab,\,ab}$ and increase $J_{ab,\,c}$ (at low enough concentration) leading to a more uniform distribution current.

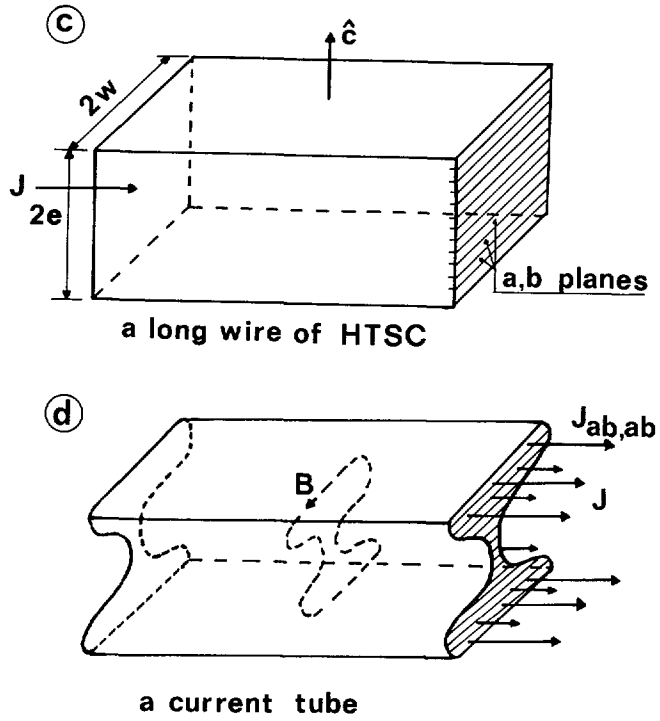


Fig. 82c, d. — c) A thick sample or wire (of thickness $2\,e \approx$ width $2\,w$) fed with an external current approximately equal to its critical current. d) Because of the layered structure, we predict that the current should be concentrated near the surfaces parallel to the *a-b* planes as sketched in the figure (but quantitative calculations are needed to clarify this point).

14.4 ANISOTROPY OF THE MAGNETIC CURRENT $J_{mag}(\theta)$ IN THICK SINGLE CRYSTALS AND ORIENTED GRAINS. — Let us consider again the three critical current densities $J_{i,j}$ of inequalities given in equations (80a) and (80b) above. It is important to emphasize that the manifestation of these currents in magnetic data is generally much more complicated to analyse than in transport data. In fact, the anisotropy of the irreversible magnetization is related not only to that of the critical current density but also to the dimensions of the sample *via* the shape dependent characteristic fields (described just below) associated with each of the currents $J_{ij}$. By convention we define these fields by the same indices as the corresponding critical currents $J_{ij}$ .

$$H_{ab,\,ab} = \frac{2\,\pi}{5}\,eJ_{ab,\,ab},\; H_{ab,\,c} = \frac{2\,\pi}{5}\,wJ_{ab,\,c},\; H_{c,\,ab} = \frac{2\,\pi}{5}\,wJ_{c,\,ab}\,. \tag{81}$$

As depicted in figure 83, $w$ and $e$ stand respectively for the width and the thickness of the sample.

In figure 76 we show (solid lines) the apparent anisotropy of $J_{mag}$ as deduced from magnetic data [50, 358, 380] (lower curve) after appropriate corrections of the shape of the sample (this point will be clarified later) and that of $J_{tr}$ determined by transport measurements on thin films [58, 60] at 4.2 K and 30 kG. We have seen that the transport curve probably reflects the passage from $J_{ab,\,ab}$ to $J_{c,\,ab}$ as **H** is rotated from the *a-b* planes to the *c*-direction (with the caveat concerning the possible contribution of the equilibrium currents as just discussed). We

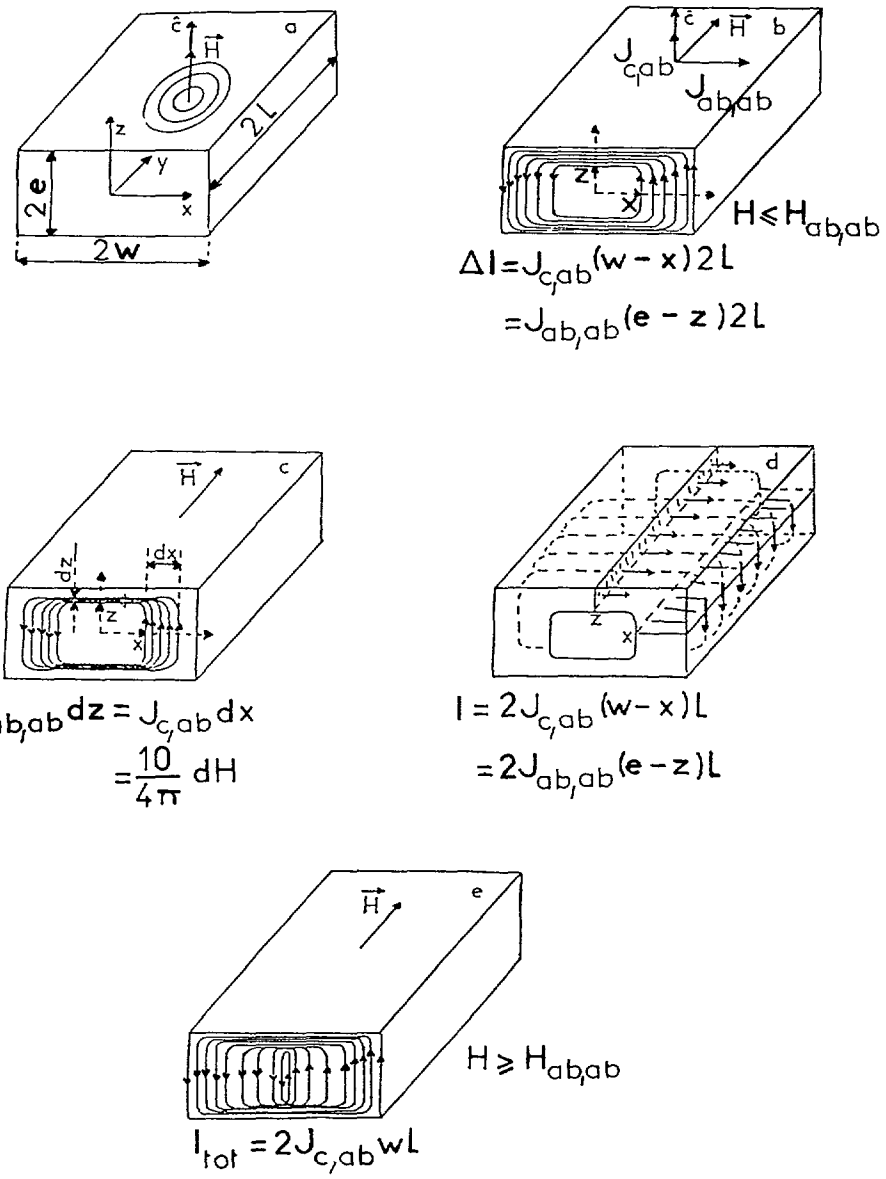


Fig. 83. — Development of currents within a single crystal of dimension $(2w) \times (2e) \times (2L)$ as a function of the applied field. a) $H$ parallel to the $c$-axis. b), c), d) and e) $H$ along the $a$-$b$ planes.

feel that the magnetic critical current curve $J_{mag}(\theta)$ of the same figure would correspond to the anisotropy $J_{ab,\,c} \rightarrow J_{c,\,ab}$ which is just the opposite of the anisotropy $J_{ab,\,ab} \rightarrow J_{c,\,ab}$ deduced from transport measurements. The dashed curve of figure 76 does not correspond to any experimental data. It represents the predicted anisotropy of $J_{mag}(\theta)$(i.e. $J_{ab,\,ab} \rightarrow J_{ab,\,c}$) in the limit of very thin samples such that $eJ_{ab,\,ab} \ll wJ_{ab,\,c}$.

To support the above claim concerning the apparent anisotropy of $J_{mag}(\theta)$ it is necessary to calculate the hysteresis cycle of single crystals in the presence of anisotropy. This can be done easily in the limit where each $J_{ij}$ is independent of **H** (the field effects have been considered

separately in Sect. 7 and 8). This calculation is interesting from other points of view as well (see next discussions) and is carried out below. For such a calculation we recall that the magnetization involves all the currents circulating in the material whatever their origins and can be written as follows (in the practical units of Bean, A/cm$^2$, emu/cm$^3$ and œ) :

$$\mathbf{M} = \frac{-1}{20\,v} \int [\mathbf{J}(r) \times \mathbf{r}]\, dv \tag{82}$$

where the integration is over the whole volume $v$ of the sample assumed to be either a long cylinder or a slab with negligible demagnetizing field. Note that for cylindric symmetry with $J$ = constant we recover the Bean model immediately.

**14.4.1** *H parallel to the c-axis, the relationship between the hysteresis cycle and the current* $J_{ab,\,c}$. — Let us first assume that $J$ is isotropic and independent of **H** (i.e. $J(r)$ = constant and cylindrical symmetry). This is approximately realized for **H** parallel to the $c$-axis at intermediate fields. In this case one has $J = J_{ab,\,c}$. Then, the equations describing the whole cycle for **H** oriented along the $c$-axis are quite simple (we still neglect demagnetizing effects) and can be written as :

$$M_c^{\mathrm{cyc}} = -\frac{J_{ab,\,c}\,R}{30} + M_{\mathrm{eq}}(H) \qquad (H \geqslant H_{ab,\,c}) \tag{83a}$$

$$M_c^{\mathrm{vg}} = -\frac{H_{\mathrm{eff}}}{4\,\pi}\left[1 - \frac{H_{\mathrm{eff}}}{H_{ab,\,c}} + \frac{1}{3}\left(\frac{H_{\mathrm{eff}}}{H_{ab,\,c}}\right)^2\right] + M_{\mathrm{eq}}(H) \tag{83b}$$

with

$$H_{\mathrm{eff}} = H + 4\,\pi M_{\mathrm{eq}}(H) \qquad \text{and} \qquad (H \leqslant H_{ab,\,c}) \tag{83c}$$

$$M_c^{\mathrm{rl}} = -\frac{J_{ab,\,c}\,R}{30} + \frac{\Delta H_{\mathrm{eff}}}{4\,\pi}\left[1 - \frac{\Delta H_{\mathrm{eff}}}{2\,H_{ab,\,c}} + \frac{1}{3}\left(\frac{\Delta H_{\mathrm{eff}}}{2\,H_{ab,\,c}}\right)^2\right] + M_{\mathrm{eq}}(H) \tag{83d}$$

with

$$\Delta H_{\mathrm{eff}} = H_{\max} - H_{\mathrm{eff}} \leqslant 2\,H_{ab,\,c}\,. \tag{83e}$$

We recall that the equilibrium magnetization $M_{\mathrm{eq}}(H)$ contributes to the total $M$ in two ways : directly and *via* its screening field which enters $H_{\mathrm{eff}}$. These equations describe the cyclic, the virgin, and the reversal branches of the hysteresis cycle respectively. Inspecting these equations, it is interesting to see that the reversal magnetization may be determined from the virgin one by a simple translation of $M$ and $H$ and by multiplying the Bean field $H_{ab,\,c}$ by 2.

**14.4.2** *H parallel to the basal plane, and the relationship between the hysteresis cycle and the currents* $J_{c,\,ab}$ *and* $J_{ab,\,ab}$. — We now consider the hysteresis cycle $M_{ab}(\mathbf{H})$ for **H** lying in the $a$-$b$ basal planes. In this configuration, the intensity of the local current density $\mathbf{J}(r)$ is no longer constant (along a given current loop), and varies from $J_{ab,\,ab}$ to $J_{c,\,ab}$ (Fig. 83b-e). This rises the important question concerning which of these two currents is really at the origin of the magnetization $M_{ab}$ ? To answer this question it is necessary to calculate $M_{ab}$ analytically, at least approximately. For this purpose, it is more physical to assume that the sample is a slab (rather than a cylinder) of dimensions $2\,e \times 2\,w \times 2\,L$ having the symmetry of the single crystal with its surface parallel to the $a$-$b$ planes and such that $L > w$. The gradual development of the magnetic currents as a function of the strength $H$ of the applied field is sketched in figures 83b to e.

We can readily calculate the whole cycle $M_{ab}(H)$ (with the help of the current loops and the definitions sketched in Fig. 83) following the same method as in the calculation of the hysteresis cycles in sections 10 and 11. The cyclic magnetization for $H$ parallel to the $ab$ planes has been first calculated by Gregory *et al.* [56]. The present treatment extends these calculations to the whole hysteresis cycle (i.e. to the virgin and reversal branches) and more importantly it considers simultaneously the contributions of both currents $J_{ab,\,ab}$ and $J_{c,\,ab}$ to the cycle, especially to the virgin curve. In addition we also account qualitatively for $M_{eq}$ and the associated surface current $J_s$ (London-Abrikosov's current). The final result depends on the ratio $(eJ_{ab,\,ab})/(wJ_{c,\,ab}) = H_{ab,\,ab}/H_{c,\,ab}$. In general $H_{ab,\,ab} \gg H_{c,\,ab}$ for single crystals (see Eq. (81)) for the definition of $H_{t,\,j}$). In this case we find for the virgin curve with $H$ parallel to the basal planes :

$$M_{ab}^{vg} = -\frac{H_{eff}}{2\pi}\left[1 - \frac{1}{2}\left(1 + \frac{wJ_{ab,\,c}}{eJ_{ab,\,ab}}\right)\frac{H_{eff}}{H_{c,\,ab}} + \frac{wJ_{c,\,ab}}{3\,eJ_{ab,\,ab}}\left(\frac{H_{eff}}{2\,H_{c,\,ab}}\right)^2\right] + M_{eq}(H)\,. \quad (84a)$$

We recall that $H_{eff}$ is given by equation (83c) (in the absence of demagnetizing effect). In the case where $H_{ab,\,ab} < H_{c,\,ab}$, the virgin magnetization is again given by the same equation except that $J_{c,\,ab}$ must be replaced by $J_{ab,\,ab}$ and *vice versa*. It is interesting to note that it is in principle possible to determine the ratio $(eJ_{ab,\,ab})/(wJ_{c,\,ab})$ from $M_{vg}$ and thus the ratio of the anisotropy of $J$. In practice, because of the low $H$ peak effect discussed in sections 7 and 10 it is necessary to account for the field dependence of $J$ in the analysis. However, in this case it is better to use the reversal curve for which $J$ is much less dependent on $H$ in the limit $H_{c_1} \ll H \ll H_{c_2}$. This condition is easily satisfied for $YBa_2Cu_3O_7$. In addition, for $H \gg H_{c_1}$ the contribution of the equilibrium magnetization to the magnetic cycle is smaller and almost independent of $H$ (we know that in this field domain $M_{eq}(H)$ varies logarithmically with the reduced field $(H/H_{c_2})$) allowing us to replace $H_{eff}$ by $H$. The equation of the reversal curve for $H$ parallel to the basal planes is related to the virgin one (given by Eq. (84a) above) by the same transformation as for equations (83b-83e). The cyclic curve is given by :

$$M_{ab}^{cyc} = -\frac{\inf\,(wJ_{c,\,ab}\,;\,eJ_{ab,\,ab})}{20}\left[1 - \frac{\inf\,(wJ_{c,\,ab}\,;\,eJ_{ab,\,ab})}{3\,\sup\,(wJ_{c,\,ab}\,;\,eJ_{ab,\,ab})}\right] + M_{eq}(H)\,. \quad (84b)$$

In general (except sometimes for thin films) we have $wJ_{c,\,ab} < eJ_{ab,\,ab}$ so that equation (84b) transforms into :

$$M_{ab}^{cyc} = -\frac{wJ_{c,\,ab}}{20}\left[1 - \frac{wJ_{c,\,ab}}{3\,eJ_{ab,\,ab}}\right] + M_{eq}(H)\,. \quad (84c)$$

It is easily seen from equation (84b) that when the shape anisotropy measured by the aspect ratio $(w/e)$ just balances that of the critical current density (i.e. when $w/e = J_{ab,\,ab}/J_{c,\,ab}$) we exactly recover the « isotropic » formula (83a). Moreover, if $J_{ab,\,ab}/J_{c,\,ab} = 1$ we obtain the classical equation for a slab as first considered by Bean. According to Cronemeyer *et al.* [57], the anisotropy ratio $J_{ab,\,ab}/J_{c,\,ab}$ exceeds 250 for YBaCuO and is probably much larger for other HTSC families (Bi, Tl, La). This implies that for **H** parallel to the $a$-$b$ planes the measured magnetization $M_{ab}$ is generally governed by $J_{c,\,ab}$. In other words, the anisotropy of $J_{mag}$ displayed in figure 76, lower curve) reflects the variation of $J_{mag}$ from $J_{ab,\,c}$ (for **H** parallel to the $c$-axis) to $J_{c,\,ab}$ and is completely insensitive to $J_{ab,\,ab}$.

Figure 84 shows the calculated (dashed line) and the experimental cycles (solid line) for **H** oriented either along ($\theta = 0$) or perpendicular ($\theta = 90°$) to the $c$-axis. It is clear that the agreement between the two cycles is remarkable, except for the small « hump », the

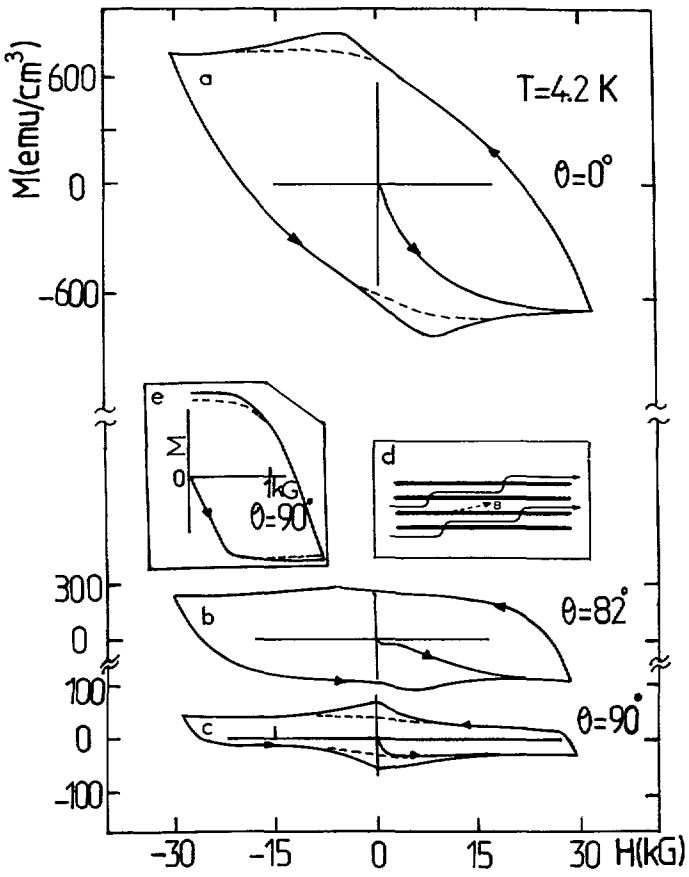


Fig. 84. — The hysteresis cycle of a single crystal at the indicated angles between $H$ and the $c$-axis. Note the anomalous virgin curve for $\theta = 82°$. d) Very close to the $a$-$b$ planes the vortices are no longer straight lines but have staircase shapes.

interpretation of which was considered in the previous sections (3 and 10). This in fact explains correctly the anisotropy of $J_{mag}$ reported in figure 76.

The evolution of the initial magnetization (Eqs. (84a, 84b)) for an anisotropy ratio $J_{ab,\,ab}/J_{c,\,ab} = 250$ and with $w/e$ varying from $10^3$ to 10 is calculated and presented in figure 85. This is performed for $J_{c,\,ab}$ and the width $w$ kept constant and equal to $3 \times 10^5$ A/cm$^2$ and 1 mm respectively. It is interesting to note that the shape of the virgin magnetization depends on the effective anisotropy and can be used to determine both $J_{ab,\,ab}$ and $J_{c,\,ab}$.

**14.4.3** *H directed out from the high symmetry directions.* — In the examples given above the applied field was assumed to be parallel to one of the symmetry directions ($c$ axis or $a$-$b$ planes). We have also noted in the introduction to this section that for an arbitrary orientation of **H** the three magnetic vectors **H**, **M** and **B** were desaligned, with **M** almost parallel to the $c$-direction. These anisotropy effects are often unavoidable in granular samples (where the crystallographic axes are distributed at random) and to some extent in textured materials. The general treatment of these cases (with **H** out of the symmetry axes) is exceedingly difficult. Here we wish to discuss this important point using a simple decomposition model [50, 358, 380] which can be justified in the limit of a truly two dimensional superconductor. A more

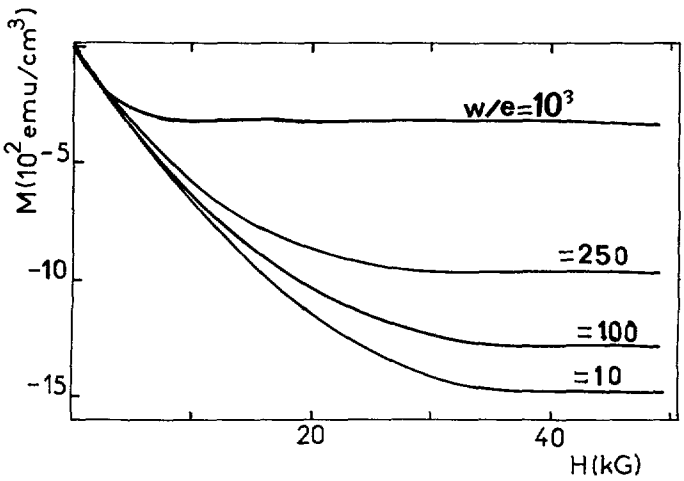


Fig. 85. — Calculated $M(H)$ curves of a slab (see Fig. 83) of variable thickness ($2e$) for $H$ parallel to the $a$-$b$ plane. The critical current density $J_{c,ab}$ along the $c$-axis, the current anisotropy ratio $J_{ab,ab}/J_{c,ab}$ and the width $2w$ are kept constant : $J_{c,ab} = 3 \times 10^5$ A/cm$^2$, $J_{ab,ab}/J_{c,ab} = 250$ and $w = 1$ mm. The curves correspond to four different aspect ratios : $w/e = 10^3$ (top curve nearest to the $H$ axis), 250, 100 and 10.

general model based on the collective pinning theory was reported very recently by Blatter *et al.* [419]. This model is based on a new scaling approach which allows to map the results obtained for isotropic superconductors to anisotropic materials whichever the angle $\theta$.

**14.5** A DECOMPOSITION MODEL FOR AN ARBITRARY ORIENTATION OF $H$. — Let us again consider the curves of figure 78 for which **H** is oriented out of the symmetry directions and the curve $\theta = 82°$ of figure 84. It is clear that in these two figures the initial magnetization exhibits a very complex behaviour and looses any connection (of the sort deduced from equation (83) with the reversal one : experimentally, the latter is indeed regular while the former exhibits a step like anomaly.

Figure 78 [50, 358] corresponds to a sample of aligned grains diluted in epoxy resin and shows an ensemble of virgin curves at different angles $\theta$. Here too the shapes of the $M_{vg}(H, \theta)$ curves are very complex. Nonetheless, it is found that they can be explained reasonably well by the following and simple decomposition procedure.

At first, we decompose **H** into a component $H_z = H \cos \theta$ along the $c$-axis and a component $H_y = H \sin \theta$ in the $a$-$b$ plane. Then, it turns out that for any fixed $\theta$ the $M$ *vs.* $H$ relationship could be (to a first approximation) deduced directly from the $\theta = 0°$ (i.e. from $M_c(H_z)$) and the $\theta = 90°$ (i.e. $M_{ab}(H_y)$) cycles of figure 84. In other words, the magnetic vector induced by the applied field would be described by :

$$\mathbf{M}(H, \theta) = \mathbf{M}_c(H_z) + \mathbf{M}_{ab}(H_y) . \tag{85a}$$

It is to be stressed that conventional magnetometers only measure the projection of the vector $\mathbf{M}(H, \theta)$ along the field direction. Thus, in this model the measured magnetization would be equal to :

$$M(H, \theta) = \frac{\mathbf{H} \cdot \mathbf{M}(H, \theta)}{H} = M_c(H_z) \cos(\theta) + M_{ab}(H_y) \sin(\theta) . \tag{85b}$$

It is found that this relation describes quite correctly the experimental data in many conditions. [50, 358, 380] particularly for fine decoupled grains. For large single crystals with

large $R$ and large $J$ the fit with experiments is found to be less satisfactory [155] probably because of the fact that the local field is very different from the applied field. In fact, this decomposition model would be reasonably well justified in two limiting cases : (1) the anisotopy is infinite (highly layered systems) and (2) the vortices are sufficiently soft (stifness modulus very low) so as to adopt a staircase shape as in the inset to figure 84 (Note that these two questions are not independent [110] since anisotropy favours the formation of kinks).

In conclusion of the above considerations, magnetic measurements are sensitive to the anisotropy of the total current which is imposed both by the shape of the sample and by the actual anisotropy of $J$ through that of the pinning forces (Fig. 81). In addition, we have seen that even when we know how to correct from the shape anisotropy it is generally not easy to get information on the critical current density $J_{ab,\,ab}$ particularly from the cyclic curve (see Eq. (80a, 80b)). Nevertheless, it is possible to have information on $J_{ab,\,ab}$ *via* either the initial or the reversal magnetizations the shapes of which depend on the ratio $J_{ab,\,ab}/J_{c,\,ab}$. At this point it is interesting to add that informations obtained from the reversal branch are more reliable than those deduced from the initial one. This is because the former includes what we have called the central peak, or $H_{c_1}$, effect (ascribed here to single vortex pinning) which makes the analysis harder.

**14.6** THE RELATIONSHIP BETWEEN THE ANISOTROPIES OF $J$ AND $M$ IN TEXTURED SAMPLES AND IN ALIGNED GRAINS DISPERSED IN EPOXY RESIN. — Magnetic anisotropy as derived from the hysteresis cycle is often used to estimate the degree of alignment of crystallites in textured samples. However from the above considerations it is clear that magnetic anisotropy generally includes a shape dependent term which reduces the total apparent anisotropy and hence reduces the apparent degree of texturing. Regarding this problem, it is interesting to mention that magnetic measurements performed on highly aligned (better thand ± 1 degree) thin crystals embedded in epoxy resin [50, 358, 380] exhibit a magnetic anisotropy ratio $M_c/M_{ab}$ of only about 4 to 10 against 15 to 25 for a « spherical » single crystal investigated in the same conditions. Such a result rises the question about the real meaning of the measured magnetic anisotropy and how to correct for the shape of the sample and grains. At first, it can be argued that since the non-equilibrium magnetization is a defect-dependent quantity it is quite possible that the measured anisotropy varies from sample to sample (even when their shapes are identical) depending on the state and the nature of the involved pinning sites. However, we know from many examples in the literature that despite these defect-dependent phenomena the critical current density is the same in order of magnitude from sample to sample and for $T \ll T_c$) whatever the method of preparation employed (for the same high $T_c$ family, particularly YBaCuO (1 : 2 : 3)).

**14.6.1** *How to correct for the shape of grains in the magnetic anisotropy of aligned and highly textured samples.* — Frequently, the grains of textured materials have either needle-like or elongated platelet shapes. We would like to show here that this can lead to a drastic decrease of the apparent magnetic anisotropy. This effect provides a part of the explanation concerning the observed difference between the magnetic anisotropy of fine grains and that of the spherical single crystal discussed before. The arguments are based on the ideas mentioned previously that the irreversible magnetization (such as $M_c$ for **H** parallel to the $c$-axis) is governed by the smallest dimension (hereafter defined as $w$ for simplicity) of the platelet in the $a$-$b$ planes. In fact, this short dimension acts as the weakest link within these planes. The same calculations as those which led to equations (84b) and (84c) show that to a first approximation the cyclic magnetization in the $c$ direction is given by :

$$M_c = -\frac{wJ_{ab,\,c}}{20}\left[1 - \frac{w}{3L}\right] + M_{c,\,\mathrm{eq}}(H) \qquad (w \leqslant L)\,. \tag{86a}$$

Now we can also derive $M_{ab}$ by adding the contributions of all grains (recall that $M_{ab}$ is the magnetization for **H** strictly parallel to the $a$-$b$ planes, neglecting for the moment any possible desorientation of **H**). For this, let us consider equations (84b, 84c) together with figure 83 and assume that the distribution of the grain dimensions $w$ and $L$ (in the plane perpendicular to the $c$ axis) is at random, we must replace in this equation the width $w$ of the platelet by the average width $\langle w + L \rangle/2$, and rewrite equation (84c) as follows :

$$M_{ab} = -\frac{J_{c,\,ab}\langle w + L \rangle}{40} + M_{ab,\,\mathrm{eq}}(H)\,. \tag{86b}$$

This qualitative evaluation shows that a more appropriate relationship connecting the anisotropy of the magnetization to that of the critical current density is obtained from equations (86a, 86b) and can be summarized (neglecting the equilibrium magnetizations) as :

$$\frac{J_{ab,\,c}}{J_{c,\,ab}} = \frac{M_c}{M_{ab}}\,\frac{\langle w + L \rangle}{2\langle w \rangle}\left[1 - \frac{w}{3L}\right] \qquad (w \leqslant L)\,. \tag{87}$$

It is important to remember that equation (87) always implies the inequality $L \geqslant w$ and that $M_{ab}$ is imposed by $J_{c,\,ab}$ rather than by $J_{ab,\,ab}$. Replacing $M_c/M_{a,\,b}$ in equation (87) by the experimental value ($\approx 10$ for the oriented grains) we immediately see that the anisotropy of the current density for aligned grains would be about the same (at least 25) as that of the single crystal considered before if $\langle L \rangle \approx 6\langle w \rangle$ (elongated platelets). Such a condition is often realized in granular superconductors. Textured materials often exhibit a very large aspect ratio too. However, we know that in the case of textured materials the problem must be considered in connection with the possible existence of weak links to define the effective grains. We indeed emphasize that the above formula assumes that the grains are perfectly aligned and decoupled with $H$ rigorously parallel to the $c$-axis for $M_c$ and to the $a$-$b$ planes for $M_{ab}$. We must also mention that in addition to this spurious size effect, the measured (or apparent) magnetic anisotropy can also be reduced severely by the imperfect alignment of the grains, which is seldom better than a few degrees.

**14.6.2** *Influence on the apparent anisotropy of a small desorientation of H from the basal planes.* — To estimate quantitatively the effect of a small desorientation $\Delta\theta$ from the basal planes on the measured anisotropy it is reasonable to assume that when **H** is directed very close to the symmetry directions the magnetization and the critical current density are still related by the same relationships.

The angular dependence of the measured magnetization of a « spherical » single crystal (at $H = 30$ kG and $T = 4.2$ K) was illustrated in figure 76. The anisotropy of $J$ given there was derived from that of $M$ by the relation $J_{ab,\,c}/J_{c,\,ab} = 1.5 \times M_c/M_{ab}$ (given by Eq. (87)) using the fact that the investigated single crystal was quasi spherical so that $w \approx L$. The real anisotropy of the critical current density is presumably larger than given by such an equation because of the following experimental fact. We indeed observe (Fig. 76) that the logarithmic derivative of $M$ (and hence of the associated $J$) as a function of $\theta$ seems to diverge in the limit $\theta \to \pi/2$ (i.e. when **H** approaches the basal planes) while it tends towards zero in the vicinity of the $c$-axis. That is :

$$\frac{1}{M_c}\left[\frac{\mathrm{d}M}{\mathrm{d}\theta}\right]_{\theta \to 0} \cong \frac{1}{J_{ab,\,c}}\left[\frac{\mathrm{d}J}{\mathrm{d}\theta}\right]_{\theta \approx 0} \cong 0 \tag{88a}$$

$$\frac{1}{M_{ab}}\left[\frac{\mathrm{d}M}{\mathrm{d}\theta}\right]_{\theta \to \pi/2} \cong \frac{1}{J_{c,\,ab}}\left[\frac{\mathrm{d}J}{\mathrm{d}\theta}\right]_{\theta \approx \pi/2} \geqslant 25\,. \tag{88b}$$

Such a singular behaviour near the $a$-$b$ planes strongly suggests that the pinning forces

acting on the vortex lattice vary rapidly close to the *a-b* planes probably because of the intrinsic pinning.

Also, in connection with such a singular behaviour, it is of interest to estimate the error in the experimental anisotropy due to the unavoidable uncertainty $\Delta\theta$ on the direction of **H** relative to the *a-b* planes. It is indeed likely that the apparent anisotropy ratio of the critical current density is notably reduced (compared to the real value) by the angular error $\Delta\theta$. In order to estimate roughly this effect let $M(\pi/2 - \Delta\theta)$ be the measured magnetization with $H$ directed as close as possible to the basal plane and $M_{ab} = M(\pi/2)$ the unknown magnetization for $H$ strictly parallel to that plane. Then, assuming that $\Delta\theta$ is small enough to allow first order Taylor's expansion, we have $M(\pi/2 - \Delta\theta) \approx M_{ab} - \Delta\theta(\mathrm{d}M/\mathrm{d}\theta)_{\theta \to \pi/2}$. Substituting in the second term of equation (88b) gives (we recall that we assume $w = L$ here) :

$$\frac{J_{ab,\,c}}{J_{c,\,ab}} = \frac{3}{2}\frac{M_{ab}}{M_c} \approx \frac{3}{2\left[1 - \left|\frac{1}{M_{ab}}\frac{\mathrm{d}M}{\mathrm{d}\theta}\Delta\theta\right|\right]}\frac{M_c}{M(\pi/2 - \Delta\theta)}\,. \tag{88c}$$

Accepting a desorientation angle $\Delta\theta \approx 1°$ (= 0.017 rd) and using the experimental value ($\approx 25$, right hand side of Eq. (83b)), we find that the true anisotropy ratio ($M_c/M_{ab}$) is underestimated by a factor as high as 100 %. In addition, a more detailed analysis suggests that even in the limit of a bi-dimensional superconductor the experimental anisotropy ratio never exceeds $1/\Delta\theta$. Of course, this is a very rough calculation. Nevertheless, it shows clearly that the effective anisotropy of the current density is, in general, significantly higher than that of the measured magnetization (i.e. probably larger than 40 in the present « spherical » $YBa_2Cu_3O_7$ single crystal). Finally, it is to be emphasized too that despite the impression that the angular derivative of $M(\theta)$ diverges as one approaches the basal plane (Eq. (88b)), it is actually probable that, this derivative goes to zero for $\Delta\theta \ll M_{ab}/M_c = 0.025$ rd = 1°, which is well below the present experimental accuracy. It is also probable that this effect reduces significantly the apparent anisotropies of textured samples and oriented grains where the alignment always presents a distribution of a few degrees in the best cases. Therefore we believe that the anisotropy of the critical current density is often about the same (~ 20 to 40) in macroscopie single crystals, in fine oriented grains and in highly textured materials of $YBa_2Cu_3O_7$ even when the associated magnetic anisotropies look quite different. We recall that the comparison between the real anisotropy of the current and that of the measured magnetic anisotropy also requires corrections from shape effects.

**14.7** INFLUENCE OF $M_{eq}$ AND THE ASSOCIATED CURRENTS $J_s$ ON THE APPARENT ANISOTROPY. — In this paragraph we present extremely simplified and very qualitative formulae intended to be useful for rapid comparison with experimental data. Quantitive comparison requires more specialised considerations as developed in references [69, 80-83, 62, 434] (see also § 3.1).

We know that magnetic and transport properties are dominated by the equilibrium surface currents $J_s$ in the two reversible regimes defined either by $H < H_{c_1}(T)$ or by $H > H^{ir}(T)$ (above the irreversibility line). The manifestation of anisotropy in the equilibrium magnetization $M_{eq}$ is expected to depend strongly on the ratio $\lambda/r_g$. This shape effect can be quite large in granular materials, in particular close to $T_c$ where the ratio $\lambda/r_g$ diverges.

To see this qualitatively, we can again decompose the applied field $H$ into $H_z = H\cos\theta$ (along the *c*-axis) and $H_y = H\sin\theta$ (in the *a-b* planes), generalize equation (60a) of section 12 to anisotropic particles and calculate the corresponding components $M_{eq,\,c}$ and $M_{eq,\,ab}$ of $M_{eq}$ along the *c*-axis and the *ab* planes respectively. We find that for a spherical grain in the limits $\lambda_c \gg \lambda_{ab}$, $\lambda_c \ll r_g$ and $H < H_{c_1}$ we can rewrite equation (60a), as

$$M_{\mathrm{eq},\,c} \approx - V_{\mathrm{p}} \frac{H \cos\theta}{4\pi(1-N_z)} \left[ 1 - \frac{3\,\lambda_{ab}}{r_{\mathrm{g}}} \right] \tag{89a}$$

$$M_{\mathrm{eq},\,ab} \approx - V_{\mathrm{p}} \frac{H \sin\theta}{4\pi(1-N_y)} \left[ 1 - \frac{3(\lambda_c + \lambda_{ab})}{2\,r_{\mathrm{g}}} \right] \tag{89b}$$

where we recall that $\lambda_{ab}$ and $\lambda_c$ are the London penetration depths in the $a$-$b$ planes (or $H$ parallel to the $c$-axis) along the $c$-axis respectively whereas $V_{\mathrm{p}}$ is the fractional volume of superconducting material. More exact calculations have been carried out by Kogan and Clem [62] in various limiting cases and by Stroumbos *et al.* [434]. We see immediately from the above equations that for $r_{\mathrm{g}} \gg \lambda$ we can neglect the ratio $\lambda/r_{\mathrm{g}}$ so that the grain behaves as perfectly isotropic whereas for $r_{\mathrm{g}}$ comparable to $\lambda$ the magnetic vector **M** is oriented nearer to the $c$ axis, if $\lambda_{ab} \gg \lambda_c$ as is the case for most HTSC materials. Neglecting the factors $\lambda/r_{\mathrm{g}}$, it is interesting to rewrite these equations in terms of longitudinal and transverse magnetizations for $H \ll H_{c_1}$.

$$M_{\mathrm{eq},\,\parallel} \approx - V_{\mathrm{p}} \frac{H}{4\pi} \left[ \frac{\cos(\theta)^2}{1-N_z} + \frac{\sin(\theta)^2}{1-N_y} \right] \tag{89c}$$

$$M_{\mathrm{eq},\,\perp} \approx - V_{\mathrm{p}} \frac{H}{4\pi} \left[ \frac{1}{1-N_z} - \frac{1}{1-N_y} \right] \cos\theta \sin\theta\,. \tag{89d}$$

It is also interesting to give the equilibrium magnetization of spherical particles in the opposite limit $\lambda/r_{\mathrm{g}} \gg 1$ (always realized near $T_{\mathrm{c}}$) and for $H < H_{c_1}$ [62] :

$$M_{\mathrm{eq},\,\parallel} \approx - V_{\mathrm{p}} \frac{H}{4\pi} \frac{r_{\mathrm{g}}^2}{10\,\lambda_{ab}^2} \frac{m_c \cos(\theta)^2 + m_{ab}[1 + \sin(\theta)^2]}{m_c + m_{ab}} \tag{89e}$$

$$M_{\mathrm{eq},\,\perp} \approx - V_{\mathrm{p}} \frac{H}{4\pi} \frac{r_{\mathrm{g}}^2}{10\,\lambda_{ab}^2} \frac{[m_c - m_{ab}] \sin\theta \cos\theta}{m_c + m_{ab}} \tag{89f}$$

We recall that the physical origin of the anisotropy of $M_{\mathrm{eq}}$ for $H < H_{c_1}$ has been considered theoretically by several other workers [417-421]. For $H \gg H_{c_1}$ the equilibrium magnetization was calculated first by Kogan [67] and then by Balatskii *et al.* [69] in the London approximation and more recently by several authors [80-83] under more general hypotheses. Combining and simplifying (for the purpose of rapid comparison with experimental data) the results of these authors we find that $M_{\mathrm{eq}}(H, \theta)$ can be written in the form (valid in the London approximation and for $H_{c_2} \gg H \gg H_{c_1}$ and $\lambda \gg r_{\mathrm{g}}$) :

$$M_{\mathrm{eq},\,\parallel} = - c_z \sqrt{\frac{m_c}{m_{ab}}} \cos\theta \frac{H_{c_1}(\pi/2 - \theta)}{4\pi} \tag{90a}$$

$$M_{\mathrm{eq},\,\perp} = - c_y \sqrt{\frac{m_{ab}}{m_c}} \sin\theta \frac{H_{c_1}(\pi/2 - \theta)}{4\pi} \tag{90b}$$

with

$$c_z \approx \left[ 1 - \frac{3\,\lambda_{ab}}{r_{\mathrm{g}}} \right] \frac{\ln(d/\xi_{ab})}{\ln(\lambda_{ab}/\xi_{ab})}, \qquad c_y \approx \left[ 1 - \frac{3(\lambda_c + \lambda_{ab})}{2\,r_{\mathrm{g}}} \right] \frac{\ln(d/\xi_c)}{\ln(\lambda_c/\xi_c)} \tag{90c}$$

$$d \approx \sqrt{\frac{\Phi_0}{B}} \qquad \text{(about the vortex spacing)}$$

and [69]

$$H_{c_1}(\theta) = \frac{H_{c_1, c}}{\sqrt{\cos\,\theta^2 + \frac{m_c}{m_{ab}} \sin\,\theta^2}} . \tag{90d}$$

We recall that here $H_{c_1}(\theta)$ is the first critical field for $H$ oriented in the $\theta$ direction, $d$ is the vortex spacing and $m_{ab}$ and $m_c$ are the masses of the normal electrons moving within and perpendicular to the $a$-$b$ planes respectively. In the above formulae we assumed (without rigorous proof however) that the correction terms from size effect (i.e. terms $\lambda/r_g$) are the same as for $H < H_{c_1}(\theta)$ in equations (89a, 89b) and that $r_g \gg \lambda$. It is possible to check that if we put $\theta = 0$ or $\theta = \pi/2$ in the above equations we recover equation (3) in the London approximation ($\alpha = \beta = 1$ and $r_g \gg \lambda$). Again, we see that for highly anisotropic materials with $m_c \gg m_{ab}$, $M_{eq}$ is essentially perpendicular to the $a$-$b$ planes whatever the direction of **H** except in a very small angle $\Delta\theta$, of order $m_{ab}/m_c$, around the $a$-$b$ planes. Note that contrary to the case $H \leqslant H_{c_1}$ this property holds true here whatever the ratio $\lambda/r_g$.

**14.8** CONCLUSION. — In this section, we have emphasized the fact that the measured magnetic as well as transport critical current densities generally correspond to a complicated distribution (both in strength and direction) of $B(r, \theta)$ across the sample and includes contributions from different currents $J_{ij}$ the weight of which depends on the experimental conditions.

It is also important to have in mind that conventional magnetometers measure only the projection of $M$ along the direction of the applied field $H$. As a consequence, in this case the signal represents the longitudinal magnetization ($M_L$) and gives no information on the transverse component ($M_T$) which, in some conditions, can be much larger than the longitudinal one. The former is often determined by means of the torque technique.

Comparison between magnetic and current anisotropies is meaningful only after appropriate corrections of the distribution in the grain dimensions and of the residual desorientations of the grains.

It is clear from the above considerations that rigorously speaking the conventional scalar-critical state breaks down in the presence of a large anisotropy and cannot be applied to calculate the hysteresis cycle and the associated critical currents, except perhaps in the limiting case of infinite anisotropy where the decomposition model proposed here becomes valid. For a more exact solution the problem of the irreversible magnetization must be treated in the more general critical state formalism by taking into account the anisotropy of the elastic constants of the vortex lattice (see Ref. [110] and [419]). This is a very hard task compared to that of the equilibrium magnetization which itself is very complicated.

Finally, the manifestation of anisotropy in equilibrium magnetization depends strongly on the dimensions of the sample and grains *via* the ratio $\lambda/r_g$ and is different from that of the irreversible magnetization. Generally, the latter is larger because it is related to the anisotropy of pinning forces themselves probably related to the anisotropy of $H_{c_2}$.

## 15. Demagnetizing effects ; the magnetization of thin films.

**15.1** INTRODUCTION. — In the major part of the preceding analysis we have neglected demagnetization effects except in the case $H < H_{c_1}$ (Sect. 12 and 15). Here we wish to reconsider again the low-$H$ limit briefly on the one hand and the extreme example of very thin films in transverse applied fields on the other hand. The treatments of these two cases are

relatively independent from each other and the reader interested in thin films can ignore the first point.

15.2 DEMAGNETIZING EFFECTS IN THE LOW $H$ LIMIT SUCH THAT $\Delta r \ll R$. — Quite generally, the $M$ *versus* $H$ relationship is governed by the usual demagnetizing field when the flux penetration distances $\Delta r$ resulting from a small variation $\Delta H$ of the field are much lower than the macroscopic dimensions of the specimen ($\Delta r \ll R$). This claim is true whichever the physical mechanism responsible for $\Delta r$, in particular for the virgin magnetization ($\Delta r = R - r^*$, Fig. 3), the reversal cycle ($\Delta r = R - r_1$, Fig. 3), the screening distances ($\Delta r = \delta$; Eqs. (14f-g)) or for the elastic depth $\lambda_{el}$ (Eq. 73b)). This is also generally the case for $R \gg \lambda$ and $H \ll H_p$ (where $H_p$ is the field of complete flux penetration) or $H \leqslant H_{c_1}$ since the penetration distance is equal to the London penetration depth in this latter case.

This low field behaviour is illustrated in figure 86 which shows the initial magnetization $M(H)$ as a function of both $H$ and the angle $\theta$ of $H$ with the $c$-axis, for a single crystal of almost spherical shape (Fig. a) and oriented grains embedded in epoxy resin (Fig. b). Note that the

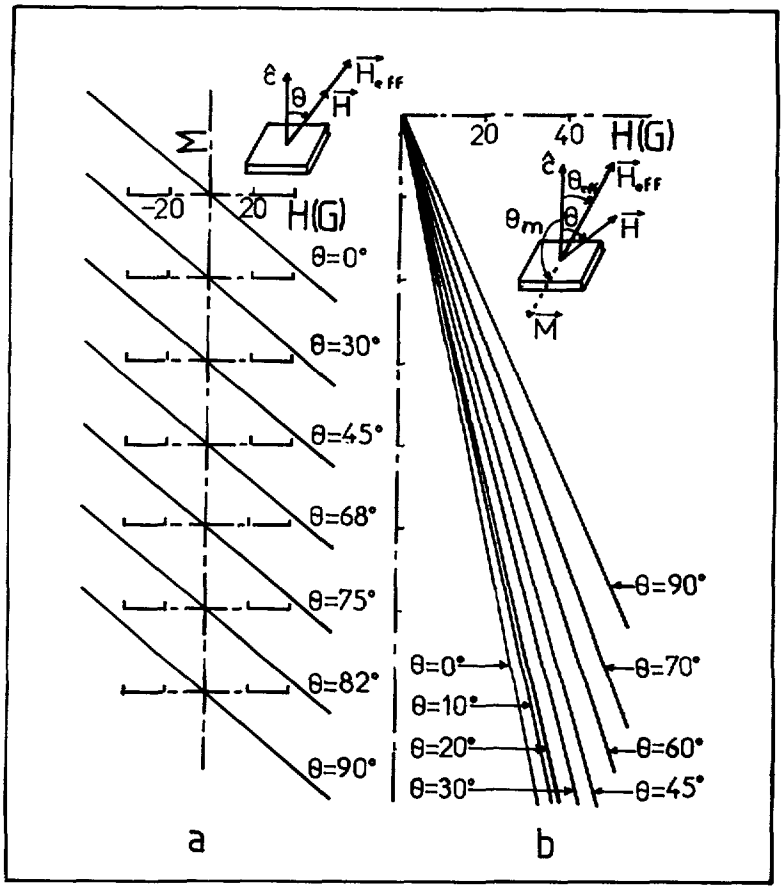


Fig. 86. — Angular dependence of the low $H$ magnetization. Left : a large, almost spherical in shape single crystal. Right : oriented grains diluted in epoxy resin (about 1 % concentration). Inset : because of the shape anisotropy of the demagnetizing factors of the grains $H_{eff}$ differs from $H$ both in amplitude and direction (see next Sect. 15), [380].

initial slope of the response of a highly textured $YBa_2Cu_3O_{7-\delta}$ thin film is almost infinite (because of the large demagnetizing factor) and cannot be visualized at the field scales ($\sim 40$ G) of this figure.

In many examples investigated in our laboratory we found that for large enough samples or grains ($r_g \gg \lambda$) the initial magnetization is given by

$$M = V_p \frac{-H}{4\pi(1-N)} \qquad (H \ll H_p,\ r_g \gg \lambda)\,. \tag{91}$$

We recall that $V_p$ is the packing factor (or the fraction) of superconducting material. The same result holds for sintered granular samples as illustrated by figure 87 (from [380] which shows that the hysteresis cycle of two sintered pellets having different radius $R$ (but the same hight $L$) exhibit the same initial slope after correcting for the macroscopic demagnetizing field [380]. It is useful to note the following formulae which allow us to derive $V_p$ in the limit $r_g \gg \lambda$. These results are valid for completely decoupled grains as well as for sufficiently compact specimens ($V_p > 80$ % for instance). Note however that the case when the dipolar coupling between grains is neigher very strong nor very weak (i.e. intermediate limit) and the Josephson coupling negligible is the most difficult to treat theoretically and requires accounting correctly for multipolar interactions [437].

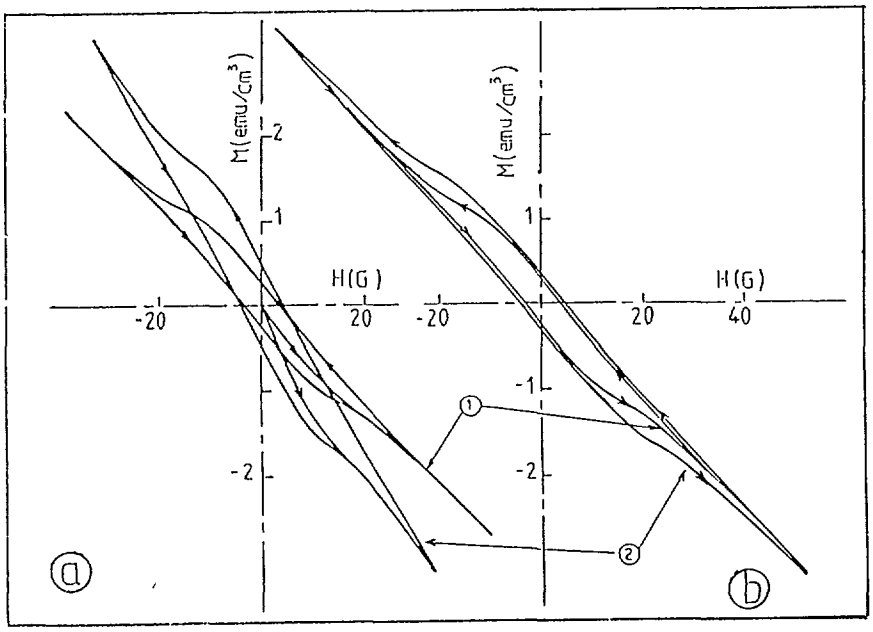


Fig. 87. — The low field hysteresis loops of two sintered pellets of YBaCuO (1 : 2 : 3, $R = 0.5$ and 2 mm, the same length 5 mm) before (left) and after (right) correcting for the macroscopic demagnetizing field [357].

For single crystals and oriented grains diluted in epoxy resin the above expressions (91) can be combined with the sum rule connecting the demagnetizing factors $N_\parallel$ and $N_\perp$ in the principal directions of the grains (assumed to have oblate ellipsoidal shapes) :

$$2N_\parallel + N_\perp \approx 1\,. \tag{92a}$$

The resolution of equations (91) and (92a) allows us to determine from experiments both these demagnetizing factors and the fractional volume $V_p$ of superconducting material. (Generally $N_\parallel$ and $N_\perp$ correspond to an applied field directed along the *ab* planes and along the *c* direction respectively). If $r_g \gg \lambda$ we have :

$$N_\perp = \frac{2\chi_\perp - \chi_\parallel}{2\chi_\perp + \chi_\parallel}, \qquad N_\parallel = \frac{\chi_\parallel}{2\chi_\perp + \chi_\parallel}, \qquad V_p = -8\pi \frac{\chi_\perp \chi_\parallel}{2\chi_\perp + \chi_\parallel}, \qquad (r_g \gg \lambda). \quad (92b)$$

Here $\chi_\parallel$ and $\chi_\perp$ are the initial susceptibilities ($\chi'$ or $\chi_{zfc}$) for $H$ respectively parallel and perpendicular to the *a-b* planes. Naturally, when possible, the demagnetizing factors can be derived directly from the dimensions of the sample using analytical formulae. For an oblate ellipsoid one has :

$$N_\perp = \frac{1+u^2}{u^3}\,[u - \arctan\,(u)], \qquad u = \sqrt{\frac{e^2}{R^2} - 1}. \quad (93a)$$

We recall that $2e$ and $2R$ refer to the thickness and the diameter of the sample respectively. For other orientations of the applied field see reference [357] and below.

To help the analysis of experimental results in the field domain $H < H_{c_1}$, we would like to add two helpful remarks.

(1) The first one concerns the determination of the angular dependence of $H_{c_1}$. It is indeed clear that, except for spherical samples with $R \gg \lambda$, the effective field $\mathbf{H}_{\text{eff, s}}$ differs from the applied field, $H(\theta)$, both in amplitude and direction. Let $\theta_{\text{eff, s}}$ be the angle of $\mathbf{H}_{\text{eff, s}}$ with the *c*-axis and assuming that $R \gg \lambda$ we obtain

$$H_{\text{eff, s}} = H \sqrt{\frac{\cos(\theta)^2}{(1-N_\perp)^2} + \frac{\sin(\theta)^2}{(1-N_\parallel)^2}} \quad (93b)$$

$$\tan\theta_{\text{eff, s}} = \frac{1-N_\perp}{1-N_\parallel}\tan\theta. \quad (93c)$$

As a consequence, the real $H_{c_1}$ is related to the apparent one (i.e. that determined naively from a direct experiment) by these two equations.

(2) It is interesting to write the total magnetization in term of a longitudinal component and a transverse component :

$$M_L = -H\left[\frac{\cos(\theta)^2}{1-N_\perp} + \frac{\sin(\theta)^2}{1-N_\parallel}\right] \quad (93d)$$

$$M_T = -H\sin(\theta)\cos(\theta)\left[\frac{1}{1-N_\parallel} - \frac{1}{1-N_\perp}\right]. \quad (93e)$$

It is to be recalled (Sect. 14) that when $\lambda$ is comparable to $R$ there is another cause of anisotropy : the difference between $\lambda_c$ and $\lambda_{ab}$ which tends to align $M$ along the *c*-direction.

**15.3** DEMAGNETIZING EFFECTS IN THIN FILMS AT ARBITRARY APPLIED FIELD. — We know from the previous sections and discussions (in particular from Fig. 1 in Sect. 2 and Fig. 82a in Sect. 15) that the local current density in thin films generally results from a complicated combination of the currents $J_s$, $J_{ab,\,c}$, $J_{ab,\,ab}$ and $J_{c,\,ab}$ (accepting again that the critical current can be described by a combination of these parameters).

The spatial distribution of the axial field $H_z(r)$ in a thin superconducting film and the

magnetization associated with it *via* the current $J = \frac{4\pi}{c} \{\partial H_z/\partial r - \partial H_r/\partial z\}$ were first calculated numerically by David Frankel [438] (using an iterative procedure). Frankel assumed that $J$ obeys a Kim model but neglected the radial contribution $(\partial H_r/\partial z)$ to $J$. Däumling and Larbastier [439] extended the numerical calculation (using finite element analysis) to thicker disks (with a variable aspect ratio $e/R$) and, more importantly, included radial effects associated with the radial field $H_r(r, z)$ generated by the screening currents themselves. The case where $J$ depends on $H$ following a Kim form was also investigated by Conner and Malozemoff [440] more recently. Due to the complexity of the problem only the saturation magnetization was reported in the main results of the above studies which can be summarized as follows :

1) The saturation magnetization is still given by Bean's model and is thus proportional to the radius $R$ of the disk.

2) The field of full flux penetration (or equivalently current saturation) is almost independent of $R$ but scales with $e$, half the thickness of the film.

3) Contrary to the usual « long cylinder » geometry, the critical current density is related principally to the gradient of the radial fields (i.e. to $\frac{\partial H_r}{\partial z}$ in cylindrical coordinates or to $\frac{\partial H_x}{\partial z}$ and $\frac{\partial H_y}{\partial z}$ in cartesian ones) rather than to the usual $\partial H_z/\partial r$ term (remember that the applied field is along the $z$ axis).

4) According to Däumling and Larbastier [439] difficulties can occur in deriving the field dependence of $J$ from the measured magnetization. In particular, the field dependence of $M$ is less steep than the field dependence of $J$.

5) In addition, a curious experimental result not generally noticed in the literature is that the hysteresis cycle of highly textured HTSC thin films is strongly dissymmetrical with respect to the field axis. This leads to an apparent reversible mgnetization $\{M^+ + M^-\}/2$, sometimes larger than $410^3$ (uem/cm$^3$). Some possible physical origins of this apparent reversible magnetization will be discussed later.

As can be expected, the numerical calculations carried out in references [438-440] are extremely tedious even for approximate solutions. Besides, anisotropy effects (not considered in the examples above) and the real variation of $J$ with $H$ (which is, as we have seen in Sects. 10 and 11, more complicated than the simple Kim form even for single crystals) make it very hard to test these calculations by means of experimental results on HTSC thin films.

Here we would like to consider the hysteresis cycles of textured thin film from a rather qualitative but somewhat more analytical approach than in the above examples. Our treatment is extremely simple : nevertheless, we shall see that it reproduces most of the characteristic features of the magnetic properties of the superconducting thin films enumerated just above.

**15.4** A SIMPLE ANALYTICAL CALCULATION OF THE HYSTERESIS CYCLE OF THIN FILMS. — To derive the hysteresis cycle of thin films and see how it is related to the local currents we use here a very simple model which only requires a few lines of analytical calculations and which avoids entering into the complexity of resolving the general critical state equations in the presence of strong demagnetizing effects. Our working hypothesis are as follows :

1) As in the case of long cylindrical samples, we assume that in response to the applied field the superconducting film will develop shielding currents starting from the edges of the disk. These currents will propagate across the film until a certain radius **r** for which the self-field induced by these currents at the centre of the film (i.e. at $r = 0$) equals in amplitude (but

opposite in direction) the applied field $H$. Thus, we have $H_{self}(r = 0) = H_{self,\,z}(r = 0) = -H$ and $H_{self,\,r}(r = 0) = 0$ by symmetry.

2) The infinitesimal field $\delta H_{self}$ induced at the centre of the film by an elemental current loop of radius $r$ and carrying a current $\delta I$ is given by the very classical formula for a single turn coil (Fig. 88a) :

$$\delta H_{self}(r = 0) = -\frac{4\pi}{c}\frac{\delta I}{2r} \quad \text{with} \quad \delta I = 2Je\,\delta r\,.$$

Putting this equation into the integral equation (94a) and assuming that flux has penetrated the film down to a circle of radius $r^*$ gives :

$$H_{self}(r = 0) = -\frac{4\pi}{c}\int_{r^*}^{R}\frac{2eJ\,dr}{2r} = -\frac{4\pi}{c}eJ\ln(R/r^*) \tag{94a}$$

or equivalently

$$r^* = R\,e^{-\frac{cH}{4\pi eJ}} = R\,e^{H/H_{fp}} \tag{94b}$$

$$H_{fp} = \frac{4\pi}{c}Je\,. \tag{94c}$$

From this formula we can define a full penetration field (right hand side of Eq. (94b)) which is exactly equivalent to the Bean field $H_b$ except that the radius $R$ of the sample is replaced here by $e$. The magnetization is then easily derived by means of the general integral equation relating $M$ and $J$ which is rewritten just below. From this equation the virgin (or initial) magnetization is given by (in practical units in which $c$ entering the above equations in cgs is replaced by 10) :

$$M_{vg}^{tf} = \frac{-1}{10R^2}\int_{r^*}^{R}Jr^2\,dr = -\frac{J}{10R^2}\left[\frac{R^3}{3} - \frac{r^{*3}}{3}\right] = -\frac{JR}{30}\left[1 - \frac{r^{*3}}{R^3}\right]. \tag{95a}$$

Using equation (94b) for $r^*$ leads to

$$M_{vg}^{tf} = \frac{-JR}{30}\left[1 - e^{-3H/H_{fp}}\right] \tag{95b}$$

and

$$M_{cyc} = M_{sat} = \frac{\pm JR}{30} \tag{95c}$$

where the sign + and − are for the upper and lower branches of the cycle. From the above equations for the virgin curve we can deduce several remarkable properties.

1) First of all, it is very interesting to note that Taylor's expansion of the virgin magnetization near $H = 0$ gives

$$M_{vg}^{tf} = -\frac{H}{4\pi}\frac{R}{e} \tag{95d}$$

which is almost exactly (within a factor of $\pi/2$) the value obtained using the demagnetizing factor $N = (1 - \pi e/2R)$ of a very thin oblate film in low transverse field.

The physical origin of this $\pi/2$ increase factor is interesting to understand for its own right : our calculation is based on the ideas that $J$ is constant and that the magnetic screening is always complete at the centre of the specimen (i.e. $H_{self}(r = 0) = -H$). The latter condition

is an approximation and is in fact too strong : we know indeed from standard textbooks that the axial component $H_{self,z}$ induced by a single turn coil passes by a minimum at the centre of the coil (this is easily justified by symmetry arguments), then through a maximum at $r \approx R$ and finally tends to zero at long distances (Fig. 88c). This result holds for the whole film except that the maximum is now smoothed out and is located somewhere between $r = 0$ and $r = R$. This is illustrated schematically in figure 88d which is consistent with the numerical calculation of [438].

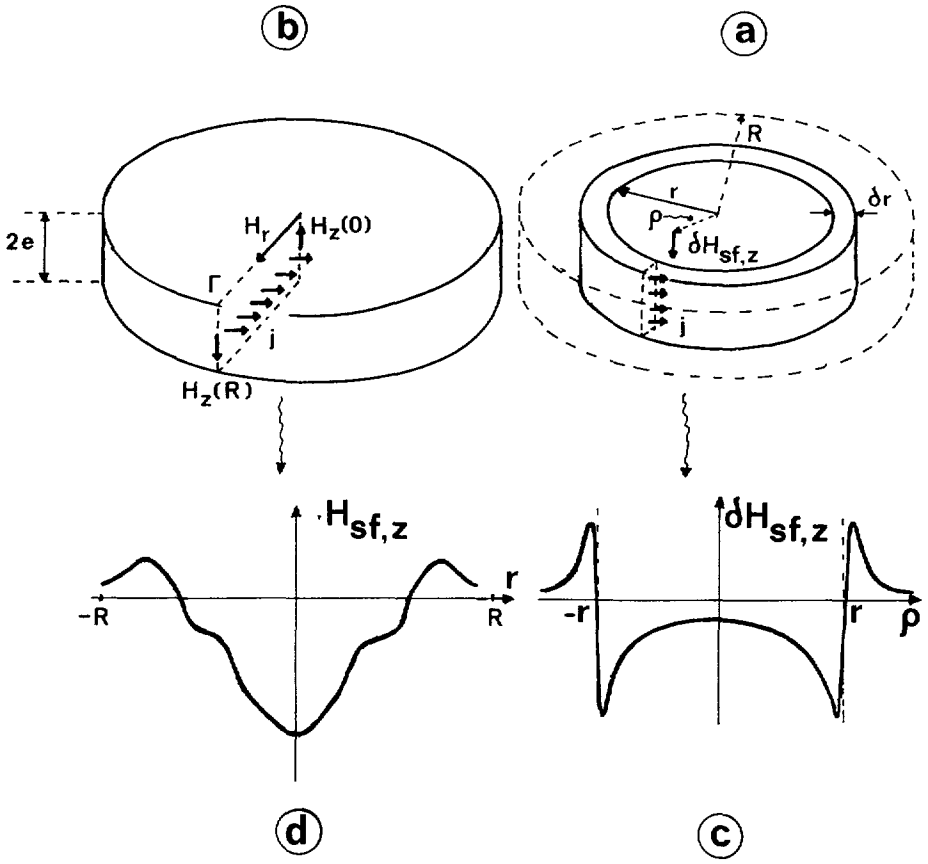


Fig. 88. — a) A coil made of a single turn carrying a current $J(2\ e\ \delta r)$. c) The elementary axial field induced by the elementary coil (a). b) Sketch of the current loops in a thin disk and the associated induced axial field (d). This field is obtained by adding up all the contributions of the elementary fields sketched in (c), see also [438]. It is to be recalled that, to a very large extent, $J$ is not imposed by this axial field but by the radial field.

2) Considering again the virgin curve we see that as $H$ is further increased the signal reaches about 95 % of its saturation value $M_{sat}$ at $H = H_{fp}$ (Eqs. (95a, 95c)), thus justifying our definition of $H_{fp}$ (Eq. (94c)) as the field of complete flux penetration throughout the film.

3) The saturation value of $M$ is still given by the usual Bean's formula (provided that the usual hypothesis that $J$ is not strongly dependent on $H$ is justified).

4) Repeating the same calculations as for the virgin curve allows us to derive the reversal

branch of the hysteresis cycle. The result is :

$$M_{rl}^{tf} = -\frac{JR}{30}\left[1 - 2\exp\left\{\frac{-3(H_{max} - H)}{2H_{pf}}\right\}\right]. \tag{96}$$

It is of interest to note that the width of this reversal branch is equal to about $2H_{pf}$ and that its initial slope is the same as that of the virgin one. Therefore as for the latter it is controlled by the film demagnetizing factor $N$ : to see this we replace $H_{pf}$ in equation (96) by (94c) and take the derivative $dM_{rl}^{tf}/dH$ at $H = H_{max}$. We then find the same slope $dM_{vg}^{tf}/dH$ (formula (95d)) at $H \approx 0$.

**15.5** WHAT IS THE CONTRIBUTION OF THE RADIAL FIELD $H_r$ TO $J_{mag}$ IN THIN FILMS ? — To see the physical origin of the apparent magnetic current in thin films let us again consider a disk geometry with uniform current density (Fig. 88b) placed in a transverse field. Applying Ampere's theorem to the closed path ($\Gamma$) of this figure and noting that by symmetry we must have $H_r = 0$ at the middle of the film (i.e. at the symmetry plane $z = 0$) we get :

$$H_r R + [H_z(R) - H_z(0)]\, e = \frac{4\pi}{c} JeR\,, \tag{97a}$$

or

$$J = \frac{c}{4\pi}\left[\frac{H_r}{e} + \frac{H_z(R) - H_z(0)}{R}\right]. \tag{97b}$$

Here $H_r$ is the effective radial field averaged at the surface whereas $H_z(R)$ and $H_z(0)$ are the effective axial field along the $z$ axis at $r = R$, (edge of the slab) and $r = 0$ (the centre of the slab) respectively.

From the results of the preceding paragraphs we know that magnetic saturation of the film is complete for an applied field $H = H_{fp}$. The contribution of the self field to the corresponding effective field $H_z(R)$ can be estimated directly by means of Biot and Savart's law. In the limit $R \gg e$ and to a first approximation one has :

$$H_z(R) - H_z(0) \approx 2\,\varepsilon H_r(e) \quad \text{(for low field such that } H \approx H_{fp}). \tag{97c}$$

Here $\varepsilon$ is a factor of the order of + 1 for the ascending field branch of the cycle and − 1 for the descending curve (in the current saturated state). Putting in equations (97a, 97b) and using the value of $H_{fp}$ given by equation (94b) we find that the average contribution of the radial field, respectively the axial field, to $J$ are about

$$J\left[1 - 2\frac{e}{R}\right] \quad \text{and} \quad 2J\frac{e}{R}. \tag{97d}$$

Consequently, in the saturated cyclic state the current is principally governed by the radial field $H_r$. Note also that the local critical current density $J(r)$ is not rigorously constant across the sample. This is particularly true for the current component related to $H_z$. We have indeed seen (Fig. 88c) that the sign of $H_z$ changes near the edge of the film, but this contribution is negligible in thin films.

**15.6** WHY IS THE CRITICAL CURRENT DENSITY SO HIGH IN THIN FILMS AND WHAT IS THE DIRECTION OF THE PINNING FORCES IN THE FILM ? — Presented in figure 89a is a typical example of the hysteresis cycle of $YBa_2Cu_3O_7$ thin films. It is clear that this cycle exhibits all of the characteristic properties already enumerated. In addition, the magnetization varies

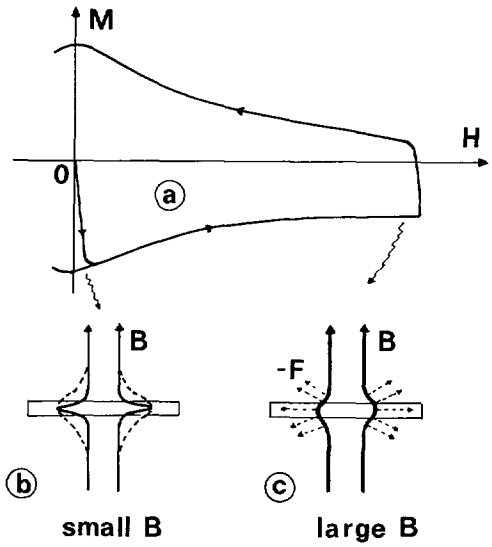


Fig. 89. — a) Example of a thin film hysteresis cycle of $YBa_2Cu_3O_7$. $R \approx 1$ mm, $e \approx 1\,500$ Å and $J_{mag}$ estimated to be about $2 \times 10^7$ A/cm$^3$. b) Suggests that because of both the anisotropy of the layered structure and the demagnetizing field the vortices prefer to lie in the *a-b* planes at low $B$. The dashed curve of (b) would correspond to the isotropic case. At large $B$ (Fig. c) the interaction between vortices favours straight lines hence diminishing the radial field and the associated current.

significantly with $H$ and is quite dissymmetrical with respect to the $H$ axis. Here, we have neglected such field variations, the possible physical origins of which are discussed briefly below.

We show in figure 90 a calculated hysteresis cycle using the various equations (95b-96) derived previously for thin films assuming $J$ independent of $H$. Also shown for comparison is a straight dashed line which corresponds to the calculated magnetization of a long cylinder assumed to have the same radius $R$ and the same current $J$ as the film (i.e. $R_{cyl} = R_{film}$ and $J_{cyl} = J_{film}$ ; in both cases the magnetizations are given per unit volume). In the field domain ($H < 2$ kG ) of this figure one has $M = -H/4\pi$ (with a very good approximation) for the cylinder the magnetization of which per unit volume is almost three orders of magnitude lower than that of the film (note the difference between the corresponding magnetization scales).

The following remarks can help understanding the field behaviour of the cycle.

(1) Firstly, the magnetization is a factor of 2 to 10 higher than in usual single crystals and oriented grains.

(2) Also, if one excepts the very low field region close to $H_{c_1}$ (not visible in Fig. 89) $M(H)$ drops with $H$ much more rapidly here than in single crystals. We believe that a significant part of this drop is due to anisotropy. Another suggestion is that the measured signal includes somehow a large contribution from the radial component of the equilibrium magnetization.

(3) From the previous paragraphs we know that when the applied field reaches the current saturation value, $H \approx H_{fp}$, $H_z$ and $H_r$ become comparable in magnitude and are both of the order of $H_{fp}$. This implies that the Lorentz force is directed far away from the $c$-axis : since $\tan(\theta_B) \approx H_r/H_z \approx 1$ one has $\theta_B \approx 45°$ where $\theta_B$ is the average angle of $B$ with the $c$-axis.

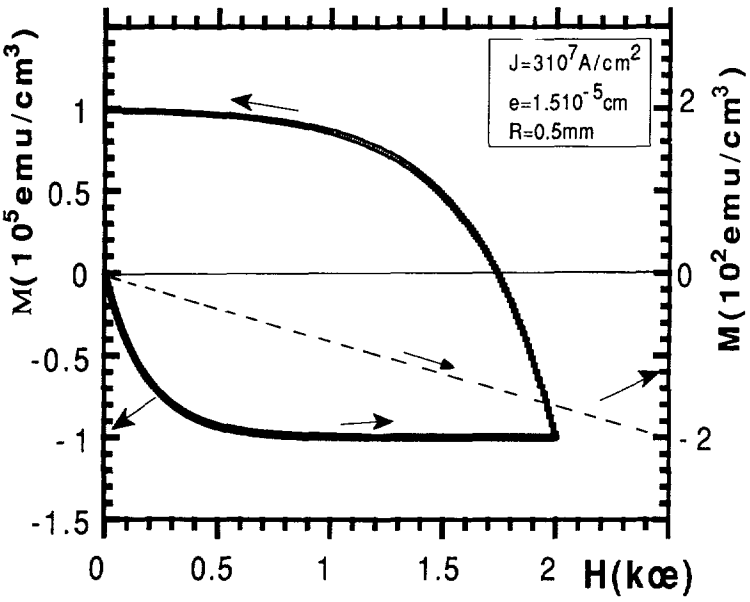


Fig. 90. — Calculated hysteresis cycle for a thin film 1 500 Å thick and $J = 3 \times 10^7$ A/cm$^2$, $R = 0.5$ mm. Shown for comparison as a dashed line (right scale) is the expected $M(H)$ curve of a long cylindrical sample with the same $R$ ($R_{\text{cylindre}} = R_{\text{film}} \gg e$) and the same $J$ as the film and in the same field range. Note the factor 500 in the vertical scales.

**15.7** DISCUSSION AND CONCLUSION OF THIS SECTION. — The reason why the critical current is much higher in thin films than in single crystals is not clear at present, at least for us. However, recent microscopic observations [441-444] revealed the presence of screw dislocations (in thin films) the density of which was found to be correlated with the critical current density. In section 14 we proposed another mechanism based on intrinsic pinning, to explain the transport current of thin films. Here, we wish to show that our mechanism can explain the magnetic data as well. This is based on the following remarks.

(1) In the field region where $H_z$ is very low the vortex segments are in the *a-b* planes and thus fully submitted to the strong intrinsic pinning forces (inset Fig. 84d).

(2) The field dependence of the experimental $J_{\text{mag}}$ is probably controlled simultaneously by a direct field dependence (i.e. at fixed direction of $BJ$ varies with the amplitude of $B$) and by the anisotropy. (The local direction of $B$ changes as the applied field is varied.) Such dependence would be introduced through $B$ and $\theta_B$ dependences of the elastic modulus of the vortex lattice, particularly the tilt and shear stiffness, $c_{44}$ and $c_{66}$ respectively.

(3) We expect that for highly anisotropic materials the radial and the axial portions of the vortices are decoupled (pancakes). Then it is difficult to imagine how the screw dislocations (which are perpendicular to the film plane [441, 444]) can pin the radial segments of the vortices which, according to the above calculations, contribute strongly to $J$.

Intuitively we expect that the layered structure will help the bending of the vortices (since an isolated vortex always prefers to lie between CuO sheets), thus increasing the radial field $H_r$ and consequently $J$ *via* equation (96b). This is schematized in figure 89b which shows that the bending of the lines would be reinforced at low flux density and lowered at high fields.

Consequently, we believe that because of the very high anisotropy of layered superconductors the critical current $J$ of thin films should be to a large extent imposed by intrinsic pinnings

at low fields and would diminish with $H$ because of the fact that repulsion between lines would oppose the bending of the lines and hence decrease $H_r$. Lastly it is possible that the equilibrium magnetization is also enhanced considerably by the radial field. One way to test this suggestion is to investigate relaxation effects which should be very weak in the case of the equilibrium contribution. This can explain some of the asymmetry of the hysteresis cycle with respect to the H axis.

### 16. Surface barrier, surface pinning and surface imperfections.

Surface pinning has been widely investigated in conventional materials. Its manifestation in the magnetic properties of conventional materials has been considered by Bean and Livingston [445] and analysed in details by Ulmaier [446] in particular in relation to the hysteresis cycles of hard superconductors. This is illustrated schematically in figure 91 which shows how the so-called minor cycle would look like in the case where the critical current is dominated by surface pinning (bottom left Fig.). More recently, surface barriers and surface pinning have been invoked by several authors [213, 348] to explain some anomalous behaviours of the hysteresis cycle of HTSC in particular near $T_c$ [348]. However, in our opinion there are not yet many convincing proofs in favour of such surface effects in the literature. In addition, we have seen in sections 7 and 8 that correct descriptions of the hysteresis cycle must take into account properly the equilibrium magnetization, especially the influence of its screening field induced by the Abrikosov-London current $J_s$, on the irreversible magnetization (see term 4 $M_{eq}$ of Eq. (39)). The influence of this shielding field is particularly important near $T_c$ as the contribution of the equilibrium magnetization becomes very essential there. The role of the demagnetizing field, which is much more complicated

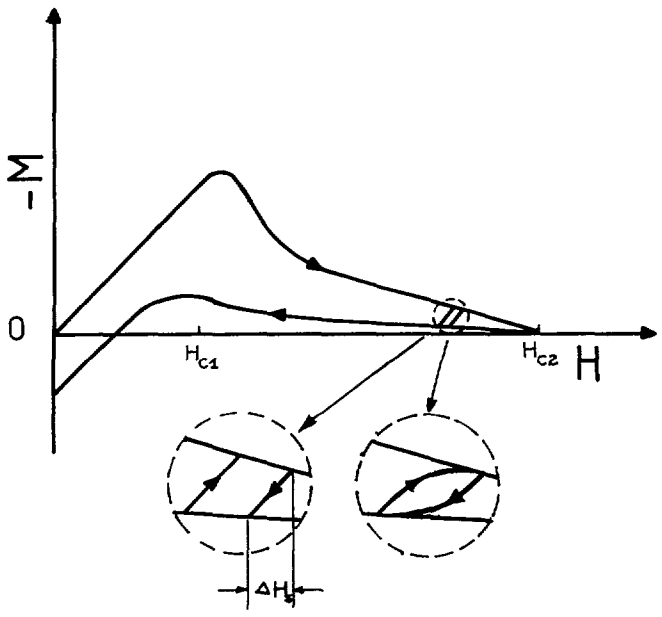


Fig. 91. — Schematic illustration of the shape of the minor hysteresis cycle [446] when the critical current is imposed either by surface currents (bottom left) or by usual bulk current (bottom right). Recall that this is only valid in the critical state limit and for conventional magnetic measurements. For instance, the situation is quite different when $M$ is measured by a tiny Hall probe fixed close to the sample.

than in homogeneous ferromagnetic materials, see Sect. 14, must also be considered correctly for quantitative interpretations. When analysing either the minor loops or the virgin curve or the reversal branches of the cycle it is important to take care of the experimental technique employed (see Fig. 3 of Sect. 2 for the definition, of these branches). For instance, the $M$ *versus* $H$ equations for these curves are quite different whether they are measured by means of a classical magnetometer placed far away from the sample or *via* a Hall probe fixed on that sample. To our knowledge, up to now these problems are generally not accounted for in the literature on HTSC. There are arguments (but only valid in the framework of the critical state model) that the minor cycle determined by such a Hall probe will always (i.e. even in the absence of any surface pinning) be similar in shape to that obtained using a magnetometer in the presence of extrinsic surface pinnings (Fig. 91, bottom left). In addition, demagnetizing fields are unavoidable there (end effects) and depend not only on the geometrical shape of the sample but also on the whole distribution of the current within it.

From the theoretical point of view, the interaction of the surface of the specimen with the vortex lines can be established in at least three distinct ways the most common of which are (1) extrinsic pinninig due to pinning centres near the surface, (2) intrinsic or thermodynamic surface barriers and (3) surface weak links connected with extended defects. Let us now discuss each of these effects consecutively.

**16.1** SOME CHARACTERISTIC FEATURES OF EXTRINSIC SURFACE PINNING IN MAGNETIC MEASUREMENTS. — Now it is important to note that, so far as surface pinning is concerned it has the three very distinctive signatures described below (assuming that the thickness of the « surface layer » is infinitely thin as compared to the sample radius).

(i) The magnetization curve in particular the minor cycle, has roughly a parallelogram-like shape (when $J$ is independent of $H$ as in the initial assumption of Bean) with sharp angular points.

(ii) The magnetization per unit volume becomes independent of the macroscopic radius $R$ of the sample (instead of being proportional to it as in the Bean model) whereas the apparent (or average) critical current density (as defined by the Bean model) decreases as $1/R$. Moreover the demagnetizing field is now given by the same formula ($H_d = H + 4\pi NM$) as in ordinary ferromagnets (homogeneous and isotropic).

(iii) A third and quite subtle feature of the surface barrier appears when the associated current density depends on $H : J = J(H)$. Then, if the equilibrium magnetization is negligible the hysteresis cycle should be symmetrical with respect to the field axis, after correcting for the demagnetizing field in the usual way. In particular, this means that any positive peak in the hysteresis cycle should be accompanied by a symmetrical peak and *vice versa*. We recall that the low-$H$ peak encountered previously, particularly in section 7, is always symmetrical with respect to the origin and not to the field axis.

**16.2** FORMAL ANALOGY WITH TUBULAR SAMPLES AND RINGS. — In fact the general problem of surface barriers is not easy to solve except when the total magnetization is strongly dominated by surface pinning and when the specimen is a long cylinder with negligible demagnetizing field (we have noted that the latter approximation is more difficult to satisfy in measurements using Hall probes because of end effects). In this case the problem becomes quite simple and is indeed equivalent to that of a hollow cylinder of thickness $e$ equal to the thickness, of the surface pinning barrier. The quadrangular shape of the minor cycle of figure 91 (bottom left) and the angular points of the same cycle are then easily explained. This is simply because the variation of $M$ with $H$ is abruptly interrupted when the flux front (and the associated currents produced for example by the reversal field) arrives at the inner surface

of the tube (*). This is very easily demonstrated by calculating the magnetization of a tubular sample.

Let us assume that the surface current $J_{sp}$ is independent of $H$ and let $e$ be the thickness of the tube (i.e. the thickness of the equivalent surface barrier) of outer radius $R$. The virgin magnetization is then given by the same equation as equation (83b) of section 14 except that the virgin interval is now very narrow and limited to the field domain $H < H_{sp} = \frac{2\pi}{5} J_{sp}\, e$ (which means that the field $H_{sp}$ of full flux penetration is now proportional to $e$ and not to $R$). Note the use of the subscript « sp » to define quantities related to surface pinning : we have calculated the whole hysteresis cycle in the presence of two field independent currents, one ($J_{sp}$) is assumed to be restricted to an outer layer of thickness $e$ and the other (called $J$ as usual) is defined in the rest of the sample, i.e. in a cylinder of radius $R - e$. The corresponding cycles are presented below (Fig. 92). Here for simplicity we only give the equations for $J = 0$ in practical units :

$$M_{vg} = -\frac{H}{4\pi}\left[1 - \frac{2\pi}{5}\frac{H}{J_{sp}R} + \frac{1}{3}\left\{\frac{2\pi}{5}\frac{H}{J_{ps}R}\right\}^2\right] \tag{98a}$$

with

$$H < H_{ps} = \frac{2\pi}{5} R J_{sp} \tag{98b}$$

$$M_{cycl} = -\frac{eJ_{sp}}{30}\left[1 - \frac{e}{R} + \frac{1}{3}\frac{e^2}{R^2}\right], \quad H > H_s\,. \tag{98c}$$

It is interesting to note that :

(1) The equation of the virgin curve is independent of the thickness $e$ of the barrier. The same statement is equally true for the reversal curve the equation of which is not given here.

(2) The derivative of $M(H)$ is discontinuous at $H = H_{sp}$ with

$$\frac{dM(H_{sp} - \varepsilon)}{dH} - \frac{dM(H_{sp} + \varepsilon)}{dH} = \frac{1}{4\pi}\left[1 - 2\frac{e}{R} + \frac{e^2}{R^2}\right]. \tag{99}$$

As we can see this discontinuity disappears for $e = R$. The same kind of calculation leads to a discontinuity in the reversal magnetization too and explains the sharp angular points of the minor cycle of figure 91. Formula (99) shows also that because of the factor $e/R$ the discontinuity in $M(H)$ and more generally the angular points in the hysteresis cycle should be much more pronounced in large samples (single crystals) than in small samples (granular materials for which $e$ can not generally be very small compared to the radius $r_g$ of the grains).

We can make the above formulae a bit more general by adding to the current $J_{sp}$ of the surface barrier of thickness $e$ a less intense bulk current $J$ located in the rest of the sample (also independent of $H$), that is in the inner region of radius $R - e$. This is performed in figure 92 which shows the calculated cycles in two cases : (1) a surface current $J_{sp} = 10^5$ A/cm$^2$ limited to a surface barrier of thickness $e = 20$ μm and a bulk current $J = 10^4$ A/cm$^2$, (2) the same values as in (1) except $J = 10^3$ A/cm$^2$. In these calculations $e$ is

(*) Note that such an abrupt interruption in the variation of the measured magnetic flux is expected to always happen (at least in the critical state model) when using a Hall probe for magnetic measurements.

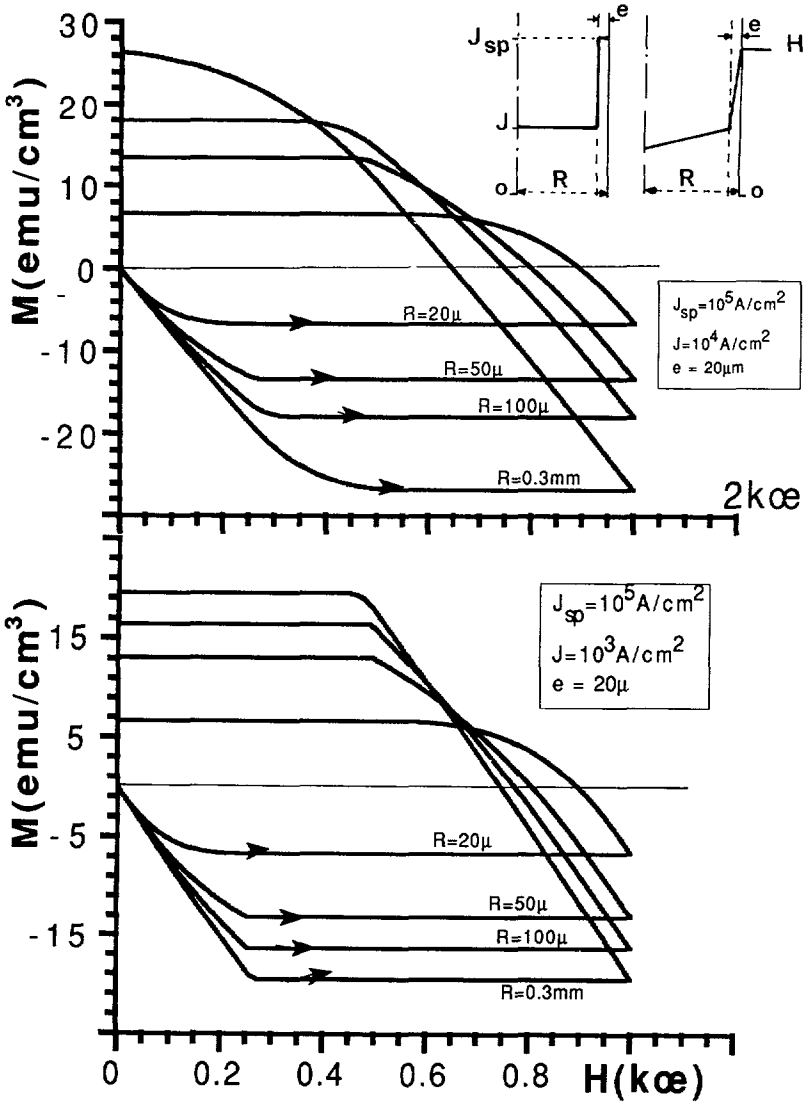


Fig. 92. — Calculated hysteresis cycles assuming that the critical current ($J_{sp}$) is large only in a tube of thickness $e = 20$ μm, and variable radius $R$. The current is significantly lower in the rest of the material (i.e. in the cylinder of radius $R - e$). The values of the critical currents and those of the radii of the sample are varied as indicated in the figure.

kept constant (20 μm) but $r_g$ is varied from about 300 to 20 μm. It is to be noted that :

(i) For $R = 20$ μm one has $e = R$ and the notion of surface pinning looses any signification ; the cycle is in fact simply that of a long filament.

(ii) The comparison with experiments can be more complicated than predicted here when $J$ depends on $H$. This is generally the case in the low-$H$ peak region ($H \gg H_{c_1}$). Therefore, the comparison with experiments would be more meaningful far from this peak region. This implies that the reversal curve would generally be closer to the experimental data than the virgin one.

**16.3** ON THE PHYSICAL ORIGINS OF THE VARIOUS SURFACE EFFECTS. — Usually, the interaction of the surface of the specimen with the vortex lines can manifest experimentally in at least three distinct ways the most common of which are now considered.

**16.3.1** *A perfect surface behaves as a thermodynamic barrier for entry and exit of vortices.* — A perfect surface leads to a severe distortion of fields and currents of any vortex line located within a distance of the order of $\lambda$ or less from that surface. The physical requirement that the currents of the vortex are necessarily tangent to the surface leads to the introduction (to facilitate the calculation) of a vortex image of opposite polarity to the real one. These two vortices interact in exactly the same way as two real vortex lines except that the interaction is attractive here whereas it is generally repulsive within the VLL (the expression of this interaction can be found in most textbooks concerned with superconductivity ; it is generally given in terms of standard Bessel functions). Moreover, as the vortex crosses the London's penetration shell around the sample it is submitted to a Lorentz force $\Phi_0 \times \mathbf{J}_s$ due to the London-Abrikosov current $J_s(r) \approx 4\ \pi M_s \exp[-r/\lambda]$ where $r$ is the position of the vortex with respect to the surface and $M_s$ the magnetization induced by these surface currents in the presence of the barrier. Note that : (1) in the absence of any barrier $M_s$ it is simply equal to $M_{eq}$ and (2) for non cylindrical specimens $M_s$ is determined by the local demagnetizing field at the point $r$ of the surface under consideration. The total energy involves also the usual unperturbed energy of the VLL. The consequence of all this is that a perfect surface behaves like a very high potential barrier opposing both the entry and the exit of vortices. According to de Gennes ([118] p. 76-80), in terms of magnetic field, this barrier would be as high as the usual thermodynamic field $H_c \approx \sqrt{H_{c_1} H_{c_2}}$ at relatively low vortex density ($H \geq H_{c_1}$) and for isotropic materials. This calculation was extended to higher fields by several authors (see Ref. [19] p. 339-41 and Refs. herein). The case of HTSC have been considered by several people [447]. Damjanovic and Simonov [448] found that $H_s$ is again given by $\Phi_0/(4\ \pi \lambda_{ab}\ \xi_{ab}) \approx H_c$. More remarkably, these authors found that $H_s$ is practically independent of the direction of the applied field with respect to the $c$-axis (in qualitative agreement with the fact that $H_c$ is isotropic in the London approximation model). Using a different approach (Josephson interlayer coupling model) Buzdin and Feinberg [449a] found that this result holds near $T_c$ but $H_s$ becomes weakly anisotropic at low temperatures, if the transverse coherence length $\xi_c$ becomes smaller than the interlayer distance $d$. For the sake of comparison, it turns out that in a Josephson junction, the entrance field is approximately equal to the first critical field $H_J$ of this section [449b]. In practice, this situation can be realised only in the case of Bi based compounds and not in that of $YBa_2Cu_3O_7$ which is the most investigated systems at present. In the case of high $T_c$ materials the calculated $H_s$ is of the order of $10^4$ œ (at $T \ll T_c$) and is thus about three orders of magnitude higher than the experimental penetration field ($\approx 50$ œ for $YBa_2Cu_3O_7$ along the $a$-$b$ planes and much less than this value for Bi based compounds) generally identified as $H_{c_1}$. This huge difference between the calculated and the experimental values holds for $T$ as high as $0.99\ T_c$. The absence of any evident surface barrier of significant magnitude (compared to $H_s$) is often ascribed to surface imperfections which are thought to enhance considerably the local demagnetizing fields and hence help overcoming the thermodynamic barrier in these regions. However, as we shall see below, we believe that the non observance in experimental data of a thermodynamic barrier of this kind is practically impossible to explain in terms of local demagnetizing fields alone.

Physically, the barrier presented by perfect surfaces would be very similar to the surface barriers encountered by Bloch and Néel domain walls in ferromagnetic materials. So by analogy with the latter it would be interesting to introduce a nucleation field, $H_n$, and a propagation field $H_{pr}$, for the individual vortices. We know that because of the very large

anisotropy of HTSC it is not necessary to consider that the vortex is a rigid line. Then we can imagine that the nucleation of a given vortex can first take place by means of a small vortex portion (pancake) which can be much more easily induced (than a whole rigid vortex) by the local demagnetizing field as well as by thermal fluctuations. This « slice » of vortex will then develop (or propagate) more easily through the specimen. In the absence of any other kind of pinning force than the thermodynamic barrier (perfect material) the propagation field would then coincide with $H_{c_1}$. We know however (see Fig. 50) that the apparent $H_{c_1}$ is in practice larger than the true one because of defects (unavoidably present in the material) which oppose the propagation of the vortex lines. We have noted that in addition to the action of the local demagnetizing field temperature fluctuations can also help the vortices to jump over the effective surface barrier [213]. The fact that the relative difference between the measured and the calculated first penetration fields are practically independent of $T$ suggests that the effective surface barrier is much smaller than the other energy scales intervening in $J$ and $M$ measurements.

**16.3.2** *Surface imperfections can behave like localized weak links.* — We have just mentioned that in real experimental conditions, the surfaces are imperfect and present various kinds of defects with different spatial dimensions. Such imperfections play a great role in microwave losses and have been extensively investigated in the past [450-452] in relation to conventional superconductors. Surface imperfections are not equivalent physically and not equally efficient in perturbing the flux penetration within the sample. Some imperfections are rather difficult to visualize by usual microscopic observation techniques. This is because these methods generally require polishing the sample thus removing some imperfections but adding new (undesirable) ones. In addition, usual microscopic observations do not make any distinction concerning the weak or strong superconducting link character of the imperfection. A new and promising E.P.R. method is being presently developed [453-455]. It investigates surface imperfections *via* the perturbations of the field $H(r)$ near and immediately above the surface by such imperfections. Concerning more usual magnetic measurements some surface imperfections can be considered as « surface weak links » which give rise to magnetic hysteresis at very low field. In addition, in the presence of sharp features near such weak links the local field seen by the link can be considerably increased by the demagnetizing fields created by these features. As a consequence, the combination of the « surface weak links » and the local demagnetizing fields would in principle lead to the existence of hysteresis effects and losses whatever small the applied field is.

In practice, however, we expect that the relative value $\Delta M/M$ of the usual irreversible magnetization associated with these surface imperfections would be of the order of $\frac{\delta v}{\pi R^2}$ (or in the worst case of the order of $\frac{\delta v}{2\,\pi R\lambda}$) where $\delta v$ is the effective volume occupied by the surface « weak links ». It is to be added however that such imperfections can lead to large ac-losses (due to flux pinning) at very high frequencies as the latter increase as $\omega$. However, at very high frequencie the losses are less due to flux pinning (or trapping) than to viscous flux flow *via* the normal electrons of the vortex cores located in the « surface weak links ». Indeed these normal electron losses are expected to increase roughly as $\omega^2$.

**16.3.3** *Surface pinning in the vicinity of the surface.* — As discussed previously in detail the term « surface pinning » is related to an anomalous increase of defect concentration very close to the surface and thus to a large « surface » like critical current density. It is of interest to note that such a layer of surface pinning can exist naturally in YBaCuO if the annealing time (in oxygen or in air) is not sufficiently long to allow for oxygen to diffuse through the whole sample. It is often found that large single crystals are oxygenated only in a limited penetration depth beyond which the material is poorly superconducting and hence would have a very low

current $J$ in these regions. In the discussion about « butterfly » shaped hysteresis cycles (Sect. 7) we have seen that such effects could lead to surface like hysteresis loops of the sort depicted in figure 92.

**16.4** CONCLUSION. — In conclusion of this section we have tempted to clarify and identify surface effects particularly extrinsic surface pinning (Fig. 92) in magnetic measurements. Concerning the thermodynamic barrier opposed by the surface to the vortices it is probable that in HTSC both local demagnetizing fields, local weak links, thermal fluctuations and more importantly anisotropy add their effects to overcome this barrier.

## 17. Thermal fluctuations, collective pinning and irreversibility line.

Up to now we have concentrated our efforts upon the interpretation of the experimental results from the usual critical state (and somewhat phenomenological) point of view (a major exception is Sect. 13). This approach was first of all intended to relate the experimental data ($M(T, H, t, R, r_g)$, $\chi''(T, H, \omega, R)$, $J_{tr}\, T, H, t, R$) to the local critical current density and to other micro and macroscopic factors such as anisotropy and demagnetizing effects and granularity. It is clear from the ensemble of the previous results and conclusions that the understanding of the so-called irreversibility or depinning line requires as a preliminary condition the correct interpretation of the measured quantities both near and far from such a line, taking into account the various parameters quoted just above. The problem of thermal fluctuations of the vortex position ( $\langle u^2 \rangle$ proportional to $T$), the physical nature of such a line and the modification of the flux creep model by such fluctuations are not independent. In the spirit of the present paper these questions can be summarized into a single one : why does the critical current density drop so abruptly with $T$, $H$ and $t$ ?

From the discussion of section 4 we concluded that the anomalous $T$, $H$ and $t$ behaviours of $M$ can be understood within the framework of the flux creep model. However according to Feigel'man *et al.* [173, 174] the usual flux creep model of Anderson would be valid only in the limit $J(t = 0) - J(t) \ll J(t = 0)$ where (as already defined) $J(t = 0)$ is the critical current density in the hyper critical state (before the starting of any flux creep). We have indeed seen that because of the exponential drop of $J_{ab,\,c}$ and $J_{c,\,ab}$ the condition $J(t = 0) - J(t) \ll J(t = 0)$ (or equivalently $J \approx J_{max}$) is rarely realized in usual experimental time scales $t$ except very close to $T = 0$ (Fig. 14). The theory of collective pinning-collective creep developed first by Larkin and Ovchinnikov [172] at $T = 0$ and then extended in references [173, 174] to finite temperature, would include the case $J(t) \ll J(t = 0)$ and, accordingly, would be valid over larger temperature and time intervals. The main results of this theory are the following.

(1) The energy barriers are smoothened by thermal fluctuations and their spatial range broadened from $r_p \approx \xi$ to $r_p \approx \sqrt{\xi^2 + \langle u^2 \rangle}$. In the limit of weak pinning the mean-squared thermal displacement is determined by equating the thermal energy to the elastic energy per degree of freedom. It seems that in the field domain $H_{c_1} \ll H \ll H_{c_2}$ the result has the form $kT \approx C \langle u^2 \rangle B^{-1/2}$ where $C$ depends on all of the elastic constants $C_{ij}$.

(2) As a function of $J$ the pinning potential would grow as $J^{-\alpha}$ with $\alpha > 0$ and notably smaller than 1. However, it is to be recalled that this singular behaviour is related to the fact that the correlation volume $V_c$ tends to infinity as $J \to 0$ (vortex glass state [106, 413]). This result is itself based on a tacit assumption of the usual collective pinning theory according to which the only effect of pinning disorder is to deform elastically the VLL. However, the presence of unavoidable irreversible deformations (particularly dislocations [411, 410]) provide a natural border for $V_c$ which therefore would be limited by the average distance between the physical defects in the VLL. At this point we also recall that the collective

pinning theory involves another characteristic volume $V_b$ of the flux bundle intervening in the plastic flux jumps through the barriers. These two volumes are related to different elastic constants of the VLL.

It is also of interest to note that in the fc-state the current density $J$ is practically zero, since generally $|M_{fc,\,ir}(T, H)| \ll |Mz_{fc,\,ir}(T, H)|$ at $T \ll T_{ir}$. As a consequence, the condition of vortex glass behaviour is reasonably realized. Then, the observation of relaxation effects in $M_{fc}$ measurements leads to some finite effective pinning potential $U_0^* = kT/S$ with $S = -(M_{fc,\,ir})^{-1}(dM_{fc}/d \ln t)$ (see Eq. (13a)). Therefore, this experimental fact is in total contradiction with the vortex glass concept which predicts that the effective potential tends to infinity as $J$ approaches zero.

(3) The magnetic relaxation also shifts from the logarithmic ($\ln t$) to a power law ($t^{-\beta}$) behaviour (but with $0 < \beta \ll 1$). Here too, some of the anomalous effects are connected with the vortex glass phase and hence need more clarifications from the theoretical point of view. Concerning the experimental side, the fact that the exponent $\beta$ is very small makes it very difficult to distinguish between the two possible relaxation laws.

(4) A more important consequence of the theory is that the critical current density would drop exponentially with $T$. As we know, this prediction is in agreement with experimental results. It seems that this approach is more general and more powerful (but also more complex) than the classical flux creep theory. However, from the experimental point of view it is not easy to distinguish between the two theories at present and decide whether the anomalous $J(T)$ drop (with $T$) is due to the collective thermal fluctuations or to spatially extended potential barriers [139-141]. In addition, the effects of $T$, $H$ and $t$ on $M$ are so different from one HTSC family to another (Y, Bi, La...) that it is not certain that they can be described within the same theoretical framework. In fact, it is likely that even for a given oxide the competition between usual flux creep and collective thermal depinning would vary as a function of temperature and field. It is to be added that the predicted exponential drop of $J(T)$ is based on the idea that the pinning is weak. Finally, it is not clear for us how these predictions are affected by plastic deformations of the VLL.

(5) We also strongly believe that the effect of thermal fluctuations are less dramatic for the intrinsic pinning and thus on $J_{ab,\,ab}$. There are at least two arguments supporting this claim : (i) Intrinsic pinning in HTSC is very strong. (ii) The elastic constants controlling the fluctuations of planar vortices (i.e. vortices lying in the *a-b* planes, see Figs. 81c, d) are probably much stiffer than in the configurations governing $J_{ab,\,c}$ and $J_{c,\,ab}$ (Figs. 81a, b). At this point we recall that according to our discussion (§ 7.4 and § 14.3) $J_{ab,\,ab}$ is expected to be deterioreted by any kind of defect, even at low concentrations, in contrast to $J_{ab,\,c}$ and $J_{c,\,ab}$. It is interesting to note that the new scaling approach of Blatter *et al.* [419], which relates the anisotropic properties (such as $J$, $C_{ij}$ etc.) to the isotropic properties, could probably help clarifying these problems.

The question concerning the possible occurrence of a melting transition or a glassy transition in the vortex lattice is of fundamental interest in its own right. Here is a brief outline of this subject : Melting of Abrikosov's vortex lattice has been envisaged long time ago by several authors (Berezinskii [456] and by Fisher [457]) who showed that a solid-liquid transition is favoured considerably in the limit of thin films (conventional superconductors) of thickness much smaller than the London penetration depth. However, for bulk (or three dimensional) conventional superconductors the melting line in the *T-H* plane is very close to the $H_{c_2}(T)$ line and therefore hard to detect.

Nelson [458] examined the case of HTSC in the anisotropic Ginzburg-Landau (G-L) model. He found that the melting temperature $T_m$ is lowered both because of the very high value of

the Landau-Ginzburg parameter $K$ and because of the high temperatures involved in HTSC measurements.

According to several authors and more particularly to Brandt [110, 459] and to Fisher *et al.* [106], the melting temperature $T_m(H)$ deduced by Nelson (in the limit of local elastic approximation) is in fact too high and is drastically reduced (by a factor of order of $[(H/H_{c_1})/(1 - H/H_{c_2})]^{1/2}$) as a result of non local elasticity of the vortex lattice (i.e. due to the $k$-dependence of the elastic moduli). Brandt also showed that the melting transition would be lowered further through the softening of the vortex lattice by flux pinning. Here, too, the experimentally determined line would result from the combination of both thermal fluctuations of the vortices and usual flux jump with a relative weight depending on $T$ and on defect concentrations. At this point it is important to note that contrary to the common belief, pinning of the vortex lines can persist above the melting line in the liquid state [110, 460]. This confirms the need for a simultaneous treatment of the two questions. Markiewicz [176] has recently given an interesting discussion concerning the consequence of the melting transition on the critical current density and the possibility to incorporate such a transition and defects into an extended flux creep model.

The various theories invoked above are more or less based on the anisotropic London theory. Doniach [460], has argued that because of the layered structure of the new high $T_c$ oxides the anisotropic London theory is valid only very close to $T_c$ and breaks down as $T$ is reduced, for $(T_c - T)/T_c$ of the order of $4 \times 10^{-2}$ in the case of YbaCuO and $4 \times 10^{-3}$ in that of BSCCO. According to Doniach, the more correct model of Lawerence and Doniach [461] which assumes weak Josephson coupling between Cu-O layers would further reduce the melting transition line with respect to the above predictions including the nonlocal ones. Physically, this is because the layered structure introduces, in addition to the « entangling » of the individual vortex lines along the $B$ direction predicted first by Nelson [458], reconnections between different lines at higher temperatures. Because of the layered structure the vortices are very soft in the interlayer regions and this can lead to the breaking of the vortex line in smaller slices (« pancake ») of dimension comparable to the lattice constant in the $c$-direction, generally much smaller than the size of the thermally activated nucleation of vortex loops in the G-L theory. This yields soliton like excitations with thermal fluctuations notably different from those of the usual vortex line of dimension equal to that of the specimen.

### 18. General conclusion.

This review was, in part meant to clarify the question of critical current density and magnetic irreversibilities in HTSC, emphasizing the novel properties of these materials. In view of the huge amount of experimental data on the subject, we also tempted to clarify the relationship between the measured critical current density, the experimental conditions and the techniques employed. Most of the analysis was based on the usual concepts of the critical state, but we also considered some specific examples (diffusive limit (Sect. 5.5), very low amplitude of the measuring field (Sect. 13), demagnetizing effects (Sect. 15, . )) where the usual critical state ceases to be valid. We also generalized this state to granular materials and showed the analogy between hysteresis cycle and $a$-$c$ susceptibility measurements. The very complex question of anisotropy was looked at from a somewhat phenomenological point of view. In the last section we referred briefly to the very important question of the theory of thermally activated collective depinning. This topic is rapidly developing at present in particular by theorecians from the Landau Institute in Moscow and is in fact beyond the scope of this review.

We excluded from this paper considerations concerning technical applications, in particular the interesting question relating thermal instabilities, thermal conductivity and specific heat.

Lastly, we believe that the classical experimental techniques examined here, though of fundamental interest, are alone not sufficient to clarify the question concerning the nature of flux depinning and the associated irreversibility line. We believe that other experimental techniques such as direct or indirect visualisation of the vortex lines (for instance *via* improved « Lorentz transmission electron microscopy » or tunneling microscopy) are needed.

Noise measurements, in particular near the irreversibility line, would be also of very great interest. For instance, we suggest that an original and new method could be the use of « microscopic » Hall probs of the order of the dimension of the vortex $\approx \lambda$. This is possible with modern lithography but the main problem is in the fact that the time scales $\tau_v$ involved can be extremely short : $\tau_v \approx \lambda / v_v \approx 10^{-6}$ s for a vortex moving at $v_v \approx 10$ cm/s.

We have also addressed a number of questions, among which that concerning the specific and opposite effects of crystalline and chemical defects on $J_{ab,\,ab}$ on the one hand and on $J_{ab,\,c}$ and $J_{c,\,ab}$ on the other hand, is probably of great importance for possible technical applications.

**Acknowledgments.**

The author is very grateful for stimulating discussions with P. Manuel and C. Aguillon. We thank E. H. Brandt, R. A. Brand and P. Regnier for the critical reading of several sections of the manuscript. I also thank F. Mosbah for his help in preparing some of the figures and Micro-print (9, rue Ferdinand Foureau, 75012 Paris, France) for having assisted us in the numerical calculations.

## Appendix A.

### Comparison of the various supercurrents flowing in type II superconductors.

We wish here to enumerate and compare some of the most characteristic current densities that can exist in type II superconductors.

**A1.** THE LONDON CURRENT. — The simplest case is probably that of the London current density defined for $H \ll H_{c_1}$ by :

$$\mathbf{J}_s = -\frac{c}{4\pi} \nabla \cdot \mathbf{H} \approx \frac{c}{4\pi} \frac{\mathbf{H}}{\lambda} \tag{A1}$$

circulating around the sample in the London penetration depth $\lambda$, as illustrated in the inset of figure 2 for example (typically for $H = H_{c_1}$ and $T \ll T_c$ on has $J_s = 1$ to $5 \times 10^7$ A/cm$^2$).

**A2.** THE CRITICAL CURRENT DENSITIES IN VERY THIN WIRES, FILMS AND NEAR VORTEX CORES. — A second important example concerns the critical currents in the limit where the thickness of the specimen becomes comparable to the coherence length $\xi(T)$. In this case and in the G-L approximation the critical current depends on the applied field and goes through a maximum at $H = H_c$ (the thermodynamic field) :

$$J_{\text{G-L}} \approx \frac{c}{3\sqrt{6}\,\pi} \frac{H_c(T)}{\lambda(T)} \tag{A2}$$

This is comparable (within a factor = 1.8) to that obtained from the London approximation (Eq. (A1)) if one replaces $H$ by $H_c$. Such a current is also comparable to the depairing current at this field (see Tinkham [120] p. 116-118). This current is also almost equal to the maximum surface curren. in the presence of the Bean-Livingston's barrier [445].

It is also of interest to compare the current values given just above with those existing in Abrikosov's vortex lines close to the cores. It is well known (see de Gennes [118] p. 59) that for isolated cylindrical vortex the magnetic field is given by :

$$h(r) \approx \frac{\Phi_0}{2\,\pi\lambda r} K_0(r/\lambda) \tag{A3}$$

where $K_0$ is a zero order Hankel function of imaginary argument which diverges as $r$ approaches zero but which is for physical reasons limited to $\ln(\xi/r)$ as $r$ tends to $\xi$. From Maxwell' equations and making use of the relationship relating $H_{c_1}$ and $H_c$ ($H_{c_1} = H_c \ln(K)/(\sqrt{2}\,K)$ where $K = \lambda/\xi$) we obtain

$$J_{c,\,\mathrm{vor}}(r) \approx \frac{c}{2\,\pi \ln(K)} \frac{H_{c_1}}{r} = \frac{c}{2\sqrt{2}\,\pi K} \frac{H_c}{r} \tag{A4}$$

We can then easily check that for $r \approx \sqrt{2} \times \xi$ (i.e. very close to the vortex core) the supercurrent deduced from equation (A4) is exactly equal to that ($J_{\mathrm{G\text{-}L}}$) obtained from formula (A3). It is now interesting to emphasize that : (i) the existence and the intensities of the above critical current densities require no pinning centres (they arise in perfect materials), (ii) the critical current density is expected to be intrinsically larger in thin wires and thin films than in bulk materials.

According to Larkin and Ovchinnikov [172] and to Geshkenbein *et al.* [462] the usual critical current density $J$ is the highest (neglecting the « phonon » like thermal fluctuations) in the limit of « collective pinning of individual flux lines » and is related to the depairing current $J_d$ by :

$$J \approx J_d(\xi/L_c)^2 \qquad (L_c > \xi)\,. \tag{A5}$$

Here $L_c$ is the correlation length along the vortex direction. $L_c$ depends upon the strength of disorder and on $H$ and $T$ and measures the « longitudinal » dimension of the correlation volume $V_c$. We believe (though we have no rigorous arguments) that equation (A5) is not valid for $L_c \leqslant \sqrt{\lambda\,\xi}$. The qualitative argument is that the critical current $J$ represents an average value of the local currents $J(\mathbf{r} - \mathbf{r}_i)$ induced by all the lines of the vortex lattice located at positions $\mathbf{r}_i$. For vortices located either sides of $\mathbf{r}$ (i.e. for $\mathbf{r}_i$ and $\mathbf{r}_j$ of opposite signs) these currents are of opposite signs. As a consequence, the real current is a strongly and a rapidly oscillating function of $r$, particularly near the vortex cores. In addition, the amplitude of $J(r)$ never exceeds $J_d$. Since the only dimensionless characteristic parameter of the superconductor material is the Guinzburg-Landau parameter $K = \lambda/\xi$ we propose that an upper limit of $J$ is given by

$$J \leqslant \frac{J_d}{K} \approx J_s(H_{c_1}) \tag{A6}$$

or perhaps $J \leqslant J_d \dfrac{\ln(K)}{K}$

Therefore if the dimension of the sample is much larger than $\xi$ and $L_c \leqslant \sqrt{\lambda\,\xi}$, we suggest that the upper limit for $J$ is of the order of the maximum London-Abrikosov current density obtained at $H = H_{c_1}$. It is interesting to pay more theoretical attention to this point.

## Appendix B.

### Units and notations.

Many of the equations reported in this article are written in the so-called practical units in which the magnetization per unit volume is expressed in emu/cm$^3$, the current density in A/cm$^2$ and the magnetic field in Oersted (Oe). These units are obtained from gauss c.g.s. units simply by replacing the velocity of light ($c$) by 10. We have chosen the practical system because it is used extensively in the literature on the magnetic properties (particularly those of the critical current density) of superconducting materials. However in the course of preparation of this article we learned that the practical system is not always so practical and we have been led to use the notations (SI and gauss c.g.s.) as well.

To help the reader who wishes for a more uniform notation, we present a brief correspondence between SI and gauss-c.g.s. units below.

| Quantity | SI | c.g.s. gauss |
|---|---|---|
| Electric field (**E**) | Volt per metre (V/m) | u.e.s. = $3 \times 10^4$ V/m |
| Electric current ($I$) | Ampere (A) | u.e.s. = $\frac{1}{3 \times 10^9}$ A |
| Resistance | Ohm ($\Omega$) | u.e.s. = $9 \times 10^{11}$ $\Omega$ |
| Magnetic flux ($\Phi$) | Weber (W) | Maxwell = $10^{-8}$ Wb |
| Magnetic induction **B** | Tesla | Gauss = $10^{-4}$ Tesla |
| Magnetic field ($H$) | Ampere per metre (A/m) | Oersted = $\frac{10^3}{4\pi}$ A/m |
| Magnetization per unit volume or magnetic intensity (**M**) | Ampere per metre (A/m) | u.e.m. = $10^3$ A/m |
| Total magnetic moment **m** | A.m$^2$ | u.e.m. = $10^{-3}$ A.m$^2$ |
| Bean's formula for cylindrical symmetry | $J = \frac{3M}{R}$ | $\frac{3cM}{R}$ |

*Some useful equations*

| SI | c.g.s. gauss | |
|---|---|---|
| $\mathbf{J} = \sigma . \mathbf{E}$ | | $\sigma$ is the conductivity of the material |
| $\mathbf{M} = \frac{\mathbf{B}}{\mu_0} - \mathbf{H}$ | $M = \frac{B - H}{4\pi}$ | $\mu_0$ is the permeability in vacuum |
| $\mathrm{d}\mathbf{m} = I . \mathrm{d}\mathbf{S}$ | $\mathrm{d}\mathbf{m} = \frac{I}{c}\mathrm{d}\mathbf{S}$ | The magnetic moment of a small circuit of surface d$S$ carrying a current $I$ |
| $\mathbf{F} = e\mathbf{v} \wedge \mathbf{B} + e\mathbf{E}$ | $\mathbf{F} = \frac{e}{c}\mathbf{v} \wedge \mathbf{B} + e\mathbf{E}$ | The force acting on a carrier moving with a velocity $v$ and carrying a charge $e$ |
| $\mathbf{F}_L = e\mathbf{J} \wedge \mathbf{B} + n_n\, e\mathbf{E}$ | $F = \frac{\mathbf{J}}{c} \wedge \mathbf{B} + n_n\, e\mathbf{E}$ | $F_L$ is the force density : $n_n$ is the number of normal electrons per unit volume |
| $\mathrm{Curl}\,\mathbf{H} = \mathbf{J} + \frac{\partial \mathbf{D}}{\partial t}$ | $\mathrm{Curl}\,\mathbf{H} = \frac{1}{c}\left(4\pi\mathbf{J} + \frac{\partial \mathbf{D}}{\partial t}\right)$ | **D** is the electric induction. The associated current is negligible in the experimental conditions considered in this paper |
| $E = -\nabla V - \frac{\partial \mathbf{A}}{\partial t}$ | $E = -\nabla V - \frac{1}{c}\frac{\partial \mathbf{A}}{\partial t}$ | $V$ and $A$ are the electric and the vector potentials respectively |
| $\mathbf{B} = \mathrm{Curl}\,\mathbf{A}$ | $\mathbf{B} = \mathrm{Curl}\,\mathbf{A}$ | |

## References


[1] Bednorz J. G. and Müller K. A., *Z. Phys. B* **64** (1986) 189.

[2] Takagi H., Uchida S., Kitazawa K. and Tanaka S., *Jpn J. Appl. Phys.* **226** (1987) 123.

[3] Chu C. N., Hor P. H., Meng R. L., Gao L., Huang Z. L. and Wang T. Q., *Phys. Rev. Lett.* **58** (1987) 405.

[4] Michel C., Hervieu M., Borel M. M., Gerandin A., Deslands F., Provost J. and Raveau M., *Z Phys. B* **63** (1987) 421.

[5] Maeda H., Tanaka Y., Fikutomi M. F. and Azano T., *Jpn J. Appl. Phys.* **27** (1988) L209.

[6] Hazen R. M., Prewitt C. T., Angel R. J., Ross N. L., Finger L. W., Hadidiacos C. G., Veblen D. R., Heaney P. J., Hor P. H., Meng R. L., Sun Y. Y., Wang Y. Q., Xue Y. Y., Huang Z. J., Gao L., Bechtold J. and Chu C. W., *Phys. Rev. Lett.* **60** (1988) 1174.

[7] SUBRAMANIAN M. A., TORARDI C. C., CALABRESE J. C., GOPALAKRISHNAN J., MORRISSEY K. J., ASHEW T. R., FLIPPEN R. B., CHOWDHRY U. and SLEIGHT A. W., *Science* **239** (1988) 1015.

[8] PARKIN S. S. P., LEE V. Y., ENGLER E. M., NAZZAL A. I., HUANG T. C., GORMAN G., SAVOY R. and BEYERS R., *Phys. Lett.* **60** (1988) 2539.

[9] SHENG Z. Z. and HERMANN A. M., *Nature* **332** (1988) 55.

[10] HAZEN R. M., FINGER L. W., ANGEL R. J., PREWITT C. T., ROSS N. L., HADIDIACOS C. G., HEANEY P. J., VEBLEN D. R., SHENG Z. Z., EL ALI A. and HERMANN A. M., *Phys. Rev. Lett.* **60** (1988) 1657.

[11] PARKIN S. S. P., LEE V. Y., NAZZAL A. I., SAVOY R., BEYERS R. and LAPLACA S. J., *Phys. Rev. Lett.* **61** (1978) 750.

[12] CAVA R. J., BATLOGG B., KRAJEWSKI J. J., RUPP L. W., SCHNEEMEYER L. F., SEIGRIST T., VAN DOVER R. B., MARSH P., PECK W. F., Jr., GALLAGHER P. K., GHARUM S. H., MARSHALL J. H., FARROW R. C., WASZCZAK J. V., HULL R. and TREVOR P., *Nature* **336** (1988) 211.

[13] OUSSÉNA M., SENOUSSI S., COLLIN G., *Europhys. Lett.* **4** (1987) 625.

[14] CHAUDHRARI P., KOCH R. H., LAIBOWITZ R. B., MC GUIRE T. R. and GAMBINO R. J., *Phys. Rev. Lett.* **58** (1987) 2684.

[15] POPPE U., SHUBERT J., ARONS R. R., EVERS W., FREIBURG C. H., REICHERT W., SCHMIDT K., SYBERTZ W. and URBAN K., *Solid State Commun.* **66** (1988) 661.

[16] XI X. X., LINKER G., MEYER O., NOLD E., OBST B., RATZEL F., SMITHEY R., STREHLAN B., WESCCHEN-FELDER F. and GEERK J., *Z. Phys. B* **74** (1989) 13.

[17] XIONG G. C. and WANG S. Z., *Appl. Phys. Lett.* **55** (1989) 902.

[18] JOSEPHSON B. D., *Adv. Phys.* **14** (1965) 419 (review article) ; *Phys. Rev. A* **152** (1966) 211 ; *Rev. Mod. Phys.* **46** (1974) 251 (Nobel prize lecture).

[19] CAMPBELL A. M. and EVETTS J. E., *Adv. Phys.* **21** (1972) 119.

[20] SENOUSSI S., OUSSENA M., COLLIN G. and CAMPBELL I., *Phys. Rev. B* **37** (1988) 9792.

[21] LABORDE O., THOLENCE J. L., LEJAY P., SULPICE A., TOURNIER R., CAPPONI J. J., MICHEL C., PROVOST J., *Solid State Commun.* **63** (1988) 877.

[22] KES P. H., VAN DEN BERG J., VAN DER BEEK C. J., MYDOSH J. A., ROAELAND L. A., MENOVESKY A. A., KADOWAKI K. and de BOER F. R., Proc. of the 1st Latino-American Conference on High Temp., Superconductivity, Brazil, 4-6 Mai (1988) ; (World Scientific Co, Singapore) p. 239.

[23] FANG M. M. FINNEMORE D. K., FARRELL D. E. and BANSAL N. R., *Cryogenics* **29** n 3A (supplément) (1989) p. 347.

[24] NAITO M., MATSUDA A., KITAZAWA K., KAMBE S., TANAKA I., KOJIMA H., *Phys. Rev. B* **41** (1990) 4823.

[25] AGUILLON C., MC CARTNEY D. G., REGNIER P., SENOUSSI S., TATLOCKT G. J., *J. Appl. Phys.* **69** (1991) 8261.

[26] MÜLLER K. A., TAKAKASHIGA M. and BEDNORZ J. G., *Phys. Rev. Lett.* **58** (1987) 1143.

[27] WORTHINGTON T. K., GALLAGHER W. J. and DINGER T. R., *Phys. Rev. Lett.* **59** (1987) 1160 ; WORTHINGTON T. K., YESHURUN Y., MALOZEMOFF A. P., ANDROFSKI R. M. Y., HOLTZBERG F. H. and DINGER T. R., *J. Phys. France Colloq.* **C 8** (1988) 2093.

[28] MOTA A. C., POLLINI A., VISANI P., MÜLLER K. A. and BEDNORZ J. G., *Phys. Rev. B* **36** (1987) 401.

[29] YESHURUN Y. and MALOZEMOFF A. P., *Phys. Rev. Lett.* **60** (1988) 2202.

[30] MALOZEMOFF A. P., KRUSIN-ELBAUM L., CRONEMEYER D. C., YESHURUN Y. and HOLTZBERG F., *Phys. Rev. B* **38** (1988) 6490.

[31] YESHURUN Y., MALOZEMOFF A. P., HOLTZBERG F., 4th Joint MMM-Inter. Conf. Vancouver, July 12-15, 1988, *J. Appl. Phys.* **64** (1988) 5797.

[32] DE SANTOLO A. M., MANDICH M. L., SUNSHINA S., DAVISON B. A., FLEMING R. M., MARSH P. and KOMETANI T. Y., *Appl. Phys. Lett.* **52** (1988) 1995.

[33] TUOMINEN M., GOLDMAN A. M. and MCCARTNEY M. L., *Phys. Rev. B* **37** (1988) 548.

[34] KES P. H., BERGHUIS P., GUO S. Q., DAM B. and STALLMAN G. M., *J. Less Comm. Metals* **151** (1989) 325.
[35] KUPFER H., APFELSTEDT I., SHAUER W., FLUKIGER R., MEIER-HIRMER R., WUHL H., *Z. Phys. B* **69** (1987) 159.
[36] PATERNO G., ALVANI C., CASADIO S., GAMBARDELLA U. and MARITATO L., *IEEE Trans. Magn.* **25** (1989) 2276.
[37] FANGI M. M., FINNEMORE D. K., FARELL D. E. and BANSAL N. R., *Cryogenics* **29** (1989) 347.
[38] MC HENRY M. E., MALEY M. P. and WILLIS J. O., *Phys. Rev. B* **40** (1989) 2666.
[39] XIA J. S., SUN S. F., ZHANG T., CAO L. Z., ZHANG Q. R., CHEN J. and CHEN Z. Y., *Physica C* **158** (1989) 477.
[40] KWASNITZA K. and WIDNER Ch., *Physica C* **171** (1990) 211.
[41] Zhou Bing, Qiu Jingwu, Tang Zhiming Miao Baicai and Qian Yongjia, *Int. J. Mod. Phys. B* **1** (1987) 521.
[42] CRABTREE G. W., LUI J. Z., UMEZAWA A., KWOK W. K., SOWERS C. H., MALIK S. K., VEAL B. W., LAM D. J., BRODSKIY M. B. and DOWNEY J. W., *Phys. Rev. B* **36** (1987) 4021.
[43] ENOMOTO Y., MURAKAMI T., SUZIKI M. and MORIWAKI K., *Jpn J. Appl. Phys.* **26** (1987) L1266.
[44] DINGER T. R., FEILD C. and HOLTZBERG F., *Phys. Rev. Lett.* **62** (1989) 827.
[45] WELP U., KWOK W. K., CRABTREE G. W., VANDER-VOORT K. G. and LIU J. Z., *Phys. Rev. Lett.* **62** (1989) 1908.
[46] DOLAN G. J., HOLTZBERG F., FEILD C. and DINGER T. R., *Phys. Rev. Lett.* (1989) 2184.
[47] DINGER T. R., WORTHINGTON T. K., GALLAGHER W. J. and SANDSTROM R. L., *Phys. Rev. Lett.* **58** (1987) 2687.
[48] NAUGHTON M. J., YU R. C., DAVIES P. K., FISCHER J. E., CHAMBERLIN R. V., WANG Z. Z., JING T. W., ONG N. P. and CHAIKIN P. M., *Phys. Rev. Lett.* **59** (1987) 1160.
[49] WORTHINGTON T. K., GALLAGHER W. J. and DINGER T. R., *Phys. Rev. Lett.* **59** (1987) 1160.
[50] SENOUSSI S. and AGUILLON C., *Europhys. Lett.* **12** (1990) 273.
[51] KES P. H., VINOKUR V. M. and VAN DER BEEK C. J., *Phys. Rev. Lett.* **64** (1990) 1063.
[52] FRUCHTER L., AGUILLON C., SENOUSSI S. and CAMPBELL I. A., *Physica C* **160** (1989) 185.
[53] JANOSSY B., HERGET R. and FRUCHTER L., *Physica C* **170** (1990) 22.
[54] FARRELL D. E., WILLIAMS C. M., WOLF S. A., BANSAL N. P. and KOGAN V. G., *Phys. Rev. Lett.* **61** (1988) 2805.
[55] FARRELL D. E., BONHAM S., FOSTER J., CHANG Y. C., JIANG P. Z., VANDERVOOST K. G., LAM D. J. and KOGAN V. G., *Phys. Rev. Lett.* **63** (1989) 782-785.
[56] GYORGY E. M., DOVER R. B., JACKSON K. A., SCHNEEMEYER L. F. and WASZCZAK J. V., *Appl. Phys. Lett.* **55** (1989) 238.
[57] CRONEMEYER D. C., MCGUIRE T. R., MALOZEMOFF A. P., HOLSBERG F., GAMBINO R. J., CONNER L. W. and MCELFRESH M. W., Conf. On Transp. Prop. of Superconductors at Rio de Janeiro 1990), ed. R. Nicolsky (World Scientific Co. Singapore) to be published.
[58] ROAS B., SCHULTZ L. S. and ENDRES G., *Appl. Phys. Lett.* **53** (1988) 1557.
[59] ROSA B., SCHULTZ L. and SAEMANN-ISCHENKO G., *Phys. Rev. Lett.* **64** (1990) 479.
[60] RAFFI H., LABDI S., LABORDE O. and MONCEAU P., *Physica B* **165-166** (1990) 1423.
[61] RAFFI H., LABDI S., LABORDE O., MONCEAU P., *Superconducting Sci. Technol.* **4** (1991) S100.
[62] KOGAN V. G. and CLEM J. R., *Japan J. Appl. Phys.* **26** (1987) 1159.
[63] KWOK W. K., WELP U., CRABTREE G. W., VANDERVOOST K. G., HULSCHER R. and LIU J. Z., *Phys. Rev. Lett.* **64** (1990) 966.
[64] RICE J. P., GINSBERG D. M., RABIN M. W., VANDERVOORT K. G., CRABTREE G. W. and CLAUS H., *Phys. Rev. B* **41** (1990) 6532.
[65] KLEMM R. A. and CLEM J. R., *Phys. Rev. B* **21** (1980) 1886.
[66] KLEMM R. A., *Phys. Rev. B* **38** (1988) 6641.
[67] KOGAN V. G., *Phys. Rev. B* **24** (1981) 1572 and 2497.
[68] CAMPBELL L. J., DORIA M. N. and KOGAN V. G., *Phys. Rev. B* **38** (1988) 2439.
[69] BALATSKII A. V., BURLACHKOV L. I. and GORKOV L. P., *Sov. Phys. J.E.T.P.* **63** (1986) 866.
[70] SCHPOHL N. and BARATOFF A., *Physica C* **153-155** (1988) 689.
[71] FIETZ W. A. and WEBBS W. W., *Phys. Rev.* **178** (1969) 657.

[72] BEAN C. P., (a) *Phys. Rev. Lett.* **8** (1962) ; (b) *Rev. Mod. Phys.* **36** (1964) 31.
[73] EVETTS E. and GLOACKI B. A., *Cryogenics* **28** (1988) 641.
[74] ANDERSON P. W. a, *Phys. Rev. Lett.* **9** (1962) 309a.
[75] FRIEDEL J., de GENNES P. G. and MATRICON J., *Appl. Phys. Lett.* **2** (1963) 119.
[76] SILOX J. and ROLLINS R. W., *Appl. Phys. Lett.* **2** (1964) 237 ; *Rev. Mod. Phys.* **36** (1963) 52.
[77] SENOUSSI S., AGUILLON C. and MANUEL P., *Physica C* **175** (1991) 202 (a) ; SENOUSSI S., AGUILLON C. and HADJOUDJ S., ibid **215** (b).
[78] a) ABRIKOSOV A., *Zh. Eksp. Theor. Fix* **32** (1957) 1442 ; translated by *Sov. Phys. J.E.T.P.* **5** (1957) 1174 ; b) Fundamentals of The Theory of Metals (Elsevier Science Publishers B.V., 1988), Amsterdam The Netherlands.
[79] LIVINGSTON J. D., *Phys. Rev.* **129** (1963) 1943.
[80] BUZDIN I. A. and SIMONOV A. Yu., *Physica C* **175** (1991) 143.
[81] BUZDIN I. A. and SIMONOV A. Yu., *Physica B* **165-166** (1990) 110.
[82] HAO Z., CLEM J. R., MCELFRESH M. W., CIVALE L., MALOZEMOFF A. P. and HOLTZBERG F., *Phys. Rev. B* **43** (1991) 2844.
[83] HAO Z. and CLEM J. R., *Phys. Rev. Lett.* **67** (1991) 2371.
[84] SHINDÉ S. L., MORVILL J., GOLAND D., CHANCE D. A. and MC GUIRE T., *Solid. State Commun.* **69** (1989) 367.
[85] MURPHY S. D., RENOUARD K., GUTTENDEN R. and BHAGAT S. M., *Solid. State Commun.* **69** (1989) 367.
[86] NIKOLO M. and GOLDFARB R. B., *Phys. Rev.* **339** (1988) 6615.
[87] PALSTRA T. T. M., BATLOGG B., VAN DOVER R. B., SCHNEEMEYER L. F. and WASZCZAK J. V., *Phys. Rev. B* **41** (1989) 6621.
[88] LUDWIG F., FORSTHUBER M., HILSCHER G., KIRCHMAYR H., HERRMANN R., *Physica C* **177** (1991) 401.
[89] DOU S. X., LIU H. K., WANG J. and SONG K. H., *Physica C* **171** (1990) 293.
[90] SAVIDES N., COLLOCOTT S. J., ANDRIKIDIS C., MÜLLER K. H., VANCE E. R., *Physica C* **171** (1990) 181.
[91] GOLDFARB R. B., CLARK A. F., BRAYINSKI A. I. and PANSON A. J., *Cryogenics* **27** (1987) 495 ; GOLDFARB R. B., CLARK A. F., *IEEE Tran may,* May **21** (1986) 332.
[92] KÜPFER H., APFELSTEDT I., FLÜKIGER R., KELLER C., MEIER-HIRMER R., RUNTSCH B., TUROWSKI A., WIECH U. and WOLF T., *Cryogenics* **28** (1988) 650.
[93] GÖMÖRY F. and LOBOTKA P., *Solid State Commun.* **66** (1988) 654.
[94] LOGEL B., BOLMONT D. and MEHDAOUI A., *Physica C* **159** (1989) 816.
[95] MAEDA A., HASE M., TSUKADA I., NODA K., TAKABAYASKI S. and UCHINOKURA K., *Phys. Rev. B* **41** (1990) 6418.
[96] SENOUSSI S., OUSSÉNA M. and HADJOUDJ S., *J. Appl. Phys.* **63** (1988) 4176.
[97] SENOUSSI S., OUSSÉNA M., BIERI J. B., ARABSKI J. and REICH R., Progress HTS, Vol. **9** ed R. Nicolsky (World Scientific Publishing Co. Singapoure, 1989) p. 127.
[98] SENOUSSI S., AGUILLON C., OUSSÉNA M. and TREMBLAY P., *J. Phys. France Colloq.* c8, **49** (1989) 2099.
[99] OSAMURA V., TAKAYAMA T. and OCHIOI S., *Supercond. Sci. Technol.* **2** (1989) 111.
[100] WONG D., STAMPER A. K., STANCIL D. D. and SCHLESINGER T. E., *Appl. Phys. Lett.* **53** (1988) 240.
[101] NARWANKAR P. K., CHANDRACHOOD M. R., MORRIS D. E. and SINHA A. P. B., *Appl. Phys. Lett.* **58** (1991) 651.
[102] STEPANKIN V., PROTASOV E. A., KUZNETSOV A. V., ZAITSEV-ZOTOV S. V., *JETP Lett.* **41** (1985) 23.
[103] BORIK M., CHERNIKOV M., IVANOV P., ISTEPANKIN V., OSIKO V. and VESELAGO V., *Physica C* **162** (1989) 727.
[104] SENOUSSI S., AGUILLON C. and HADJOUDJ S., ICMAS-90 (17-19 October 1990 (Grenoble, France) Edit. IITT Int. ; page 159.
[105] LIKHAREV K. K., *Rev. Mod Phys.* **51** (1979) 101.
[106] FISHER D. S., FISHER M. P. A. and HUSE D. A., *Phys. Rev. B* **43** (1991) 130.

[107] MANUEL P., Conférence de la Société des Electriciens et des Electroniciens (SEE) held in Paris, October 1987.
[108] MALOZEMOFF A. P. in « Physical Properties of High Temperature Superconductors-I », ed D. M. Ginsberg, World Scientific Singapour (1989) page 71.
[109] THOLENCE J. L., SAINT-PAUL M., LABORDE O., MONCEAU P., GUILLOT M., NOËL H., LEVET J. C., POTEL M., PADIOU J. and GOUGEON P., to appear in « Studies of High Temperature Superconductors » (NOVA Science Publishers Inc., New York) Ed. A. V. No.
[110] BRANDT E. H., *J. Mod. Phys. B* **5** (1991) 751 (a) ; *Physica C* **162-164** (1989) 1167 (b).
[111] FISANICK G. J., AIP Conf. Proc. **182** (1988), 180 (Atlanta).
[112] EKIN J. W., *Appl. Phys. Lett.* **55** (1989) 905.
[113] GOODRICH L. F. and BRAY S. L., *Cryogenics* **30** (1990) 667.
[114] GUPTA A., ESQUINAZI P., BRAUN H. F., GERHAUSER W., NEUMÜLLER H. W., HEINE K. and TENBRINK J., *Europhys. Lett.* **10** (1989) 663.
[115] HAMPSHIRE D. P., LARBALESTIER D. C., *IEEE Trans. Magn.* **25** (1989) 1956.
[116] HÜPFER H., KELLER C., MEIER-HIRMER R., SALAMA K., SELVAMANIKAM V., TARTAGLIA G. P., *IEEE Trans. Magn.* **27** (1989) 1369.
[117] YAMADA Y., NOMURA S., ANDO K. and HORIGAMI O., *Cryogenics* **30** (1990) 643.
[118] DE GENNES P. G., in « Superconductivity of Metals and Alloys, W. A. Benjamin Incorporat, New York (1966), p. 69.
[119] DE GENNES P. G., MATRICON J., *Rev. Mod. Phys.* **36** (1964) 45.
[120] TINKHAM M., « Introduction to Superconductivity », Ed. Robert E. Krieger (Publishing Comp. Malabar, Florida) p. 152.
[121] KRAMERS H. A., *Physica* **7** (1940) 284.
[122] FEIGEL'MAN M. V. and VINOKUR V. M., *Phys. Rev.* **B 41** (1990) 8986.
[123] COFFEY M. W. and CLEM J. R., *Phys. Rev. Lett.* **67** (1991) 386.
[124] SENOUSSI S., AGUILLON-LEVILLAIN C., MOSBAH F. and REGNIER P., Proceedings of the International Workshop On Critical Current limits, Worsow Poland (Sept. 1991) ; To be published by World Scientific (Singapore) 1992.
[125] MARTINOLI P., FLUECKIGER Ph., MARSICO V., SRIVASTAVA P. K., LEEMANN Ch. and GALIVANO J. L., *Physica* **165-166B** (1990) 1163.
[126] LABUSCH R., *Phys. State Solids* **19** (1967) 715 ; *Cryst. Lattice Defects* **1** (1969) 1 ; *Phys. Lett.* **22** (1969) 9.
[127] WORDENWEBER R. and KES P. H., *Cryogenics* **29** (1989), 321.
[128] ANDERSON P. W. and KIM Y. B., *Rev. Mod. Phys.* **36** (1962) 39.
[129] BEASLEY M. R., LABUSCH R. and WEBB W. W., *Phys. Rev. B* **181** (1969) 682.
[130] XU Y., SUENAGA M., MOODENBANGH A. R. and WELCH D. U., *Phys. Rev. B* **40** (1989) 10882.
[131] SUN J. Z., CHAR K., HAHN M. R., GEBALL T. H., KAPITULNIK A., *Appl. Phys. Lett.* **54** (1989) 663.
[132] LI J. N., KADOWAKI K., MENKEN M. J. V., MENOVSKY A. A., FRANSE J. J. M., *Physica C* **161** (1989) 313.
[133] KAMBE S., NAITO M., KITAZAWA K., KOJIMA H., *Physica C* **160** (1989) 243.
[134] XUE Y. Y., HOR P. H., CHU C. W., *Physica C* **176** (1991) 195.
[135] HAGEN C. W. and GRIESSEN R., Thermally activated Magnetic Relaxation in High-Tc Superconductors in studies of High Temperature Superconductors, Ed. A. V. Narlikar, *NOVA Sc. Publ.* (1989).
[136] HAGEN C. W., GRIESSEN R. P. and SALOMONS E., *Physica C* **157** (1989) 199 ;
HAGEN C. W. and GRIESEN R., *Phys. Rev. Lett.* **62** (1989) 2857 ;
GRIESSEN R., *Phys. Rev. Lett.* **64** (1990) 1674.
[137] GESHKENBEIN V. B. and LARKIN A. I., *Zh. Eksp., Teor. Fiz.* **95** (1989) 1108 ; *Sov. Phys. JETP* **68** (1989) 639.
[138] NEEL L., EVETTS J. E., *Europhys. Lett.* **15** (1991) 453.
[139] MANUEL P., AGUILLON C. and SENOUSSI S., *Physica C* **177** (1991) 281.
[140] ZELDOV E., AMER N. M., KOREN G., GUPTA A., MCELFRESH M. W. and GAMBINO R. J., *Appl. Phys. Lett.* **56** (1990) 680.

[141] ZELDOV E., AMER N. M., KOREN G. and GUPTA A., *Appl. Phys. Lett.* **56** (1990) 1700.
[142] FEIGEL'MAN M. V., GESHKENBEIN V. B. and LARKIN A. I., *Physica C* **167** (1990) 177.
[143] NEEL L., EVETTS J. E., *Europhys. Lett.* **15** (1991) 453.
[144] MOTA A. C., POLLINI A., VISANI P., MÜLLER K. A. and BEDNORZ J. G., *Physica Scripta* **37** (1988) 823.
[145] HAMZIC A., FRUCHTER L. and CAMPBELL I. A., *Nature* **345** (1990) 515.
[146] BLATTER G., GESHKENBEIN V. B. and VENOKUR V. M., *Phys. Rev. Lett.* **66** (1991) 3297 (a) ; BLATTER G., GESHKENBEIN V. B. (preprint).
[147] FISHER M. P. A., TOKUYASU T. A. and YOUNG A. P., *Phys. Rev. Lett.* **66** (1991) 2931.
[148] MALEY M. P., WILLIS J. O., LESSURE H. and MCHENRY M. E., *Phys. Rev. B* **42** (1990) 2639.
[149] HART H. R., LUBORSKY Jr. F. E., ARENDT R. H., FLEISCHER R. L., TKACZYK J. E. and ORSINI D. A., *IEEE Trans. Magn.* **27** (1991) 1375.
[150] HSU H. W., CHEN Y. C., CHEN K. and LEE W. H., *Solid. State Commun.* **77** (1991) 843.
[151] WEIR S. T., *Solid. State Commun.* **77** (1991) 839.
[152] ROSSEL C., SANDVOLD E., SERGENT M., CHEVREL R. and POTEL M., *Physica C* **165** (1990) 233.
[153] FRUCHTER L., AGUILLON C. and CAMPBELL I. A., *Phys. Rev. B* **42** (1990) 2627.
[154] AGUILLON-LEVILLAIN C. *et al.* submitted to *Physica C.*
[155] OUSSÉENA M., unpublished.
[156] LICHTENBERGER K. S., SANDERS S. C., FINNEMORE D. K., *IEEE Trans. Magn.* **27** (1991) 1387.
[157] MOSCHALKOV V. V., ZHUKOV A. A., KUZNETSOV V. D., METLUSLIKO V. V. and LEONYUK L. I., *JETP Lett.* **50** (1989) 92.
[158] LESSURE H. S., SIMIZU S. and SANKAR S. G., *Phys. Rev. B* **40** (1990) 5165.
[159] REISSNER M., AMBROSCH R., STEINER W. and SCHAFFARICH P., LT-19 Brighton (1990).
[160] CAMPBELL I. A., FRUCHTER L. and CABANEL R., *Phys. Rev. Lett.* **64** (1990) 1561.
[161] PALSTRA T. T. M., BATLOGG B., SCHEEMEYER L. F. and WASZCZAK J. V., *Phys. Rev. Lett.* **64** (1990) 3090.
[162] HUDSON P. A., YIN F. C. and JONES H., *IEEE Trans. Magn. Mag.* **17** (1981) 1649.
[163] HUDSON P. A., YIN F. C. and JONES H., *IEEE Trans. Magn. Mag* **17** (1983) 903.
[164] HAMPSHIRE D. P., JONES H. and MITCHELL E. J. W., *IEEE Trans. Magn. Mag.* **21** (1985) 289.
[165] TURCHINSKAYA M. J., ROYTBURD A. L., BENNETT L. H., SWARTZENDRUBER L. J. and SAWANO K., *Physica C* **182** (1991) 297 ; see also [15] of this reference.
[166] THOMPSON J. R., SUN Y. R., HOLTZBERG F., CAMPBELL I. A., *Phys. Rev. B* **44** (1991) 403.
[167] MOTA A. C., VISANI P. and POLLINI A., *Phys. Rev. B* **37** (1988) 9830.
[168] MITIN A. V., EKSP Zh, *Theor. Fiz.* **93** (1987) 590 ; *Sov. Phys. JETP* **66** (1987) 335.
[169] MATSUSHITA T., OTABE E. S., MATSUNO T., MURAKAMI M., KITAZAWA K., *Physica C* **170** (1990) 375.
[170] HETLINGER D., SWANSON A. G., SKOEPOL W. J., BROOKS J. S., GRAYBEAL J. M., MANKIEWICH P. M., HOWARD R. E., STRAUGHN B. L. and BURKHARARDT E. G., *Phys. Rev. Lett.* **62** (1989) 2044.
[171] MALOZEMOFF A. P., WORTHINGTON T. K., ZELDOV E., YEH N. C., MC ELFRESH M. W. and HOLTZBERG F., Springer Ser. in Physics-Strong correlation and Superconductivity, Eds. H. Fukuyama, S. Maekawa and A. P. Malozemoff (Springer-Verlag, Heidelberg, 1989) p. 349-360.
[172] LARKIN A. I., OVCHINNIKOV Yu. N., *J. Low Temp. Phys.* **34** (1979) 409.
[173] FEIGEL'MAN M. V., VINOKUR V. M., *Phys. Rev. B* **41** (1990) 8986.
[174] FEIGEL'MAN M. V., GESHKENBEIN V. B., LARKIN A. I., VINOKUR V. M., *Phys. Rev. Lett.* **63** (1989) 2303.
[175] GESHKENBEIN V. B., LARKIN A. I., *Zh ETF* **95** (1989) 1108.
[176] MARKIEWICZ R. S., *Physica C* **171** (1990) 479.
[177] GAMMEL P. L., SCHEEMEYER L. F., WASZCZAK J. V. and BISHOP D. J., *Phys. Rev. Lett.* **61** (1988) 1666.
[178] BRANDT E. H., ESQUINAZI P. and WEISS G., *Phys. Rev. Lett.* **62** (1989) 2330.
[179] TINKHAM M., *Phys. Rev. Lett.* **61** (1988) 1658.

[180] PALSTRA T. T. M., BATLOGG B., SCHEEMEYER L. E. and WASZCZAK J. V., *Phys. Rev. Lett.* **61** (1988) 1662 ; *Appl. Phys. Lett.* **54** (1989) 763.
[181] BARDEN J. and STEPHEN M. J., *Phys. Rev.* **140A** (1965) 1197.
[182] LEBWOHL P. and STEPHEN M. J., *Phys. Rev.* **163** (1967) 376.
[183] CLEM J. R. and COFFEY M. W., *Phys. Rev.* **B 42** (1990) 6209.
[184] CAROLI C., DE GENNES P. G. and MATRICON J., *Phys. Lett.* **9** (1964) 307.
[185] BARDEN J., KUMMEL R., JACOBS A. E. and TEWORDT L., *Phys. Rev.* **187** (1969) 556.
[186] LIN T. X., ZHANG J. L., WANG S. Z., XIONG G. C. and YIN D. L., *J. Less. Comm. Met.* **164, 165** (1990) 1408.
[187] GROSS R., HIPLER K., MANHART J., HUEBENER R. P., CHAUDARI P., DIMOS D., TSUEI C. C., SCHUBERT J. and POPPE U., *Appl. Phys. Lett.* **55** (1989) 2132.
[188] BUDHANI R. C., WELCH D. O., SUENAGA M. and SABATINI R. L., *Phys. Rev. Lett.* **64** (1990) 1666.
[189] DEVRIES J. W. C., STOLMAN G. M. and GIJS M. A. M., *Physica C* **157** (1989) 406.
[190] KOCH R. H., FOGLIETTI V., GALLAGHER W. J., COREN G., GUPTA A. and FISHER M. P. A., *Phys. Rev. Lett.* **63** (1989) 1511.
[191] XIONG G. C., WANG S. Z., WANG F. R., JIANG Q. D., YIN B., LI C. Y. and YIN D. L., *J. Less Common. Met.* **164, 165** (1990) 1316.
[192] NICOLSKY R., *Cryogenics* **29** (1989) 388 ;
KÜMMEL R., GUNSCENHEIMER V., NICOLSKY R., *Phys. Rev. B* **42** (1990) 3992.
[193] ANDREEW A. F., *Sov. Phys. JETP* **19** (1964) 1228.
[194] KES P. H., AARTZ J., VAN DEN BERG J., VAN DEN BEEK C. J. and MYDOSH J. A., *Supercond. Sci. Technol.* **1** (1989) 242.
[195] CLEM J. R., KERCHER H. R. and SEKULA T. S., *Phys. Rev.* **B14** (1976) 1893.
[196] BERGHUIS P. and KES P. H., *Physica B* **165-166** (1990) 1169.
[197] DEW-HUGHES D., Proceedings Int. Conf. on Transp. Properties of Superconduct., April-May (1990), Rio de Janeiro (Brasil) (World Scientific, Singapore).
[198] MAURY R., Thesis, Université Paul Sabatier Toulouse, France (1991).
[199] KOPPÉ H., *Phys. State Solids* **17** (1966) K229.
[200] a : KIM Y. B., HEMPSTEAD C. F. and STRAID A. R., *Phys. Rev. Lett.* **9** (1962) 306 ;
b : *Phys. Rev.* **129** (1963) 528 ;
c : *Rev. Mod. Phys.* **36** (1964) 43.
[201] MOSCHALKOV V. V., ZHUKOV A. A., PETROV D. K., VORONKOVA V. I. and YANOVSKU V. K., *Physica C* **166** (1990) 185.
[202] MOSCHALKOV V. V., ZHUKOV A. A., KUZNETSOV V. D., MELLUSHKO V. V. and LEONYUK L. I., *Pisma Zh. Eksp. Teor. Fiz.* **50** (1989) 81.
[203] QUITMAN C., EBELS U., SPLITTGERBER P. C., HÜNNEKES, GUNTHERODT G., *Physica B* **165-166** (1990) 1143.
[204] ECKSTEIN J. N. and BOZOVIC I., *Appl. Phys. Lett.* **57** (1990) 1049.
[205] GIERLLOWSKI P., GORECKA J., SOBOLEWSKI R. and LEWANDOWSKI S. J., *Physica B* **165-166** (1990) 1485.
[206] TAI M. F., TU Y. K. and JOU I. C., *Physica B* **165-166** (1990) 1401.
[207] MORRIS D. E., CHANDRACHOOD M. R. and SINHA A. P. B., *Physica C* **175** (1991) 156.
[208] HARMANN A. M., DUAN H., KIEHL W., YUAN LIULI L. S., DIAM-LIN Z., AIP Conf. Proc. (USA) **219** (1991) 364.
[209] MALEY M. P., VOGT G. J., PHILIPS D. S., GOULTER J. Y., ARENDT P. N., ELLIOT N. E., *IEEE Trans. Magn.* **27** (1991) 1137.
[210] LIOU S. H., CHAN V. K., FOONG F., LEE W. Y., GOU Y. S. and UEN T. M., *IEEE Trans. Magn.* **27** (1991) 1227.
[211] SATO K., HIKATA T., MUKAI H., UEYMA M., SHIBUTA N., KATO T., MASUDRA T., NAGATA M., IWATA K., MITSUI M., *IEEE Trans. Mag.* **27** (1991) 1231.
[212] TENBRENK J., WILHELM M., HEINE K., KRANTH H., *IEEE Trans. Magn.* **27** (1991) 1239.
[213] KOPYLOV V. N., KOSHELEV A. E., SCHEGOLEV I. F. and TOGONIDZE T. G., *Physica C* **170** (1990) 291.

[214] CHEN C. H., CHEONG S. W., WERDER D. J., COOPER A. S. and RUPP L. W. Jr., *Physica C* **175** (1991) 301.

[215] NAITO M., MATSUDA A., KITAZAWA K., KAMBE S., TANAKA I., KOJIMA H., *Phys. Rev. B* **41** (1990) 4823.

[216] KHISHIOL K., NAKATANIL K., KITAZAWA K., TANAKA I., KOJIMA H. and YAMAFUJI K., Proc. 3rd Int. Symp. Superconductivity (ISS '90), (Nov. 6-9, 1990), Sendai, Japan, to be published in Springer-Verlag, Tokyo.

[217] SIEGRIST T., SCHNEEMEYER L. F., WASZCZAK J. V., SINGH N. P., OPILA R. L., BATLOGG B., RUPP L. W. and MURPHY D. W., *Phys. Rev. B* **36** (1987) 8356.

[218] TARASCON J. M., BARBOUX P., HULL G. W., RAMESH R., GREENE L. H., GIROUD M., HEGDE M. S. and MCKINNON R., *Phys. Rev. B* **39** (1989) 4316.

[219] WEINBERGER B. R., LYNDS L., PORREPKA D. M., SNOW D. B., BURIKA C. T., EATON H. E. Jr. and APOLLI, *Physica C* **161** (1989) 91.

[220] SEN S., CHEN I., CHEN C. H. and STEFANESCU D. M., *Appl. Phys. Lett.* **64** (1989) 766.

[221] MASUDA H., MIZUNO F., HIRAHAYASHI I. and TANAKA S., *Jpn J. Appl. Phys.* **28** (1989) L-1226.

[222] OKAI B., KOSUGE M., TAHAHASHI K. and OTHTA M., *Jpn J. Appl. Phys.* **27** (1988) L-1843.

[223] DOU S. X., GUO S. J., LUI H. K. and SASTERLING K. E., *Supercond. Sci. Technol.* **2** (1989) 380.

[224] WAGENER T. J., GAO Y., VITOMIROV I. M., ALDAO C. M., JOYCE J. J., CAPASSO C., WEAVER J. H., CAPONE D. W., II, *Phys. Rev. B* **38** (1988) 232.

[225] TARASCON J. M., BARBOUX P., MICELI P., GREENE L. H., HULL G. W., EIBSCHUTZ M. and SUNSHINE S. A., *Phys. Rev. B* **37** (1988) 7458.

[226] XIAO G., CIEPLAK M. Z., GAVRIN A., STREITZ F. H., BAKSHAI A. and CHIEN C. L., *Phys. Rev. Lett.* **60** (1988) 1446.

[227] JAYARAM B., AGARWAL S. K., RAO C. V. N. and NARLIKAR A. V., *Phys. Rev. B* **38** (1988) 2903.

[228] HILSCHER G., PÖLINGER S., FORSTHUBER M., PILLMAYR N., REMSCHNIG K., ROGEL P., REISSNER M., STEINER W., *Physica C* **167** (1990) 472.

[229] ODA Y., FUJITA H., TOYODA H., KANEKO T., KOHARA T., NALADA I. and ASAYAMA K., *Jpn J. Appl. Phys.* **26** (1987) L-1660.

[230] SHIMAKAWA Y., KUBO Y., UTSUMI K., TAKEDA Y. and TAKANO M. T., *Jpn J. Appl. Phys.* **27** (1988) 1071.

[231] SANKAWA I., SATO M. and KONAKA T., *Jpn J. Appl. Phys.* **27** (1988) L-28.

[232] LUO J. S., FAUDOT F., CHEVALIER J. P. and MICHEL D., *J. Less Common. Metals* **164-165** (1990) 1428.

[233] SINGH J. P., LEN H. J., POEPPEL R. B., VAN VOORKEES E., GOUDEY G. T., WINSLEY K. and DONGLU SHI, *J. Appl. Phys.* **66** (1989) 3154.

[234] JIN S., DAVIS M. E., TIEFEL T. H., VAN DOVER R. B., SHERWOOD R. C., O'BRYAN H. M., KAMMLOTT G. W. and FASTNACHT R. A., *Appl. Phys. Lett.* **54** (1989) 2605.

[235] ZHANG PINGXIANG, ZHOU LIAN, JI PING, DU SHEJUN, WANG JINGRONG, WANG KEGUANG and WU XIAOZU, ICMC'91 June 11-14 Hunsville Alabama, USA.

[236] DWIR B., AFFRONTE M. and PAVUNA D., *Phys. Lett.* **55** (1989) 399 ;
DWIR B., PAVUNA D., AFFRONTE M., BERGER H. and THOLENCE J. L. (to be published).

[237] PRASED R., CONI N. C., MOHAN A., KHERA S. K., NAIR K. U., GUPTA C. K., TOMY C. V. and MALIK S. K., *Mater. Lett.* **7** (1988) 9.

[238] JUNG J., MOHAMED M. A.-K., CHENG S. C. and FRANCK J. P., *Phys. Rev. B* **42** (1990) 6181.

[239] FUKUSHIMA N., NIU H., NAKAMURA S., TAKANO S., HAYASHI M. and ANDO K., *Physica C* **159** (1989) 777.

[240] HUANG C. Y., SHAPIRA Y., MCNIFF E. M., PETERS J. R. P. N., SCHWARTZ B. B., WU M. K., SHULL R. D. and CHIANG C. K., *Mod. Phys. Lett.* **B** (1988) 869.

[241] SHAPIRA Y., HUANG C. Y., MCNIFF E. J. Jr., PETERS P. M., SCHARTZ B. B., WU M. K., *AMMM* **78** (1988) 19.

[242] MORITA M., MURAKAM M., MIYAMOTO K., SAWANO K. and MATSUDA S., *Physica C* **162-164** (1989) 1217.

[243] MENG R. L. and CHU C. W., *Nature* **345** (1990) 326.

[243a] DONGLU SHI, MING XU, FANG M. M., CHEN J. G., CORNELUS A. L. and LANAN S. G., *Phys. Rev. B* **41** (1990) 8833.

[244] WISNIEWSKI A., BARAN M., PRYSLUPSKI P., SZYMZAK H., PAJACZKOWSKA A., PYTEL B., PYTEL K., *Solid State Commun.* **65** (1988) 577.

[245] MCHENRY M. E., WILLIS J. O., MALEY M. P., THOMPSON J. D., COST J. R. and PETERSON D. E., *Physica C* **162-164** (1989) 689.

[246] SCHINDLER W., ROAS B., SAEMANN-ICHENKO G., SCHULTZ L. and GERSTENBERG H., *Physica C* **1-2** (1990) 117.

[247] KUPFER H., APFELSTEDT I., SCHAUER W., FLÜKIGER R., MEIER-HIRMER R., WÜHL H. and SCHEWRER H., *Z. Phys. B* **69** (1987) 167.

[248] UMEZAWA A., CRABTREE G. W., LIU J. T. Z., WEBER H. W., KWOK W. K., NUNEZ L. H., MORAN T. J., SOWERS C. H. and CLAUS H., *Phys. Rev. B* **36** (1987) 7151.

[249] VAN DOVER R. B., GYORGY E. M., SCHNEEMEYER L. F., MITCHELL J. W., RAO K. V., TUROWSKI A., WIECH U. and WOLF T., *Nature* **342** (1989) L-1561.

[250] SAUERZOPF F. M., WIESENGER H. P., KRITSHA W., WEBER H. W., CRABTREE G. W. and LIU J. Z., *Phys. Rev. B* **43** (1991) 3091.

[251] KRITSCHA W., SAUERZOPF F. M., WEBER H. W., CRABTREE G. W., CHANG Y. C. and JIANG P. Z., *Europhys. Lett.* **12** (1990) 179.

[252] WHITE A. E., SHORT K. T., DYNES R. C., LEVY A. F. J., ANZBOVAR M., BLANDWIN K. W., POLAKOS P. A., FULTON T. A. and DUNKLEBERGER L. N., *Appl. Lett.* **53** (1988) 1010.

[253] VICHERY H., RULLIER-ALBENQUE F., PASCAROL H., KONCZYKOWSKI M., KORMANN R., FAVROT D. and COLLIN G., *Physica C* **159** (1989) 697.

[254] RULLIER-ALBENQUE F., ARDONCEAU J. and KORMANN R., *J. Phys. France I* **1** (1991) 395.

[255] KATO T., SHIRAISKI K. and KUNIJA J., *Jap. J. Appl. Phys.* **58** (1989) L-766.

[256] ROAS B., HENSEL B., SAEMANN-ISHENKO G. and SCHULTZ L., *Appl. Phys. Lett.* **54** (11) (1989) 105 ; *Jap. J. Appl. Phys.* **28** (1989) L-1521.

[257] NEUMÜLLER H. W., RIES G., SCHMIDT W., GERHÄUSER W., KLAUMÜNZER S., **1** ICMAS-90 (17-19 October 1990 Grenoble, France) Edit. IITT Int. ; page 1351.

[258] CIVALE L., MARWICK A. D., WORTHINGTON T. K., KIRK M. A., THOMPSON J. R., KRUSIN-ELBAUM L., SUN Y., CLEM J. R. and HOLZBERG F., *Phys. Rev. Lett.* **67** (1991) 648.

[259a] KIRK M. A., Proceedings of the International Workshop On Critical Current limits, Worsow Poland (Sep. 1991) ; To be published by World Scientific (Singapore) 1992 ; and a review article to appear in 1992.

[259b] HARDY V., PROVOST J., GROULT D., HERVIEU M., RAVEAU B., BURRCOK S., POLLERT E., FRISON J. C., CHAMINADE J. P. and POUCHARD M., to appear in *Physica C* ;
HARDY V., PROVOST J., GROULT D., RAVEAU B., TESSLER L. R., FRISON J. C., CHAMINADE J. P. and BOUFFARD S., preprint.

[260] KES P. H., PRUYMBOOM A., VAN DEN BERG J., MYDOSH J. A., *Cryogenics* **29** (1989) 228.

[261] BLATTER G., RHYNER J. and VENOKUR V. M., *Phys. Rev. B* **43** (1991) 7826.

[262] IYE Y., NAKAMURA S., TAMEGAI T., TEREASHIMA T., YAMAMOTO Y. and BANDO Y., *Physica C* **166** (1990) 62.

[263] GYORGY E. M., VAN DOVER R. B., SCHNEEMEYER L. F., WHITE A. E., O'BRIAN H. M., FELDER R. L., WASZCZAK J. V., RHODES W. W. and HELLMAN F., *Appl. Phys. Lett.* **56** (1990) 2465.

[264] SCHEGOLEV I. F., private communication, at ISSP Chernogolovka (USSR).

[265] HOFF H. A. *et al.*, studies of High Temperature Superconductors, Edited by Anaut Narlikar (Nova Sciences Publishers) **6** (1990).

[266] GRANADOS X., CARRERA M., OBRADORS X., FERRER N., FONTCUBERTA J., LERA F., RILLO C., BARTOLOME J., NAVARRO R., VALLET M., CABANAS M. V., GONZALEZ CALBET J. M., *Cryogenics* **29** (1989) 350.

[267] RICE J. P., GENSBERG D. M., RABIN M. W., VANDERVOORT K. G., CRABTREE G. W. and CLANS H., *Phys. Rev. B* **41** (1990) 6532.

[268] KRAMER M. J., *Appl. Phys. Lett.* **58** (1991) 1086.

[269] AYACHE J., SABRAS J., GASGNIER M., MONTY C., MAURY R., BOZEC X., FERT A. R., REDOULES J. P., SNOECK E. and ROUCAU C., *J. Less Common. Metals* **164, 165** (1990) 152.
[270] PRATIBHA GAI L. and MCCARRON E. M., *Science* **247** (1990) 553.
[271] CHAKRAVARTY S., IVLEV B. I. and OVCHINIKOV Y., *Phys. Rev. B* **42** (1990) 2143.
[272] AGOSTINELLI A., FIORANI D., FOLCH R., TEJADA J. and TESTA A. M., preprint and Studies of High Temperature Superconductors, Edited by Anaut Narlikar (Nova Sciences Publishers) **5** (1990).
[273] NARWANKAR P. K., CHANDRACHOOD M. R., MORRIS D. E. and SINHA P. B., *Appl. Phys. Lett.* **58** (1991) 651.
[274] KISHIO K., GREEN M. L., NAKATANI K. and KITAZAWA K., *Mol. Cryst. Liq. Cryst.* **184** (1990) 369.
[275] HARSHMANN D. R., SCHEEMEYER L. F., WASZCZAK J. V., AEPPLI G., CAVA R. J., BATLOGG B., RUPP L. W., *Phys. Rev.* **B 39** (1989) 851.
[276] PUMPIN B., KELLER H., KUNDINGETOL W., *Physica C* **162-164** (1989) 151.
[277] KRUSIN-ELBAUM L., GREENE R. L., HOLTZBERG F., MALOZEMOFF A. P., YESHURUN Y., *Phys. Rev. Lett.* **62** (1989) 217.
[278] COOPER J. F., CHU C. T., ZHOU L. W. *et al., Phys. Rev.* **B 37** (1988).
[279] STROUMBOS H. and MONOD F., *J. Less. Comm. Met.* **164-165** (1990) 1009.
[280] DOLGOV O. V., GOLUBOV A. A. and KOSHELER A. E., *Solid State Commun.* **72** (1989) 81.
[281] OSAMURA K., TAKAYAMA T., OCHIAI S., *Supercond. Sci. Technol.* **2** (1989) 111.
[282] DIMOS D., CHAUDARI P., MANNHART J. and LEGOVES F. K., *Phys. Rev. Lett.* **61** (1988) 219.
[283] GROSS R., CHAUDARI P., DIMOS D., GUPTA A. and KORE G., *Phys. Rev. Lett.* **64** (1990) 228.
[284] KORMANN R., LAINEE F., GANNE J. P. and LLORET B. ; *Eur-Ceramics* **2**, ed. by G. de With, R. A. Terpstra and R. Metsel (Elsevier Applied Sciences London and New York, 1989, 441.
[285] ALFORD N. McN, BUTTON T. W., JONES D. H., GOUGH C. E. and PENN S. J., KARLHSRUE, *Cryogenics* **30** (1990) 434.
[286] REGNIER P. and CHAFFRON L. and SCMIGELD L., ICMAS-90 (17-19 October 1990 Grenoble, France) Edit. IITT Int., p. 93.
[287] MAURY R., FERT A. R., REDOULES J. P., AYACHE J., SABRAS J. and MONTY C., *Physica C* **167** (1990) 591.
[288] SCHULTZ B., SCHLIEPE B., WISNY W. and BABERSCHKE K., *Solid State Commun.* **80** (1991) 111.
[289] SUENAGA M. and GHOSH A., *IEEE Trans. Mat. Magn. Mag.* **21** (1985) 1122.
[290] OGALE S. B., DIJKKAMP D. and VENKATESAN J., *Phys. Rev. B* **36** (1987) 7210.
[291] KUPFER H., APFELSTADT I., SHAUER W., FLUKIGER R., MEIER-HIRNER R., WUHL H., *Z. Phys. B* **69** (1987) 159.
[292] EBERHARDT F. J., HIBBS A. D., CAMPBELL A. M., *IEEE Trans. Magn.* **25** (1989) 2146.
[293] PAVUNA D., BERGER H., AFFRONTE M., VAN DER MASS J., CAPPONI J. J., GUILLOT M., LEJAYAND P. and THOLENCE J. L., *Solid State Commun.* **68** (1988) 535.
[294] AGUILLON C., SENOUSSI S., unpublished.
[295] VAN DUZER T., TURNER C. W., Principles of Superconductive Devices and Circuits, Elsevier North Holland, New York (1981).
[296] DEW-HUGHES D., Proceedings of First European Workshop on High $T_c$ Superconductors Genova, Italy (1987) 67.
[297] KWAK J. F., VENTURINI E. L., GINLEY D. S. and FU W., In Novel Superconductivity (Eds S. A. Wolf and V. Z. Kresin) Plenum Publishing corporation, New York, USA (1987) 983.
[298] PETERSON R. L. and EKIN J. W., *Phys. Rev. B* **37** (1988) 9848.
[299] SENOUSSI S., HADJOUDJ S., WEYL C. and FONDER P., *Physica C* **165** (1990) 199.
[300] GRADER E. M., GYORGY L. G., VAN UITERT W. H., GRODKIEWICZ T. R., KYLE and ELSBSCHUTZ M., *Appl. Phys. Lett.* **53** (1988) 319.
[301] HSIANG T. Y. and FINNEMOR D. K., *Phys. Rev. B* **22** (1980) 154.
[302] ROSENBLAT, LEBEAU C., PEYRAL P. and RABOUTOU A., Josephson effect Achievement And Trends, ed. A. Barone (World Scientific, Singapoure, 1986) p. 320.
[303] EBNER C., STROUD D., *Phys. Rev. B* **23** (1981) 6147 ; *Phys. Rev. B* **25** (1982) 5711 ; STROUD D., EBNER C., *Physica C* **153** (1988) 63.

[304] MOGENSTERN I., MULLER K. A., BEDNORZ J. G., *Z. Phys. B* **69** (1987) 33.
[305] GIOVANNELLI A., GIOVANNELLA C., *J. Less Common. Metals* **164-165** (1990) 1488.
[306] JIN S., TIEFEL T. H., SHERWOOD R. C., VAN DOVER R. B., DAVIS M. E., KAMLOTT G. W. and FASTNACHT R. A., *Phys. Rev. B* **37** (1988) 7850.
[307] JIN S., TIEFEL R., SHERWOOD R., DAVIS M., VAN DOVER R., KAMMLOTT G., FASTNACHT R. and KEITH H., *Appl. Phys. Lett.* **52** (1988) 7074.
[308] JIN S., SHERWOOD R., GYORGY E., TREFEL T., VAN DOVER R., NAKAHARA S., SCHNEEMEYER L., FASTNACHT R. and DAVIS M., *Appl. Phys. Lett.* **54** (1989) 584.
[309] MURAKAMI M., MORITA M., DOI K. and MIYAMOTO K., *Jpn J. Appl. Phys.* **28** (1989) 1189.
[310] MURAKAMI M., MOROTA M. and KOYAMA N., *Jpn J. Appl. Phys.* **28** (1989) L-1125.
[311] LAY K. W., AIP Conf. Proc. (USA) **219** (1991) 119.
[312] SALAMA K., SELVAMANICKAM V., GAO L. and SUN K., *Appl. Phys. Lett.* **54** (1989) 2352.
[313] CHAFFRON L., REGNIER P., SCHMIRGELD L., MAURICE F., AGUILLON C. and SENOUSSI S., International Conf. on Mod. Aspects of Superconductivity (ICMAS), Paris (1991) p. 319-324, Published by IITT.
[314] AGUILLON-LEVILLAIN C., Thesis : Université Paris Sud, Orsay (France) 1991.
[315] JIANG X., HUANG J., YU Y., JIANG M., QUIO G., GE Y., HU Z., SHI C., ZHAO Y., WANG Y., XU G. and ZHOU Y., *Supercond, Sci. Technol.* **1** (1988) 102.
[316] MORRIS P., BAGLEY B., TARASCON J., GREEN L. and HULL G., *J. Am. Ceram. Soc.* **71** (1988) 334.
[317] MCGINN P., BLACK M. and VALENZUELA A., *Physica C* **156** (1988) 57.
[318] MCGINN P., CHEN W. and BLACK M. A., *Physica C* **161** (1989) 198.
[319] DAS B. N. *et al., J. Supercond.* **2** (1989) 253.
[320] DE RANGO P., GIORDANENGO B., TOURNIER R., SUPPLICE A., CHAUSSY J., DEUTSCHER G., GENICON J. L., LEJAY P., RETOUX R. and RAVEAU B., *J. Phys. France* **50** (1989) 2857.
[321] LUSNIKOV A., MILLER L. L., MCCALLUM R. W., MITRA S., LEE W. C. and JOHSTON D. C., *J. Appl. Phys.* **65** (1989) 3136.
[322] FARREL D. E., CHADRASEKHAR B. S., DEGUIRE M. R., FANG N. M., KOGAN V. G., CLEM J. R. and FINNEMORE D. K., *Phys. Rev. B* **36** (1987) 4025.
[323] REGNIER P., to be reported elsewhere.
[324] FERREIRA J. M., MAPLE M. B., ZHOW H., HAKE R. R., LEE B. W., SEAMAN C. L., KURIC M. V. and GUERTON R. P., *Appl. Phys. A* **47** (1988) 105.
[325] SHAW G., BHAGAT S. M., *J. Appl. Phys.* **69** (1991) 5373.
[226] MIMURA M., EKOMOTO N., UNO M., NAKAJIMA M., KUMAKURA H. and TOGANO K., Proc. ICMC Conf. May-1990 Garmish-Partenkirchen.
[327] GLOWACKI B. A. and EVETTS J. E., Proc. 1st Europ. Workshop on High-$T_c$ Mat. Geneva (1987) p. 447.
[328] FLUKIGER R., MÜLLER T., GOLDACKER W., WOLF T., SEIBT E., APFIELSTEDT I., KÜPPER H. and SCHAVER W., *Physica C* **153-155** (1988) 1574.
[329] REGNIER P., LE HAZIF R. and CHAFFRON L., Proceedings of the Inter. Conf. on Mod. aspects of superconductivity (Paris, 1989), Edit. IITT Int. p. 133.
[330] REGNIER P., CHAFFRON L., SCHMIRGELD L., Proceedings of the International Conf. ICMAS-90 from Modern Superconductivity towards Applications (Grenoble 1990), Edit. IITT, p. 93.
[331] FLÜKIGER R., GROTH C., GOLDACKER W. and XU J. Q., Proceedings of the Inter. Conf. on Mod. aspects of superconductivity (Paris, 1990), Edit. IITT Int., p. 165.
[332] OH S. S., OCHIAI S. and OSAMURA K., Proc. 2nd Int. Symp. on Superconductivity (ISS'89), Eds T. Ishiguro and K. Kajimara (Springer, Berlin 1990).
[333] SATO S. K., MIKATA T., MUKAI H., MASSUDA T., UEYAMA M., HITOTSUUYANAGI H., MITSWI T. and KAWASIMA M., Proc. 2nd Int. Sympos. on Superconductivity (ISS'89), Eds T. Ishiguro and K. Kajimura.
[334] KUMAKURA H., TOGANO K. and MAEDA H., *J. Appl. Phys.* **67** (1990) 3443.
[335] YAMADA Y., KCHARA K. J., HUSEB T., YANGIYA T., YASUHARA S. and ISHUHARA M., *Cryogenics Eng.* **25** (1990) 82.
[336] SOOH S., TADESKI KUBOTO and KOZOOSAMURA, *Physica C* **171** (1990) 265.

[337] HIKATA T., NISHIKAKAWA T., MUKAI H., SATO K., HITOTSUYANAGI H., *Japan J. Appl. Phys.* **28** (1989) L-2161.
[338] SCHAÜFELE J., GROTH C., GOLDACKER W., KÜPFER H. and FLÜKIGER R., Proc. ICMC, Conf. May-1990, Garmisch-Partenkirchen, FRG.
[339] AMBEGAOKAR V. and BARATOFF A., *Phys. Rev. Lett.* **10** (1963) 486 ; *errata* **11** (1963) 104.
[340] FERREL R. A. and PRANGE R. E., *Phys. Rev. Lett.* **10** (1963) 479.
[341] JOSEPHSON B. D., *Rev. Mod. Phys.* **36** (1964) 216 ;
MATISSO J., *J. Appl. Phys.* **40** (1969) 1813.
[342] CLEM R., BUMBLE B., RAIDER S. I., GALLAGHER W. J. and SHIH Y. C., *Phys. Rev. B* **35** (1987).
[343] CLEM R., *Physica C* **153-155** (1988) 50.
[344] SENOUSSI S., submitted to *Phys. Rev. Lett.*
[345] KANITHI H. C., MOTOWILDO L. R., OZERYANSKY G. M., HAZLTON D. W. and ZEITLIN B. A., *IEEE Trans. Magn.* **25** (1989) 2204.
[346] MALOZEMOFF P., Private suggestion.
[347] GRIESSEN R., Private Communication.
[348] KONCZYKOWSKI M., BURLACHKOV L. I., YESHURUN Y. and HOLTZBERG F., *Phys. Rev.* **B 43** (1991) 13707.
[349] DAMJANOVIC V. P. and SIMONOV A. Yu., *J. Phys. I France* **1** (1991) 1639.
[350] DAEUMLING M., SEUNTJENS J. M. and LARBALESTIER C., *Nature* **256** (1990) 332.
[351] CAVE J. R., CRITCHLOW P. R., LAMBERT P. and CHAMPAGNE, *IEEE Trans. Magn.* **27** (1991) 1379.
[352] BHAGWAT K. V. and CHADDAH P., *Phys. Rev. B* **44** (1991) 6950.
[353] DERSCH H. and BLATTER G., *Phys. Rev. B* **38** (1988) 11391.
[354] PETERSON R. L., *Phys. Rev. B* **40** (1989) 2678.
[355] MEILIKHOV E. and GERSHANOV Yu., *Physica C* **157** (1989) 431.
[356] DE LUCAS R., PACE S. and SAVO B., *Phys. Lett. A* **154** (1991) 185.
[357] SENOUSSI S., HDJOUDJ S., MAURY R., FERT An., *Physica C* **165** (1990) 364.
[358] AGUILLON C. and SENOUSSI S., *J. Less Common. Met.* **164-165** (1990) 1061.
[359] DEW-HUGHES D., *Cryogenics* **27** (1987) 476.
[360] FEVRIER A., *Cryogenics* **23** (1983) 185.
[361] DUBOTS P. and CAVE J., *Cryogenics* **28** (1988) 661.
[362] CAMPBELL A. M., *J. Phys. C* **2** (1971) 1492 ; *Ibid.* **4** (1971) 3136.
[363] LOVE G. R., *J. Appl. Phys.* **37** (1966) 3336.
[364] ULLMAIER N. A., *Phys. State Solid.* **17** (1966) 631.
[365] CLEM J. R., *Physica C* **153-155** (1988) 50.
[366] MÜLLER K. H., MAC FARLANE J. C. and DRIVER R., *Physica C* **158** (1989) 158.
[367] MÜLLER K. H., *Physica C* **159** (1989) 117.
[368] GESKEINBEIN V. B., VINOKUR V. M. and FEHRENBACHER R., *Phys. Rev. B.*
[369] FEIGEL'MAN M., LOFFE L., LARKIN A. and VINOKUR V., Preprint.
[370] ROSSEL C., MAENO Y. M. and MORGANSTROM I., *Phys. Rev. Lett.* **62** (1989) 681.
[371] GREGORY S., ROGERS C. T., VENKATESMA T., WU X. D., INAM A. I. and DUTTA B., *Phys. Rev. Lett.* **62** (1989) 1548.
[372] PUREUR P., SCHAF J., KUNZLER J. V. and FRAGES E. R., *Solid. State Commun.* **66** (1988) 931 ;
SCHAF J., PUREUR P., KUNZLER V., *Phys. Rev. B* **40** (1989) 6948.
[373] PUREUR P., SCHAF J., *Solid. State Commun.* **78** (1991) 723.
[374] MALOZEMOFF A., WORTHINGTON T. K., YESHURUN Y. and HOLTZBERG F., *Phys. Rev. B* **38** (1988) 7203.
[375] AKSENOV V. L. and SERGEENKOV S. A., *Physica C* **165** (1988) 18.
[376] MEHDAOUI A., BOLMONT D. and LOGEL B., ICMAS-90 (17-19 October 1990 Grenoble, France) Edit. IITT Int. p. 191.
[377] GUPTA A., ESQUINAZI P., BRAUN H. F., GERHAUSER W., NEUMULLER H. W., HEINE K. and TENBRINK J., *Europhys. Lett.* **10** (1989) 663 ;
GUPTA A., ESQUINAZI P., BRAUN H. F. and BRANDT E. H., *Physica C* **162-164** (1989) 667 ;
ESQUINAZI P., *Solid State Commun.* **74** (1990) 75.

[378] SAGDAHL L. T., GJOLMESLI S., TUSET P., NES O.-M., LAGREID T., FOSHEIM K. and ASSMUS W., *Physica C* **165-166** (1990) 1149.
[379] LI J. N., KADOWAKI K., MENKEN M. J. V., MENOVSKY A. A. and FRANSE J. J. M., *Physica C* **161** (1989) 313.
[380] OUSSÉNA M., Thèse, Université Paris-Sud Orsay 91405, France (1989).
[381] CIVALE L., HAFAR H., DE LA CRUZ F., ESPAEZA D. A. and D'OVIDIO C. A., *Solid State Commun.* **65** (1988) 129.
[382] KRUSIN-ELBAUM L., MALOZEMOFF A. P. and YESHURUN Y., HTS Sympos., Boston, USA, 30 Nov.-4 Dec. 1987 (Pittsburg, P.A., USA, Res. Soc. 1988).
[383] SENOUSSI S., *Phys. Rev. Lett.* **51** (1983) 2218 ; *Phys. Rev. Lett.* **56** (1986) 2314 ; *J. Mag. Mag. Mat.* **54-57** (1986) 153.
[384] SENOUSSI S. and ONER Y, *J. Mag. Mag. Mat.* **40,** 12 (1984) 39 ; *J. Phys. France* **46** (1985) 1435.
[385] GOTOH S., MURAKAMI M., FUJIMOTO H., KOSHIZUKA N. and TANAKA S., *Physica C* **166** (1990) 215.
[386] GJOLMESLI S., LÆGREID T. and FOSSHEIM K., *Physica C* **162** (1989) 339.
[387] OKUDA K., NOGUCHI S., YOSHIKAWA M., IMANAKA N., IMAI H. and ADACHI G., *Physica B* **165-166** (1990) 1397.
[388] VAN DEN BERG J., VAN DEN BEEK C. J., KES P. H., MYDOSH J. A., MENKEN M. J. V. and MONOVSKY A. A., *Supercond. Sci. Technol.* **1** (1989) 249.
[389] NELSON D., *Phys. Rev. Lett.* **60** (1988) 1973.
[390] TAKACS S., GÖMORY F., *Supercond. Sci. Technol.* **3** (1990) 94.
[391] TAKACS S., GÖMORY F. and LOBOTKA P., *Physica B* **165-166** (1990) 1399.
[392] MARCON R., FASTAMPA R. and GIURA M., *Europhys. Lett.* **11** (1990) 1399.
[393] GESHKENBEIN V. B., VINOKUR V. M., FEHRENBACHER R., *Phys. Rev. B* **43** (1991) 37-48.
[394] BRANDT E. H., *Z. Physik B* **80** (1990) 167.
[395] INUI M., LITTLEWOOD P. B. and COPPERSMITH S. N., *Phys. Rev. Lett.* **63** (1989) 2421.
[396] LONDON F., Superfluids, Macroscopic Theory of Superconductivity (Dover, New York) p. 31, 32.
[397] MELVILLE P. H., *Phys. Lett.* **39A** (1972) 373.
[398] GRADNER G. S., GRADER G. S., GYORGY E. M., VAN UITERT L. G., GRODKIEWICZ W. H., KYLE T. R. and EIBSCHUTZ M., *Appl. Phys. Lett.* **53** (1988) 319.
[399] TJUKANOV E., CLINE R. W., KRAHN R., HAYDEN M., REYNOLDS M. W., HARDY W. N., CAROLAN J. F. and THOMPSON R. C., *Phys. Rev. B* **36** (1987) 7244.
[400] WEI-JIANG YEH, LIE CHEN, FENGZKI XU, BAOKANG BI and PEIRAN YANG, *Phys. Rev. B* **36** (1987) 2415.
[401] GIORGY E. M., GRADER G. S., JOHNSON D. W., Jr., FELDMAN L. C., MURPHY D. W. and RHODES W. W., *Appl. Phys. Lett.* **52** (1988) 328.
[402] LI J. N., KADOWAKI K., MENKEN M. J. V., MENOVSKI A. A. and FRANSE J. J. M., *Physica B* **165-166** (1990) 1429.
[403] EBERHARDT F. J., HIBS A. D. and CAMPBELL A. M., *Cryogenics* **28** (1988) 681.
[404] CAMPBELL A. M., *J. Phys. C* **2** (1969) 1492.
[405] GITTLMAN J. I. and ROSENBLUM B., *Phys. Rev. Lett.* **16** (1966) 7''' ; *J. Appl. Phys.* **39** (1968) 2617.
[406] An extensive analysis of the torque technique is reported in the thesis of C. W. Hagen (1991), Vrije Universitteit Te Amsterdam, The Netherlands.
[407] LOWELL J., Low-Temperature Physics-LT13 (1972) vol. 3, edited by K. D ; Timmerhauss *et al.* (Plenum Press, New York-London).
[408] KOSHELEV A. E. and VINOKUR V. M., *Physica C* **173** (199&) 465.
[409] YEH N. C., *Phys. Rev. B* **43** (1991) 523.
[410] JENSEN H. J., BRASS A. and BERLINSKY A. J., *Phys. Rev. Lett.* **60** (1988) 1676) ; BRASS A., JENSEN H. J. and BERLINSKY A. J., *Phys. Rev. B* **39** (1989) 102.
[411] SHI A. C., BERLINSKY A. J., *Phys. Rev. Lett.* **67** (1991) 1926.
[412] BRANDT E. H., *Phys. Rev. Lett.* (oct. or sept. 91) ; Proc. Conf. $M^2S$-HTSCIII, Kanazawa, July (1991) ; *Physica C* **185** (1991) 270.
[413] FISHER M. P. A., *Phys. Rev. Lett.* **62** (1989) 1415.
[414] VAN DER BEEK C. J. and KES P. H., *Phys. Rev. B* **43** (1991) 13032.

[415] VINOKUR V. M., KES P. H. and KOSHELEV A. E., *Physica C* **168** (1990) 29.
[416] SUDBO A. and BRANDT E. H., *Phys. Rev. Lett.* **66** (1991) 1781.
[417] BULAEVSKII L. N., *Zh. Eksp. Teor. Fiz.* **64** (1973) 2241 ; *sov. Phys. JETP* **73** (1973) 1133 ; *Int. J. Mod. Phys.* **B 4** (1990) 1849 (a review).
[418] TACHIKI M. and TAKAHASHI S., *Solid State Commun.* **70** (1989) 291 ; **72** (1989) 1083.
[419] BLATTER G., GESHKENBEIN V. B. and LARKIN A. I., Preprint.
[420] FEINBERG D. and VILLARD C., *Mod. Phys. Lett. B* **4** (1990) 9.
[421] BUDZIN A. and FEINBERG D., *J. Phys. France* **5** (1990) 1971.
[422] FEINBERG D. and VILLARD C., *Phys. Rev. Lett.* **65** (1990) 919.
[423] MASLOV S. S., POKROVSKII V. L., *Europhys. Lett.* **14** (1991) 591.
[424] BULAEVSKII L. N., *Phys. Rev.* **B 44** (1991) 910.
[425] FRIEDEL J., *J. Phys. France* **49** (1988) 1561.
[426] FEINBERG D., Preprint.
[427] BLATTER G., GESHKENBEIN V., Preprint.
[428] CARTON J. P., *J. Phys. I*, **1** (1990) 113.
[429] TONER J., *Phys. Rev. Lett.* **66** (1991) 2523.
[430] CHUDNOVSKY E. M., *Phys. Rev. B* **43** (1991) 7831 ; *Phys. Rev. Lett.* **66** (1991) 7831.
[431] CLEM J. R., *Phys. Rev.* **B 42** (1990) 6244 ; *ibid.* **B 43** (1991) 7837.
[432] KWOK W. K., WELP U., VINOKUR V. M., FLESHER S., DOWNEY J. and CRABTREE G. W., *Phys. Rev. Lett.* **67** (1991) 390.
[433] OUSSÉNA M., SENOUSSI S., COLLIN G., BROTO J. M., RAKOTO H., ASKENAZY S. and OUSSET J. C., *Phys. Rev. B* (rapid communication) **36** (1987) 4014.
[434] STROUMBOS H., LAROUI A., MONOD P., DECAMPS B., DUBOIS J. P. and ODIER P., *Physica C* **167** (1990) 375.
[435] MOSHALKOV V. V., HENRY J. Y., MARIN C., ROSSAT-MIGNOD J. and JAQUOT J. F., *Physica C* **175** (1991) 407.
[436] BRANDT E. H., *J. Low Temp. Phys.* **26** (1977) 709.
[437] METTOUT B., LIMAGNE D., WAYSAND G., CAPITELLA E., DE BELLEFON A. and ESPIGAT P., *Solid State Commun.* **64** (1987) 1069.
[438] FRANKEL D., *J. Appl. Phys.* **50** (1979) 5402.
[439] DAÛMLING M., LARBALESTIER D. C., *Phys. Rev. B* **40** (1989) 9350.
[440] CONNER L. W. and MALOZEMOFF A. P., *Phys. Rev. B* **43** (1991) 402.
[441] Group of Los Alamos, APS Meeting, Cincinnati, March 91.
[442] GERBER C., ANSELMETTI D., BEDNORZ J. G., MANNHART J., SCHLOM D. G., *Nature* **350** (1991) 279 ; APS Meeting, Cincinnati, March 91.
[443] MANNHART J., ANSELMETTI D., BEDNORZ G., GERBER Ch., MÜLLER K. A. and SCHLOM D. G., Preprint : Proc. of the Int. Workshop on Critical Currents in Superconductors, Churchill College, Cambridge, England, July 1991.
[444] SCHLOM D. G., ANSELMETTI D., BEDNORZ J. G., BROOM R., CATANA A., FREY T., GERBER Ch., GUNTHERODT H. J., LANG H. P., MANNHART J. and MÜLLER K. A., *Z. Phys. B* **86** (1991) 163.
[445] BEAN C. P. and LIVINGSTON J. D., *Phys. Rev. Lett.* **12** (1964) 1.
[446] ULMAIER H. (Springer Tracs in Modern Physics-New York) **76** (1975) 1.
[447] KRZYSTON T., *Phys. Status Solidi (b)* **158** (1990) K21.
[448] DAMJANOVIC V. P. and SIMONOV A. Yu., *J. Phys. I France* **1** (1991) 1639.
[449a] BUZDIN A. and FEINBERG D., Preprint.
[449b] BARONE A. and PATERNÔ G., Physics and Applications of the Josephson Effect (Wiley-Interscience, 1982).
[450] BUCHHOLD T. A., *Cryogenics* **3** (1963) 141.
[451] MELVILLE P. H., *J. Phys. C, Solid State Phys.* **4** (1971) 2833.
[452] PORTIS A. M., BLAZEY K. W., MÜLLER K. A., BEDNORZ J. G., *Europhys. Lett.* **5** (1988) 467.
[453] BONTEMPS N., DAVIDOV D., MONOD P. and EVEN R., *Phys. Rev. B* **43** (1991) 11512.
[454] FRAITSCZECH Z., *J. Phys.* **9** (1959) 750.
[455] FRAIT Z., FRAITOVA D. and PUST L., *J. Phys. Colloq. France C8* **49** (1988) 2235.

[456] BEREZINSKII V. L., *Zh. Eksp. Theor. Fiz* **59** (1970) 907 ; *Sov. Phys. JETP* **32** (1971) 493.
[457] FISHER D. S., *Phys. Rev. B* **22** (1980) 1190.
[458] NELSON D. S., *Phys. Rev. Lett.* **60** (1988) 1973 ;
NELSON D. S. and SEUNG H. S., *Physica C* **162** (1989) 1156.
[459] BRANDT E. H., *J. Low Temp. Phys.* **73** (1988) 355.
[460] DONIACH S., in High Temp. Superconduct. : Proc. of the Los Alamos Sympos. (1989) ed. by K. S. Bedell, D. Coffey, D. E. Meltzer, D. Pines and J. R. Shrieffer (Addison-Wesley Publishing Co., Redwood City, California, 1990) p. 406.
[461] LAWRENCE E. W. and DONIACH S., Proc. 12th Internat. Conf. of Low Temp. Physics LT12 (E. Kanda, ed., Academy Press Japan, Kyoto, 1991) p. 361.
[462] GESHKENBEIN V., LARKIN A., FEIGEL'MAN M., VINOKUR V., *Physica C* **162** (1969) 239.